

Durham E-Theses

*The structural and kinematic evolution of an upper
crustal transpression zone: The Lusitanian Basin,
Portugal.*

Curtis, Michael L.

How to cite:

Curtis, Michael L. (1993) *The structural and kinematic evolution of an upper crustal transpression zone: The Lusitanian Basin, Portugal.*, Durham theses, Durham University. Available at Durham E-Theses Online: <http://etheses.dur.ac.uk/5680/>

Use policy

The full-text may be used and/or reproduced, and given to third parties in any format or medium, without prior permission or charge, for personal research or study, educational, or not-for-profit purposes provided that:

- a full bibliographic reference is made to the original source
- a [link](#) is made to the metadata record in Durham E-Theses
- the full-text is not changed in any way

The full-text must not be sold in any format or medium without the formal permission of the copyright holders.

Please consult the [full Durham E-Theses policy](#) for further details.

**THE STRUCTURAL AND KINEMATIC
EVOLUTION OF AN UPPER CRUSTAL
TRANSPRESSION ZONE:
THE LUSITANIAN BASIN, PORTUGAL.**

by

Michael L. Curtis

The copyright of this thesis rests with the author.
No quotation from it should be published without
his prior written consent and information derived
from it should be acknowledged.

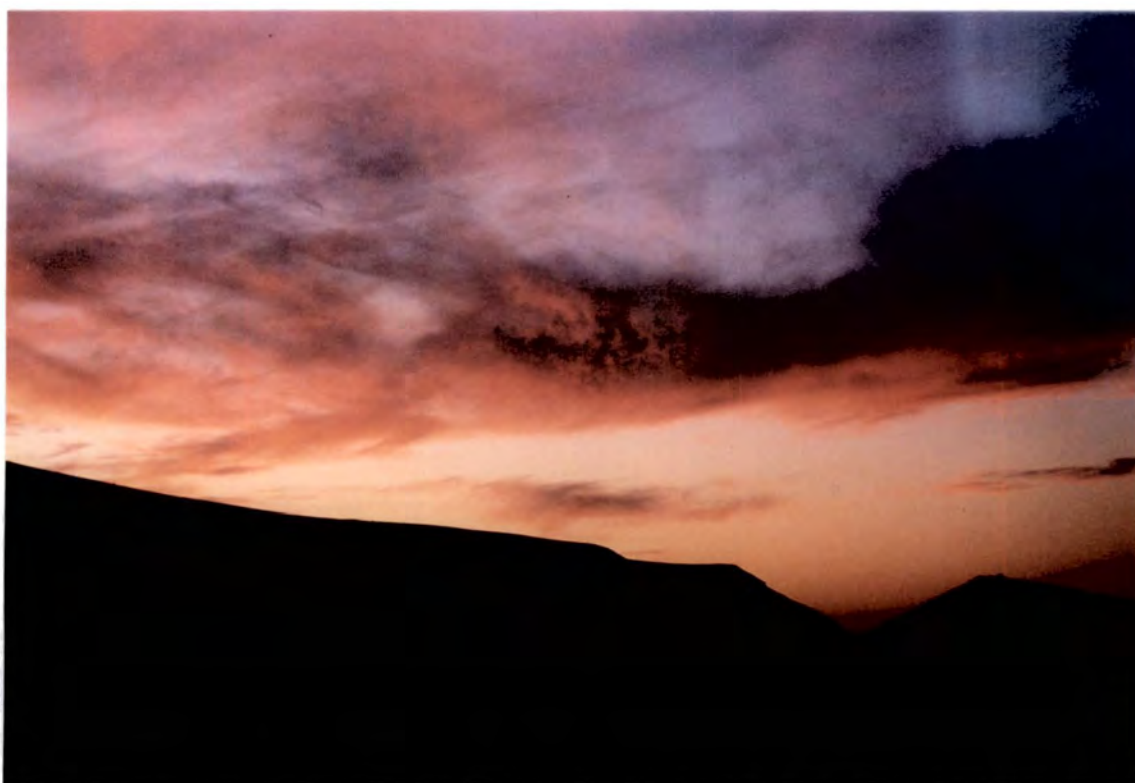
**A thesis submitted in partial fulfilment of the degree of Doctor of Philosophy at
the Department of Geological Sciences, University of Durham.**

1993.



i
10 AUG 1994

To Mum



Frontispiece

'Sunset over the Costa de Alvados'

(October 1989)

Copyright

The copyright of this thesis rests with the author. No quotation from it should be published without prior written consent and any information derived from it should be acknowledged.

No part of this thesis has been previously submitted for a degree at this university or any other university. The work described in this thesis is entirely that of the author, except where reference is made to previous published or unpublished work.

© 1993 Michael L. Curtis

ABSTRACT

The Lusitanian Basin forms a long (250km), narrow (50-100km), NE-SW trending outcrop of inverted Mesozoic carbonates and clastics. The outcrop of the Mesozoic sequence is flanked by two Neogene sub-basins, the contact between which is commonly faulted indicating that the Lusitanian basin underwent inversion during the Miocene. This inversion was achieved by reactivation of Jurassic extensional faults, which were originally formed above reactivated Hercynian basement faults during the Atlantic rifting event. The Serra de Montejunto/Candeeiros fault system (SMCF) forms the eastern boundary to this inverted zone, and is dominated by the NNE trending Serra dos Candeeiros fault (SCF). Towards the northern end of this fault system is a complex, uplifted, 15x20km fault bounded block, the Candeeiros block. At the southern termination of the SMCF, the fault orientation changes abruptly from NNE to ENE. This change in fault orientation coincides with the Serra de Montejunto mountain range, a narrow zone of tectonic uplift.

Detailed studies of the main fault zones and adjacent wall rock deformation, allows the kinematics and strain to be characterised. These studies have revealed a complex history of Miocene to Recent reactivation along the boundaries of the Candeeiros block. Initial reactivation of the cross-faults of the block was synthetic to the sinistral SCF. Initial sinistral motion along the cross-faults was superimposed by a late period of dextral transpression, as evidenced by the inverted Alvados pull-apart basin preserved along the Alvados/Minde cross-faults. Dextral transpressive strains along the cross faults of the Candeeiros block, appear to be intimately related to the southerly directed extrusion and anti-clockwise rotation of the block. Structural relationships suggest up to 30° of rotation has occurred. Rotation of the Candeeiros Block is believed to be associated with the change from sinistral simple shear to sinistral transpression along the SCF, during the Late Miocene.

The Serra de Montejunto region also displays a complex kinematic history, initiated by N-S shortening across the range, which was superseded by a late stage of sinistral transpression. This transpressive phase manifests itself as both simple and complex transpressive strains. The overall structural geometry of the region is that of a flower structure, formed in a major restraining bend at the termination of the SMCF.

The kinematic and deformation style of the early Miocene reactivation in both the Candeeiros and Montejunto regions are consistent with the application of a N-S regional shortening direction, or σ_1 , on the pre-existing Jurassic age structure of the areas. This initial phase of deformation is overprinted by a distinct late phase of deformation related to sinistral transpression along the SCF, which was probably responsible for the inversion of the Lusitanian Basin. The orientation, and chronology of the regional shortening directions responsible for the evolution of the SMCF are in agreement with the relative plate motion history for Africa-Europe (Dewey et al., 1989).

A comparison of instrumental seismicity and neotectonic surface faults associated with the SMCF, suggests that the basin is undergoing basement driven sinistral deformation, which is decoupled from the cover sequence by a thick evaporite sequence. The sinistral displacement along the proposed concealed, steep, basement faults appears to be transferred laterally along the sub-horizontal evaporite horizon, for up to 20km, to the steep cover faults of the SMCF.

*"We've done the bugger!"**

Sherpa Tenzing Norgay (1914-1986)

29th May 1953

(Attr., on conquering Mount Everest.)

* Source: The New Penguin Dictionary of Quotations, eds., J.M. & M.J. Cohen

Acknowledgements

First and foremost, I would like to acknowledge my supervisor and friend Dr. Donny Hutton, for his all round enthusiasm toward structural geology, and the confidence he imparted to me during the past three years. Hope you enjoyed the Portuguese experience as much as I did.

As for the Durham experience, the list is long, but not often that distinguished!! So here goes: Firstly, to the old gits, 'McCaffers' and Chris Jones, who referred to me as the 'young pup', or simply 'Boyo', when I first arrived. Thanks for introducing me to the Vic (I think!). A big thanks to Steve Jolley for leaving the weekend I arrived. To all the 'lads' in the department "SMC AMAT !!". Firstly, a big thanks to Gerald, and Dave for introducing me to those rare and splendid things - the college bars. A special SMC to Gary 'Sploob' Ingram for being so outrageously intolerant of everything, and keeping me company for 3 years in that wastepaper recycling bin we lovingly called an office. 'Top-of-the-Morning' to Big Andy of champagne airways, who like a loyal friend accompanied me on numerous sharking excursions to the 'Hill', and to Mark 'Rigsby' Wharton, thanks for the Karakoram expedition, that was one hell of an adventure (let's do it again sometime!). To the other people who have occupied CG212 during my period of tenancy, Jipper 'give-it-some-jip' Jaques, Stan, and Michele, thanks a lot for talking sooo much about granite. Moving swiftly along to the students of those lesser disciplines (Geochem, Seddies, Bugs, and Geofizz). General salutations to the following people (In no particular order): Ian 'the Beast' Parkinson, keep tuning in to Radio Moscow!!!, Steve 'Filth-Merchant' Edwards for getting me to Cambridge, Nilpf (thanks for the Amsterdam trip), Steve Moss, Dougie, Chezer, Timmy & Billy Bairn (the new breed of post-grad), Jane Keaton (a.k.a. Eric Bristow), Paul Field, John Booter, Sue, Boo, Sarah A., Zoë (I live in Switzerland you know) Sayer, J. Bole a.k.a. Andy Kerr, Hugh Sinclair, and anyone else I may have unwittingly missed out.

A special mention must go to the undergrad class of '92, notably the Castle and Hatfield boys (completely mad!). No mention of the undergrads would be complete without a special reference to *'The Firm'*, thanks for brightening up the view around the department, and taking this old wrinkly on a few good nights to Rixies and Riverside! Thanks also to the Karakoram expedition team: Cal, Goody, Amanda, and McCann. Special thanks to Cal for proof reading a large chunk of this thesis.

In Portugal: *Moito Obrigado* to João Batista Lopes, without whose help and friendship my fieldwork would not have been possible. Special thanks to the *Moita bela* Silvia Ferreira, and the Residencial Glória swimming pool, both made my fieldwork around Serra D'Aire a lot more tolerable. Special note is made of that most excellent of beers 'Super Bock'. However, I won't miss the salted cod!

The Department: Firstly, I'd like to thank 'Grand pops' Thuggy Alsop, and Bob H., for their valuable discussion regarding squashed, and broken stones. Thanks also to the other members of staff who almost convinced me there is more to geology than faults and folds. A huge debt of gratitude is owed to Karen, Carol, and Lynne whom I pestered incessantly about all things to do with paper!, my thanks also to Jerry Dresser and Alan Carr for photos (I haven't forgotten those maps you enlarged Alan, Cheers!), to Dave Stevenson for saving chapter 3, and last, but by no means least, a big thank you to the man who makes the department tick, Dave Asbery.

Thanks!!

Contents

Copyright	iii
Abstract	iv
Acknowledgements	vi
Contents	vii
Chapter 1	
Overview of strike-slip and transpressional tectonics	1
1.1 Strike-slip tectonics	1
1.1.1 Introduction	1
1.1.1.1 Classification and terminology	2
1.1.2 Mechanics of strike-slip faulting	3
1.1.3 Secondary fault sets and fault geometries	7
1.1.4 En echelon folds	16
1.1.5 Steppovers along strike-slip faults	19
1.1.5.1 Pull-aparts and rhomb grabens	19
1.1.5.2 Pressure ridges, push-ups and restraining bends	28
1.1.6 Tectonic rotations in strike-slip environments	29
1.2 Transpressional tectonics	34
1.2.1 Introduction	34
1.2.2 Modelling of transpressive strains	35
1.2.2.1 Finite transpressional strain	36
1.2.2.2 Incremental transpressional strain	36
1.2.2.3 Secondary structures	42
1.2.3 Complex transpression and kinematic partitioning	43
1.2.3.1 Spatial strain partitioning	43
1.2.3.2 Temporal strain partitioning	44
1.2.4 Transpression and associated en echelon folding	45
1.2.4.1 Folds and cleavage transection	47
1.2.5 Flower structures	50
1.3 Sense of movement determination in a brittle deformation regime	52
1.3.1 Slickenside striations	52
1.3.2 Sense of movement structures involving secondary fractures	54

Chapter 2	
The Mesozoic to Cenozoic evolution of the Lusitanian Basin	59
2.1 Introduction	59
2.2 The plate kinematics of Africa-Europe since the Middle Jurassic	62
2.3 Basin structure	65
2.3.1 Basement structure	65
2.3.2 Halokinetic structures and faulting	67
2.4 Stratigraphy	70
2.4.1 Aborted rift stage	72
2.4.2 Successful rifting stage	73
2.4.3 Post rift passive margin phase	76
2.4.4 Emergence and tectonic inversion of the Lusitanian Basin	78
Chapter 3	
The structure and Kinematics of the Serra dos Candeeiros region	81
3.1 Introduction	81
3.2 Serra dos Candeeiros Fault	82
3.2.1 The pre-Miocene history of the Serra dos Candeeiros Fault	82
3.2.2 Kinematics of the Serra dos Candeeiros Fault	85
3.2.2.1 Kinematics derived from mesoscopic and secondary faults	85
3.2.2.2 En-echelon folding	87
3.2.2.3 Cleavage	88
3.2.3 Cleavage development and fold relationship	88
3.2.4 Deformation style of the Serra dos Candeeiros Fault	90
3.3 The Alvados-Minde fault system	91
3.3.1 The Alvados fault zone	91
3.3.1.1 Kinematics and deformation style	94
3.3.2 The Minde fault	97
3.3.2.1 Fault kinematics	97
3.3.2.2 En-echelon folding	98
3.3.3 The inverted Alvados pull-apart basin	102
3.3.3.1 Structure and kinematics of the Alvados pull-apart basin	103
3.4 The Alcanede fault zone	119
3.4.1 Southeastern segment	119
3.4.1.1 Mesoscopic faulting along the southeast fault segment	120
3.4.2 Northwestern segment	121
3.4.2.1 Shear sense evidence along the northwest fault segment	121
3.4.3 The deformation style and kinematics of the Alcanede fault	124

3.5 The Mendiga fault zone	124
3.5.1 The northeastern segment	124
3.5.2 The southwestern segment	127
3.6 The southeastern thrust zone of the Candeeiros block	129
3.6.1 The Amiais de Baixo thrust zone	129
3.6.1.1 Southwestern sub-area	130
3.6.1.2 The Revinhas sub-area	131
3.6.1.3 Detailed strain evolution of Amiais de Baixo thrust sheet	133
3.6.1.4 The Perched Oligocene basin	136
3.6.2 Monsanto thrust zone	137
3.6.2.1 Thrust zone kinematics	138
3.6.2.2 Large scale fold geometry and associated structures	138
3.6.2.3 Strain and small scale structures associated with folding	142
3.6.2.4 Evidence within the Monsanto thrust zone for the rotation of the Candeeiros block	148
3.7 Serra D'Aire thrust zone	148
3.7.1 Moitas Venda region	149
3.7.2 Northern region	151
3.7.3 Fault kinematics	155
3.7.3.1 Moitas Venda region	155
3.7.3.2 Northern region	155
3.8 Structural and Kinematic evolution of the Candeeiros block	158
3.8.1 Model for the rotation of the Candeeiros block	161
Chapter 4	
Structure and Kinematics of the Serra de Montejunto range	163
4.1 Introduction	163
4.2 Structural domains of the Montejunto anticline	165
4.2.1 The Espigão plateau	165
4.2.1.1 The Rocha Forte fault	165
4.2.1.2 The Pragança fault	170
4.2.1.3 The Cercal fault	171
4.2.1.4 Arieiro anticline	174
4.2.2 The Main Montejunto massif	174
4.2.2.1 The Northern limb of the Montejunto massif	175
4.2.2.1.1 Tojeira thrust fault	175
4.2.2.1.2 Folding	176
4.2.2.1.3 Faulting	179

4.2.2.2 Arieiro fault zone	182
4.2.2.2.1 Main Arieiro fault	182
4.2.2.2.2 Northern Arieiro fault	185
4.2.2.2.3 Southern Arieiro fault	186
4.2.2.2.4 Southern fault splays	188
4.2.2.3 Southern limb of the Montejunto massif	193
4.2.2.3.1 Folding	193
4.2.2.3.2 Serra de Montejunto thrust	197
4.3 Late extensional veining and faulting within the Espigão plateau and Montejunto massif	203
4.4 Strain orientations within the Montejunto anticline	204
4.4.1 Methodology	204
4.4.2 Strain distribution and orientation	205
4.5 Structural and kinematic evolution of the Montejunto region	208
4.5.1 Initial phase of north-south shortening	208
4.5.2 Late sinistral transpression	209
Chapter 5	
Neotectonics of the Lusitanian Basin	215
5.1 Introduction	215
5.2 Neotectonic surface structures	215
5.3 Geometry of the Serra dos Candeeiros fault system at depth	219
5.4 Intraplate seismicity within the Lusitanian and Lower Tagus Basins	224
5.4.1 The Nazaré - Vilariça lineament	225
5.4.2 The Lower Tagus Valley lineament	225
5.4.3 Seismicity associated with the Lusitanian Basin	227
5.5 Summary: Neotectonics of the Lusitanian Basin	228
Chapter 6	
The Serra de Montejunto-Candeeiros fault system: Its evolution and implications	231
6.1 Serra de Montejunto-Candeeiros fault system	231
6.1.1 Fault system evolution	231
6.1.1.1 Middle Miocene initialisation of the fault system	232
6.1.1.2 Late transpressional structures	232
6.1.2 Estimates for the Miocene to Recent displacement along the S. dos Candeeiros - Cercal fault zone	235
6.2 Relationship between fault system kinematic and the relative plate motions of Africa- Europe	236

6.3 tectonic style of the Lusitanian Basin	238
6.3.1 Previous interpretations	239
6.3.2 Revised tectonic model for the Lusitanian Basin	240
6.3.3 Neotectonic model for the Lusitanian Basin	241
6.3.4 Summary: Alpine evolution of Lusitanian Basin Tectonics	243
References cited in text	246
Appendix	267
Reconstruction of principal strain axes from en echelon vein arrays	

CHAPTER 1

Overview of strike-slip and transpressive tectonics

1.1 Strike-slip tectonics

1.1.1 Introduction

The first scientific recognition of a strike-slip fault was probably made by Arnold Escher von der Linth, a Swiss geologist, who in the 1850's correctly mapped an 8km trace of the "Sax Schwendi fault". Observations of the horizontal slickenlines lead to the discovery of a 500-800m sinistral displacement. However, this work was not published until 1885 by Suess (Sylvester, 1988). Anecdotal reports of the first strike-slip surface rupture due to an earthquake were made in the 1857 earthquake along the San Andreas fault, where a sheep corral that lay astride the fault was distorted into an "S" shape (Wood, 1955). Freund (1971) credits the first published reports of a strike-slip rupture to Mckay (1890, 1892) who observed the 1888 earthquake along the Hope fault of southern New Zealand. These initial observations on strike-slip faults were brought abruptly to the scientific fore by the 1906 earthquake that occurred along the San Andreas fault, when 4.7m of dextral motion occurred along a fault which prior to 1906 would probably have been classified as a normal fault (Willis, 1938).

Several decades passed after the observations in New Zealand before the geological community had sufficient evidence to extrapolate from instantaneous strike-slip in earthquakes to interpretations that involved tens, or even thousands of kilometres of horizontal slip. The key to this thinking was the seminal paper of Kennedy presented to the Geological Society of London in 1939 (Kennedy, 1946), who correlated rocks and structures on either side of the Great Glen fault that were separated by 100km of sinistral displacement since the Middle Carboniferous. This work spawned several papers that recognised large displacements along strike-slip



faults around the world; 450km along the Alpine fault, (Wellman in Benson, 1952); more than 560km dextral displacement along the San Andreas fault (Hill and Dibblee, 1953); and 100km offset along the Dead Sea Rift (Quennell, 1958, 1959). The development of plate tectonics allowed geologists to overcome the limitations of fixist tectonics which prevailed before the late 1960's and led to an understanding of the mechanical complexities and tectonics of strike-slip fault zones. Extensive field observations, experimental studies, three-dimensional imaging by seismic reflection and drilling, refined dating techniques, paleoseismic investigations, and analysis of modern earthquakes provide a theoretical basis to relate strike-slip faulting to the concepts of pure and simple shear.

The following section is intended to discuss the pertinent features of strike-slip faulting and associated structures, as they will be applied and interpreted within this thesis. It is not intended to be an exhaustive review of the subject matter, although there is additional discussion of some subjects omitted from, or insufficiently discussed, in Sylvester's excellent review of strike-slip tectonics (1988). No attempt has been made to discuss the seismotectonics of strike-slip faults.

1.1.1.1 Classification and terminology

A strike-slip fault is "a fault on which most of the movement is parallel to the fault's strike" (Bates and Jackson, 1987), however, faults displaying this basic relationship have been described using various terminology¹⁰³. The term "wrench fault" was proposed by Kennedy (1946) who had been influenced by Anderson (1905) who had used "wrench plane" in the Scottish Geological survey for many years. These authors, and latterly Moody and Hill (1956), used this term to describe a deep-seated, regional, nearly vertical strike-slip fault which involves igneous and metamorphic basement rocks as well as supracrustal sedimentary rocks. Geikie (1905) referred to similar faults as "transcurrent faults". Increasingly "wrench fault" has frequently been used to describe any and all strike-slip faults by many authors, whether or not they conform to the characteristics of Moody and Hill (1956). Wrench faults have also been linked to

late compressional regimes that pass into transpression (Harland, 1971), thus adding even more confusion to the nomenclature. In this text, the author agrees with Sylvester (1988) who recommends that *strike-slip fault* be used for a fault of any scale which moves dominantly parallel to its strike. Strike-slip faults can be sub-divided into two general groups based on their relationship to the lithosphere; strike-slip faults that bound plates are termed *transform faults*, whereas *transcurrent fault* can be used to generally group the wide variety of strike-slip faults which do not cut the lithosphere (Sylvester, 1988). Woodcock (1986) has further classified the above groups on their plate-tectonic setting (figure 1.1), a summary of which can be found in Table 1.1. In depth discussions of the various attributes of the various types of transform and transcurrent faults are provided in Woodcock (1986) and Sylvester (1988).

Within this section words highlighted in *italics* will represent the terminology employed throughout the rest of text.

1.1.2 Mechanics of strike-slip faulting

The presence of shortening structures such as folds and thrust faults, of extensional structures including normal faults and dykes, and structures representing horizontal shear on nearly vertical surfaces, together in a single deformational regime represent the concept of strike-slip tectonics (Anderson, 1942; Moody and Hill, 1956; Wilcox et al., 1973). Two principal mechanisms explain the geometric and dynamic relations between these faults and associated structures: pure shear or Coulomb-Anderson model, and simple shear

Pure shear

This mechanism was originally proposed by Anderson (1905), it predicts that a conjugate set of complementary sinistral and dextral strike-slip faults will form at an angle of ϕ and $-\phi$ about the shortening direction, where ϕ is the angle of internal

INTERPLATE (DEEP-SEATED)	INTRAPLATE (THIN-SKINNED)
TRANSFORM faults (delimit plates, cut lithosphere, fully accommodate motion between plates)	TRANSCURRENT faults (confined to the crust)
Ridge transform faults Displace sediments of oceanic crust having similar spreading vectors Present examples: Owen, Romanche and Charlie Gibbs fracture zones	Indent-linked strike-slip faults Separate continent-continent blocks which move with respect to one another due to plate convergence Present examples: North Anatolian fault (Turkey); Karakoram fault (Pakistan)
Boundary transform faults Join unlike plates which move parallel to the boundary between the plates. Present example: San Andreas fault (California), fault (Pakistan), Alpine fault (New Zealand)	Tear faults Accommodate differential displacement within a given allochthon or between the allochthon and adjacent structural units (Biddle and Chisman Christie-Blick, 1963). Present example: northwest- and northeast striking faults in Asiatic fold-thrust belt.
Trench-linked strike-slip faults Accommodate horizontal component of oblique subduction; may cut and localise arc intrusions volcanic rocks; located approx. 100km inboard of trench. Present examples: Semanko fault (Burma), Atacama fault (Chile), Median Tectonic line (Japan)	Transfer faults Transfer horizontal slip from one segment of a major strike-slip fault to its overstepping neighbour. Present example: Lower Hope valley and Upper Huranui valley faults between the Hope and Kakapo faults (New Zealand)
	Intracontinental transform faults Separate allochthons of different tectonic styles. Present example: Garlock fault (California)

Table 1.1 Classification of strike-slip faults

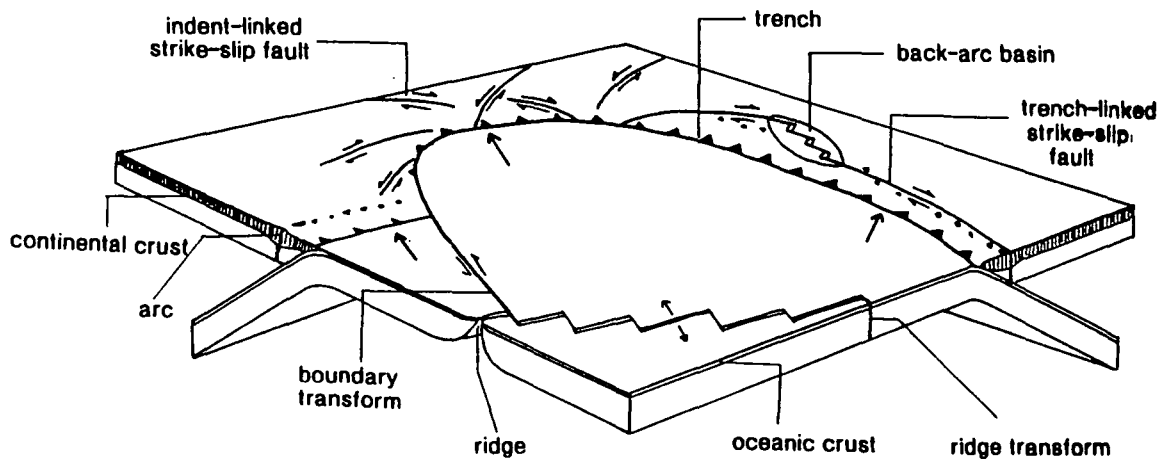


Figure 1.1 Summary of the major classes of strike-slip fault in their plate tectonic setting (Woodcock, 1986)

friction. It also predicts that extension fractures or normal faults will form perpendicular to the elongation axis, and that folds and thrusts will form perpendicular to the shortening axis (figure 1.2). These conjugate faults can accommodate

irrotational bulk strain as long as they operate simultaneously, otherwise space problems occur that can only be resolved by rotational strain and alternating differential slip on each of the conjugate faults. Strike-slip faults in areas of pure shear do not exhibit displacements measurable in hundreds of kilometres, because of the room problems produced by the convergence of large crustal masses (Sylvester, 1988), however, conjugate faults displaying many kilometres displacement are well documented. These fault sets are commonly found in fold-thrust systems, and frequently transect the fold trends. The conjugate faults develop on all scales, both pre- and post-folding, and help to accommodate the brittle component of strain in regimes of crustal shortening.

Simple shear

The major strike-slip faults of the world are in domains of simple shear which can be thousands of kilometres long, and tens of kilometres wide, with the most recently active fault only a few metres wide.

Simple shear has a monoclinic symmetry of strain as it is rotational. Due to this fact, a greater variety of structures form in a simple shear domain as opposed to pure shear (Sylvester, 1988). The complexity and variety of these structures individually or in combination have three main aspects; (1) the faults and folds form en-echelon arrays in relatively narrow zones; (2) complications related to components of reverse or normal slip on the basement fault; and (3) the formation of localised areas of extensional or shortening structures due to the lateral offsets_{or bends} in the master strike-slip faults (Naylor et al., 1986).

The various structures developed within a simple shear regime, although commonly found in association with one another, merit individual discussion which form the remainder of section 1.1.

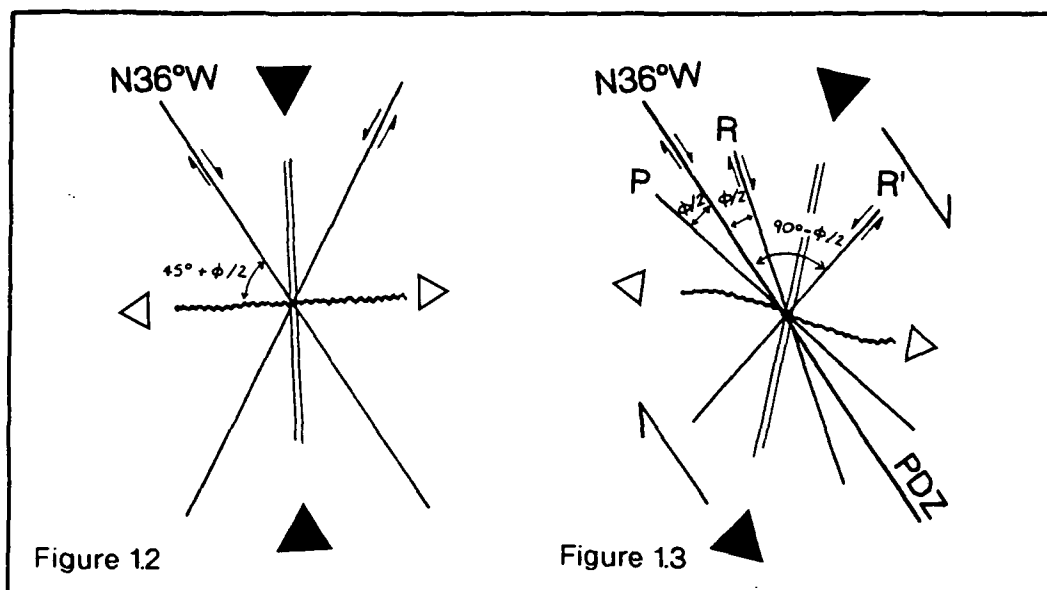


Figure 1.2 Plan view of incremental geometric relationship among structures for a Coulomb-Anderson model or Pure shear (Sylvester, 1988).

Figure 1.3 Riedel model of simple shear displaying incremental orientations of structures in a dextral system. (Sylvester, 1988)

Key to figures 1.2 and 1.3- Double parallel lines represents extensional structures, wavy line represents fold axes, or compressional structures, P= P fracture, R and R' are Riedel and Antiriedel faults, PDZ= principal displacement zone. Short black arrows = shortening axis, open arrows = axis of lengthening.

1.1.3 Secondary fault sets and fault geometries

From observations of model simple shear experiments, deformation experiments of homogeneous rocks under confining pressure, and surface ruptures in alluvial deposits, six sets of faults have been seen to form. These fractures form en-echelon arrays of kinematic and spatially distinct faults: (1) *Riedel* (R) shears (Tchalenko, 1970), or "synthetic" (Cloos, 1928) strike-slip faults; (2) conjugate *Riedel* (R') shears (Tchalenko, 1970), Antithetic *Riedel* shears (Naylor, 1986), or more concisely *Antiriedel shears*; (3) secondary synthetic strike-slip faults or *P shears* (Skempton, 1966; Tchalenko, 1970); (4) extensional fractures (*T fractures* of Tchalenko and Ambraseys, 1970) or normal faults; (5) reverse and thrust faults; and (6) faults parallel to the principal displacement zone (*Y shears* Morgenstern and Tchalenko, 1967; and Logan et al., 1979).

Figure 1.3 shows the incremental orientation of the above fault sets for a sinistral simple shear regime. The R, P, and Y shears are synthetic to the sense of shear along the principal displacement zone, whereas the R' shears are antithetic. All of the faults within this system are nearly vertical, except for the thrust faults. Thrust, reverse, and extensional faults form perpendicular and parallel, respectively to the maximum principal shortening direction across the fault zone, which forms an angle of 45° for simple shear. The conjugate R and R' shears form symmetrically about this principal shortening direction, defining angles of $45^\circ - \phi/2$ and $45^\circ + \phi/2$ to the maximum compressive stress σ_1 (Naylor et al., 1986), respectively. This relationship means that R faults form between $15\text{-}20^\circ$ to the principal displacement zone, while the R' faults form at $60\text{-}75^\circ$ (Tchalenko and Ambraseys, 1970).

Fault zone evolution

The evolution of strike-slip fault zones have been studied experimentally by several authors (Cloos, 1928; Riedel, 1929; Tchalenko, 1968; Wilcox et al., 1973, Bartlett et al., 1981; and Naylor et al., 1986). These analogue models consisted of either clay (Tchalenko, 1970), or loosely packed sand (Naylor et al., 1986) to represent

sedimentary cover, that overlies a "basement fault" represented by two plates that are free to move laterally past each other. The results of these experiments were largely compatible with one another, and displayed a consistent kinematic and structural evolution with increasing "basement fault" displacement. The fault zone development proceeds as follows:

- (1) Initial displacement results in the formation of en-echelon Riedel shears that strike at an average of 17° (Naylor et al., 1986) to the "basement fault". The R shears overlap slightly, and commonly have lengths between 1 and 2 times the overburden thickness. Each fault has a helicoidal geometry, so that the sense of vertical displacement changes across the "basement fault" (figure 1.4).
- (2) Short lived splays develop at or near the tips of the R shears, the strike of which curve towards parallelism with the principal shortening axis, resulting in the extremities of the shears commonly becoming extensional.
- (3) With further displacement, lower angle splays form after the short lived splays become inactive. They form either at the tips of the R shears, or from the inactive splays. Occasionally Antiriedel shears develop at approximately 72° to the "basement fault", but their formation is dependant on a substantial overlap between the adjacent R shears, hence in nature they are rarely developed (Keller et al., 1982).
- (4) The discontinuous R shears are incapable of taking up all the "basement" displacement, thus interconnecting shears are required. These typically occur between two R shears where the direction of the shortening axis becomes reoriented toward the R shear (figure 1.5), resulting in P shears forming at an angle of $-\phi/2$ to the underlying basement fault (Naylor et al., 1986).
- (5) The final fault pattern is that of an anastomosing zone of faults that define shear lenses, with displacement concentrated on the central throughgoing faults (figure 1.6 and plate 1.1).

During the deformation of media with a much greater elastic stiffness, such as limestone, the R and P shears form almost simultaneously (Bartlett et al., 1981). In such rock models the limestone accommodates very little displacement along the R

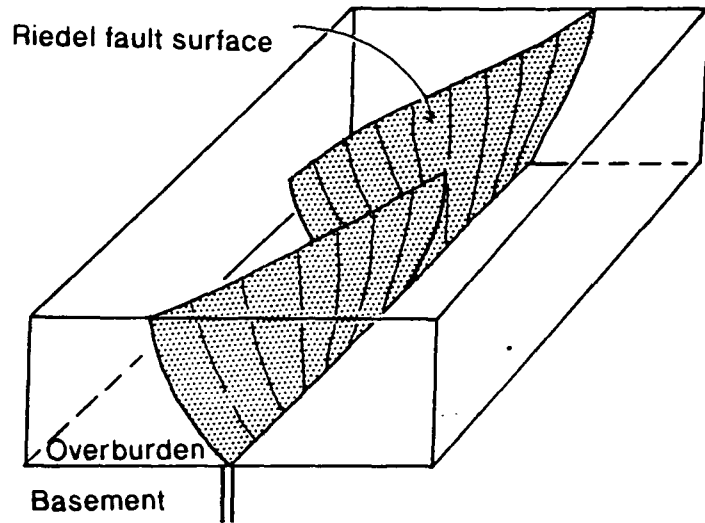


Figure 1.4 Helicoidal geometry of an individual Riedel shear (Re drawn from Naylor et al., 1986)

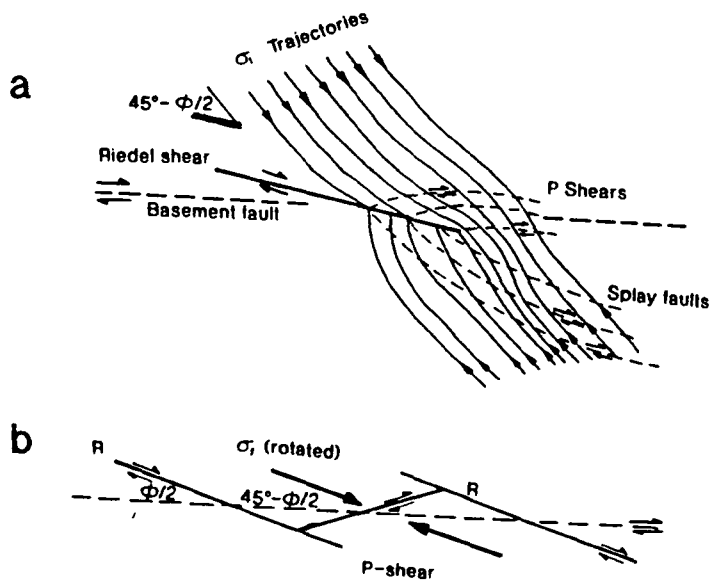


Figure 1.5 A) Stress re-orientation at the compressive and extensional sides of a Riedel shear tip, showing the potential secondary faults. B) Stress re-orientation between two Riedel shears, generating P shears. (Naylor et al., 1986)

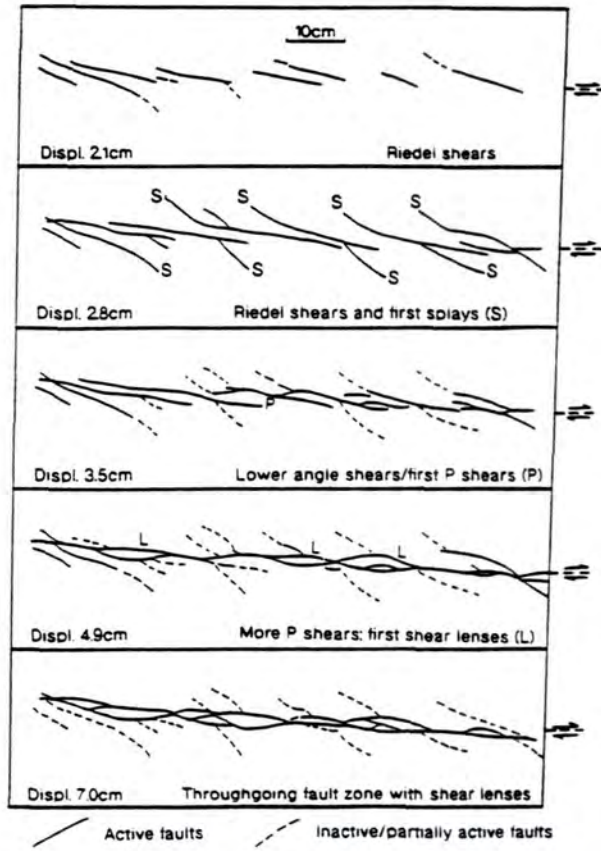


Figure 1.6 The evolution of an experimental strike-slip zone (Naylor et al., 1986)



Plate 1.1 Minor strike-slip fault zone, from Whitley Bay, NE England. Zone displays well developed shear lenses.

shears, therefore, P shears must form to allow continued displacement within the fault zone.

Although there may be slight variations in the chronology of the shear sets for different rock types, their geometric relationships are quite consistent and have been observed from the microscopic scale (Tchalenko, 1970) to the macroscopic scale in earthquake rupture patterns (Tchalenko and Ambraseys, 1970).

Variations in fault zone geometries

The dominance, and indeed the presence of Riedel shears is not a prerequisite in a strike-slip fault system. Gamond (1983) demonstrated experimentally that if the normal stress across the deformation zone is sufficiently low, dilation can exist and P shears will become the locus of slip with continued offset. Moore and Byerlee (1991) have recognised the dominance of P shears along 'creeping' or stable sliding segments of the San Andreas fault, which have been interpreted as being the result of near-lithostatic fluid pressures along these creeping sections (Moore and Byerlee 1991a). These observations have an important bearing on the possible structure of strike-slip regimes with components of shortening or dilation across them, i.e. transpressional or transtensional fault zones, respectively. In transtensional fault zones the normal stress will be low, producing stress conditions favourable for the development of P shears. Transpressional fault zones will have a much greater normal shear stress which may possibly lead to an increased dominance of R shears, (which due to their geometry and kinematics will tend to narrow the fault zone), to the P shears (which have the opposite tendency), resulting in a bulk shortening across the fault zone.

Transpressional and transtensional strains also have theoretical and experimental (Sanderson and Marchini, 1984; and Naylor et al., 1986) effects on the geometry of the secondary fault sets and associated structures (see section 1.2).

Additional secondary fault sets associated with strike-slip fault zones

Strike-slip faults commonly have an offset and/or overlapping geometry producing an echelon arrangement in map view. These stepovers are a fundamental feature along strike-slip faults of varying lengths (Aydin and Nur, 1985). They have been described by several authors in terms of dilational and antidilational jogs (Sibson, 1985), and compressive and tensile bridges (Gamond, 1987), on a larger scale as pull-apart basins (see section 1.1.5.1) and push-ups or pressure ridges (see section 1.1.5.2) at extensional and compressional stepovers, respectively. Where the rupture of these bridges has led to the formation of fault bounded lenses and slabs they are described in terms of duplex nomenclature (Woodcock and Fischer, 1986), see figure 1.7. Unlike their dip-slip counterparts, strike-slip duplexes are commonly not affected by strong anisotropies parallel to the fault orientation, resulting in the braided and apparently disorganised nature of many strike-slip fault zones (ibid.). Where strong vertical anisotropies are found (e.g. mylonitic fabrics at seismogenic depths, or vertical bedding), far more consistent fracture geometries are produced, albeit more complex. Swanson (1988) has recognised several new fracture sets from stepover zones along the Fort Foster Brittle Zone, southern Maine, USA. These extensional and contractional duplexes contain all the fractures previously noted by Logan et al., (1979), plus several extra. The resultant composite fracture pattern is considerably more complex than a simple shear system, but it still maintains its overall asymmetry to the fault zone and sense of shear (figure 1.8). The fractures can be segregated into conjugate sets and related faults that correspond to simple shear, and fault parallel contraction and extension, as follows:

Typical Riedel faults (R and R') are present with associated oblique T₁ fractures, which jointly are related to layer parallel simple shear. A second set of conjugate shears is present, the X-X' set, that together with T₂ extensional fractures, accommodate layer parallel extension (see figure 1.9). Shear fractures similar to the P shears of Logan et al., (1979), form lateral ramp structures between the layer parallel

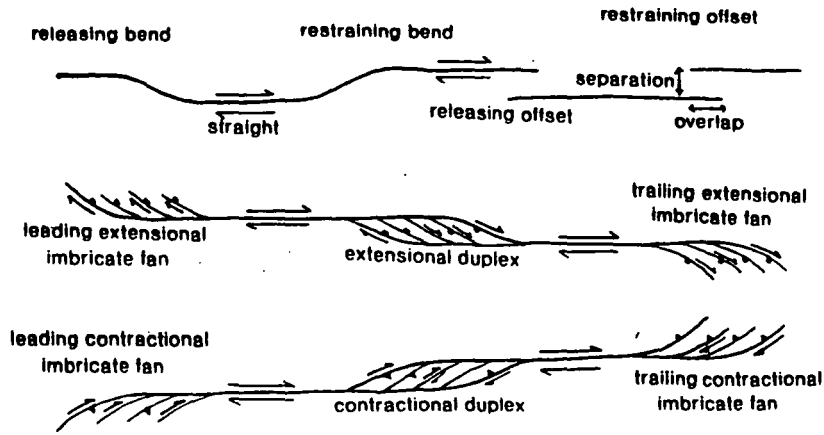


Figure 1.7 Nomenclature related to strike-slip duplexes (from Woodcock and Fischer, 1986)

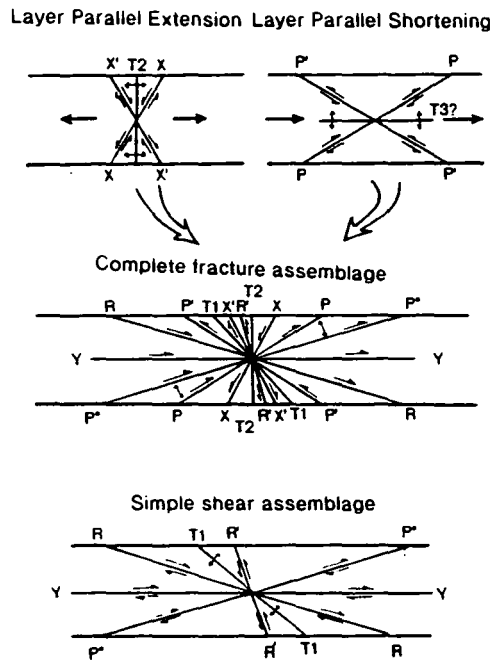


Fig. 1.8

Fig. 1.9

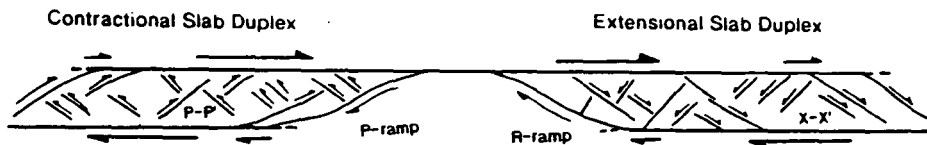


Figure 1.8 Incremental orientations of fracture sets formed in slab duplexes. Fracture sets associated with layer parallel extension, layer parallel shortening, and simple shear are shown. A composite diagram of potential fracture sets features in the centre of the figure.
 Figure 1.9 Idealised fault slab-duplex configurations for contractional and extensional slab-duplexes. (Both figures taken from Swanson, 1988)

faults, and form in two orientations. The third conjugate shear set, the P-P' shears (Tchalenko, 1968) with associated T3 extensional fractures that lie parallel to the layering, are related to layer parallel shortening. A second lower angle P* shear commonly links layer parallel surfaces. Y shears cut through the duplexes forming multiple slab duplexes (Swanson, 1988).

The spatial distribution of the various fracture sets within the slab duplex depends on the overstepping configuration of the main layer parallel shear surfaces. In a dextral system, left-stepping contractional duplexes develop the P-P' fracture sets, with leading or trailing P* or P shear fractures, that together accommodate layer parallel shortening (figure 1.9). Right-stepping extensional duplexes will develop the X-X' shear set and T2 tension fractures, with leading and trailing R and X' shears, that together accommodate layer parallel extension (figure 1.9). Simple shear related R-R' and T1 fractures may also develop in the slab duplex.

Cross-cutting relationships within extensional duplexes suggest that duplex development occurs by alternating sequences of R-R' and X-X' shear fractures. Assuming that the shear fractures are each conjugate Coulomb shear sets, the maximum principal stress directions can be constrained to lie at $\sim 48^\circ$ to the main fault, bisecting the R-R' set, and at $\sim 85^\circ$ bisecting the X-X' (figure 1.10). Changes in the stress orientation, and the observed cross-cutting relationships indicate cyclic stress field variations. Slip along the dominant fault segments and rupture of the linking R shears in response to the pre-failure stress orientations result in localised decoupling of the stepover zone, which effectively eliminates shear stress on the layer parallel segments. This would in turn lead to later adjustments on X-X' shear sets in response to post-failure stress conditions (figure 1.10). Strain hardening effects along the stepover lead to a build up of shear stress, until the cycle begins again (Swanson, 1990).

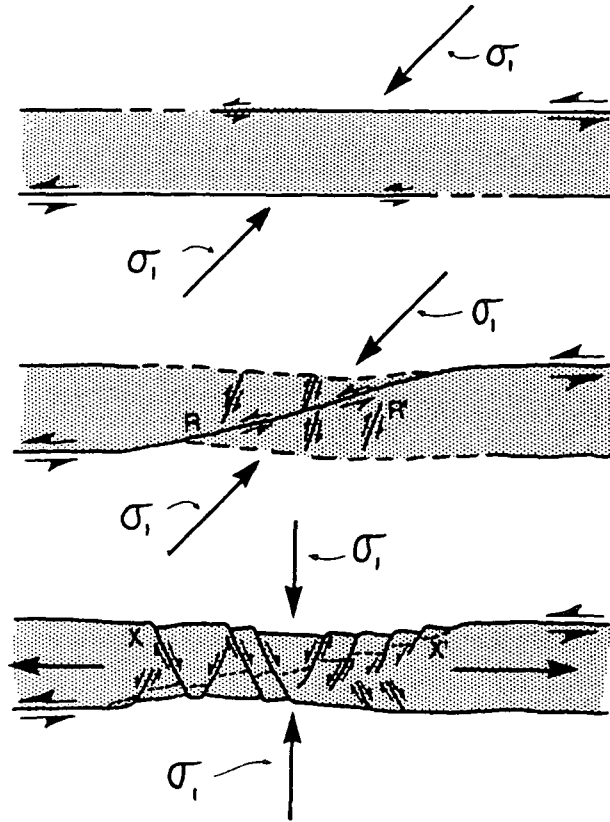


Figure 1.10 Local stress configurations for a left stepping releasing offset between sinistral strike-slip fault segments where principal stress orientations bisect sets of conjugate Coulomb shear fractures: (a) pre-failure stress orientations at offset during slip on weaker layer-parallel segments; (b) failure of intervening competent slab by early R-R' ruptures; and (c) post-failure stress orientations during additional fault parallel extension along late X-X' ruptures. (From Swanson, 1990).

1.1.4 En echelon folding

Typically, en echelon folds are distributed in relatively narrow, persistent zones above or adjacent to the master fault or principal deformation zone. However, they can form in regions of broad deformation between two strike-slip faults, such as occurs in the East Bay Hills of the San Francisco Bay region (Aydin and Page, 1984). The overstepping relationship of the en echelon folds reveal the direction of shear along the adjacent zone of principal displacement; right-stepping folds form in zones of dextral shear, and left-stepping folds form in sinistral shear regimes (figure 1.11).

En echelon folds develop during the initial stages of deformation in clay model experiments, becoming dissected by R shears during further increments of shear, to form half-anticlines and synclines (Wilcox et al., 1973). With increased displacement on the master fault, the early folds become complexly faulted in association with a general widening of the deformation zone and a progressive extension of the en echelon folds away from the master fault (figure 1.12). The largest amplitude folds are found at depth adjacent to the main fault, while the least developed occur at the margins of the deformation zone (Harding, 1976).

In ideal simple shear, the crestral traces of incremental en echelon folds should form an angle of 45° , in plan view, to the fault zone. However, in practice, en echelon folds form lower angles to the fault zone of $10\text{-}35^\circ$ (Harding and Lowell, 1979). This is not unexpected as the first increments of strain will initiate folding at 45° to the fault, with an interlimb angle of 180° . The presence of the folds will not be realised until the bulk strain has tightened the folds, and in doing so will have rotated the fold axis toward the fault. Little (1992) documents a consistent relationship between a clockwise rotation of the strike of the fold axial planes, and fold appression adjacent to the Boarder Ranges Fault system, southwest Alaska. Theoretical curves have been constructed to describe the relationship between fold appression and the orientation of the axial plane strike, for different strain paths (ibid.), i.e. simple shear, transtension, and transpression (figure 1.13). The strain path followed by the folds control the initial orientation of the folds and the rate of subsequent rotation and

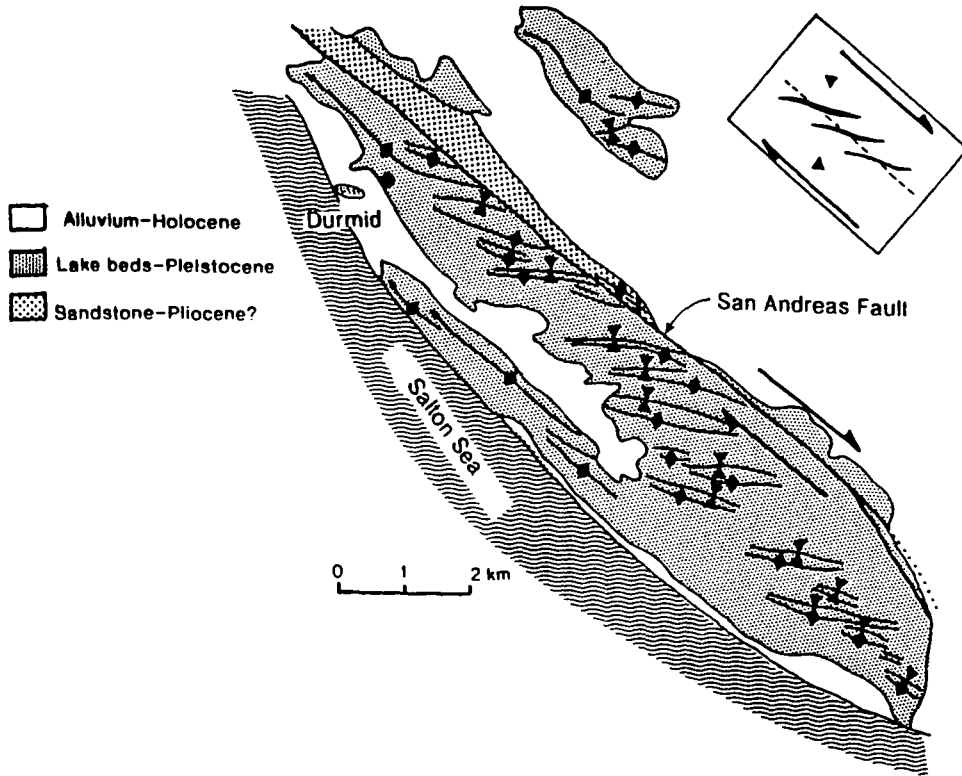


Figure 1.11 Multiple right-stepping en echelon folds in Plio-Pleistocene lake beds along the southern end of the San Andreas fault near the Salton Sea (re drawn from Sylvester, 1988). Box summarises the relationship between fault/folds, for fault movement determination.

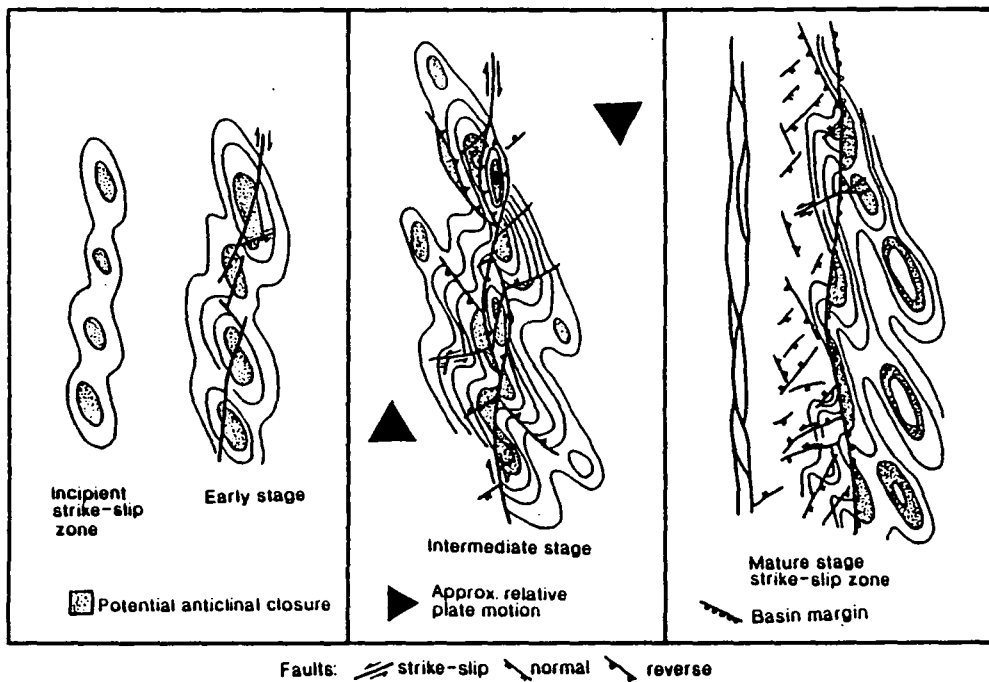


figure 1.12 Schematic diagrams of en echelon fold development, and their relationship to the rest of the structural assemblage (re drawn from Harding and Lowell, 1979)

appression (Sanderson and Marchini, 1984). As can be seen in figure 1.13, a transpressive strain path requires a smaller strain (γ -value) to produce a fold with the same apparent rotation as that formed by simple shear or transtension. In the latter, folds initiate at angles greater than 45° to the fault zone (Sanderson and Marchini, 1984; and Little, 1992). Other variables may effect the fold orientation and the interlimb angle, i.e. heterogeneities, variations in the strain rate, and the rigidity or anisotropy of the multilayers.

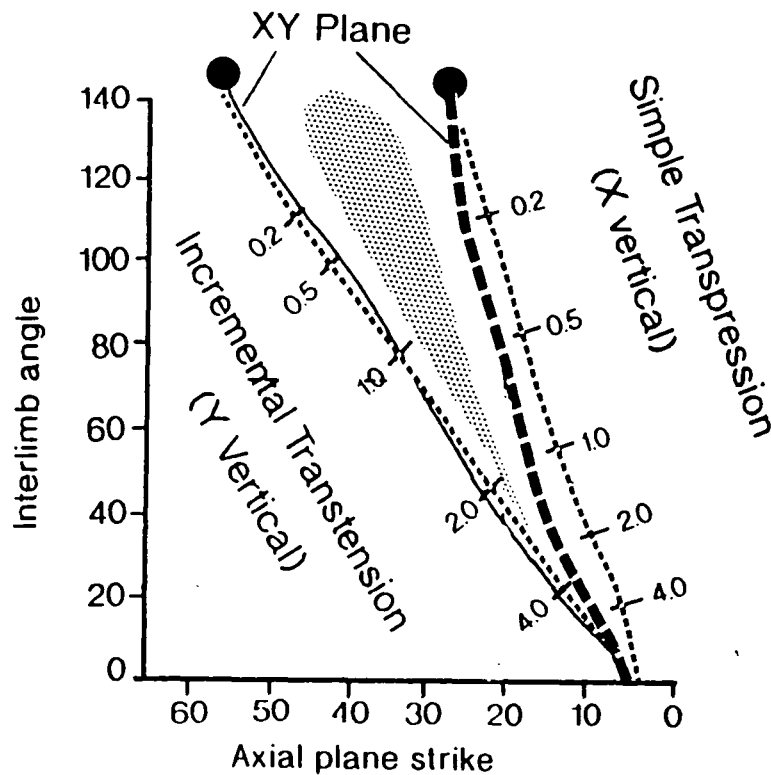


Figure 1.13 Graph displaying the relationship between fold appression, and the strike of the fold axial plane. Theoretical curves representing simple transpressional, and transtensional deformation paths are shown. Stippled area represents a simple shear deformation path. Shear strain (γ) marked along thin dashed lines. (Modified from Little, 1992)

In three dimensions, the axial surfaces of en echelon folds in a sedimentary sequence above a rigid basement fault, are nearly vertical, and parallel to the fault at basement levels. At higher levels the surfaces flatten upward and twist away from the fault strike (Gamond and Odonne, 1984; and Koral, 1983), with the fold axes generally plunging away from the zone of principal displacement (Harding and Tuminas, 1988). These observations imply that the observed angular relationship

between the en echelon fold axis and the master fault may depend on the depth of local erosion, as well as the amount of internal rotation of the shear zone (Sylvester, 1988). Bearing this in mind, alternative evidence is desirable, such as the secondary fault geometries and incremental structures (Little, 1992), to characterise the strain path of en echelon fold arrays developed in such a scenario.

1.1.5 Steppers along strike-slip faults

Steppers are fundamental features along strike-slip faults (Aydin and Nur, 1985), the geometry of which is the most important factor governing localised uplift or subsidence (Sylvester, 1988). If the sense of stepper or fault bend is the same as the sense of fault slip (i.e. right overstep along a dextral fault), crustal extension, subsidence and pull-apart basin (Burchfiel and Stewart, 1966) or rhomb-shaped graben (Freund, 1971) formation occurs. Where the sense of overstep contrasts with the shear sense, crustal shortening occurs with the formations of push-ups (Aydin and Nur, 1985) or pressure ridges (Aydin and Nur, 1982). The following section aims to describe; (1) the basic types of stepper, and their formation; and (2) the geometry of secondary structures associated with these steppers.

1.1.5.1 Pull-aparts and rhomb grabens

Extensional overstepping en echelon faults or releasing bends (Crowell, 1974b) form sites of local extension and basin formation along strike-slip faults. In general, these structures have a rhomboidal geometry, exceptions to which occur during the early stages of basin evolution.

Controls on the shape and geometry of pull-aparts

Numerous field and theoretical studies have been made regarding the shape and geometries of pull-apart basins. The majority of models suggest that the basin width is controlled by the original separation of the en echelon master faults, or the width of the restraining bend, while the length of the basin is related to the amount of displacement along the master fault (Rodgers, 1980; and Mann et al., 1983). The simplest model of basin formation suggests that the dip-slip faults at each end of the

basin were once a single fault prior to extension, therefore the length of the pull-apart basin equals the displacement along the master faults (Crowell, 1974b; Quennell, 1959; and Freund & Garfunkel, 1976). However, mathematical modelling by Mann et al., (1983) predicts that this is a gross simplification of the geometry of a basin initiating with zero fault overlap (see below). Aydin and Nur (1982) suggest that there is a scale independent relationship between the length and width of pull-aparts in map view, forming an approximate aspect ratio of 3:1. For this relationship to be valid, it necessitates an increase in the width of the basin relative to the increase in displacement along the master faults. It is proposed that this is achieved by a coalescence of neighbouring pull-aparts, as they increase in length, or new faults form parallel to existing ones, aiding the accommodation of large displacements. However, the observed aspect ratio of a pull-apart may vary widely, depending on whether the structural, physiographic or active dimensions are measured (Sylvester, 1988). Although the process of basin capture does occur, (e.g. the coalescence of small adjacent pull-aparts may occur along releasing bends with large widths during the early stages of evolution), the aspect ratio of the main basin is still controlled by the initial bend width and total displacement (Mann et al., 1983).

Evolution and structural patterns of pull-apart basins.

The structural and sedimentary evolution of pull-apart basins has been modelled for various fault configurations. Mann et al., (1983) has produced a generalised *continuum* model for the formation of basins that nucleate at releasing bends along fault segments. In this model the initial opening produces "spindle shaped" basins defined by oblique transverse faults (Ben-Avraham and Garfunkel, 1986) that connect the ends of the master faults (figure 1.14b). Along releasing bends with large widths or master fault separation, several pull-aparts may nucleate across the bend. Increased displacement along the master faults produces pull-aparts with 'lazy-S' shapes at sinistral releasing bends, and 'lazy-Z' shaped basins at dextral bends (figure 1.14c), at this stage, deep topographic depressions form. Again, for larger bend separations the extension can be achieved by two or more smaller pull-aparts that relay extension

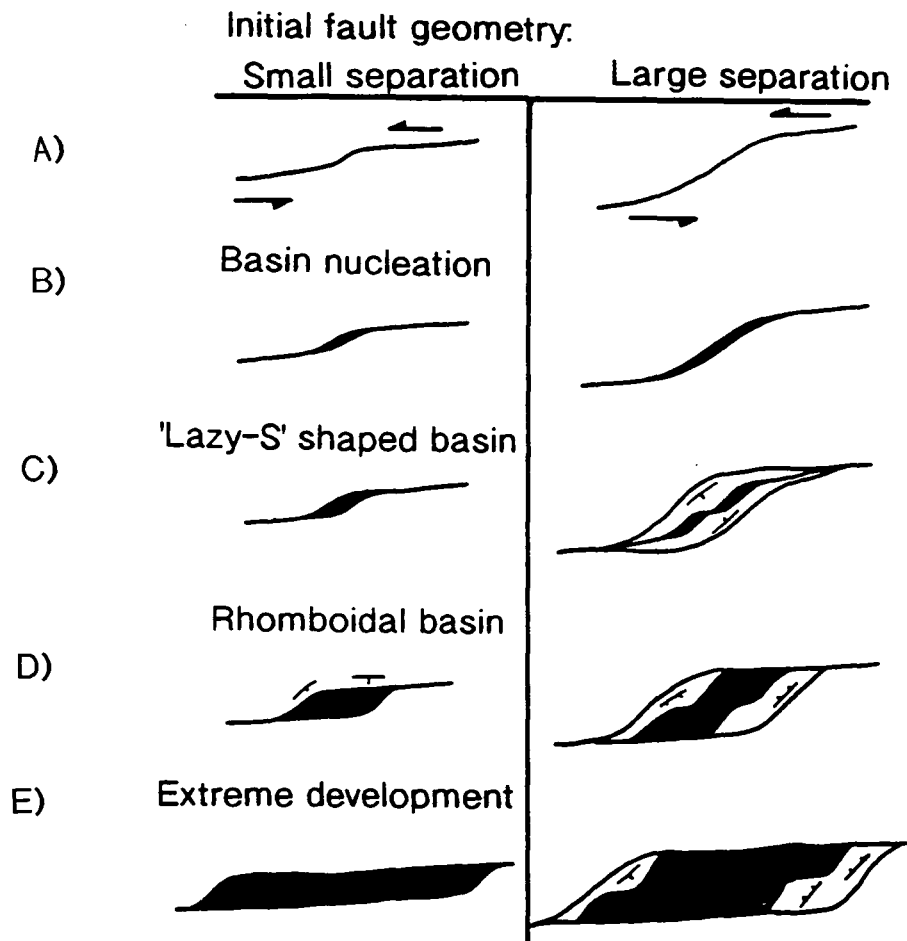


Figure 1.14 *Continuum model* for pull-apart basin development. (a) Pull-aparts nucleate at releasing fault bends along faults which are oblique to the direction of relative plate motion. (b) Spindle-shaped pull-aparts nucleate on releasing bends. (c) Continued offset produces "lazy S" basin geometries ("lazy Z" in a dextral system); extension across bends with a large separation may be relayed by two or more buried pull-aparts. (d) Continued offset of lazy S-shaped basins produces rhomb-shaped grabens; buried pull-aparts within bends with large fault separations may coalesce. (e) With steady offset rhomb-shaped grabens can develop in to long narrow troughs, within which at some point, short spreading ridges and oceanic crust will initiate. (From Mann et al., 1983)

across the basin. Continued strike-slip offset along the master faults results in the lengthening of the 'lazy-S or Z' basins, forming rhomb-shaped grabens (figure 1.14d). As the width of the basins are fixed by the initial bend width, continued displacement results in an increase in the aspect ratio, which can occur to extremes, (figure 1.14e) e.g. the Cayman trough, which has a fault overlap of 1400km, and a fault separation of 100-150km producing an aspect ratio of 10. The general aspect ratio of less than 4 (Aydin and Nur, 1982), probably reflects the tendency of pull-aparts to become deformed by the rapidly changing conditions common to strike-slip environments (Mann et al., 1983).

Mathematical modelling of pull-apart basins formed between overstepping en echelon faults by Rodgers (1980), and Segall & Pollard (1980), has allowed the displacements, stresses, and strains for fault configurations with varying degrees of fault overlap and separation, to be calculated. These models indicate that the basin depth and shape is directly related to these two parameters. In en echelon fault configurations where the overlap is between zero, and equal to the separation of the master faults, a basin forms that possesses a single deep-elongate depositional centre, the axis of which forms a line joining the ends of the master faults (figure 1.15). In models where the fault overlap is greater than the fault separation, two depositional centres form adjacent to the extensional tips of the master faults, the maximum depth of which is less than basins where the overlap is less than, or equal to the separation, given the same amount of displacement along the master faults (figure 1.15). These models also predict that uplift occurs at the outer-compressional tips of the master faults, the spatial extent of which is also related to the master fault configuration.

The pattern of predicted secondary fault formation is also intimately related to the master fault configurations, producing a complex distribution of faults for the various en echelon fault arrangements. When the master fault overlap is less than or equal to the fault separation, normal faulting occurs at the centre of the developing basin, and synthetic strike-slip faults form the basin bounding transverse faults (figure 1.16a & b). Where the overlap of the master faults is greater than the fault

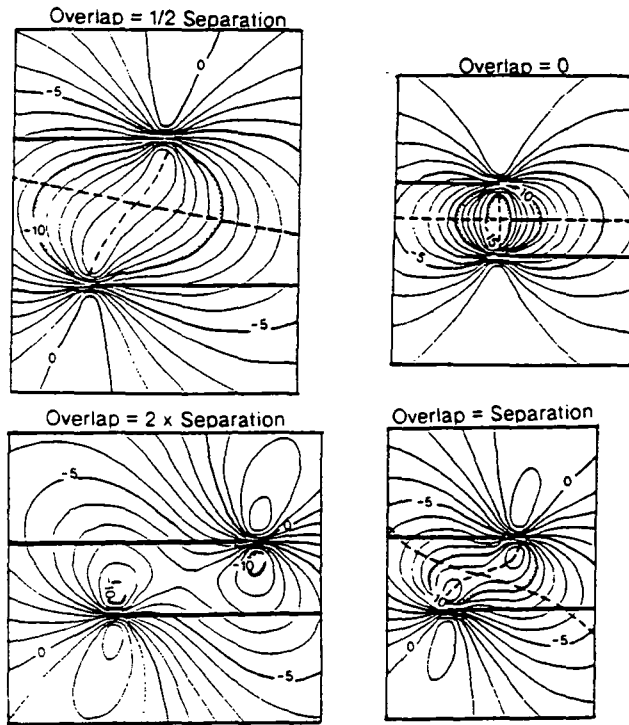


Figure 1.15 The vertical displacement in cm of the ground surface, associated with extensional stepovers along en echelon strike-slip faults (from Rodgers 1980). In the upper pair of diagrams fault overlap is less than or equal to the separation. In the lower pair, fault overlap is greater than the separation.

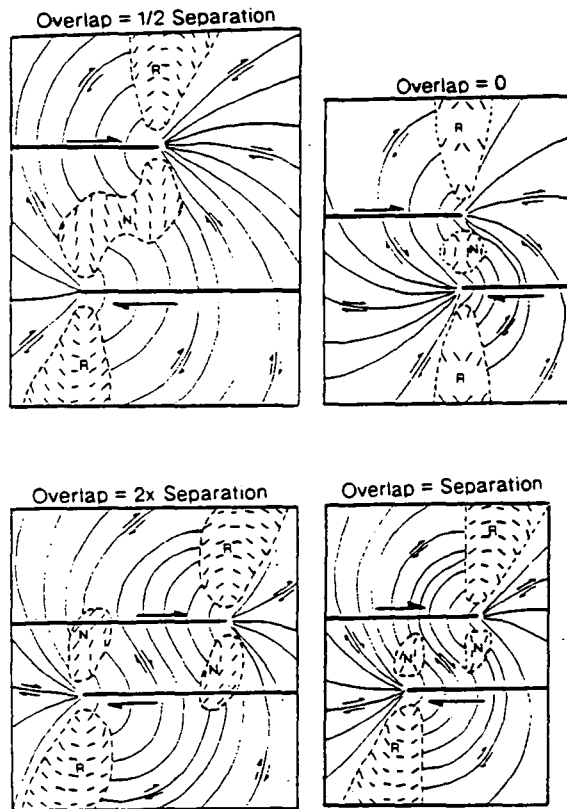


Figure 1.16 Potential fault pattern related to various en echelon fault configurations (from Rodgers, 1980). In the upper pair of diagrams fault overlap is less than or equal to the separation. In the lower pair, fault overlap is greater than the separation. N denotes normal faults, R denotes reverse faults. Single lines represent potential sinistral fault orientations.

separation, normal faults form two distinct zones near the ends of the basin, with strike-slip faults forming in the centre of the basin (figure 1.16c & d). As can be seen from figures 1.16a to d, the normal faults start out on the basin side of the master faults as strike-slip faults, that transform into normal faults as they are followed into the basin. This suggests that oblique-slip faulting occurs at the internal ends of the en echelon master faults.

The predictions of the secondary fault distributions and kinematics have important implications for the development of pull-aparts. If it is assumed that during the accumulation of displacement, the master faults propagate along strike, the predicted basin geometries and fault patterns, as seen in figures 1.15 and 1.16, can be used to predict the structural implications of the development of this hypothetical pull-apart basin.

If the faults start with a zero overlap, normal faulting will occur in the centre, with strike-slip faults forming at the ends of the basin. As the master faults propagate to an overlap of $\frac{1}{2}$ the fault separation the systems remain the same, except that the zone of normal faulting becomes enlarged. When the fault overlap becomes equal to the separation, the kinematics and geometry of the basin begin to change. Two distinct depocentres begin to form near the ends of the master faults with strike-slip faulting occurring in the centre. Assuming the orientations of the initial secondary faults have remained similar to their initiation positions, they represent a pre-existing fabric. The stress associated with the new overlapping fault configuration will act on this existing structural fabric, probably resulting in its reactivation, even though the stress system may be quite different, therefore, some of the faults must change from strike-slip to normal, and vice-versa (figure 1.17).

This model suggests an extremely complex kinematic history for the basement fault patterns, with changes in the sense of shear on many of the faults. Such complex changes in the kinematics of transverse faults has been described at the northern end of the southern basin of the Dead Sea graben (Ben-Avraham et al., 1990), where

Miocene - Early Pleistocene normal faulting has been replaced by Late Pleistocene - Recent strike-slip.

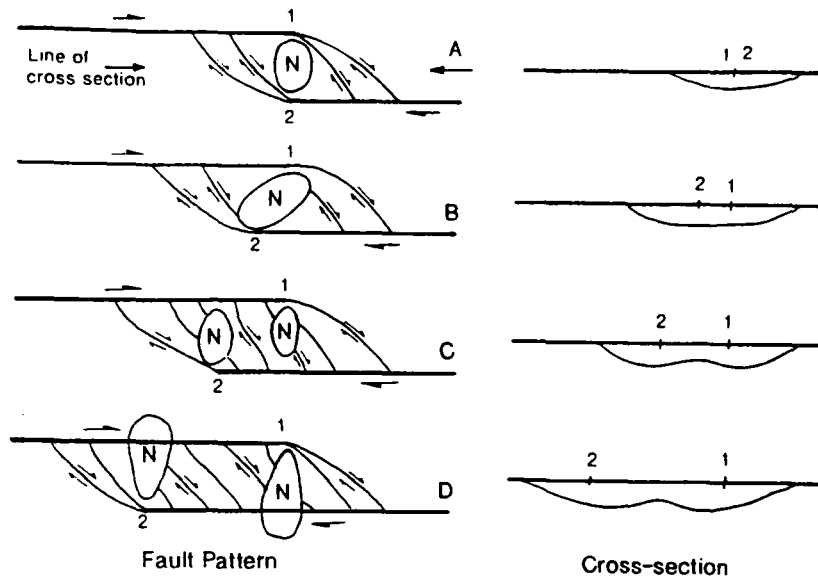


Figure 1.17 Sketch of possible pull-apart basin evolution based on figures 1.15 and 1.16. Numbers refer to locations of the ends of the master faults. Zones labelled 'N' are zones of normal faulting.

Floors to pull-apart basins

Pull-apart basins can be divided into two groups with regard to their style of floor. One group form true rifts that extend at depth to the hot rocks of the upper mantle, similar to those found above an oceanic spreading ridge. These basins are formed by attenuation of the upper crust during extension, which is followed by the forceful upwelling of hot mantle material. These basins lack true basement, however, the lower sediments do lie above a volcanic sill and dyke complex, but this is seen to intrude the older sediments. The Salton Sea basin is an example of such a basement. (Kerr & Kidwell, 1991)

The second group of pull-aparts are those who floor along a detachment or décollement surface. This style of basin can be further divided into two subgroups: 1) Those that detach against flat lying tectonic surfaces, and 2) those that bottom out unconformably along older basement, or large rheological contrasts within a sedimentary sequence. Seismic profiling and other geophysical observations, show that

much of southern California is underlain by sub horizontal tectonic surfaces (Cheadle et al., 1986). These surfaces may possibly represent the decollements on which crustal blocks may pull-apart, or rotate. (J.C. Crowell, unpub. data). The Vienna basin (Royden, 1985), and of particular relevance to the thesis, the Dead Sea basin (Manspeizer, 1985) terminate on detachments at shallow crustal levels. Seismic profiles across the Amaziahu fault, a major transverse fault in the Dead Sea basin, show the fault has a spectacular listric geometry (ten Brink and Ben-Avraham, 1989). The fault surface bends abruptly as it intersects an extensive evaporite layer, which effectively decouples the formation of the pull-apart basin in the overlying sedimentary fill, from the deformation occurring in the underlying basement (figure 1.18).

Sedimentation related to pull-apart basins

Many basins are typified by high sedimentation rates, rapid facies changes, abrupt thickening of sedimentary sequences over short distances, numerous unconformities which reflect syntectonic sedimentation, and the presence of locally derived, skewed fan-bodies of fault margin breccia facies representing talus detritus or alluvial fans (Crowell, 1974a, 1974b; Mitchell and Reading, 1978; Hempton et al., 1983; Dunne and Hempton, 1984; Nilsen and McLaughlin, 1985).

The most distinctive stratigraphic feature of pull-apart basins is the extreme thickness of onlapping sedimentary sequences relative to their area. This occurs due to the migration of the depocentre by means of syndepositional strike-slip faulting (Crowell 1974b, 1982a). The centre of deposition migrates in the direction opposite to that of strike-slip movement of the basin, so that as the basin lengthens over time, sediments are deposited in an overlapping "venetian blind" arrangement (Crowell, 1982a, 1982b; Hempton and Dunne, 1984). The Hornelen Basin of western Norway has an areal extent of less than 1,250 km², but it has a stratigraphic thickness approaching 25km in a basin 60-70km long, by 15-25km wide. The true maximum vertical thickness of the succession at any one point, is probably less than 8km (Steel and Gloppen, 1980).

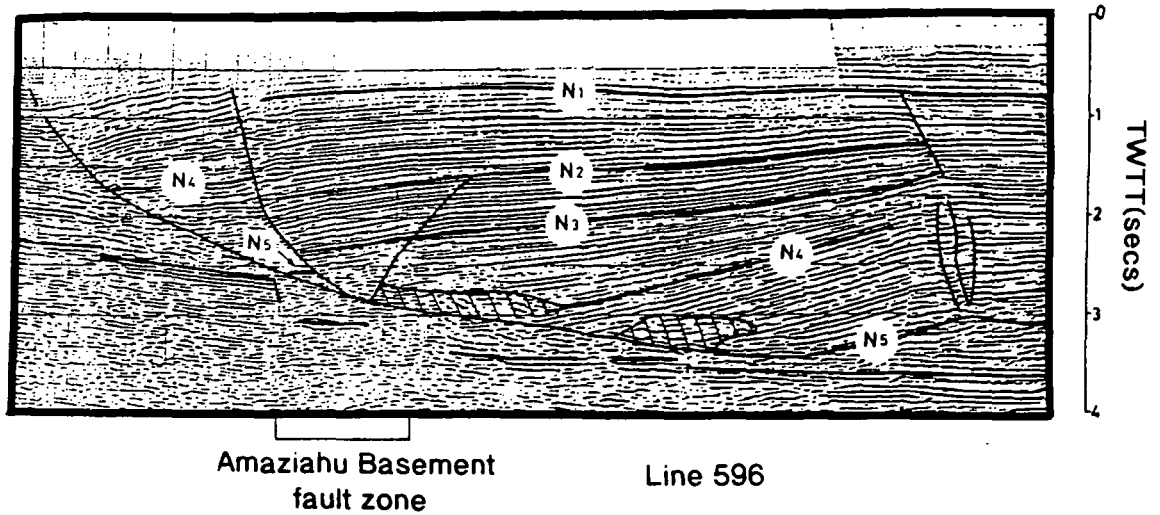


Figure 1.18 Interpreted migrated seismic sections across the Amaziaha fault, displaying its spectacular listric nature. Sub-horizontal segment of the fault runs along a Pliocene evaporite horizon. The hatched areas probably represent salt pockets. (Taken from ten Brink and Ben-Avraham, 1989).

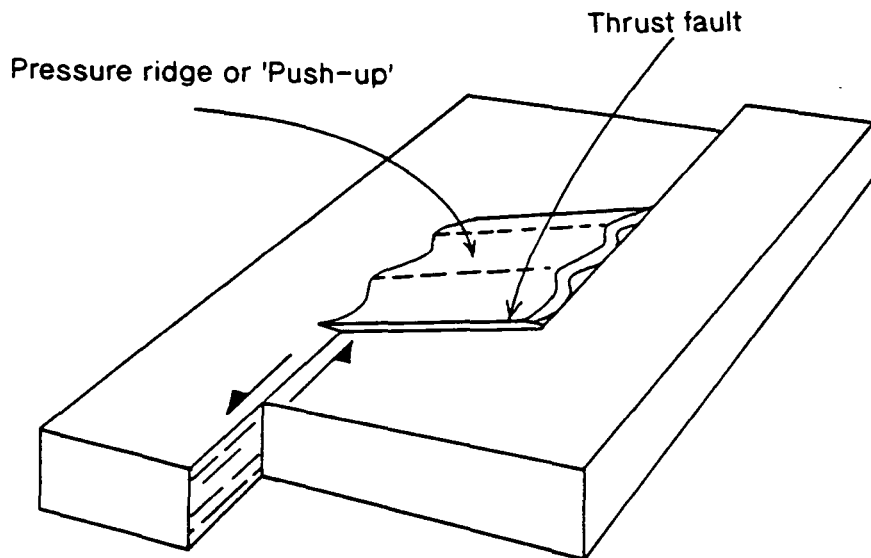


Figure 1.19 Schematic diagram of a compressional overstep between en echelon strike-slip faults, forming a pressure ridge, or push-up. (Adapted from Ramsay and Huber, 1987)

1.1.5.2 Pressure ridges, push-ups and restraining bends

Where the sense of shear and overstep along a strike-slip fault differ, a localised area of compression exists, resulting in significant uplift (Aydin and Page, 1984). Due to the reduced hydrocarbon potential of compressional oversteps, detailed experimental and field descriptions of their structure and kinematics is sparse in comparison to their extensional counterparts. The compression within these stepovers may be accommodated by pressure solution surfaces and cleavages (Moore, 1963; and Segall & Pollard, 1980) or folds, thrust faults, and possibly secondary strike-slip faults (Sharp & Clark, 1972; and Aydin & Page, 1984), see figure 1.19. As with extensional overstepping en echelon faults, the orientation at the time of initiation of these secondary structures is strongly influenced by the geometry of the en echelon master faults, i.e. overlap, separation, and length. Considering the stress orientations present in a compressional overstep with a fault overlap equal to the fault separation (Segall and Pollard, 1980), and assuming the contractional structures will form perpendicular to the maximum compressive stress, the average angle of folds and reverse faults at initiation is approximately 65° to 75° to the strike-slip master faults (Aydin and Page, 1984). In order to accommodate the shortening within the compressed stepover, the reverse faults should dip toward the compressed domain. In addition, reverse faulting and / or folding may occur parallel to the overlapping segments of the master faults (ibid.). In general, the orientation of secondary structures within a compressed overstep will be approximately 90° from those developed within extensional oversteps along the same fault zone (Aydin and Nur, 1985).

Restraining bends along strike-slip faults result in compression and uplift. The style of deformation, however, is very different from that associated with en echelon oversteps. As mentioned above, the orientation of secondary structures formed at pressure ridges is dependent on the state of stress at the fault tips, whereas, deformation at a restraining bend predominantly results from convergent strike-slip or transpression. The strain associated with these transpressional restraining bends is commonly manifest as flower structures, e.g. the Mecca Hills, southern California

(Sylvester and Smith, 1976). These structures will be discussed more thoroughly in section 1.2.3.

1.1.6 Tectonic rotations in strike-slip environments

The governing constraints on distributed deformation within a strike-slip environment are kinematic: the fault bounded blocks must remain in contact with each other and the deformation must fit its surroundings. As a result, blocks moving laterally without significant internal deformation will rotate about a vertical axis (Garfunkel and Ron, 1985). This combination of strike-slip faulting and block rotation provides an efficient mechanism of deformation compared with other types of coeval deformation, as modest offsets and rotations change the linear dimensions of faulted areas by several tens of percents (*ibid.*).

Tectonic block rotation about a vertical axis has recently been recognised as a common, if not essential, manifestation of large scale shearing of the brittle crust. This phenomenon was suspected or postulated to occur along the American Pacific coast and Dead Sea region by many authors during the middle 1960's to 1970's. Jones et al., (1976) noted a 90° contrast between the structural grain of the Catalina and Santa Cruz islands of off-shore southern California, compared with the Sierra Nevada foothills. Although the authors speculated that tectonic rotation was responsible, no sense of rotation was specified. Inspired by these early indications of block rotations Luyendyk et al., (1980, 1985) applied paleomagnetic techniques on Neogene volcanic rocks in the western Transverse Ranges in an attempt to determine the amount and sense of rotation. The results of these studies confirmed the clockwise rotation inferred by Hamilton and Myers (1966), but more importantly it determined the dimensions of the domains of rotation. Luyendyk et al., (1980) proposed a geometric model, albeit a parochial one, to describe these rotations, the essentials of which are: (1) that the blocks are defined by antithetic cross faults between a zone of dextral shear, that slipped simultaneously with the block rotation, (2) the amount of slip on the antithetic faults is related to the width and amount of rotation of the block (or vice-

versa), (3) the rotation causes the assemblage of blocks to extend within the shear couple resulting in compression at their ends. This compression is manifest as folds, thrust / reverse faulting and crush zones, (4) triangular or deltoid basins open at the junction of the rotated and unrotated blocks. Garfunkel and Ron (1985) concur with the initial two points of the Luyendyk et al., (1980) geometric model.

McKenzie and Jackson (1983) modelled tectonic rotations using a velocity gradient model, deriving an instantaneous rotation rate equal to $\omega/2$ for small blocks 'floating' in the deformation zone, where ω is the vorticity of the ductile substrate. In such a model the continuous, ductile deformation at the middle and lower crustal levels controls the displacement rate, strike, and finite rotation of the brittle faults. Lamb (1987) modelled tectonic block rotation about vertical axes as isolated rigid ellipses within a highly viscous fluid, assuming a constant relative motion vector across the deforming zone. The model has some major differences to a zone of distributed deformation in the upper crust as: (1) continental crust is not a highly viscous fluid, (2) the rigid blocks are not elliptical, and may not maintain the same shape, and (3) rigid blocks are not in isolation, but are in contact with neighbouring blocks / inclusions. However, continental crust may approximate to a viscous fluid containing rigid blocks if the block size is much smaller than the overall zone of deformation, and the motion of the blocks is mainly driven by shear stresses at their base, as suggested by McKenzie and Jackson (1983). This modelling shows that the rate of rotation varies with time and is dependent on: the instantaneous orientation of the block, the aspect ratio of the block dimensions, and the relative plate motion vector. A constant rate of rotation is found only for near circular blocks, with a rate equal to $\omega/2$. Nelson and Jones (1987), use this model to describe the deformation style within the Las Vegas Valley Shear Zone (LVVSZ), where the amount of rotation, derived from paleomagnetic studies, displays a smooth increase toward the LVVSZ. This indicates that deformation is occurring via many small-rigid blocks, relative to the width of the deformation zone, unlike the large blocks modelled by Luyendyk et al., 1980; and Ron et al., 1984.

Where elongate blocks are "pinned" or mechanically connected to the edges of the zones, the rotation rate of the blocks is equal to the velocity gradient across the zone i.e. equal to ω , which is twice the rate of blocks driven mainly by viscous forces at the bottom of the blocks (McKenzie and Jackson, 1986). This "pinned block" model, raises a number of important points with regards to the kinematic and tectonic environment expected in zones of block rotation. The model predicts that for deformation to become distributed across a zone and not concentrated along a single strike-slip fault, there must be a component of shortening or extension across the deformation zone, i.e. transpression or transtension. Slip along the block bounding cross faults is predicted to be oblique, displaying antithetic strike-slip, relative to the main faults, and a dip-slip component of motion, synthetic to that occurring across the deformation zone. Therefore, the cross faults may display antithetic transpressive or transtensive strain, depending on the type of stress applied across the main deformation zone. The analogue model does not allow finite rotations of the blocks to occur due to their totally rigid nature, but rotation can be accommodated by internal deformation between the blocks and the rigid plates on either side of the deformation zone (figure 1.20).

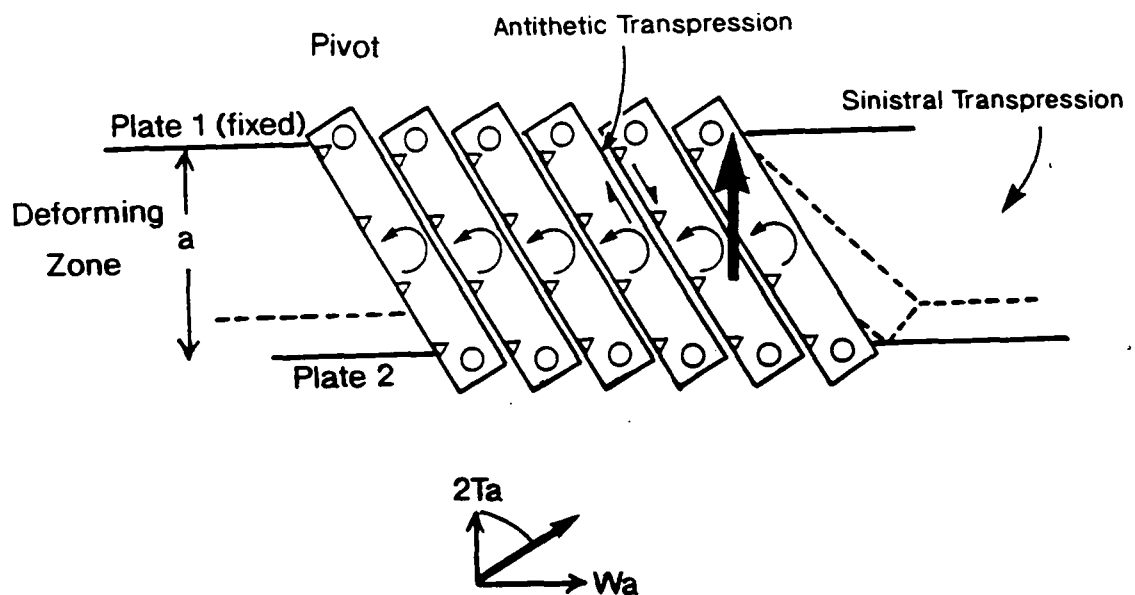


Figure 1.20 'Pinned' block model for block rotations about a vertical axis (modified from McKenzie and Jackson, 1986). The model has been re drawn to display block rotations induced by a transpressional regime. W_a - Component of oblique motion parallel to the deformation zone, $2T_a$ component normal to zone, $2T$ rate of crustal thickening. Large black arrow is the slip vector between the adjacent blocks. Dashed lines represent position of zone margins and blocks after displacement and rotation.

Variations in the relative motion vectors between two plates can have fundamental effects on the deformation style of strike-slip systems. Studies of the Neogene block rotations within the Transverse Ranges of California, where significant changes in the relative plate motion vectors occurred, have important implications for block rotations (Luyendyk, 1991). During the Middle Miocene, a transtensional regime existed along the deformation zone, this resulted in the rotating blocks rapidly becoming disconnected from the zone boundaries. As the zone widened the blocks effectively "floated" within the deformation zone being driven by the viscous forces along their bases, hence they possessed a rotation rate of $\omega/2$ (McKenzie and Jackson, 1983, 1986). In the Pliocene, the relative plate motion vector changed, inducing transpression along the deformation zone. The resulting component of shortening reconnected the blocks to the zone boundaries, effectively "pinning" the blocks, therefore increasing the rotation rate equal to ω (McKenzie and Jackson, 1986). As well as these fundamental changes in the control on block rotation rates, transtensional deformation zones develop elongate sedimentary basins parallel to both the zone boundaries and the antithetic transtensive cross faults (Luyendyk, 1991).

A consequence of block rotation is the space problems that occur between the ends of rotating blocks and the deformation zone boundaries. Regions of shortening and dilation form at opposite corners of rotating blocks due to the block edges impinging and "pulling-away", respectively from the zone boundaries. Where the rotating block "pulls-away" from the unrotated zone boundary, deep-triangular or deltoid transrotational basins form (Luyendyk et al., 1980 and Luyendyk, 1991). However, basins need not form at all extensional joints between rotated and unrotated blocks. In Southwest Japan, plutonic intrusions have occupied these triangular gaps adjacent to the Median Tectonic Line (Kanaori, 1990). Freund (1974) has shown how these spaces may also be accommodated by splay faulting, indeed Horns (1991) observed pervasive extensional normal faulting at the location of an extensional block corner, at Pt. Año Nuevo, along the San Gregorio fault zone, California. The adjacent compressional block corner is characterised by numerous reverse faults, due to the

impingement of the block against the fault zone boundary. Thrusting, folding and crush zones may also accommodate shortening at these compressional block corners (Luyendyk et al., 1980).

A further consequence of block rotations, is the requirement for the block bounding cross-faults to rotate. Based on simple mechanical considerations the amount of fault rotation permissible under a stationary stress field is limited to between 20° and 45° . Consequently, block rotations larger than 40° to 45° require more than one set of faults to accommodate the rotation (Nur et al., 1986).

Rotating blocks possess a variety of aspect ratios, but their scale in the vertical dimension is rarely seen. Intuition suggests that these blocks must detach on some decollement surface in order to facilitate the rotation, therefore, rotating crustal blocks must be flakes (Oxburgh, 1972), slabs, or crustal panels (Dickinson, 1983). In a homogeneous brittle crust it would be expected that the decollement horizon would locate along the brittle-ductile transition. The slab geometries of crustal blocks form due to weak horizons or variations in the underlying lithologies (Brown, 1928), or changes in pore fluid pressures which cause modifications in the applied shear stress on the sides of the block, which produces a torque and eventually leads to block break-up (Horns, 1991). Terres and Sylvester (1981) observed elongate blocks of soil, originally defined by plow-cuts, rotated between 20° and 40° , forming deltoid 'basins' and slipping along anithetic cross faults, as a result of dextral shear during the 1979 Imperial earthquake. The rotation had detached at a mechanical anisotropy 15cm below the surface: the dry-soil / wetted-soil interface. A similar mechanical analogy was observed by Wilson (1960), where large slabs of ice rotated in a simple shear zone between the Filchner Ice shelf and the Antarctic mainland. Horns (1991) suggests from seismic reflection data, and observed exposures, that the shallow-dipping faults of flower structures may act as decollements for rotating blocks along the San Gregorio fault zone. In a similar style much of the Transverse Ranges is detached on deep, blind, northward dipping thrust faults (Webb and Kanamori, 1985).

Many authors suggest that rotating blocks will have a thickness : width ratio of 1:1 (ibid.), however, this relationship is probably fortuitous, as it appears to be the rheological variations within the crust, either stratigraphic or structural, that controls the vertical dimensions of the blocks

1.2 Transpressional tectonics

1.2.1. Introduction

Transpression is a term that has become increasingly widely used within the published literature. However, as with its extensional counterpart transtension, it is often abused in reference to the tectonic setting being described. The term, therefore, requires defining in order to prevent any misconceptions in its use within this text.

Harland (1971) defined transpression in terms of stress, as those regimes which "operate in zones with oblique compression", this definition unfortunately infers an association with oblique collision processes due to its application to the Caledonian of Spitsbergen, which is clearly not the exclusive tectonic setting of transpression zones. Sanderson and Marchini (1984) redefined transpression as "*.....a wrench or transcurrent shear accompanied by horizontal shortening across, and vertical lengthening along, the shear plane*". This definition is non specific to any one tectonic setting, and provides a basic description of the gross finite strain state within a transpressional environment. The complexity of the strain within natural examples of transpression zones makes the evaluation of the principal stress direction extremely difficult, therefore the finite strain concept is far easier to elucidate. For these reasons, the author will use transpression as defined by Sanderson and Marchini in the ensuing chapters.

More succinct definitions such as "convergent strike-slip" (Sylvester, 1988), allows transpression to be invoked wherever zones of uplift or shortening occur as a result of strike-slip deformation, e.g. pressure ridges or push-ups developed between

overstepping en echelon faults (Erdlac, 1990). As discussed in section 1.1.5, pressure ridges and pull-apart basins formed between such en echelon fault configurations, are the result of fault tip stress interactions, and not due to a component of shortening *across* a strike-slip fault, therefore, transpression should be reserved for continuous fault planes displaying a component of shortening. Where stepovers are achieved by restraining bends, transpression may be used, as the fault segment is subject to strike-slip plus a component of shortening, fulfilling the required strain state. These localised structures are referred to as secondary transpressive structures (Harland, 1971).

1.2.2 Modelling of transpressive strains

Sanderson and Marchini (1984) produced a general model for transpression by factorizing the deformation into its pure and simple shear components. The assumptions made were that the deformation occurs in isotropic rock and that no volume change or lateral extrusion occurs along the zone, therefore, shortening across the zone must result in vertical thickening to conserve volume. Figure 1.21 defines the factorisation and the parameters used in this model; α^{-1} specifies the shortening across the zone, or more specifically the ratio of the deformed to original width of the zone; α the vertical stretch; and γ the shear strain parallel to the zone.

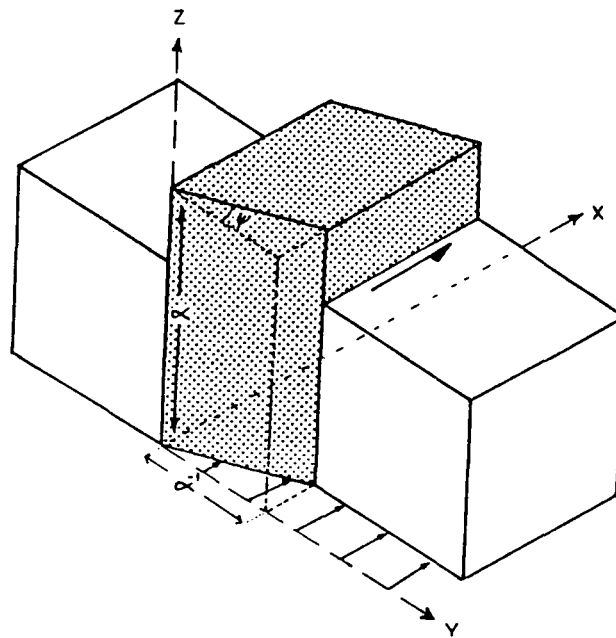


Figure 1.21 Transpression geometry, showing deformation of a unit cube by shortening parallel to Y-axis and shear parallel to X-axis. Volume is conserved by lengthening parallel to Z-axis (vertical). from Sanderson & Marchini, 1984.

Finite transpressional strain

This factorisation process (equation 1, *ibid.*) enables the strain to be defined in terms of two factors α and γ . By assigning different values to the parameters α^{-1} and γ the finite strain can be evaluated for varying amounts of shortening and shear strain (figure 1.22). Obviously, as seen in figure 1.22, the shape of the strain ellipsoid varies with α^{-1} : when $\alpha^{-1} < 1$, k -values less than 1 are produced; an $\alpha^{-1} = 1$, results in k -values equal to 1; and when $\alpha^{-1} > 1$, k -values greater than 1 result. Although figure 1.22 gives the shape of the finite strain ellipse, it does not show the variations in the orientation of the principal strain axis, one of which is always vertical. For simple shear ($\alpha^{-1} = 1$) the Y axis is vertical, for $\alpha^{-1} < 1$ the vertical axis maybe X or Y, therefore the XY plane is always vertical, but at an angle of θ' to the deformation zone boundary (see figure 1.23). Where $\alpha^{-1} > 1$, either Z or Y may be vertical, therefore the XY cleavage plane converts from vertical to horizontal. Observations of figures 1.22 and 1.23 reveal an important concept, that of lineation switching. In figure 1.22, the X-axis switches from vertical to horizontal with increasing shear strain (γ) where the solid lines 'bounce' off the b-axis of the graph, within the oblate field of the Flinn plot. This relationship is also seen in figure 1.23. However, it is important not to assume that these lines are deformation paths, as a multitude of superimposed deformation paths can combine to produce any given finite strain, hence the progressive formation of structures within the deformation zone will depend on the actual deformation path followed. In order to fully understand transpressional kinematics further assumptions about the deformation must be made.

Incremental transpressional strain

Constant incremental strain - By letting $\gamma \rightarrow 0$ and $\alpha^{-1} \rightarrow 1$ the incremental strain can be approximated, allowing the deformation path resulting from a constant incremental strain to be modelled (see Sanderson & Marchini, 1984). This allows plots of constant incremental deformation paths to be plotted (figure 1.24). As with the finite models presented above, the swapping of the principal strain axes can occur along paths of

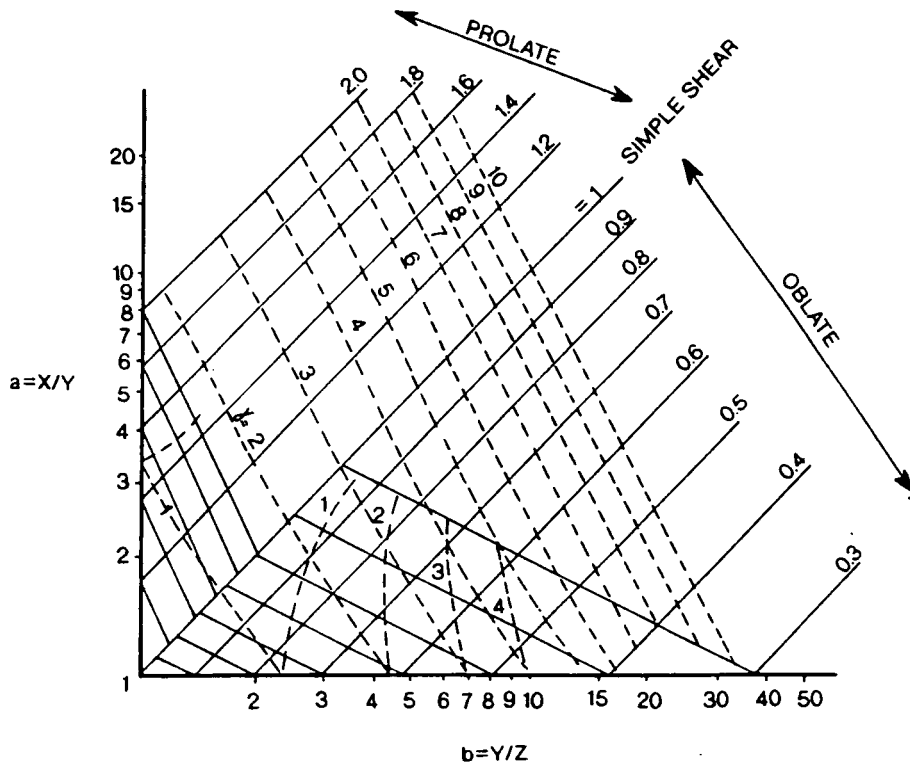


Figure 1.22 Flinn diagram showing axial ratios $a=X/Y$ and $b=Y/Z$ produced by transpressional model for various values of α^{-1} (continuous lines) and γ (dashed lines). (Sanderson & Marchini, 1984)

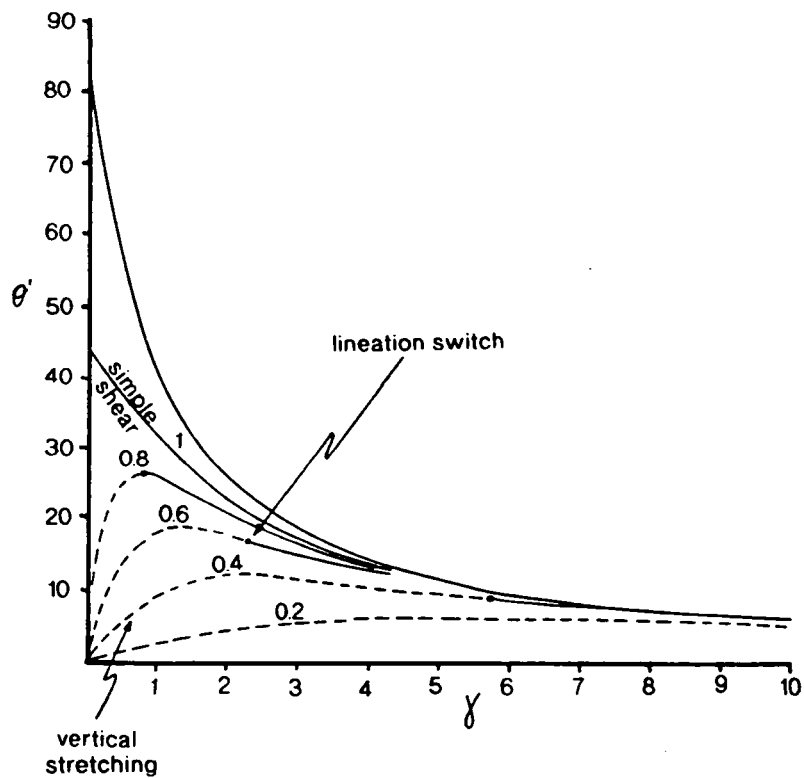


Figure 1.23 Plot of orientation of long axis of strain ellipse in horizontal plane (θ'). Continuous lines indicate X-axis horizontal, dashed lines indicate X-axis vertical. Note for α^{-1} values between 0.8 and 0.4 stretching axis (X) switches from vertical to horizontal with increasing γ . (Sanderson & Marchini, 1984).

constant incremental strain (swapping occurs where path 3 'bounces' off the b -axis in figure 1.24). The Flinn diagram also shows a change from low k -values and X vertical, to higher k -values and X horizontal. The presence of axis swapping indicates that the finite stretching direction may be normal to the incremental stretching direction, resulting in a complex relationship between finite strains (cleavages and stretching lineations) and incremental strains (fractures). The presence of these incremental strains, help to constrain the deformation path followed.

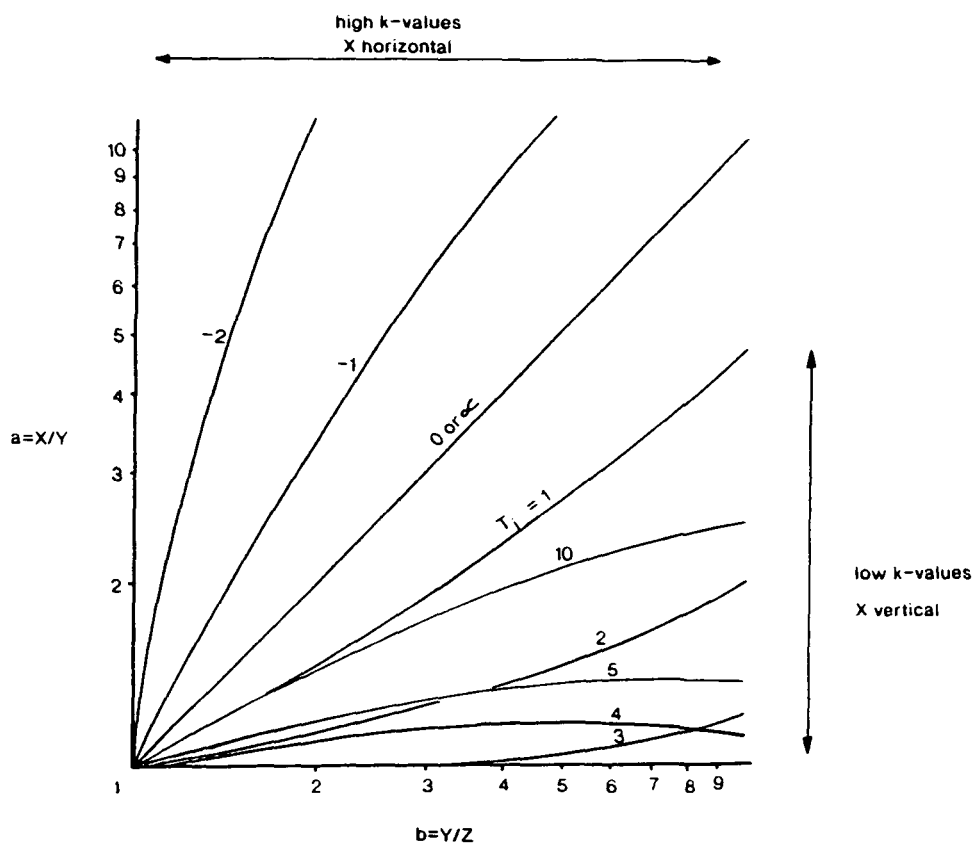


Figure 1.24 Constant incremental strain paths for transpressional model. Values on paths are numerical labels derived by dividing incremental shear strain by $(1-\alpha^{-1})$. Note the switching of axes indicated by 'bouncing' of strain path off the b -axis for path number 3 (from Sanderson & Marchini, 1984).

Simple Transpression - Deformation paths are probably determined by two main factors, the external boundary displacement of the system, and internal rheological variations, such as differential layering (Sanderson & Marchini, 1984). Harland (1971) suggested a scenario in which the deformation can be quantified in terms of boundary conditions, which involves two rigid boundaries approaching one

another obliquely. Assuming the deforming material is isotropic, the finite strain can be determined at various increments of shortening (S), and hence the deformation path may be defined. The parameters α^{-1} and γ used in the constant incremental strain model, can be expressed in terms of S for any given value of β (see figure 1.25a), where β is the angle between the relative movement vector and the rigid boundary. Figure 1.25b shows the deformation paths for the various values of β . Again, very similar results to the constant incremental strain model are obtained, with axis swapping occurring in cases where β is small.

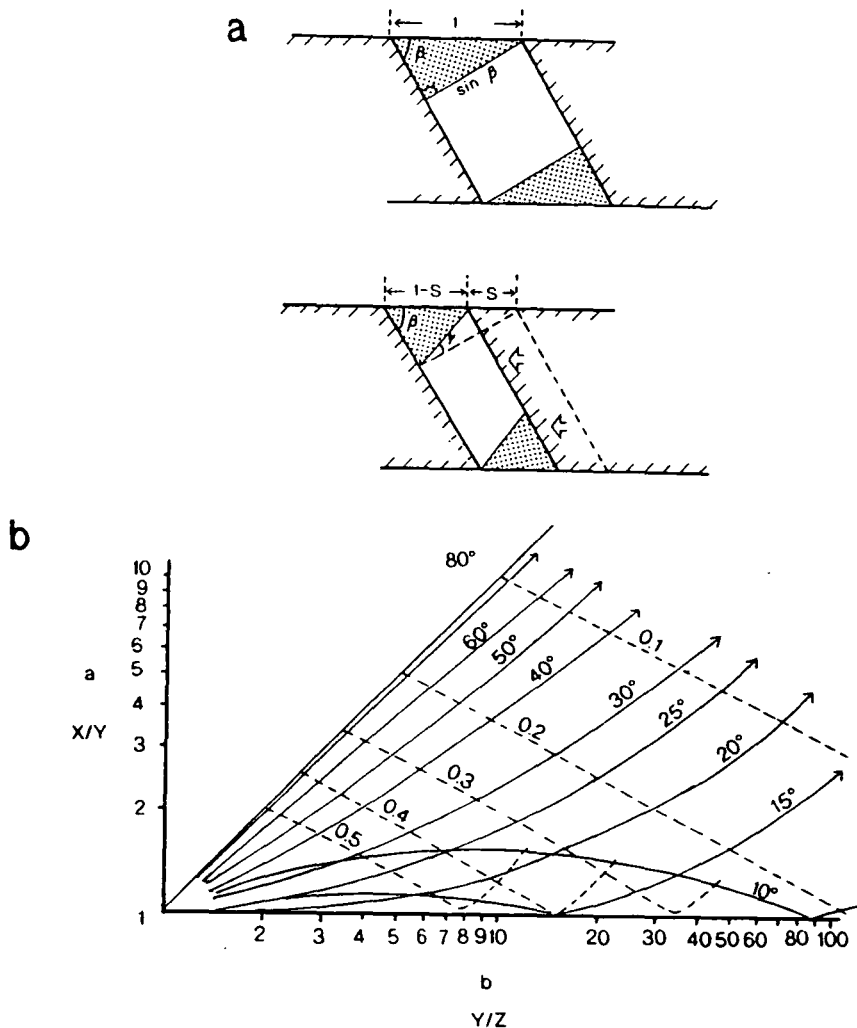


figure 1.25 (a) Simple transpressive model involving the movement of rigid blocks (diagonal shading), defining S and β . (b) Strain paths for Simple Transpression model. Continuous lines are strain paths for labelled β angles, dashed lines indicate amount of shortening across the zone (α^{-1}), $a=X/Y$, $b=Y/Z$. (Both figures taken from Sanderson & Marchini, 1984).

The relative magnitudes of the principal incremental strain axes for simple transpression can be determined by a geometrical construction (McCoss, 1986), assuming the constant volume model of Sanderson and Marchini, (1984). This is achieved by measuring the angle (A) between S and the zone normal (figure 1.26a). The incremental relative magnitudes, orientations and ellipsoid shapes are a function of A , and are outlined in figure 1.26b.

In figure 1.26b eight precise values of A can be recognised, which bound distinctly different tectonic regimes ($A = 0^\circ, 180^\circ$, the sinistral and dextral systems where $A = 90^\circ$, and where $A = 70.5^\circ, 109.5^\circ$), which define more concisely terms such as compression, extension, and strike-slip. These critical field boundaries can be followed into the finite strain field where the angles remain stable with increasing strain, except where $A = 70.5^\circ$ (ASTP or axially symmetric transpression angle) and 109.5° (ASTT or axially symmetric transtension angle), these boundaries migrate slowly towards 90° with increasing strain. The field of finite general compression expands from its incremental limits with increasing strain, at the expense of the general strike-slip field, which contracts. This has two important consequences on the kinematics and deformation paths of transpressional zones. First, if the direction of displacement is constant, A will be fixed, therefore only within the regime of incremental general strike-slip ($70.5^\circ < A < 109.5^\circ$) can axes switching occur, and then at only fairly high strains, except where A is very close to the ASTP angle. The angle between S the relative motion vector and the zone boundary (McCoss, 1986), or the β angle (Sanderson and Marchini, 1984), when lineation switching occurs are very similar, i.e. low (see figures 1.25b and 1.26b). Secondly, the stability of a regime with a constant motion direction suggests that if axis switching does occur it is more likely to be due to changes in the displacement direction relative to the zone boundary than progressive strain. Therefore, at high crustal levels where incremental strains dominate, the latter scenario is probably occurring. Where multiple switches occur within a zone of superimposed incremental strains, it suggests that the relative displacement direction is varying slightly about the critical ASTP angle. Using such

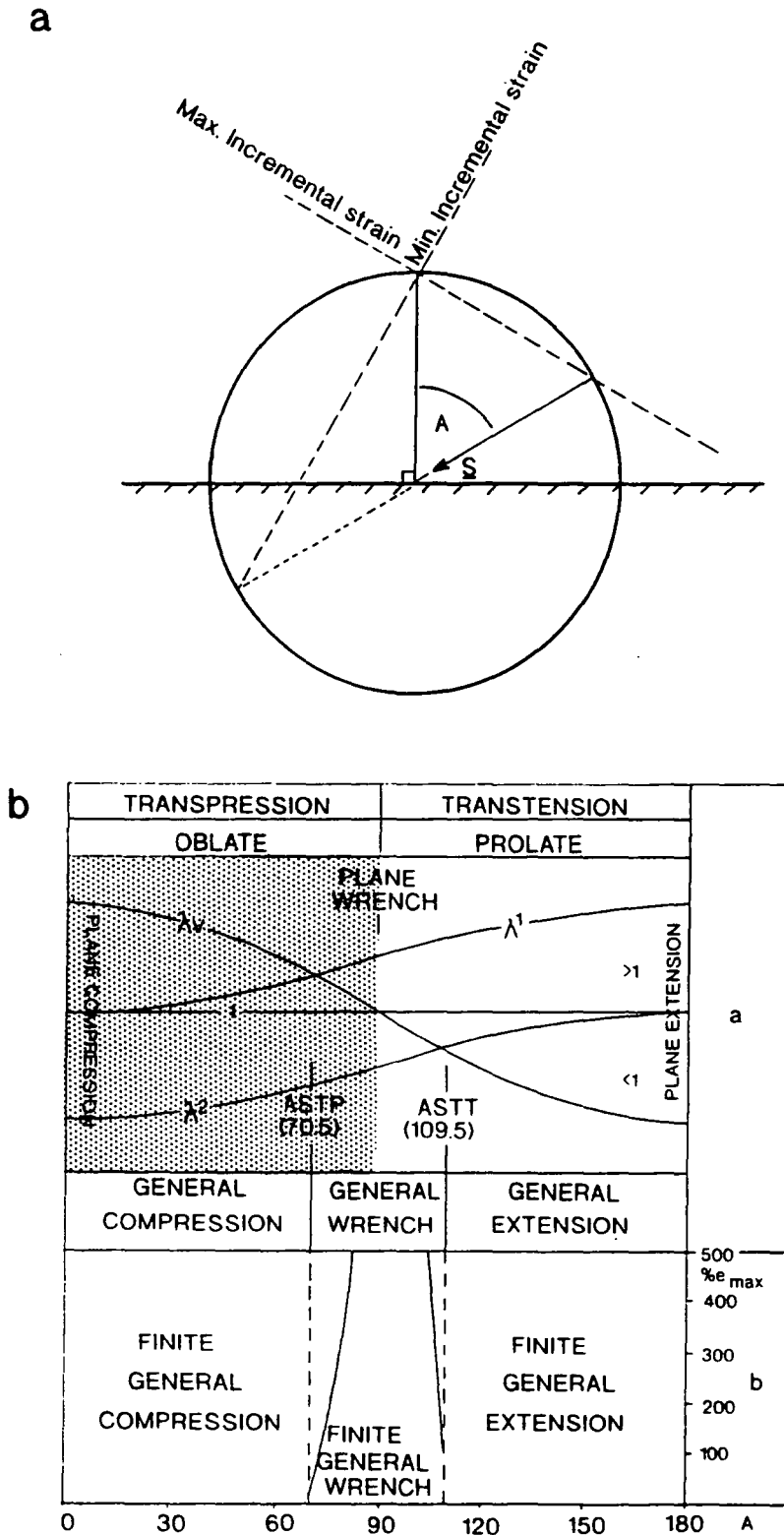


Figure 1.26 (a) The geometric construction for ASTP transpression, modified from McCoss, 1986. See text for detail. (b) A graphical solution for determining the characteristics of (a) the incremental strain ellipsoid and (b & a) the finite ellipsoid. The orientations where axially symmetric transpression and transtension occur are shown by ASTP and ASTT, respectively. λ_v is the vertical principal quadratic elongation. $\lambda_1 > \lambda_2$ are horizontal principal strains. e_{max} is the maximum finite extension. Shaded quadrant highlights transpressional regime. Note that lineation switching occurs at ASTP where λ_v crosses λ_1 . (Re drawn from McCoss, 1986)

construction methods as that of McCoss (1986) the deformation style of a zone may be characterised with either some knowledge or assumption of the boundary condition.

Secondary structures

Incremental strain axes are parallel to the principal stress axes, therefore, the orientation of faults, fractures, and folds at initiation can be predicted (figure 1.27). The effect of α^{-1} on the orientation of the maximum compressive stress axis for transpression ($\alpha^{-1} < 1$), relative to strike-slip ($\alpha^{-1} = 1$) and transtension ($\alpha^{-1} > 1$) is clearly seen in figure 1.27. Where $\alpha^{-1} < 1$ the maximum compressive stress direction forms an angle greater than 45° to the deformation zone. The secondary structures are arranged about this maximum compressive stress, therefore, folds and thrusts will initiate at angles much lower to the zone than in simple shear, and extensional structures will form at higher angles. Subsequent rotation as the strain progresses will modify these original orientations as with simple shear, but their rate of rotation will depend on the bulk strain path.

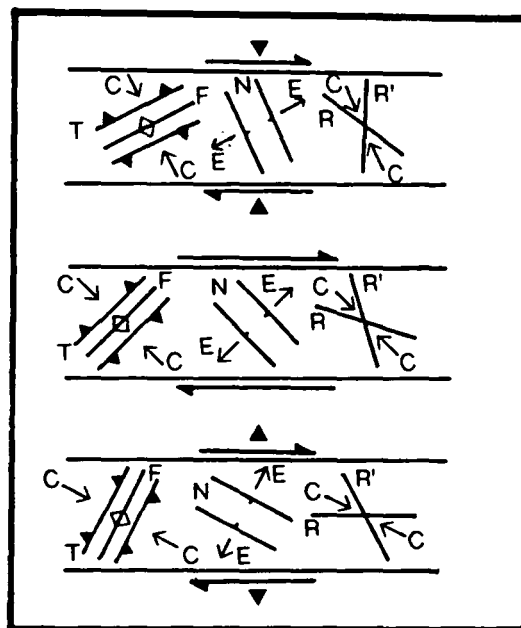


Figure 1.27 Diagram to show the initiation orientations of fractures and associated structures for a Simple Transpression model (top), compared with simple shear (centre) and transtension (bottom). C, 'compression axis'; E, 'extension axis'; N, normal faults; T, thrust faults; R, R', conjugate Riedel shears; and F, fold axis. (Re drawn from Sanderson & Marchini, 1984).

1.2.3 Complex transpression and kinematic partitioning

In recent years the identification of regions of partitioned strain and kinematics (Harland, 1971; Woodcock et al., 1988; Holdsworth & Strachan, 1991; and Sanderson et al., 1991) has become intimately associated with 'complex' transpressional deformation. The models of transpression presented above all assume that deformation occurs within an isotropic medium, however, as areas of natural deformation are rarely homogeneous the effects of previous anisotropies and rheological variations must be taken into consideration.

Strain or kinematic partitioning results from the resolution of the oblique relative plate motion vector, into its two components perpendicular and parallel to the plate margin, with shortening structures forming parallel to the margin and strike-slip along the deformation zone (Woodcock et al., 1988). The style of partitioning tends to be manifest into two types defined by the chronological relationship of kinematics: (1) Spatial strain partitioning, and (2) Temporal strain partitioning.

Spatial strain partitioning - *'Spatial strain partitioning occurs when the resolved components of the oblique relative motion vector are manifest as synchronous, spatially distinct domains of deformation.'*

Modelling of constant incremental and simple transpressive strains (section 1.2.2) does not predict the synchronous development of zone normal shortening structures, and zone parallel strike-slip. Instead the deformation paths predict a gradational change in the finite strain ellipsoid relative to the increasing shear strain, with lineation switching occurring at specific points for given deformation paths (see figures 1.24 & 1.25b). However, Holdsworth and Strachan (1991), and Strachan et al., (1992) provide persuasive evidence for the coeval formation of spatially partitioned strain within NE Greenland, but the presence of a possible pre-Caledonian shear zone architecture may be responsible for this deformation style (Holdsworth, R.E., *pers. comm.*). The influence of pre-existing basement structure has been invoked by Woodcock et al., (1988) to explain the structure and kinematics observed across north and west Wales,

suggesting that even the partitioned component of shortening can be further partitioned into discrete zones of simple and pure shear. The most obvious present day examples of spatial strain partitioning are trench-linked strike-slip faults (e.g. Segmangko system, Sumatra), which accommodate oblique subduction (Woodcock, 1986). The central Californian region also displays synchronous fault parallel thrusts and folds, accommodating $8\text{mm}\cdot\text{yr}^{-1}$ displacement, and a narrow (3-10metre wide) strike-slip fault accommodating $43\text{mm}\cdot\text{yr}^{-1}$ (San Andreas fault). Mount & Suppe (1987) have demonstrated that the partitioned nature of the San Andreas fault in this region is due to the very low shear stress of the main fault zone, relative to the Coast Ranges, which causes the principal stresses to be almost perpendicular and parallel to the fault. In regions that have suffered prolonged transpressive deformation vertical anisotropies can form that possibly result in spatial strain partitioning. However, the time aspect involved in such a deformation history leads to the introduction of temporal strain partitioning.

Temporal strain partitioning - *'Temporal strain partitioning describes the change in deformation style from one resolved component to the other, with respect to time, in a region suffering a constant incremental transpressive strain'*.

Unlike spatial partitioning, temporal strain partitioning is predicted in the transpressive models of Sanderson & Marchini (1984) and McCoss (1986), and is dependent on the specific deformation path followed, i.e. depends on the values of γ and α^{-1} (see figures 1.24 and 1.25b). In these cases, the orientation of the X-axis of the finite strain ellipsoid transforms from vertical to horizontal (Sanderson & Marchini, 1984) or vice-versa (McCoss, 1986) at high values of shear strain (γ). As mentioned earlier, the progressive development of vertical anisotropies such as slaty cleavage or the rotation of incompetent layers into the vertical by tight folding (Harland, 1971) can result in the introduction of the strike-slip component of the transpressive strain. Therefore, the individual rheology of different layers within a sequence can cause partitioning, as can the changing rheological behaviour of a deeply exhumed rock. Within the southern Bohemian massif (Fritz & Neubauer, in press) recognised that at

lower crustal levels ductile deformation accommodated the transpressive stress as a large reverse shear zone, but with increased exhumation more brittle behaviour resulted in partitioned strain along discrete fault zones, with plate boundary parallel and perpendicular components. Another obvious cause of temporal strain partitioning is a change in the incremental strain either due to a change in the relative plate motion vector, or a change in the value of α^{-1} (shortening across the zone) due to irregularities along the deformation zone, with time.

It is quite evident that the parameters controlling the partitioning of transpressive strains, are varied and are often of a transient nature. The definitions presented are for ideal situations, however, it appears that neither phenomena is mutually exclusive of the other. Commonly a lack of certainty regarding the relative chronologies of the kinematics within the deformation zone, means that quite often it is not known if the partitioned components occurred simultaneously or were differentially distributed or indeed formed in sequence. Perhaps a more reasonable expectation would be a complex distribution of deformation modes that possess an intricate chronological relationship. This is likely to be especially true for brittle upper crustal deformation, which due to its very nature, induces extremely heterogeneous strain, and is strongly effected by local anisotropies.

1.2.4 Transpression and associated en echelon folding

In simple shear the incremental shortening direction (Z_i) is at 45° to the shear plane, therefore, folds would be expected to initiate normal to this direction. However, documented en echelon folds commonly form angles much less than 45° to the main fault zone (Moody and Hill, 1956; Harding, 1973; and Wilcox et al., 1973). Folds formed in an ideal simple shear regime would not be expected to display a 45° relationship to the zone as at initiation the folds will possess an interlimb angle of 180° , only after rotation and fold appression, will the fold develop enough to become recognised. To achieve an angle of less than 25° (Moody and Hill, 1956) in a simple shear system requires high shear strains ($\gamma > 2$) which corresponds to 60% shortening

across the folds, a value which is clearly in excess of that observed in southern California. A transpressive model, however, allows fold initiation at angles $<45^\circ$, and requires a much smaller amount of shear strain to achieve a given amount of rotation when compared to simple shear. Figure 1.28 shows the angle of initiation (θ') of folds and their subsequent rotation due to increasing shear strain γ .

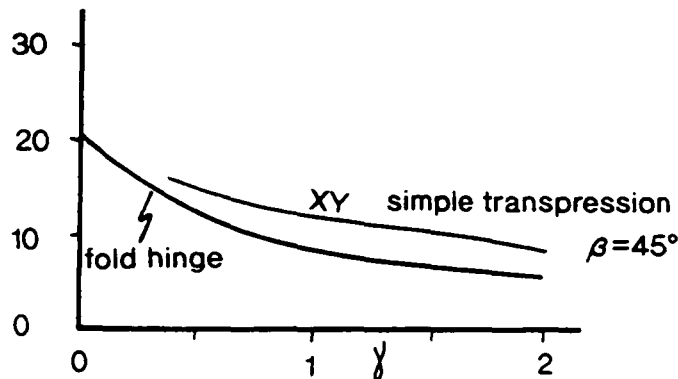


Figure 1.28 Initiation angle of fold axis within a simple transpression model, assuming the fold developed as a material line during the first increments of strain and then rotated passively. F, refers to fold axis. XY, cleavage plane. (Re drawn from Soper, 1986).

Theoretical curves have been constructed by Little (1992) to describe the relationship between fold appression and the axial plane strike. The construction procedure assumes that the hinges of ideal chevron-shaped folds initiate and subsequently behave as passive material lines or they migrate in order to remain parallel to the XY plane of the finite strain ellipsoid. Using the equations of Sanderson and Marchini (1984) curves can be derived for 'simple transpression' and constant incremental transpression (figure 1.13). The behaviour of certain fold types at higher strains, i.e. chevron folds tend to lock up at an interlimb angle of 60° , can result in curves with very similar slopes from their initiation orientations to their tightly appressed, and rotated equivalent. Therefore, independent incremental strain data is required to discriminate a true ideal transpressive path. It is important, however, not to overlook the possibility of strain variations, rigidity differences, or anisotropies within the folded layers which may exert an influence over the orientations of folds (Little, 1992).

Folds and cleavage transection

Cleavage transection has become synonymous with transpression, in particular clockwise transection with sinistral transpression in the British Caledonides (Soper & Hutton, 1984; Soper et al., 1987, Woodcock et al., 1988). Soper (1986) modelled cleavage transection as a series of incremental pressure solution cleavages, that sequentially become passively rotated, which are all superimposed upon a fold whose hinge initiated and 'passively' rotated prior to the first increments of cleavage development. This model produced a range of transection angles up to 10° , however, it requires specific assumptions regarding fold and cleavage development. Soper himself recognised the importance of the timing between the two structures and their effect on the sense of transection, with both axial planar and anticlockwise transection possible in a sinistral event. If cleavage development initiated during layer parallel shortening and continued into the buckling stage an axial planar relationship would be formed, or if the cleavage development was confined to the early layer parallel shortening an anticlockwise transection angle would be formed.

The model of fold development considered has a strong bearing on the modelled transections. Sanderson and Marchini (1984), and Soper (1986) considered fold hinges to be incremental strain markers, that become passively rotated with further increments of strain, i.e. the hinge does not remain parallel to the finite XY plane, and in fact rotates faster. However, as mentioned in the section on *transpression and associated en echelon folding*, and also by Treagus and Treagus (1992), no fold would be visible after the first increments of strain, and that only after considerable layer shortening and fold development by an 'active' hinge migration mechanism (the fold hinge tracks the XY plane of the finite strain ellipsoid) does the fold hinge become fixed, and hence passively rotated. Thus the fold axis will only lie slightly closer to the zone margin than the cleavage (approximately $1-2^\circ$). Therefore, the transpressive deformation of horizontal layers cannot account for folds transected by cleavage by as much as 10° (ibid.).

The above models assume non-dipping, strike-parallel beds. By considering inclined layered systems a variation in transection relationships can be modelled, which are controlled by two different cases of inclined layers: (1) dipping layers that strike parallel to the zone margin, and (2) layers oblique in both strike and dip. (All the models described are sinistrally transpressive)

In the first case, the XY plane (cleavage) trace forms *anticlockwise* of the fold axis developed within the various dipping layers, opposite to the relationship commonly associated with sinistral transpression. Also the transection angle increases relative to the amount the layer dips (figure 1.29a). In the second case, dipping layers that strike oblique to the rigid plate margin display a wide range of discordance in transection angles and sense, between the expected fold axes and the XY plane (figure 1.29b). The orientation of the layering to the XY plane is critical, and divides fields of anticlockwise, axial planar, and clockwise transection. Figure 1.29c summarises the fields of transection sense, which distinguish fields in which poles to bedding will develop folds with either anticlockwise or clockwise transection. Hence, it is theoretically possible to get the complete variation of relationships, however the first case of simple dipping layers is more likely to be the 'normal' situation for the closure of a sedimentary basin.

These models assume a constant transpressive incremental strain history. If the strain path varies from shortening dominated transpression to strike-slip dominated transpression, a clockwise transection angle (or vice-versa) can form in a sinistral event. The resultant finite strains can be the same as for constant incremental transpressive strains, but the relationships between the coaxial and non-coaxial microstructures evidence the strain paths followed (figure 1.30).

The consistency of the sense of cleavage transection in the British Caledonides is strong evidence for its use in determining the sense of transpression, however, theoretical evidence suggests that it should not be used to assume the sense of transpression without additional supporting kinematic and structural data (Soper, 1986; and Treagus & Treagus, 1992).

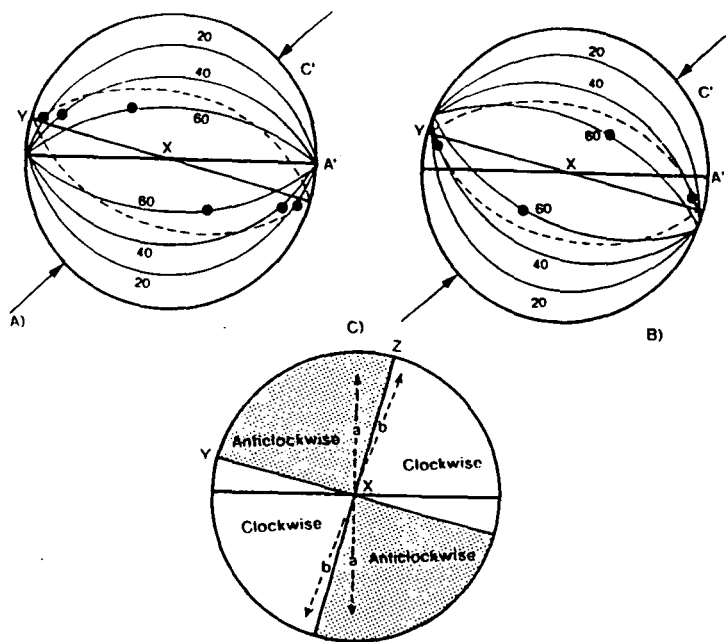


Figure 1.29 The effect of inclined and oblique layering on cleavage transection, with respect to a sinistral transpressional deformation. Transpression vector is bold arrow, transpression zone margin (a) east-west. Solid line is XY plane, broken curves circular sections. (a) Planes striking parallel to zone margin, dips 20°, 40° and 60°. Fold axes (solid dots) are cut anticlockwise by the XY plane. (b) Planes striking 20° to the zone margin, otherwise as (a). Fold axes are transected clockwise. (c) Fields for which bedding poles would have anticlockwise transection of fold axes by XY plane (ACL shaded), and clockwise (CL, blank). Positions for examples in (a) and (b) indicated by broken lines, labelled a,b.

(from Treagus & Treagus, 1992)

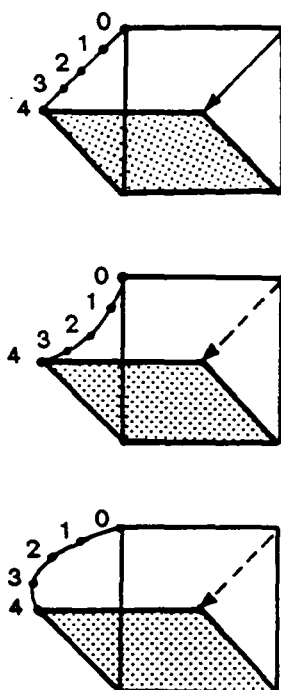


Figure 1.30 Three deformation histories producing an identical finite transpressive strain. (a) Incremental simple transpression. (b) initial pure shear to later simple shear, producing clockwise transection of folds by the XY plane. (c) Opposite deformation path, with a late reversal of shear direction (producing anticlockwise transection of folds by the XY plane). (after Harland, 1971)

1.2.5 Flower structures

Transpression zones located within the upper levels of the crust are commonly characterised by a distinctive structural geometry. This commonly comprises a central vertical zone which rises upward and outward along convex-up faults. The geometry of these structures, as imaged in seismic sections, lead Wilcox et al., (1973) to describe them as 'positive flower structures', which have become known simply as 'flower structures'. Although Sylvester (1988) argues that the term 'palm-tree structure' more adequately describes the geometry of the structure, the more widespread acceptance of the meaning of 'flower structure' prompts this author to employ its use within this text. Transtensional structures will not be discussed in any detail within the following chapters. However, it is important to distinguish the nomenclature of the transtensional counterpart of the flower structure as the plethora of botanical jargon could cause some confusion. The term 'negative flower structure' (Harding & Lowell, 1979) is redundant without its 'positive' variation, therefore the more descriptive term 'tulip structure' (Naylor et al., 1986) is adopted, although it is not meant to imply a circular structure in plan view.

The type example of a flower structure was described by Sylvester & Smith (1976) along one of a series of secondary transpressive structures or restraining bends along the San Andreas fault, namely the Mecca Hills (Sylvester, 1991). Within the central Mecca Hills, the San Andreas, Skeleton Canyon, and Painted Canyon faults dip 60°-70° toward the central uplifting block in the deepest exposures. The faults flatten upward into short, oblique-slip (presumably) thrust faults beneath rocks of the central block that have been thrust between 50 and 200 metres upon the footwall of the adjacent block (see plate 1.2 and figure 1.31. Convex upward strike-slip faults are common elsewhere, e.g. the Alpine fault (Wellman, 1955), and San Jacinto fault (Sharp, 1967). Nappe displacements of 1km along the 'Big Bend' section of the San Andreas (Davis & Duebendorfer, 1987), and 5km in West Spitsbergen (Craddock et al., 1985) represent some of the largest observed shortening displacements. Strachan et al., (1992) describe a mid-crustal transpression zone in which the zone normal



Plate 1.2 View looking NW along the Painted Canyon fault, Mecca Hills, southern California. The shallowing upward geometry of this fault is quite evident.

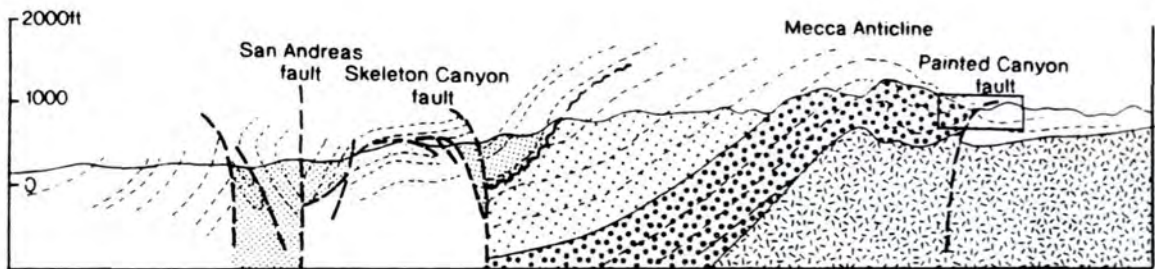


Figure 1.31 Structural cross section through the central Mecca Hills, southern California. The shallowing upward geometry of the bounding faults near the surface are shown. Box indicates the view shown in plate 1.2 above. (Re drawn from Sylvester & Smith, 1976).

movement amounts to tens of kilometres, and recognised that movements of this magnitude cannot be accommodated easily by a steeply-rooted shear zone, therefore, in examples where large shortening displacements are observed the steep shear zone / fault is envisaged to root onto a low-angle regional detachment / thrust fault.

As highlighted above, the cross-sectional geometry, and in the case of the Mecca Hills, the three dimensional geometry of flower structures are relatively well understood. However, as these structures are commonly identified on seismic sections, or unfortunately within rocks rheologically unsuitable for the preservation of kinematic indicators, the dynamic element to such structures is seldom known.

1.3 Sense of movement determination in a brittle deformation regime

The determination of the direction and sense of movement from fault surfaces is a basic requirement for the study of upper crustal tectonics, and is indispensable in establishing the kinematics of individual faults, and the regional evolution. This is especially true when the sense of slip cannot be determined from offset of geological structures. Observation of the minor structures (sense of movement criteria) associated with slickensides and slickenlines, the presence of secondary structures associated with faults, and the adjacent wallrock deformation can be used independently, but preferably together, to infer the relative sense of movement on brittle faults. When considering the larger scale, the asymmetry of structures formed in simple shear, or for that matter transpressional and transtensional regimes can be used to determine the sense of movement (i.e. the skewed distribution of fault populations, en echelon folding, and general fold vergence).

1.3.1 Slickenside striations

The morphology and cause of lineations on a slickenside fault surface may be varied, depending on the lithology, and seismic behaviour of the fault. Figure 1.32 illustrates several slickenside lineations, and their sense of movement interpretation.

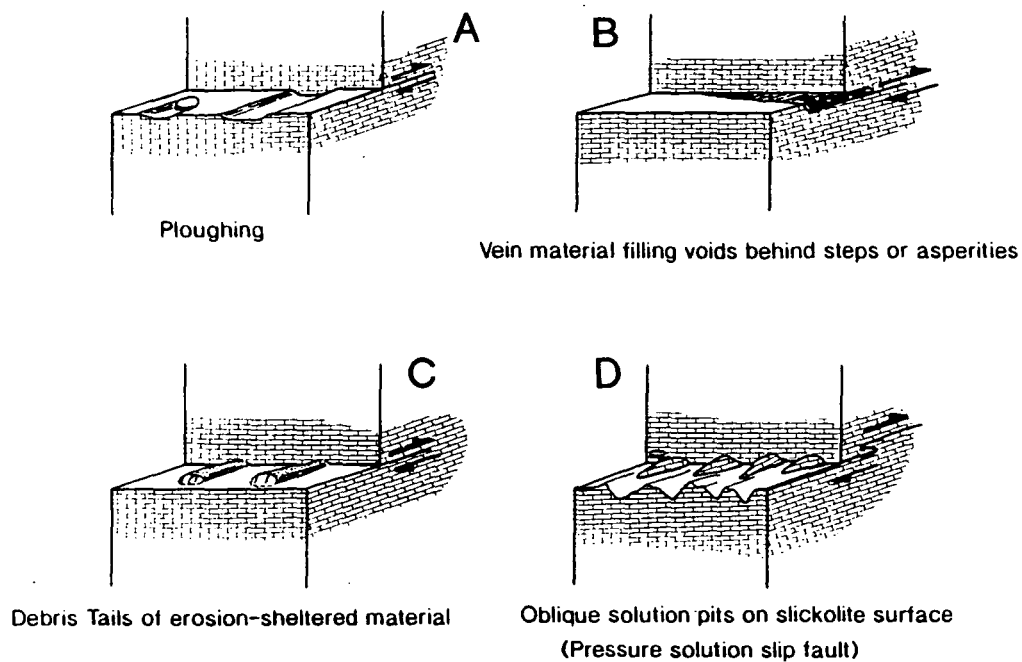


Figure 1.32 Types of slip parallel movement indicators found on slickensides. (a) Asperity ploughing, (b) accretion steps and fibres, (c) Tails or ridges of erosion-sheltered material on the down-slip side of hard asperities, (e) Oblique spikes on slickolite surfaces. (Adapted from Means, 1987)

Asperity ploughing (Means, 1987)

This is represented by furrows, grooves or scratches on slickenside surfaces, which are produced by resistant protuberances on one side of a pair of surfaces moving relative to one another, scoring a groove in the opposite block. The grooves terminate in the final ploughing element position, the end of which points toward the movement of the missing fault-wall. Excavation of the groove may be accomplished by brittle or ductile (i.e. pressure solution) processes (figure 1.32a).

Erosional sheltering

When a surface containing hard asperities becomes eroded by fault movement, elongate ridges are preserved behind the hard particle parallel to the slip direction. The leading face of this hard particle may display minor pressure solution effects, especially within carbonate rocks (figure 1.32c).

Crystallisation linked to steps along the fault surface

These steps generally form perpendicular to the striation on the fault surface, the risers to which face the direction of movement of the missing block (figure 1.32b and plate 1.3). These accretion steps (Petit, 1987) produce potential voids that can either be filled by elongate crystals of calcite (in the case of limestones) during slow dilation of the voids (Durney & Ramsay, 1973), or blocky euhedral calcite precipitation in rapidly opened voids, i.e. microseismic events. Individual accretion steps can display a combination of these crystal growth styles, indicating a change between aseismic and seismic motion.

Slickolites (Bretz, 1940)

Slickolites are similar to stylolites in being dissolution surfaces, however, unlike stylolites the spikes and columns of slickolites point sub parallel to the slip surface, and parallel to the direction of movement. The solution spikes and columns observed on a slickolite surface point in the direction relative motion of the block containing them (figure 1.32d).

1.3.2 Sense of movement structures involving secondary fractures

An important feature commonly observed along fault planes is the presence of secondary repeated fractures of the same type, that possess a regular angle with respect to the mean fault plane. These structures were reviewed by Petit (1987), whose nomenclature will be employed in this sub-section unless otherwise stated. This terminology is based mainly on Riedel-type experimental nomenclature, to describe the geometrical position of the fractures, but does not imply that the fractures can be explained mechanically by Riedel experiments.

These secondary fractures can be divided into three groups based on fracture type (striated or non-striated), and orientation: *group T*, includes repetitive tension fractures and no shear fractures, *group R*, all synthetic shear fractures of R orientation,

and *group P*, all types of secondary shears of P orientation. Within groups R and P morphological differences can be distinguished by use of a second letter: O, if only R or P secondary shear fractures are present; M, if the main or mean fault plane is completely striated; and T, if non-striated secondary fractures are present (see figure 1.33a to c).

T criteria:

The characteristic of T criteria movement sense indicators is the mean fault plane is fully striated, and intersected by fractures that are dominantly perpendicular to the striations, which are themselves non-striated. These 'tensile' fractures make an angle of 30° to 90° to the main fault plane, can be open or filled, and their intersections with the main fault either planar or curved. In the latter case the fractures tend to be perpendicular to the main fault, forming a crescent shape, the 'horns' of which point in the direction of movement of the missing block (figure 1.33a and plate 1.4). These directly correspond to 'crescentic fractures' associated with glacier striations.

R criteria:

R criteria indicators are characterised by a mean fault plane which is joined by repeated secondary striated fractures, which describe a small angle to the fault wall, and have a R shear orientation. Again, their intersection with the main fault is virtually perpendicular to the slip direction (figure 1.33b).

RO (R only) type. There is no mean striated fault plane. The R shears are very closely and regularly spaced, displaying a slight striation. The fault displays a serrated profile, due to the intersection of R and R' secondary shears. This type is uncommon.

RM type. The main fault plane is fully striated, with irregularly distributed R shears of various size intersecting the fault surface.

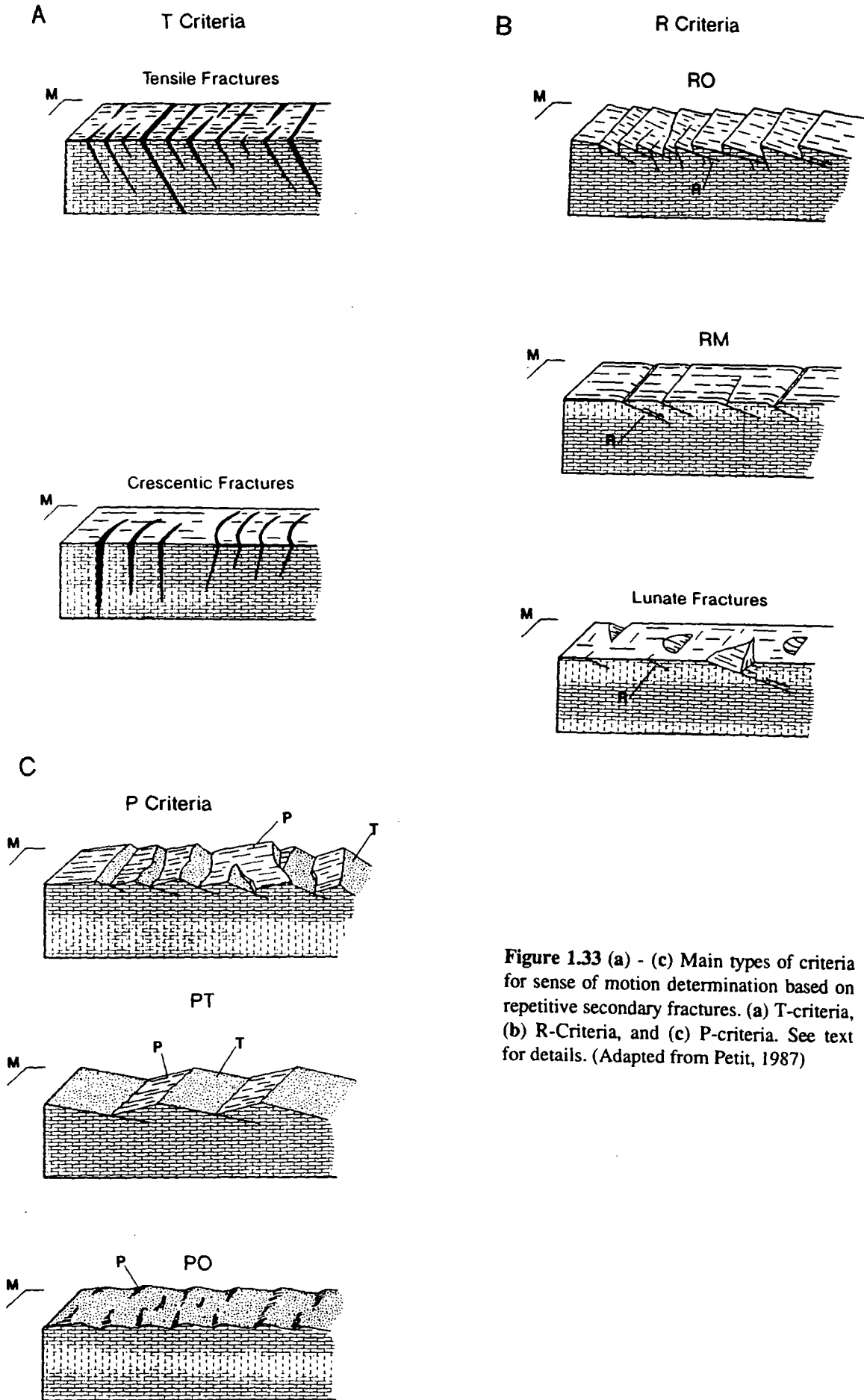


Figure 1.33 (a) - (c) Main types of criteria for sense of motion determination based on repetitive secondary fractures. (a) T-criteria, (b) R-Criteria, and (c) P-criteria. See text for details. (Adapted from Petit, 1987)

P criteria:

Characteristically the fault plane is always incompletely striated, but where developed, it appears on the side of asperities facing the movement of the missing block (figure 1.33c). The formation of this criterion implies very small slips, otherwise the striation would have become more extensive and could have led to a fully striated slickenside. Again, this category can be split into two types:

PT type. Planar non-striated surface clearly dip into the fault-wall at a small angle, where as the P shears are well developed and strongly striated. Some of the more strongly striated P surfaces show shallow steps which always ascend in the direction of the missing block.

PO (P only) type. The non-striated (protected) surfaces of the asperites (lee side) do not project into the fault-wall. The P shears display only a weak striation.

Bridge structures

In addition to the secondary fractures associated with slickensides and main fault planes, Gamond (1987) describes a fundamental relationship between first-generation en echelon faults at any scale. Depending on the sense of fault stepover compressive or tensile bridges form. Small compressive bridges provide criteria based on the increase in the linear density of solution seams at the stepover relative to the en echelon fault trace, while tensile bridges yield criteria based upon vein fillings (figure 1.34). On the large scale these features manifest as 'push-ups' and pull-apart basins.

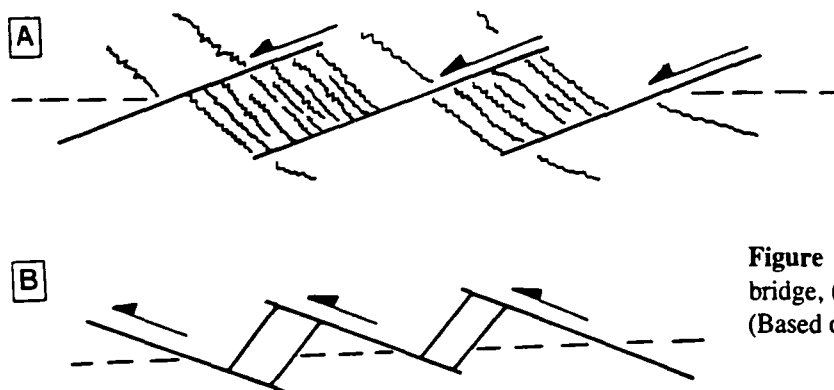


Figure 1.34 (a) compressive bridge, (b) Extensional bridge. (Based on Gamond, 1987)

Cleavages and cataclasites

The development of pressure solution cleavages in association with simple shear produces a characteristic asymmetric relationship with the fault plane, the vergence relationship between which indicates the sense of fault movement. Pressure solution cleavages can be strongly developed in coherent cataclasites, and especially in the narrow zones of residual clay squeezed between the two fault planes (Petit, 1987). Small elongate clasts of wallrock are commonly found within these clayey fault rocks, with their long axes lying within the cleavage planes. The clast sides parallel to the cleavage planes display dissolution effects, therefore, these clasts have been modified by the same incremental strain that forms the cleavage, allowing them to be used as sense of movement indicators.

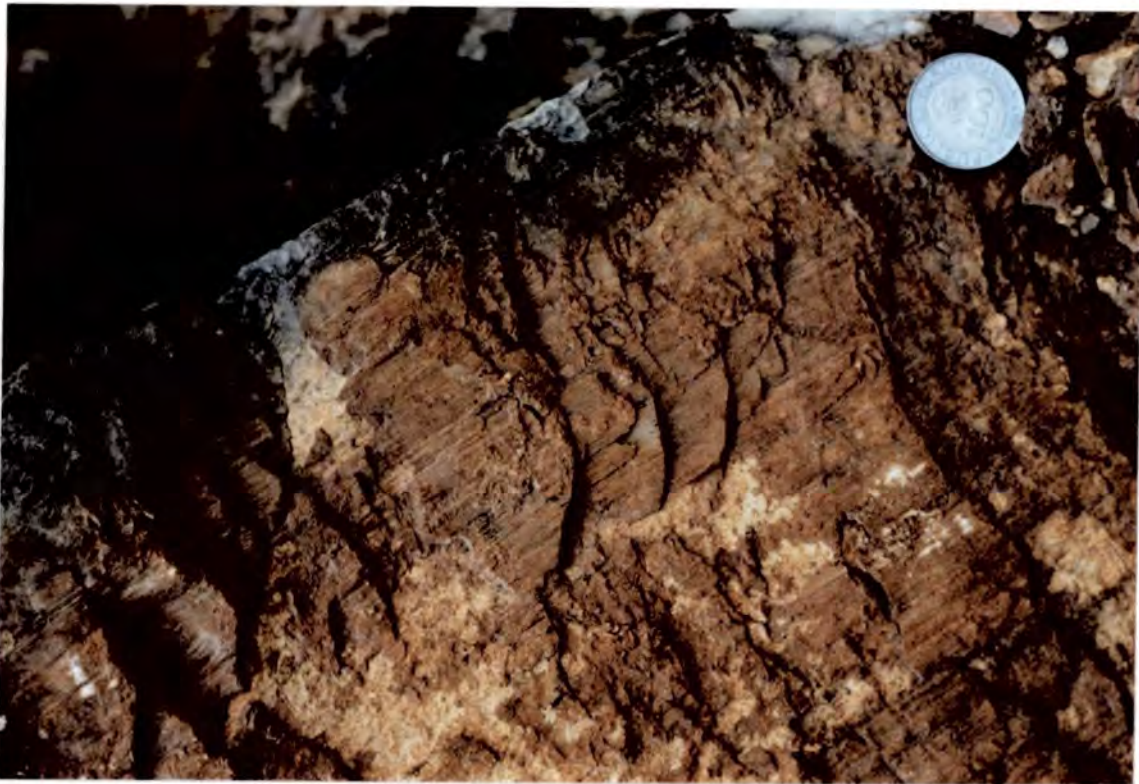


Plate 1.3 Accretionary calcite steps along fault plane. Moitas Venda, Portugal.

CHAPTER 2

The Mesozoic to Cenozoic evolution of the Lusitanian basin

2.1 Introduction

The Lusitanian Basin forms a narrow coast-parallel outcrop of Mesozoic sediments, that extend approximately 250km from Coimbra in the north, to Setúbal, south of Lisbon. These outcrops do not exceed 60km in width, and form a total onshore area of 23,000 km². The Lusitanian Basin *sensu stricto*, is characterised by an inverted zone of Mesozoic sediments which are flanked by Tertiary sub-basins to the NW and SE, the Monte Real filled mainly with Paleogene sediments, and the Lower Tagus basins possessing Neogene fill (figure 2.1). The boundary between the Monte Real and Lusitanian basin is the Nazaré fault, a major tectonic feature associated with the Nazaré submarine canyon (see later)^(figure 2.2). Between the Lusitanian and the Lower Tagus Basins the boundary is marked by a more complex series of faults that have facilitated basin inversion; namely the NNE Vila-Franca fault immediately north of Lisbon, then a less distinct N-S trending fault toward the Montejunto Range, where the NNE trend is regained and can be followed for 60km along the Serra dos Candeeiros fault zone to Leiria. The northern end of the Serra dos Candeeiros fault displays a complex geometry of distributed deformation due to the interaction of large fault bounded blocks. These latter faults and their southern extensions at Serra de Montejunto constitute one of the major basin structures, the Serra de Montejunto - Candeeiros (SMC) fault system.

The aim of this thesis is to characterise the kinematics and style of deformation responsible for basin inversion along this fault system, with particular interest in two areas; the Candeeiros block region immediately east of Porto de Mós;

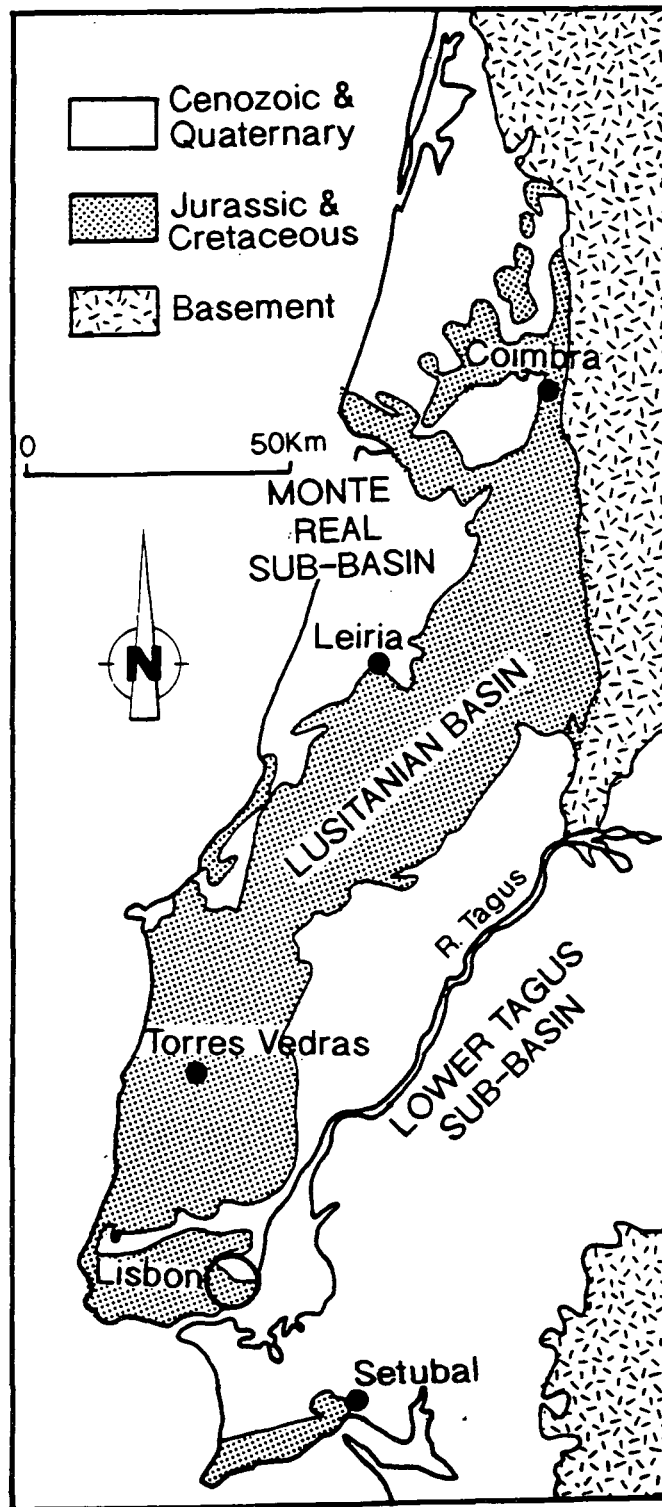


Figure 2.1 General geological map to show the distribution of the Lusitanian Basin *sensu stricto*, and the adjacent Tertiary sub-basins

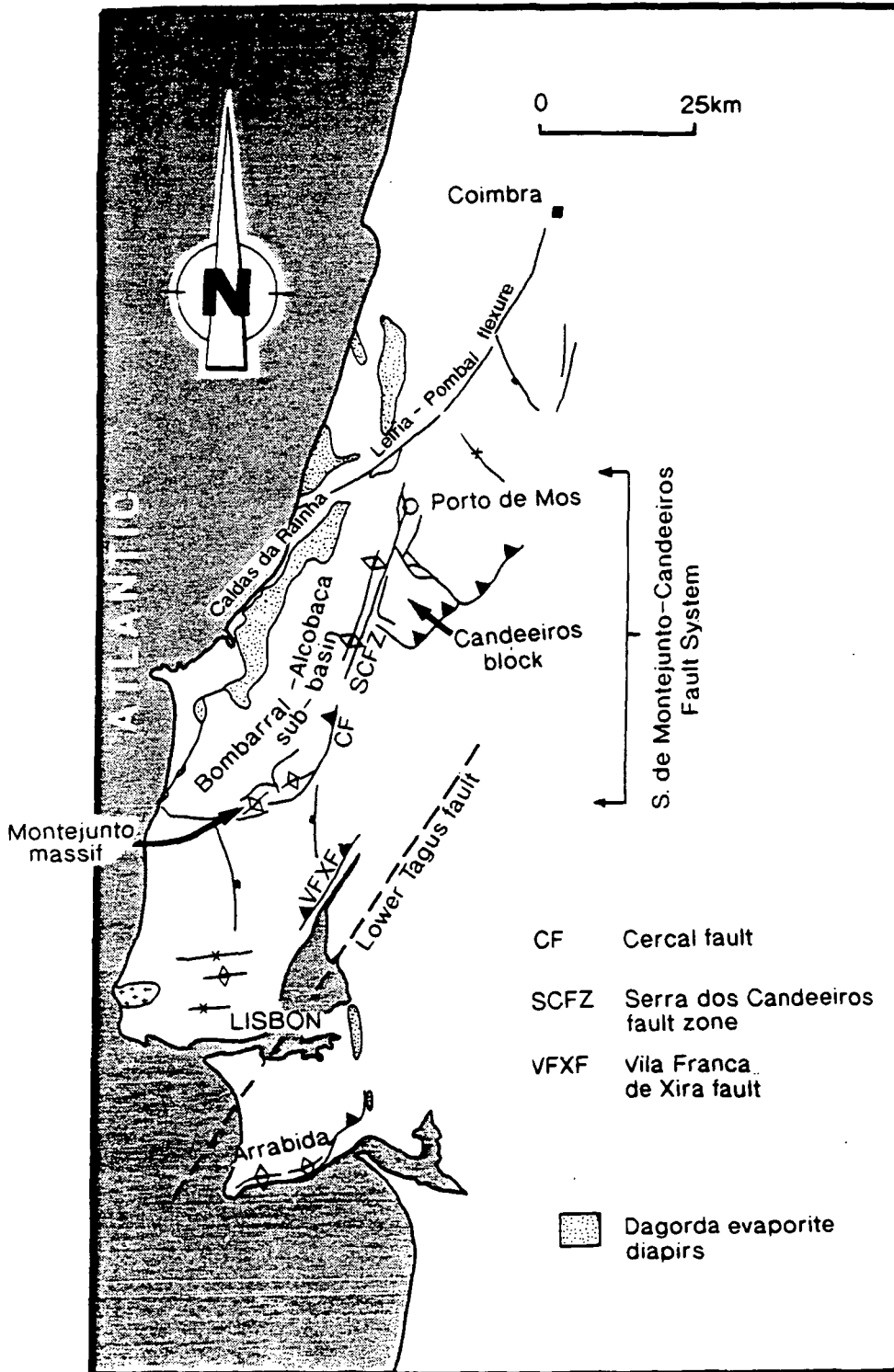


Figure 2.2 Generalised structural map of the Lusitanian Basin, displaying the dominant NNE and NE trends to the structure. Figure also displays the component structures of the S. de Montejunto-Candeeiros fault system. To the south, the Montejunto massif, joined by the NNE trending Cercal -S. dos Candeeiros faults, to the Candeeiros fault block.

and the southern termination of the Serra dos Candeeiros fault, at Serra de Montejunto (figure 2.2). This inversion is, however, only the last event in a long history of tectonic activity since the inception of the basin. The Lusitanian basin has undergone two phases of continental rifting, and latterly two phases of inversion, including the subject inversion event which occurred during the Late Miocene to Recent. The combination of structural, sedimentological, and seismic stratigraphic analysis by many authors (Guery, 1984; Wilson, 1988; Montenat et al., 1988; Leindfelder & Wilson, 1989; Ellis et al., 1990; Wilson et al., 1990), has provided a relatively comprehensive study of the basin development, emphasising the influence of pre-existing Hercynian basement structures (Wilson et al., 1990). The following chapter summarises the essential sedimentary and structural features of the basin during its evolution, to determine the basin architecture prior to inversion, and in doing so, provide a reference point when assessing the influence of pre-existing structures and lithologies on the structural style and kinematics of the inversion event documented in later chapters.

2.2 The plate kinematics of Africa-Europe since the Middle Jurassic

The relative plate motion vectors between Africa and Europe/Iberia have ultimately been responsible for the geological evolution of the Portuguese region, therefore, a discussion of the plate kinematics is essential. The most recent reconstruction of the palaeopositions of the African plate relative to the European plate was conducted by Dewey et al., (1989). This model is based on a re-identification of all magnetic anomalies in the Late Cretaceous to Tertiary sequence (Anomalies 1-34) in the North and Central Atlantic Ocean, combined with bathymetric maps and SEASAT altimetry data and gravity images. The model also introduces geological data from the western Mediterranean region which correlates with the plate motions, allowing the relative motion paths of the plates to be adjusted and smoothed (figure 2.3), unlike the earlier

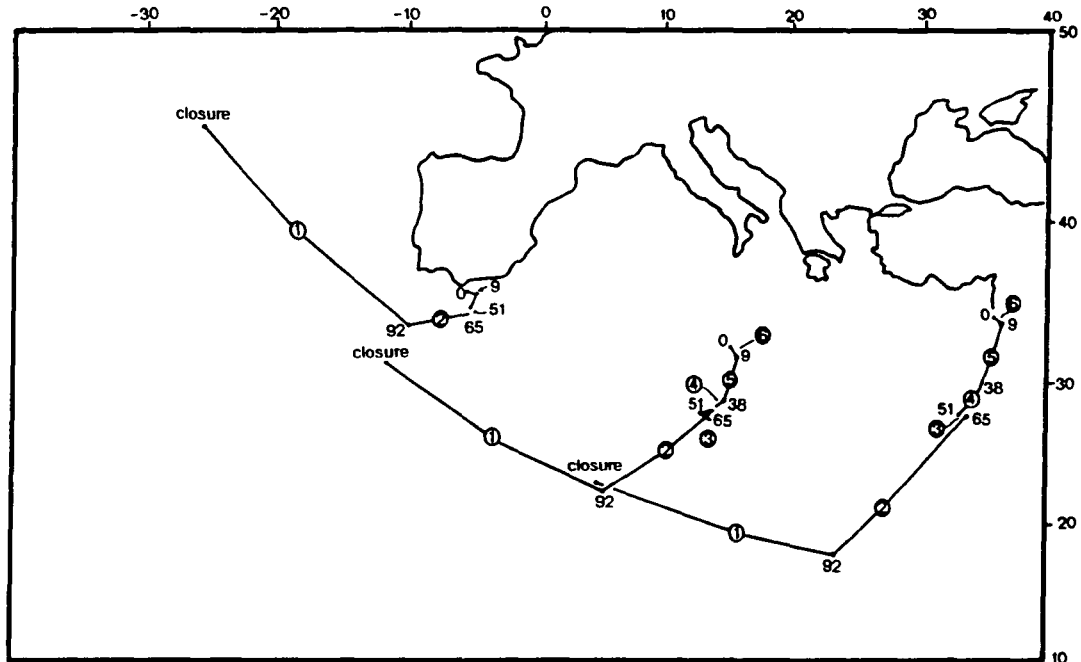


Figure 2.3 Smoothed and corrected flow lines depicting the path of Africa's motion relative to Europe, corrections made by correlations with geological events (Dewey et al., 1989). Numbers in circles refer to dominant motion phase (1-6), numbers sitting off the flow lines, refer to time before present (Ma).

models of Smith (1971), Dewey et al., (1973), Biñu-Duval et al., (1977) which have portrayed drastic changes in Africa's motion with respect to Europe.

Several distinct phases of relative motion can be distinguished from figure 2.3. During the first phase of motion, >175 Ma until Anomaly M-O (118 Ma), Africa moved sinistrally with respect to Europe, due to the differential opening of the Central Atlantic, while the north and south Atlantic regions had not begun separating, but were undergoing rifting (Pindell et al., 1988).

Between Anomaly M-O (118 Ma) and Anomaly 34 (84 Ma), the relative motion changed to a northeasterly directed compression. However, as this time period coincides with the Cretaceous Quiet Zone, a period when no large scale magnetic reversal occurred, the precise timing of this change in relative plate motion is difficult to establish. It was during this period that sea floor spreading initiated between Iberia and North America, north of the Azores-Gibraltar fracture zone. Anomaly M-O has

been identified off Iberia by Group Galice (1979) which has been suggested to correlate to the J-Anomaly Ridge of off-shore Newfoundland. However, Anomaly 34 (84 Ma) is the first clearly identifiable anomaly seen on both sides of the Atlantic, between the Azores-Gibraltar and Charlie-Gibbs fracture zones (Dewey et al., 1989). The presence of Cenomanian-Turonian aged (92 Ma) high pressure metamorphism in the Alps, prompts Dewey et al. (1989) to suggest that this age coincides with the observed change in relative plate motion.

During this period of plate vector change Iberia rotated 35° anti-clockwise, as established by the classic work of Van der Voo (1969) and Van der Voo and Zijderweld (1971). However, the exact mechanism of the rotation is debatable. LePichon and Sibuet (1971a,b) and Schott and Peres (1988) argue for a transcurrent model whereby large amounts of dextral strike-slip occurred along the Pyrenees during the opening of the Bay of Biscay. More radical solutions such as Galdeano et al. (1989) suggest that the opening of the Bay of Biscay was due to the transcurrent movement of Iberia without rotation, and introduce an earlier Late Jurassic simple rotation of Iberia. The relative plate motion vectors of Dewey et al. (1989) derived from sea floor spreading evidence, appears to be more compatible with contemporaneous rotation of Iberia and the opening of the Bay of Biscay after the late Aptian, which is the proposed time of plate vector change.

The third motion phase commenced shortly after Anomaly 30 (66.7 Ma), in the earliest Palaeocene. This phase is marked by a dramatic slowing of the convergence rate, and a somewhat variable motion. This apparent complexity of relative motion between Africa and Europe "may be the consequence of the errors involved in combining north and central Atlantic rotation parameters" (Dewey et al., 1989). However, similar relative motion paths for Africa-Europe are suggested by the published poles of Srivastava and Tapscott (1986), and Klitgord and Schouten (1986), plus the motion paths of Livermore and Smith (1985).

Resumption of the northward motion of Africa occurred after Anomaly 24 (55.7 Ma), and with only minor variations between a N and NNE direction, continued

until Anomaly 5 (8.9 Ma), in the late Miocene. This period of motion accounts for phases 4 & 5 identified by Dewey et al., (1989). The final phase of motion represents a marked change in the relative plate motion vector, from a dominantly northwardly directed compression, to a northwesterly directed closure, after Anomaly 5 (8.9 Ma, late Tortonian to Messinian).

The effects of these tectonic phases have been directly correlated by Dewey et al., to specific Alpine events in the western Mediterranean. However, only the final two tectonic phases effect west central Portugal and the Lusitanian Basin. Chapters 3 and 4 discuss how these tectonic phases are manifest within the basin, whereas the complexities of relating continental crustal response to these relative plate motions will be addressed in chapter 6.

2.3 Basin structure

2.3.1 Basement structures

The structural grain of the Lusitanian basin is the result of the reactivation of Hercynian basement structures during both the Mesozoic extensional, and Tertiary compressional episodes (LePichon et al., 1977; Wilson, 1988; Wilson et al., 1990). Therefore, a brief overview of the Hercynian orogeny and the resultant structures formed within the western Iberian Meseta is necessary before the Mesozoic and Cenozoic evolution of the Lusitanian Basin can be discussed.

Hercynian structural architecture

After the final closure of the Iapetus Ocean in the Mid Devonian, the tectonic setting of western Europe was dominated by the northerly subduction of the Proto-Tethys Ocean beneath the southern border of the Laurasian Megacontinent (Ziegler, 1982). Several microcontinents (Austro-Alpine, Avalon, Iberia), were sequentially accreted at the plate boundary, causing a step by step southward migration of the subduction zone. Iberia collided with Laurasia during the late Early Carboniferous, and a zone of N-S sinistral shear (NNW-SSE in present orientation) probably linked two

offset zones of subduction during the latest stages of the northward displacement, leading to the complex shape of the Iberian part of the Hercynian fold belt. The major tectonic boundaries of the western Iberian Meseta are sinistrally transpressive in nature, as evidenced by the southern margin of the Central Iberian Zone (Sanderson et al., 1991), and suggested by the downward convergence of the bounding reverse faults of the 100km wide Ossa Morena Zone (Fonseca, 1989).

The consolidation of the Hercynian fold belt was not synchronous along its length; by the end of the Carboniferous the mountain building process was already dormant in western and central Europe, but crustal shortening continued to the west (Appalachians) and to the east (Urals) until the end of Early Permian times (Ziegler, 1982). This was achieved by the development of a dextral 'Megashear' zone, 10,000 km long and 1000 km wide, connecting the two active belts through most of the recently consolidated section of the orogen (Arthaud and Matte, 1977). The main strike-slip faults had an east-west strike, forming angles of 20-30° with the strike of the shear zone. These synthetic shears measure several hundred kilometres in length and show tens of kilometres of offset, e.g. South Atlas Fault of Morocco, and the Biscay-North Pyrenean fault. In western Iberia, a set of left lateral strike-slip shears were particularly well developed, with dominant directions of 030° and 015°. Several dextral faults striking approximately 130° also originated in this period.

Figure 2.4 shows the spatial arrangement of the principal zones of Hercynian basement in western Iberian and their relationship to the Lusitanian basin. These zones are separated by major thrusts which strike NW-SE or NNW-SSE. The Central Iberian and Ossa Morena zones consist of metamorphosed Precambrian and Lower Paleozoic rocks, where as, the south Portuguese zone consists of low-grade Upper Paleozoic metasediments. All the zones are characterised by two phase folding that possesses a NW-SE orientation.

When the transpressional setting of the Late Palaeozoic gave way to the tensional regime of the Mesozoic, a vast network of strike-slip shears dissected the Hercynian basement of western Europe. A comparison of these trends with that of the

successively younger structures of the Lusitanian basin (figure 2.2), displays their dominance over the mechanical behaviour of the crust during the subsequent 250 million years of Iberian geological history (LePichon et al., 1977).

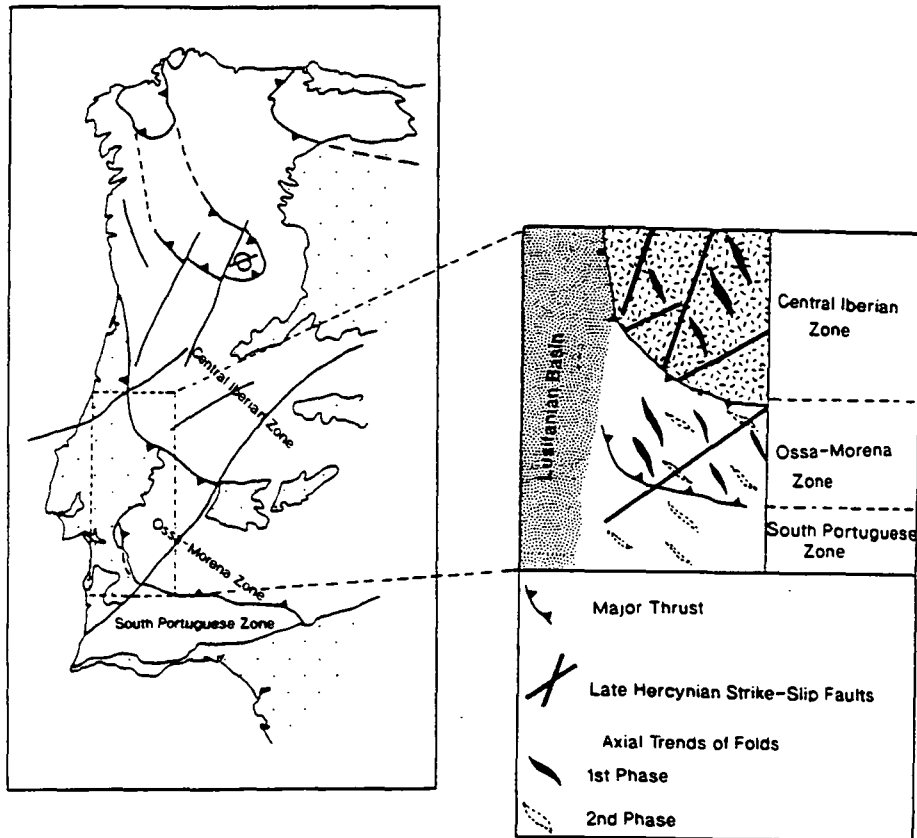


Figure 2.4 Sketch summarising the principal zones of Hercynian basement in western Iberia, and the orientation of the major Hercynian structures within the vicinity of the Lusitanian Basin. Comparison with structures within the Lusitanian Basin, fig. 2.2, reveals the significant control exerted on later deformation by basement anisotropies. (Adapted from Wilson et al., 1990)

2.3.2 Halokinetic structures and faulting

Broad geometry

A structural map of the Lusitanian basin depicts a relatively simple NE-SW trending outcrop of Mesozoic sediments, possessing a parallel depositional axis in which just over 4km of sediment has accumulated. However, in the southern part of the basin (the Estremadura trough) this interpretation proves to be an over-

simplification, where several sub-basins are present. These basins were particularly active during the Late Jurassic (Wilson, 1979), one of which, the Bombarral sub-basin, subsided largely due to salt withdrawal during the formation of large diapiric structures along its flanks, whereas the Arruda and Turcifal sub-basins developed in grabens and half-grabens. The exceptionally thick lower Kimmeridgian sequence ($>2.2\text{km}$) within the Arruda sub-basin, which accumulated at a rate of $850\text{m}\cdot\text{m}\cdot\text{y}^{-1}$, suggests that the sub-basin may have in fact formed as a pull-apart basin (Wilson et al., 1990). The northern half of the basin also displays a salt withdrawal sub-basin, the Alcobaça sub-basin, which represents the along-strike northern end of the Bombarral sub-basin (figure 2.2).

Halokinetic structures

These structures are common in the northern part of the basin, where they form NNE-SSW, and to a lesser extent, NE-SW linear structures, which mirror the trend of the basement strike-slip faults. The spatial distribution of these Halokinetic structures is probably related to the original depositional thickness of the Hettangian evaporites of the Dagorda formation, which was in turn controlled by the Hercynian basement faults that became reactivated during the initial rift phase (see 2.3). Where the evaporite formation was thick, diapiric structures developed over the reactivated basement faults, but where the formation was thin or absent the faults propagated into the cover sequence (Zbyszewski, 1959; and Wilson, 1988). Such an evaporitic structure is suggested to exist along the Torres Vedras-Montejunto anticline, which separates the Bombarral sub-basin (containing a thick Dagorda sequence), from the Arruda sub-basin (containing only thin evaporites). The onlapping and thinning of the formations toward the axis of the structure indicates that the Montejunto anticline initiated as a salt pillow (ibid.). The largest of these diapiric structures is the Caldas da Rainha diapir, a 35km by 7km , NNE trending structure that forms the western flank of the Bombarral-Alcobaça sub-basin.

Faulting

As mentioned above most of the linear halokinetic structures within the basin are suggested to be related to Mesozoic extensional reactivation of Hercynian basement faults. The major normal faults bounding the sub-basins and also those found in the northern half of the basin display dominant activity during the Late Jurassic and Early Cretaceous. Significant Late Jurassic faulting occurred to the east of the Serra dos Candeeiros region, along a NW-SE trend (Alvados, Minde and northwestern Alcanede faults), some of which are intruded by dolerite dykes that have produced ages of 140Ma (Willis, 1988). Transtensional motion has been suggested for the Vila Franca de Xira fault (Wilson et al., 1990), and by its association with the Arruda pull-apart basin, the Serra dos Candeeiros fault may also have been transtensional, with a dextral strike parallel component of motion (see 2.4.2).

Miocene compressional structures

Most of the structures already mentioned have been reactivated during Miocene to Recent times, and in the case of the Montejunto anticline, have undergone extensive deformation and modification of the original structure (Guery, 1984, and this work, chapter 4). In general, the Miocene tectonics of onshore Portugal can be split into two distinct structural styles: NNE-SSW oriented faults and salt ridges commonly display sinistral strike-slip motion, whereas ENE-WSW oriented structures display contractional or transpressional deformation. The tectonic style of Portugal during the Miocene has been described as a thrust and lateral ramp system, driven by a NNE directed compressive stress (Ribeiro et al., 1988; 1991).

The continental margin of Portugal displays extensive deformation predominantly by three sets of faults; a NNE-SSW set displaying strike-slip motion, possibly transpressional (flower structure geometries) with a sinistral sense of displacement; a N-S trending set of normal faults that bound possible pull-apart basins; and finally a NE-SW set of reverse / transpressive faults. An upper Miocene unconformity overlies most of these structures indicating that the majority of

deformation occurred during the middle Miocene, however, late reactivations are evident (Mauffret et al., 1989) indicating that the Miocene to Recent tectonics of western Portugal represent a progressive, albeit waning, event.

The tectonic interpretation of Ribeiro et al. (op. cit.) is somewhat simplistic in that it ignores the importance of sinistral transpression within the Lusitanian Basin, and the western margin of Portugal in general. It also fails to take into account the changing regional stress field that occurred during the Miocene to Recent. An alternative tectonic model for the Miocene to Recent will be presented and discussed in chapter 6.

2.4 Stratigraphy

This section deals predominantly with the Mesozoic sedimentary fill of the Lusitanian Basin, which represents the only onshore exposure of pre-, syn-, and post-rift sediments related to the opening of the North Atlantic. Due to the efforts of many workers, notably Wilson (1975, 1979, 1988, and 1990), Guery (1984, and 1986), and Montenat et al. (1988), the Mesozoic evolution of the basin is extremely well understood. In contrast, the Late Mesozoic to Cenozoic sediments have received little attention and therefore are poorly understood, with no modern interpretation available.

According to Wilson et al., (1990) the sedimentary fill of the Lusitanian Basin consists of five mega-sequences separated by basin-wide unconformities. The mega-sequences represent two periods of Late Triassic and Late Jurassic rifting, and later tectonic inversion. The unconformity bounded sequences are as follows:

- 1 Upper Triassic - Upper Callovian.
- 2 Middle Oxfordian - Berriasian.
- 3 Valanginian - Lower Aptian.
- 4 Upper Aptian - Turonian.
- 5 Uppermost Cretaceous - Miocene

Figure 2.5 summarises the Mesozoic stratigraphy within the Lusitanian Basin as proposed by Wilson (1988). The stratigraphic nomenclature shown below will be employed throughout this thesis.

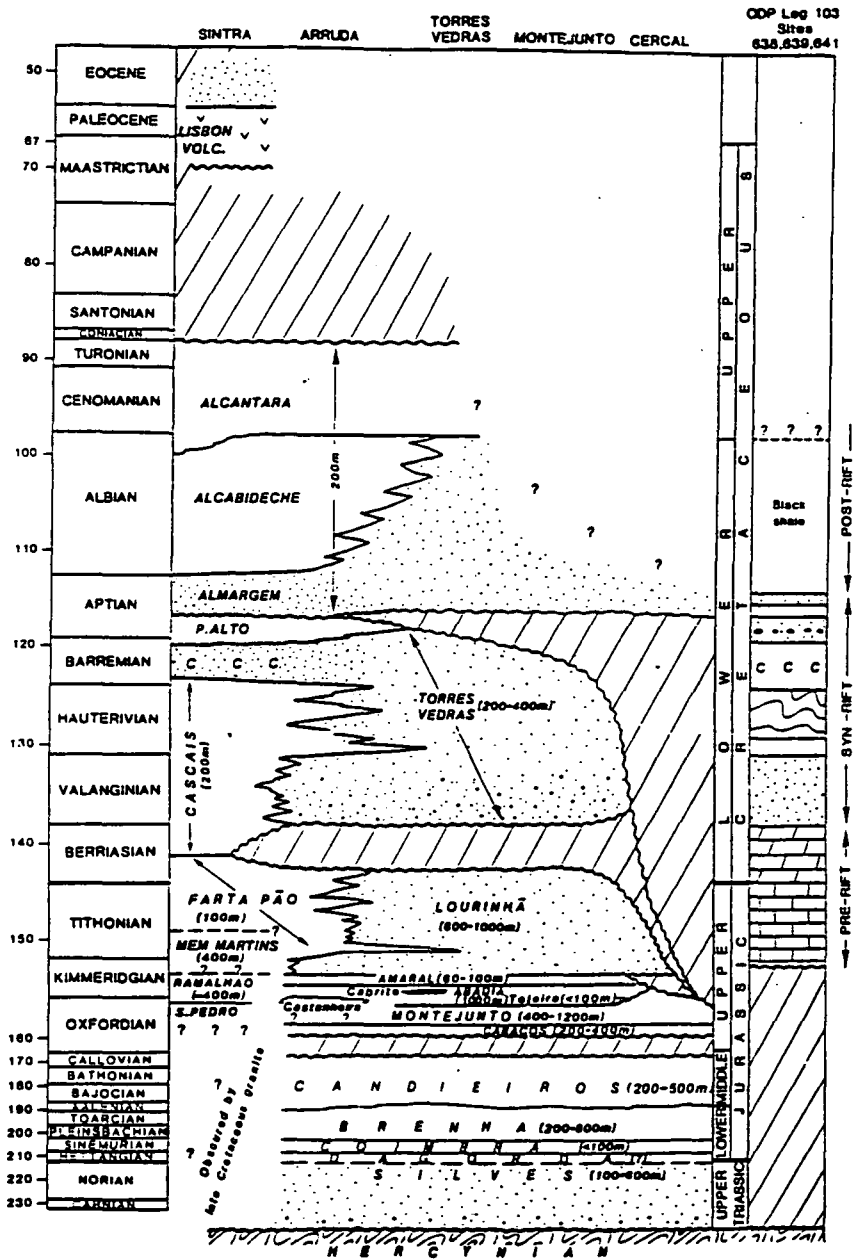


Figure 2.5 Summary of the Mesozoic and earliest Tertiary lithostratigraphy in the southern part of the Lusitanian Basin, and the succession drilled during ODP Leg 103 (from Wilson et al., 1990). Formations are shown in capitals, and members in lower-case letters. Note the five unconformity bounded sequences: (1) Upper Triassic - Upper Callovian; (2) Middle Oxfordian - Berriasian; (3) Valanginian - Lower Aptian; (4) Upper Aptian - Turonian; (5) Uppermost Cretaceous - Miocene

2.4.1 Aborted rift stage

Upper Triassic - Upper Callovian

The basal sequence is formed of Late Triassic fluviatile sediments of the Silves formation which lies unconformably upon the Hercynian basement. Overlying these sandy marls and sandstones are clays and evaporites of the Dagorda sequence, the age of which is subject to argument. Montenat et al., (1988) assigns a Carnian age to the Dagorda marls based on microflora, therefore indicating that the underlying evaporites are Triassic in age. However, Wilson et al., (1990) assigns a Hettangian (base Jurassic) age for the Dagorda sequence.

The Dagorda sequence is not uniformly deposited across the Lusitanian Basin. As mentioned ^{previously,} the distribution of halokinetic structures is interpreted to represent thickness variations, or localised depocentres, inferred to have formed in graben or half-graben structures. This in turn suggests that initial rifting and subsidence started possibly as early as the Late Triassic with the reactivation of NNE trending basement faults. These same faults may also have controlled the intrusion of Triassic mafic volcanics which are commonly associated with the halokinetic structures.

During the Lower to Middle Jurassic, open marine conditions prevailed across the Lusitanian Basin, with the deposition of marls interbedded with fine grained limestones. No abrupt lateral facies or thickness changes are seen in outcrop or on seismic section, instead, the Lower Jurassic shows a general northward thickening approximately coincident with the present day Atlantic coastline (Wright & Wilson, 1984). The absence of siliciclastic input in the east of the basin, within the Coimbra, Brenha, and Candeeiros formations, suggests that the marine carbonate conditions extended into the interior of Iberia. Wilson et al., (1990) suggest that the facies distributions within the Lower Jurassic formations indicate the presence of a westerly dipping carbonate ramp, as opposed to an easterly inclination as proposed by Montenat et al., (1988), with barrier-system ooid grainstones separating lagoonal and peritidal facies to the east, from deeper water micritic limestones and shales of the Brenha formation to the west. This carbonate ramp is believed to have been located above the

hanging wall of an easterly dipping bounding fault on the west of the basin (op. cit.). Faulting does not have a significant influence on the sedimentation except for the Nazaré fault which was active from the Middle Lias (Montenat et al., 1988). When the influences of the limited faulting are combined with the facies thickness and distribution, the Lower Jurassic sequence probably represents a regional sag due to thermal relaxation of the thinned lithosphere caused by the aborted Late Triassic rifting event, which appears to be combined with an element of extensional faulting.

By the Middle Jurassic (Toarcian and Aalenian), resedimented carbonate and siliciclastics, with a northwest derivation, were appearing within the basin indicating that the Berlegas horst block system, presently located offshore Peniché, was active. The Bajocian to Bathonian shallow water carbonates of the Candeeiros formation result from a long term Middle Jurassic sea-level fall which affected the carbonate ramp (Wilson et al., 1990)

The main control on the distribution of sedimentation during the Lower, and more importantly, the Middle Jurassic are the halokinetic structures, which initiated as early as the Toarcian along such structural lineaments as the Caldas de Rainha, Rio Maior/Candeeiros, and Torres Vedras salt ridges. These salt ridges formed above NNE and NE trending basement faults, forming steep asymmetric structures, displaying rim synclines along their steep eastern sides. The initiation of these salt ridges is evidenced by synsedimentary slumps on the flanks of the structures, and emersion of the capping facies. The thinning of Middle Jurassic sediments against the diapiric ridges indicate that the greatest halokinetic activity took place at this time (Montenat, op. cit.).

2.4.2 Successful rifting event

Middle Oxfordian to Berriasian

The absence of latest Callovian - early Oxfordian sediments represents the first megasequence boundary (Wilson et al., 1990), and forms a basin wide hiatus marking the beginning of a new tectonic setting, related to the early stages of the opening of the North Atlantic. The Middle Oxfordian sediments are commonly underlain by karstified

surfaces (Wright & Wilson, 1987). The lower parts of the mega-sequence are characterised by abrupt changes in facies and thickness, indicating the presence of localised fault and halokinetic movement. Several of the N-S trending faults, that are not easily related to the basement structures, subdivide the Lusitanian Basin into a number of sub-basins. These structures (e.g. Pragança, Sobral, and Alcochete faults) created a complex structural pattern consisting of half-grabens, as well as true horst and graben structures.

The post-hiatus Cabaços formation is dominated by lacustrine carbonates, characterised in the Serra dos Candeeiros region by lignite horizons. The Cabaços formation is overlain by marine carbonates of the Montejunto formation, within which two types of carbonate build-ups have formed (Ellis et al., 1990): Fault controlled build-ups on the east side of the basin, forming relatively thin (200-500m) sequences over tilted fault blocks. These build-ups display well developed lateral facies zonation and are dominated by lime mudstones and wackestones; the second form of build-up, salt controlled build-ups, are seen on the northwestern margin of the basin and are relatively thick (500-1500m) forming as rapidly subsiding salt withdrawal basins, dominated by grainstones and packstones that display only gradual lateral facies variations. During the latest Oxfordian - early Kimmeridgian, rejuvenation of the Berlengas block coincided with a sudden relative sea-level rise, drowning or partially drowning the carbonate build-ups and depositing dominantly marine marls (Abadia formation) with localised siliciclastic sediments (Tojeira member) over the entire basin (Leinfelder & Wilson, 1989). The upper Abadia formation is characterised in seismic sections by southward dipping clinoforms, indicating a southward prograding slope system (ibid.). The Abadia formation is believed to have formed at water depths of 200-500m (Stam, 1986), and coincided with the maximum rates of apparent basement subsidence (Wilson et al., 1990).

In the Arruda sub-basin, to the SE of Montejunto, 2200m of arkosic gravel filled the sub-basin during the lower Kimmeridgian at a rate of 850m^{m.y.}, which has been interpreted by Wilson et al., (op. cit.) to be a pull-apart basin. The presence of

NW-SE oriented dykes, and similarly oriented synsedimentary normal faults within the Serra dos Candeeiros region (Montenat et al., 1988), has lead Wilson et al. (1990) to propose a pulse of NE-SW lithosphere extension. This oblique extension is cited as the cause of the 'pull-apart' nature of the Arruda sub-basin, however, the sense of movement derived for the Montejunto fault (fig.18 in Wilson et al., 1990) is dextral, which clearly conflicts with the expected sinistral component of motion associated with such a fault configuration (figure 2.6). A sinistral system appears to explain the fault geometries and depositional pattern more adequately than the dextral, however, structures consistent with an early (late Oxfordian/Kimmeridgian) period of dextral transtension are present along the S. dos Candeeiros fault (section 3.2.1). In addition, the estimated extension direction associated with a dextral system correlates with that suggested by Dewey et al., 1989 (figure 2.6a).

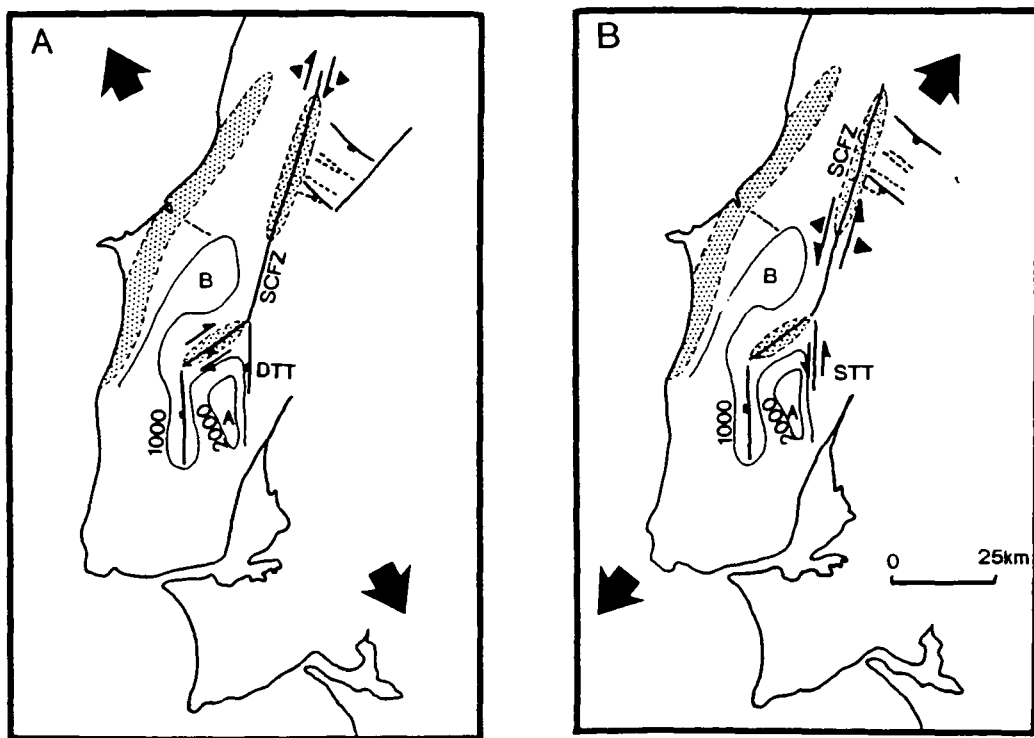


Figure 2.6 Kinematics of the Arruda sub-basin. (A) Dextral transtensional motion (DTT) along the S. dos Candeeiros fault (SCFZ), as suggested by Wilson et al., 1990 and this thesis. Arrows refer to suggested extension direction (Dewey et al., 1989). (B) The kinematics associated with the NE-SW extension indicated by Wilson et al., 1990. Sinistral transtension (STT). A, Arruda sub-basin, B, Bombarral sub-basin. Stipple refers to diapiric salt walls.

The effect of this extensional pulse was to trigger salt migration above reactivated basement faults during the Oxfordian and early Kimmeridgian, with fault movements only becoming significant in the Kimmeridgian. Stratigraphic constraint can be placed on age of these movements, as the Abadia formation does not thin over the Montejunto salt pillow or the Arruda sub-basin (Wilson, op. cit.) indicating that salt migration and fault movement in the Montejunto region, and along the Candeeiros salt ridge ceased in middle Kimmeridgian times. After the deposition of the upper Abadia formation thermal uplift of the basement occurred, counteracting the subsidence due to sediment loading. This late Kimmeridgian regressive period resulted in almost total emersion of the Lusitanian Basin, with the deposition of Portlandian aged red marls and continental fluvial sandstones that constitute the Lourinhã formation. The Lourinhã formation has a variable thickness due to the inherited structure of the basin, with over 400m of sediment deposited in the Bombarral sub-basin compared with their absence or reduced thickness on the structural highs, such as the Espigão plateau (Montenat et al., 1988). Tectonic activity appears to have been restricted to the south of the basin, with erosional processes prevailing in the northern half of the basin (ibid.).

By the end of this rifting event, the majority of structures presently seen within the Lusitanian Basin were already established (figure 2.7).

2.4.3 Post rift passive margin phase

The Valanginian-Lower Aptian, and Upper Aptian-Turonian mega-sequences

Both of these mega-sequences display very similar facies distributions, and hence will be discussed together. Both sequences are thin (200-300 metres) relative to their deep marine counterparts drilled off-shore northwest Iberia (Sibuet & Ryan, 1979; and Boillot et al., 1987). Onshore the sequences consist of fluvial sands in the north, that became replaced to the south by marine marls and rudist limestones (Wilson et al., 1990). Within the Serra dos Candeeiros and Montejunto study areas, these mega-sequences are undifferentiated, and in the case of the Candeeiros region the presence

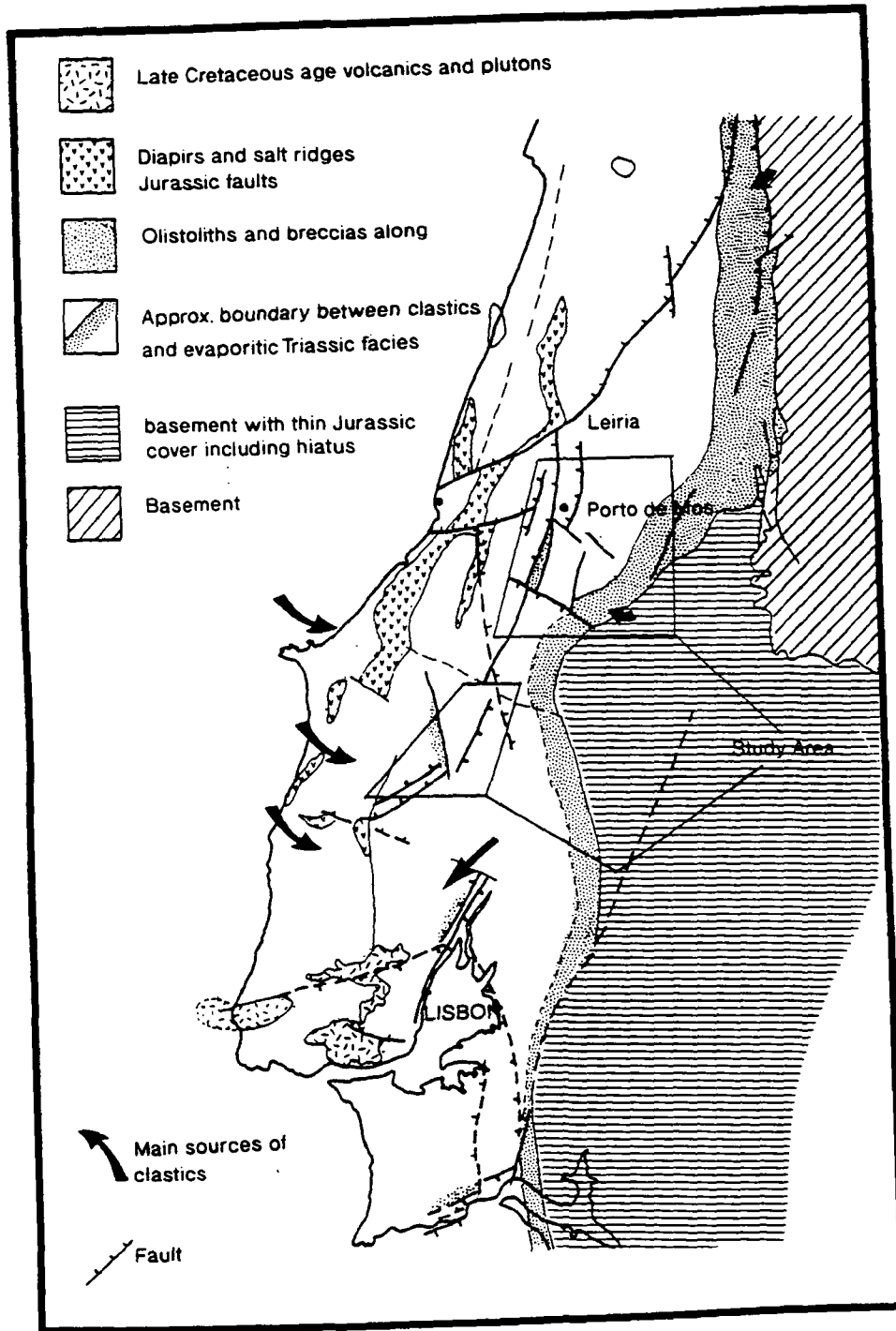


figure 2.7 Mesozoic structural framework of the Lusitanian Basin, at 80-70Ma (Late Cretaceous). Boxes highlight the southern Montejunto region, and the Candeeiros block region. Note that the major structures of the S. de Montejunto-Candeeiros faults system are already defined. (Compiled from Montenat et al., 1988; and Wilson et al., 1990).

of the Neocomian (i.e. Valanginian-Lower Aptian) mega-sequence is uncertain. However, in both regions the sequences lie unconformably on strata ranging from Middle Jurassic to Portlandian in age. The Cretaceous sequences have a characteristic yellow / gold weathering colour within the Candeeiros region, and are formed of coarse grained sandstones with intercalated conglomerates and purple marl horizons. In the Montejunto region the Cretaceous is characteristically a red coloured coarse grained sandstone. The extent of these Cretaceous facies was controlled by the variable degree of transgression, with marine deposits restricted to the west of a line running from Torres Vedras through Lisbon, to Sezimbra (Montenat et al., 1988). The unconformities found at the base of these mega-sequences increase in magnitude in the eastern margin of the Lusitanian Basin, suggesting that continued movement along the basin-bounding faults was occurring, which are related to the onset of rifting and ocean opening documented further to the west by ODP Leg 103 results (Wilson et al., op. cit.). The presence of late Mesozoic and early Tertiary igneous activity, and the lack of significant subsidence during these periods indicates that very little post-rift thermal subsidence took place in the Lusitanian Basin, which lead Wilson (1988), and Montenat et al. (1988) to suggest an upper-plate passive-margin setting for the onshore Lusitanian basin at this time.

2.4.4 Emergence and tectonic inversion of the Lusitanian Basin

Latest Cretaceous - Miocene

During the Cretaceous-Miocene period significant compressional events occurred along the various margins of Iberia, ending the typical passive margin setting of western Iberia (Rehault and Mauffret, 1979). Along the northern margin the first compressional events of the Pyrenean orogeny occurred in the Late Cretaceous as Iberia began its 100km northwestward movement toward Europe, which continued into the Paleocene with ocean crust subduction (Boillot, 1984). The culmination of this mountain building phase occurred during the Eocene with Pyrenean nappe emplacement.

The focus of deformation changed to the southern margin of Iberia during early Oligocene times, with the onset of subduction beneath the Betics. This period of compression is marked by north-south nappe emplacement during the early Miocene (25-15Ma), which was followed by major thrusting during the Tortonian (Leblanc & Oliver, 1984). The Miocene age of these Betic compressional events is clearly evidenced in the Arrábida region south of Lisbon, where unconformable middle Miocene and Plio-Pleistocene sediments overlie folded Jurassic to Lower Miocene strata, which are themselves cut by a reverse fault carrying Middle Jurassic carbonates in its hanging wall (Choffat, 1908). In post-Tortonian times, c.9Ma (Dewey et al., 1989), the regional compressive stress rotated to a NNW-SSE orientation across the Lusitanian Basin (Ribeiro et al., 1988), which according to Hutton & Gawthorpe (1988), and Wilson et al. (1990) induced transpression along the NNE-SSW oriented structures of the Lusitanian Basin. The timing of this Miocene deformation has not been so tightly constrained within the Lusitanian Basin as it has been in the Arrábida region, but the detailed structural and kinematic analysis of several of the major basin structures allows the deformation to be dated relatively between the Middle Miocene and possibly the Recent (see sections 3.8 and 4.5, this thesis).

This complex period of superimposition of compressive stresses is reflected in the stratigraphy of the basin during this time period. During the Turonian the whole of the area between the Nazaré fault and Arrábida emerged causing a depositional hiatus in the southern half of the basin which spanned the uppermost Cretaceous. The only deposition during this period occurred to the north of the Nazaré transform fault, where marine siliciclastic sediments are found. The end of this period of emergence is marked by the intrusion of the Sintra granite, 68 Ma (Ribeiro et al., 1979), and the basaltic lava flows of Lisbon, which are mainly Paleocene in age (Wilson et al., 1990). Sedimentation resumed during the Eocene, with thick clastics deposited south of the River Tagus, however, the sequence is thin or absent within the northern study areas of Serra de Montejunto, and the Serra dos Candeeiros - Serra D'Aire. In the Alcanede region of the Serra dos Candeeiros area, the Oligocene sequence crops out along the

Alcanede fault zone as a thin (200 m+), unconformable sequence, the base of which is locally formed by a 20-30m thick carbonate unit. This limestone unit consists of micrite with occasional marly layers, which gives way to a heavily, non-tectonically, brecciated upper surface which probably represents a karstified surface. Overlying this emergent surface are coarse grained sandstones and conglomerates that have a basement provenance.

The Lower Tagus Sub-basin, and to a lesser extent the Monte Real Sub-basin, possess between 1000 metres (Wilson et al., 1990) and 1400 metres (Dunod, 1980) of Miocene siliciclastic sediments, which alternate from coarse sandstones to silty mudstones (Ribeiro et al., 1979). Carbonate horizons become increasingly more significant towards the top of the Miocene, reflecting the maximums of late Miocene marine transgressions. In the Lisbon area, the Miocene sequence displays a depositional hiatus during late Tortonian and Messinian times (Ribeiro et al., 1979) which may correspond to the onset of inversion tectonics, especially within the central area of the Basin (see Chapter 6). Based on the thermal maturation studies of Middle and Upper Jurassic organic matter by Willis (1988), Wilson et al. (1990) suggest that the central inversion zone of the Lusitanian Basin may have been buried by 1000 metres of Miocene sediments, which in turn suggests significant uplift has occurred to remove this Miocene overburden and produce the present day mountain ranges of up to 677 metres in height (Serra D'Aire).

The deformation and kinematics of this Miocene inversion event will be discussed in the following chapters, based on extensive fieldwork in the S. dos Candeeiros and S. de Montejunto regions, and integrated with geophysical data to produce a new tectonic model for the Lusitanian Basin.

CHAPTER 3

The structure and kinematics of the Serra dos Candeeiros region

“Traditionally, structural geologists have been preoccupied with the complexity of the finite deformation within fault zones and with the stress states prevailing at the initiation of faults in intact crust. Future work should be directed more towards understanding the dynamic character of fault reactivation during incremental slip, and related effects.”

(Richard H.Sibson, 1989)

3.1 Introduction

The town of Porto de Mós is located approximately 35km due south of the city of Leiria, and lies along the western edge of a narrow zone of uplifted Mesozoic carbonates, that form two fault bounded blocks (Figure 3.1). The southern block (Candeeiros block) has dimensions of approximately 15x20km, producing a plateau between 250 and 600 metres high. The adjacent northern block has produced a similar plateau and contains the largest mountain in central and southern Portugal, Serra D'Aire (677 metres). Both of these blocks testify to the uplift and inversion that has occurred within the Lusitanian basin during the Miocene period. The internal geometry of the blocks is remarkably undeformed in contrast to the block boundaries which display complex kinematic and strain histories. The aim of this chapter is to characterise the deformation style within the bounding faults of the Candeeiros block, paying particular attention to the kinematics of both macro and mesoscale structures. As the deformation within the cover of the Lusitanian basin has occurred within the upper 2km of the crust, many of the strains preserved are incremental and have later become passively rotated either by folding, or block rotation. Therefore, the detailed structural study of these fault zones has enabled the construction of the relative structural and kinematic evolution of the Candeeiros block.

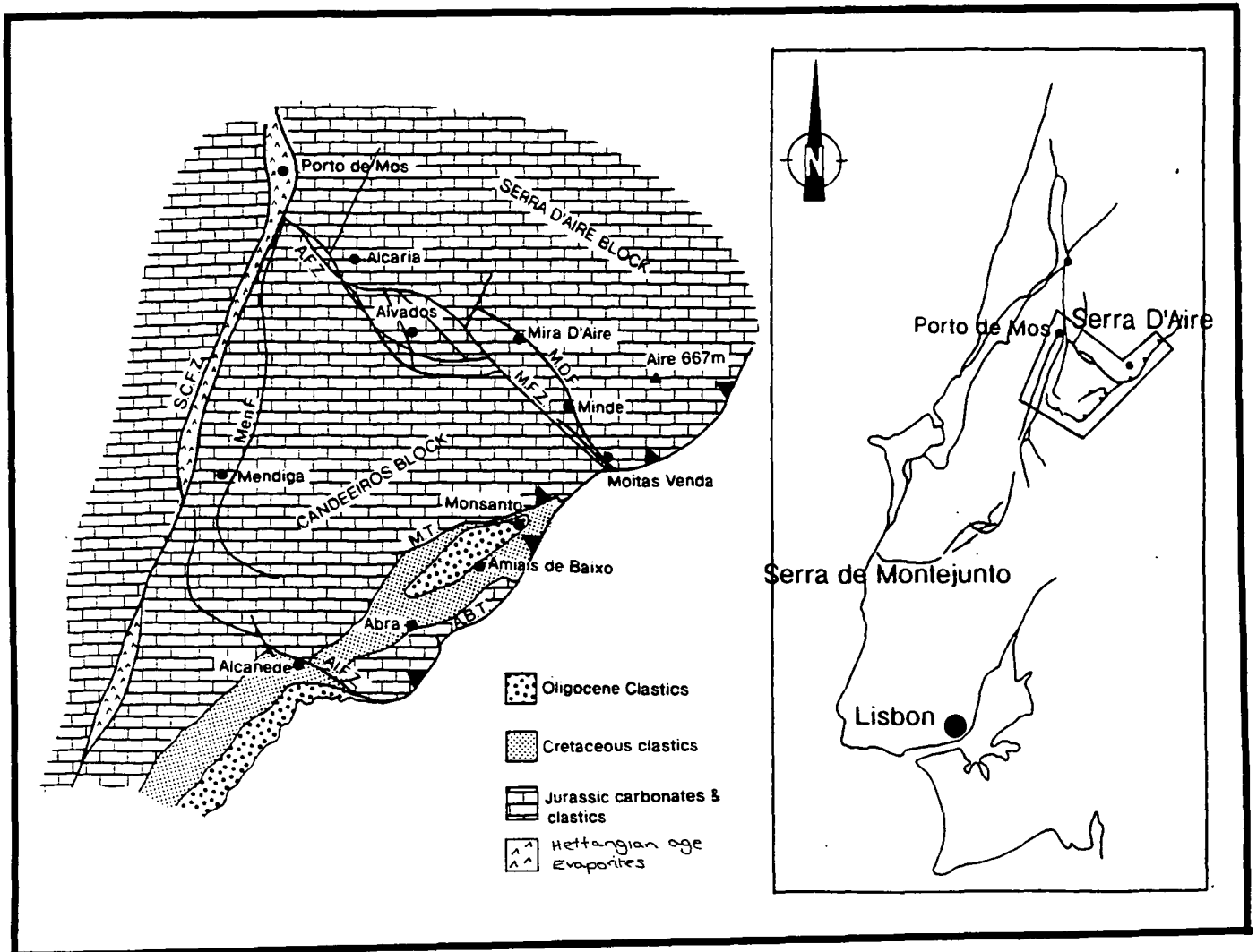


Figure 3.1 General geological map of the Porto de Mós, and Serra dos Candeeiros region displaying the main towns (solid dots) and main faults: S.C.F.Z., Serra dos Candeeiros fault zone; A.F.Z., Alvados fault zone; M.F.Z., Minde fault zone; M.D.F., Mira D'Aire fault; M.T., Monsanto thrust; A.B.T., Amiais de Baixo thrust; Al.F.Z., Alcanede fault zone, Men.F., Mendiga fault.

3.2 Serra dos Candeeiros Fault

3.2.1 The pre-Miocene history of the Serra dos Candeeiros fault

The NNE-SSW oriented Serra dos Candeeiros fault zone (S. dos Candeeiros fault zone) extends approximately 70km from Leiria in the north to Cercal in the south. Along the northern half of its trace the fault zone is marked by a pronounced topographic scar formed, due to the presence of Hettangian aged Dagorda evaporites intruded along its trace (Rio Maior or Candeeiros salt wall). The presence of

evaporites within the fault zone is virtually continuous from Leiria to Rio Maior (Figure 3.1). The S. dos Candeeiros fault zone forms one of several significant north-northeast trending faults, along which halokinetic structures occur. The spatial distribution of these faults is controlled by the Mesozoic extensional reactivation of Hercynian age basement shear zones on the same trend. Synsedimentary extensional faulting and halokinetic movement occurred along the S. dos Candeeiros fault zone as early as the Toarcian producing the Candeeiros anticlinal ridge in the hanging wall, parallel to the fault zone (Montenat et al., 1988). Wilson et al., (1990), in an attempt to explain the Arruda sub-basin as a pull-apart, imply that the S. dos Candeeiros fault zone may have possessed a dextral component of motion during the Late Jurassic. Most of the extensional and possible transtensional fault movement occurred during the Late Jurassic, and maybe into the Cretaceous. The Mesozoic extensional history of the S. dos Candeeiros fault zone is probably represented by the preservation of large amounts of calcite extensional vein systems, that have since undergone extensive faulting and pressure solution during Miocene to Recent reactivation (see 3.2.3). The calcite is present in three forms: massive calcite, distinct calcite zones coating hydraulically brecciated wall rock clasts, and earlier generations of calcite, and as thick (up to 10cm wide) discrete calcite veins with oblique crystal growth.

Mesoscopic structural field evidence supporting a pre-Miocene period of dextral transtension, as suggested by Wilson et al., (1990), is meagre. At Serra de Lua, a pair of gentle anticlines are present in the Oxfordian argillaceous limestones, that describe an anti-clockwise fold axis to fault zone angle (θ') of 63° . Such high angles for θ' suggests a dextral transtensional deformation style (Sanderson & Marchini, 1986; and Little, 1992). Rare examples of dextral transtensional calcite veins are also present along the outer extremes of the fault zone (plate 3.1). The age of these dextral structures is difficult to constrain. As will be demonstrated in section 3.2.2, the S. dos Candeeiros fault system had a consistent sinistral strike-slip history from the Miocene to Recent, therefore, the dextral structures are unlikely to be of the same age and are thus earlier and of pre-Miocene age. The anomalous presence of numerous northeast verging thrusts along the S. dos Candeeiros fault zone west of Serro Ventoso are consistent in both geometry, and principal displacement direction, with a dextral transtensional incremental strain. The thrusts truncate the sub-vertically bedded Oxfordian limestones, formed by the forceful asymmetric emplacement and development of the Candeeiros salt wall (Montenat, 1988), indicating that dextral transtension was operative until at least the full development of the Rio Maior salt wall, and lithification of the Oxfordian strata. The development of contractional structures within a transtensional environment may be explained by the buoyancy force of the emplacing salt wall being in excess of the extensional tectonic force,



Plate 3.1 Oblique calcite crystal growth in a fault parallel vein along the outer extreme of the S. dos Candeeiros fault zone, suggesting dextral transtension, location: Serra de Lua.

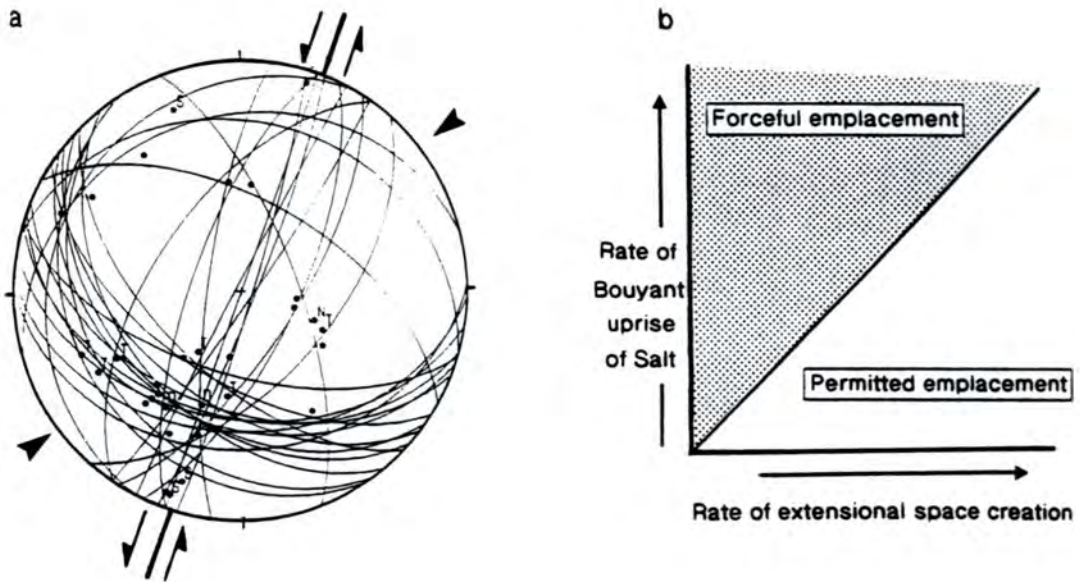


Figure 3.2 a) Equal area stereonet revealing highly oblique thrust faults to the S. dos Candeeiros fault zone. Geometry and sense of obliquity of the thrusts to the SCFZ implies dextral transtension. b) Simplified relationship between halokinetic buoyancy forces and strain rates, and extensional tectonic 'space creating' rates. Salt ridge along the SCFZ will plot in the stippled field. Modified from Hutton, 1988.

resulting in the localisation of shortening across the fault zone which, coupled with the dextral shear component of the transtensional tectonics, produced dextral contractional structures (Figure 3.2).

3.2.2 Kinematics of Serra Dos Candeeiros fault

Kinematic analysis of the S. dos Candeeiros fault was carried out mainly on the eastern fault contact between the Dagorda evaporites and the Oxfordian wall rocks, along a composite length of road cuttings totalling 450 metres. In these road cuts 197 measurements of fault plane orientations and slickenline lineations for mesoscopic faults were recorded. Where it was possible to determine, the sense of shear was also recorded. Shear sense was determined using the following characteristics: consistent accretion steps on mineralised fault surfaces (Hancock, 1985), debris trails (Means, 1987), erosional shelter behind asperites, plough marks (Petit, 1987; and Means, 1987), slickolite spikes (Means, 1987; and Bretz, 1940), 'T' and 'R' criteria, and crescentic tension fractures (Petit, 1987). To a lesser extent: en-echelon folding (Wilcox et al., 1973), oblique tectonic cleavages, visible offsets, asymmetries of fault zone clasts or "bull nose" clasts (Skempton, 1966), and mesoscopic fault relationships i.e. Horse-tails (Segall and Pollard, 1983), and bridge structures (Gamond, 1987) were used (See section 1.3).

3.2.2.1 Kinematics derived from mesoscopic and secondary faults

Mesoscopic faults measured along these road cuts can be split into several sets based on fault orientation and shear sense. One set occurs parallel to the main fault trace, with several en-echelon faults sets oblique to it.

A total of 32 fault zone parallel 'Y' shear plane surfaces were measured, the statistical mean strike of which is 031.6° . These measurements compare very favourably with the orientation of the fault trace measured directly from the Portuguese 1:50,000 geological map (031°). Where the sense of shear could be determined, all 'Y' shears displayed a sinistral sense of offset. However, the 'Y' shears do not display pure strike-slip motion, since a minor component of dip-slip is present within the fault zone (plate 3.2). The mean lineation vector for 14 sinistral slickenlines measured on 'Y' shear planes is $12^\circ/200$ (figure 3.3a).

The most consistent oblique mesoscopic fault set consists of synthetic sinistral faults that form an angle of $40-50^\circ$ anti-clockwise of the 'Y' shears. These synthetic faults correspond to Riedel or 'R' shears observed in numerous simple shear experiments (Cloos, 1928; Riedel, 1929; Tchalenko, 1970; and Naylor et al., 1984). Rare antithetic dextral shears are present oriented between $85-95^\circ$ anti-clockwise of the 'Y' shear orientation, and correspond to antiriedel or 'R' faults. These two sets form

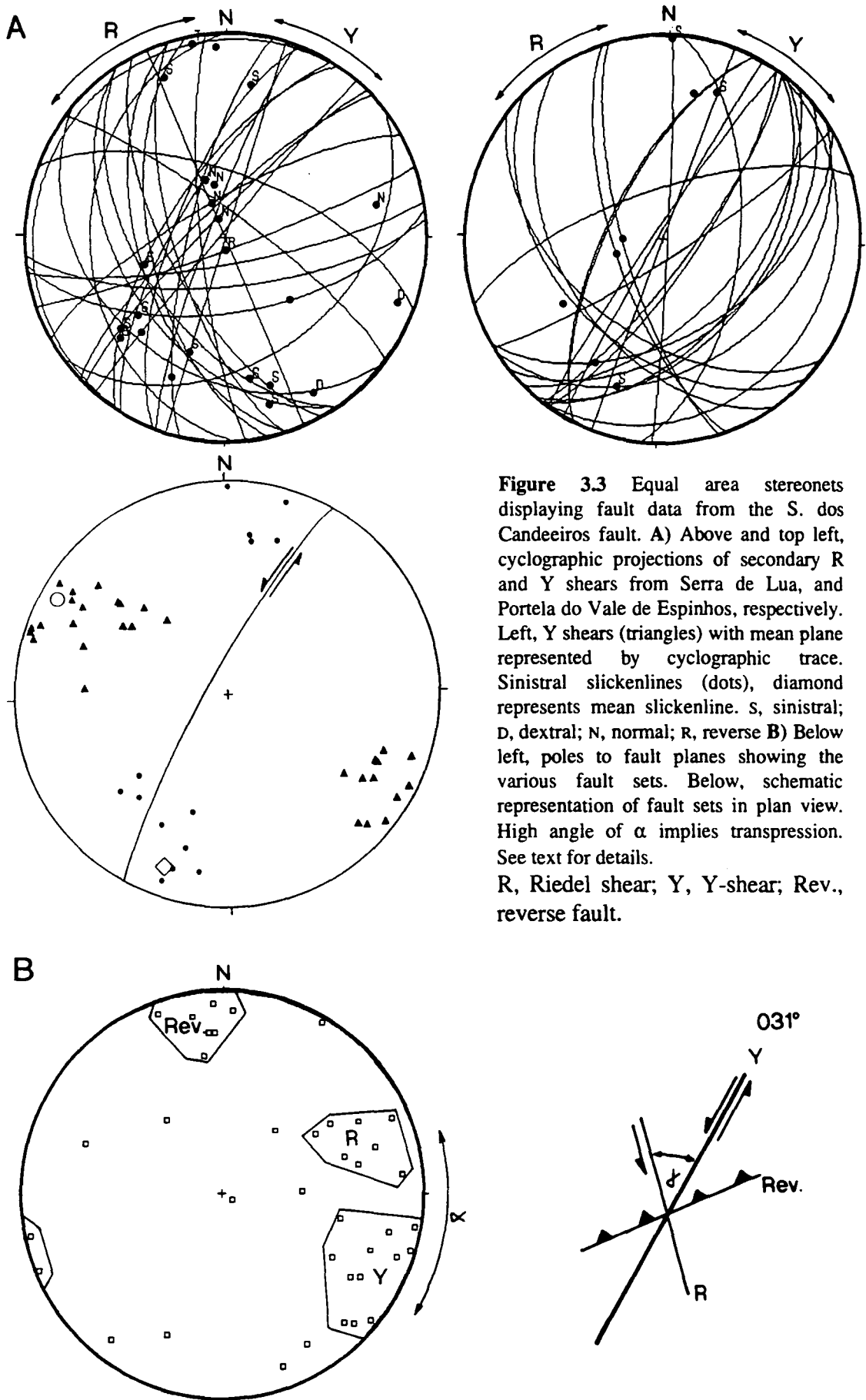


Figure 3.3 Equal area stereonets displaying fault data from the S. dos Candeeiros fault. A) Above and top left, cyclographic projections of secondary R and Y shears from Serra de Lua, and Portela do Vale de Espinhos, respectively. Left, Y shears (triangles) with mean plane represented by cyclographic trace. Sinistral slickenlines (dots), diamond represents mean slickenline. S, sinistral; D, dextral; N, normal; R, reverse B) Below left, poles to fault planes showing the various fault sets. Below, schematic representation of fault sets in plan view. High angle of α implies transpression. See text for details. R, Riedel shear; Y, Y-shear; Rev., reverse fault.

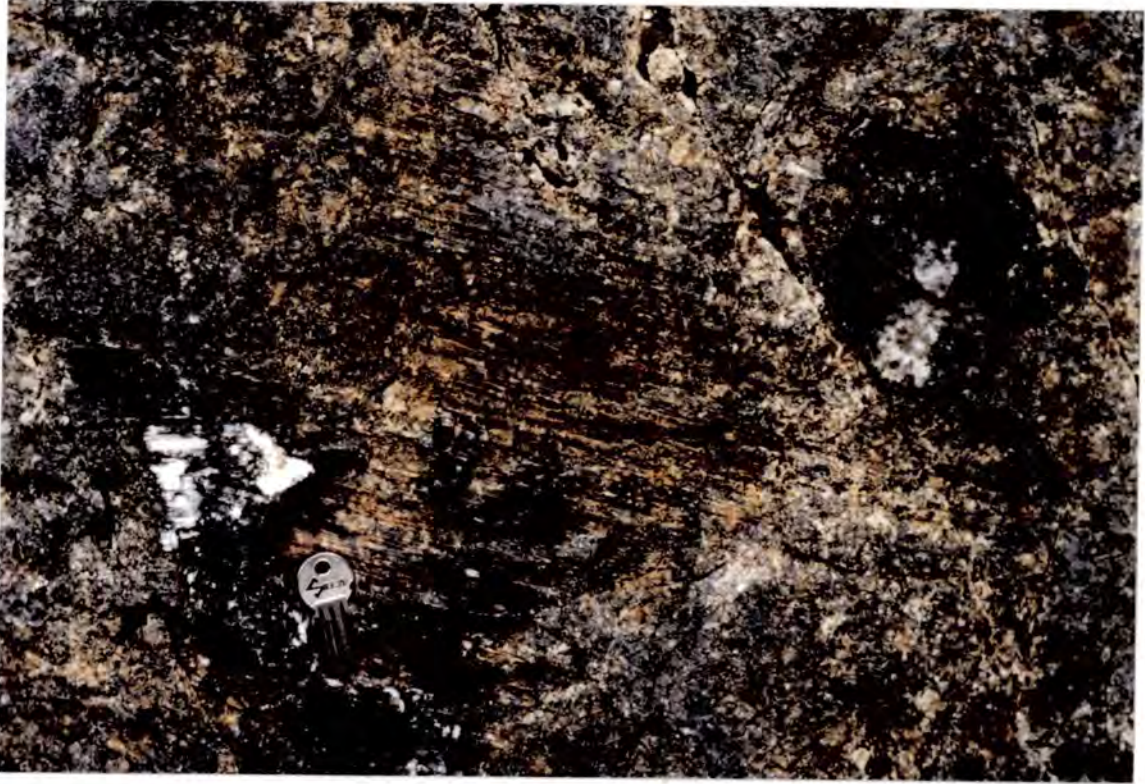


Plate 3.2 Sinistral calcite accretionary steps on a Y-fault plane, along the S. dos Candeeiros fault zone. Photograph looking toward the ESE.

an asymmetrical development of conjugate en-echelon faults characteristic of rotational shear, and consistent with sinistral strike-slip motion.

In addition to the three sets of strike-slip faults, two dip-slip sets are present, albeit in reduced numbers. Thrust and reverse faults define a 10-40° clockwise angle to the 'Y' shears, with slickenlines indicating a NW-SE direction of thrust transport. Extensional faults define a 50-60° anti-clockwise angle to the 'Y' shears, and a NE-SW extension direction (figure 3.3b). These fault sets are also consistent with sinistral motion.

3.2.2.2 En-echelon folding

En-echelon folds are an extremely common and characteristic structural feature of most ancient and recent strike-slip and transpressional fault zones (Wilcox et al., 1973; Harding, 1973; Aydin & Page, 1984; Sylvester, 1988; Little, 1990; 1992; Sanderson & Marchini, 1984; and Burgmann, 1991). However, they are not very common along the S. dos Candeeiros fault zone, with only small isolated oblique folds mapped along the fault trace between Porto de Mós and Portela do Vale de Espinho. The only example of an en-echelon fold array was observed at Serra de Lua along a short (2km) segment of the S. dos Candeeiros fault where no evaporites are present along the fault zone.

The folds vary from gentle to open with axes several tens of metres in length. They describe a mean clockwise θ' angle (fold axis to fault angle) of 32° , again consistent with a sinistral sense of motion.

The paucity of en-echelon folds may be due to the presence of the salt wall, which intruded along the S. dos Candeeiros fault during the Late Jurassic. The evaporites within the fault zone may have represented a mechanically weak, and easily deformable material therefore making it unnecessary for high threshold strains to develop before fault movement took place (i.e. preventing low strain rate folding in the wall rocks). The evaporites therefore, effectively lower the fault zone shearing resistance (f). Where no evaporites occur within the fault zone, the increased shear resistance induces fault-drag en-echelon folding. Hence, the effect and presence of evaporitic material along the fault zone may explain the localised development of fold arrays. A similar mechanism involving the factoring of relative plate motions into independent components based on the variation in shear stress has been proposed by Mount & Suppe (1987) for the San Andreas fault zone. The authors suggest that strike-slip zones with low shear stresses effectively behave as an 'almost free surface'.

Wall rock anisotropy may also contribute to the scarcity of folds, as the sub-vertical fault parallel bedding produced by Late Jurassic evaporite diapirism, may lie in a mechanically unfavourable orientation for the development of en-echelon folding.

3.2.2.3 Cleavage

Cleavage is largely absent in the wall rocks, but where present it forms a weak, spaced cleavage within the argillaceous limestones of the Oxfordian, and tectonic stylolites within more pure limestone lithologies. The cleavage lies at an oblique clockwise angle to the S. dos Candeeiros fault zone, with a mean orientation 080/82 NW (Figure 3.4) indicating sinistral displacement along the S. dos Candeeiros fault zone.

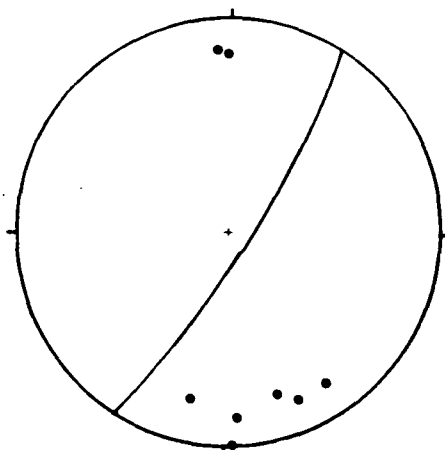


Figure 3.4 Poles to cleavage planes (solid circles) from Serra dos Casais, adjacent to the S. dos Candeeiros fault zone (SCFZ). The clockwise obliquity of the cleavage relative to the mean fault orientation (cyclographic trace) indicates a sinistral sense of displacement for the SCFZ.

3.2.3 Cleavage development and fold relationship

The cleavage defines a 32° clockwise transection angle with the fold axis of the Serra dos Casais (S. dos Casais) syncline which is itself obliquely clockwise to the S. dos

Candeeiros fault. Several authors have discussed the implications for the kinematic and strain evolution of cleavage transected folds (Murphy, 1985; Soper, 1986; Borradaile, 1978; Soper and Hutton, 1984; Treagus and Treagus, 1981; and Sanderson et al., 1980). The formation of contemporaneous transecting cleavage may be produced by the superimposition of two geometric systems: coaxial strain on bedding not initially parallel to the principal strain plane, and, non coaxial strains on originally orthogonal bedding, or by a combination of these two end member geometries (Soper, 1986). The cleavage transection associated with the Serra dos Casais syncline falls in the latter of the possibilities. The S. dos Casais syncline was originally a large fault-zone-parallel overturned syncline, related to halokinesis along the S. dos Candeeiros fault zone during the Upper Jurassic. Subsequent Late Miocene reactivation superimposed a sinistral transpressive incremental strain across the S. dos Candeeiros fault zone (see this chapter 3.8.1). Rotation of the syncline was possibly induced by a synthetic fault splay that formed a strike-slip duplex adjacent to the northeast trace of the syncline. Figure 3.5a shows the deformation associated with the duplex formation, clearly there is a striking similarity between the theoretical and observed structure.

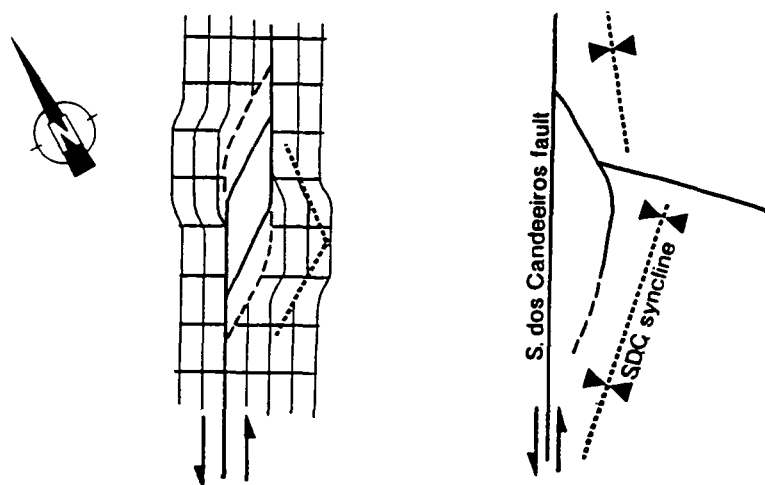


Figure 3.5a A comparison of the observed structural geometry of the Serra dos Casais syncline (SDC), and theoretical wallrock deformation associated with strike-slip duplex formation (top), from Woodcock & Fischer, 1986.

The pattern of cleavage transection suggests that it was formed by the superimposition of incremental strains onto the passively rotating syncline. Successive later increments of cleavage have increasingly lower transection angles as the rotating fold approaches parallelism with the incremental XY plane of the strain ellipsoid. If this cleavage spread does represent the incremental rotation of the fold, it suggests a 38° clockwise rotation. This figure seems plausible when compared with the orientation of the northern end of the S. dos Casais synclinal axis which indicates a 35° clockwise rotation. The rocks do not display a penetrative deformation fabric, indicating that the

rotation did not occur by bulk deformation, instead the rotation appears to have been facilitated by an accommodation fault trending NW-SE, allowing a rigid block to rotate passively (Figure 3.5b).

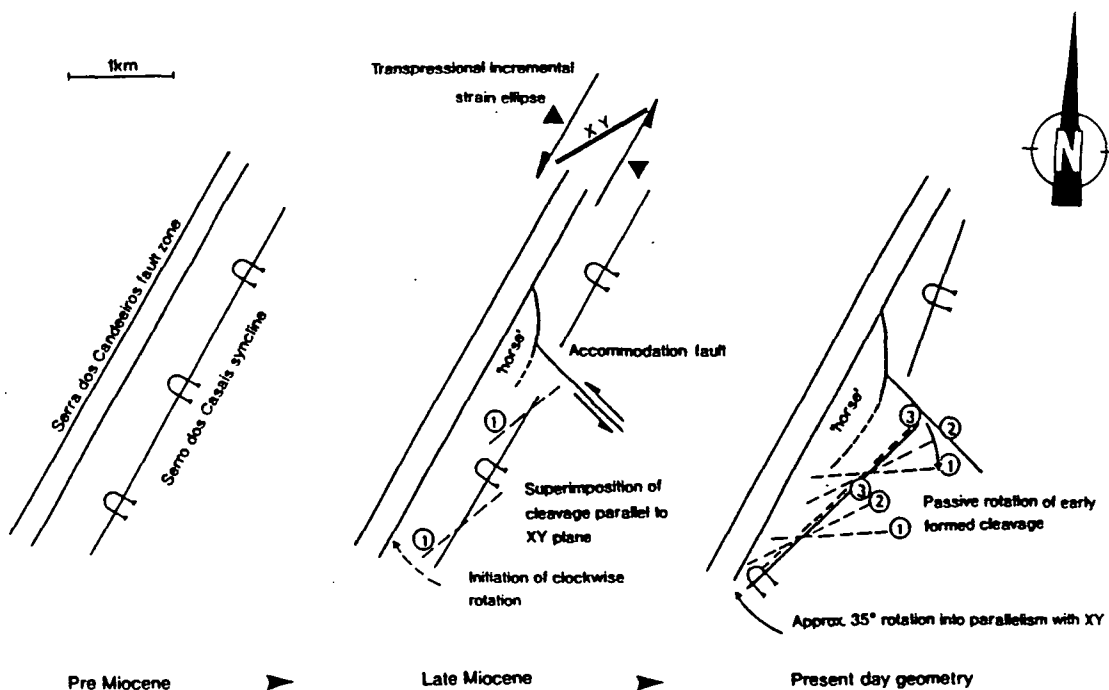


Figure 3.5b Model for the structural evolution of the Serra dos Casais syncline, and development of cleavage transection relationships.

3.2.4 Deformation style of Serra dos Candeeiros fault

Data pertaining to the kinematics of this fault have been described above (section 3.2.2). However, the oblique en-echelon folds and secondary fault sets do not conform to the observed and experimentally derived geometries and structural orientations for a simple shear system (Various authors, section 1.1.3). Experimental results show that for a sinistral simple shear system Riedel or R shears initiate at an average anti-clockwise angle of 12° (Tchalenko, 1970) to $17\text{--}20^\circ$ (Naylor et al., 1986), and that Antiriedel or R' faults strike approximately 72° anti-clockwise of the fault trace (Naylor et al., 1986). Clearly the observed secondary faults present along the S. dos Candeeiros fault have a strike at least 20° greater than is predicted. The orientations of reverse/thrust faults ($<45^\circ$) and extensional faults ($>45^\circ$) also conflict with a simple shear system. These geometric relationships can be explained by using a simple transpressive model as proposed by Sanderson and Marchini (1984). In the case of simple transpression the incremental strain ellipse has a Z axis (maximum principal axis of shortening) at an angle $>45^\circ$ to the fault zone. Riedel faults or shears will develop with orientations much greater than the $12\text{--}20^\circ$ seen in simple shear systems, likewise

Antiriedel faults will be oriented $> 72^\circ$ anti-clockwise of the fault zone. Contractional and dilational structures will form perpendicular and parallel to the Z axis respectively. In simple shear experiments en-echelon folds have been shown to form early in the deformation of a fault or shear zone (Wilcox, 1973), at an initiation angle of approximately 45° . The low ($<45^\circ$) clockwise fold axis to fault angle (θ') of the fold array, relative to their open to gentle interlimb angles, indicates a sinistral transpressive motion for the S. dos Candeeiros fault zone (Little, 1992).

3.3 The Alvados-Minde fault system

The Alvados-Minde fault system can be traced from the town of Porto de Mós southeast to Moitas Venda along a length of approximately 17 km. The fault system is composed of two major left stepping faults (Alvados and Minde faults), the traces of which are marked by pronounced fault scarps. Wilson et al., (1990) suggest that both the Alvados and Minde faults were originally Late Jurassic extensional faults, which became reactivated during the Miocene. In the stepover zone between these two overlapping faults is a rhombohedral arrangement of faults, dominantly oriented along an east-west trend (Figure 3.6). Again these faults have a prominent topographic expression that is suggestive of their neotectonic nature (Cabral and Ribeiro, 1988).

3.3.1 The Alvados fault zone

The Alvados fault zone forms a northwest to southeast trending compound fault zone, bounding a tectonic sliver of Bathonian and Oxfordian aged limestones. The sliver varies in width from 200m to 5m, and forms a pronounced topographic lineament (plate 3.3). The fault zone has been exposed by quarrying behind the Restaurante Bela Vista near Alcaria, forming a superb transverse section (Figure 3.7). The fault zone displays a complex array of mesoscopic faults bounded by two upward divergent faults, whose gross geometry is reminiscent of a flower or palm tree structure (Wilcox et al., 1973, and Sylvester & Smith, 1976, respectively). Open to close upright folds are present in the Aalenian aged shales and argillaceous limestones bordering the southwest side of the fault zone. Although data collection was greatly impeded due to the inaccessibility of the outcrop, the measurements obtained revealed that the folds have sub-horizontal hinges that describe a 20° anti-clockwise angle to the Alvados fault zone. Tectonic stylolites from the SW edge of the Alvados fault

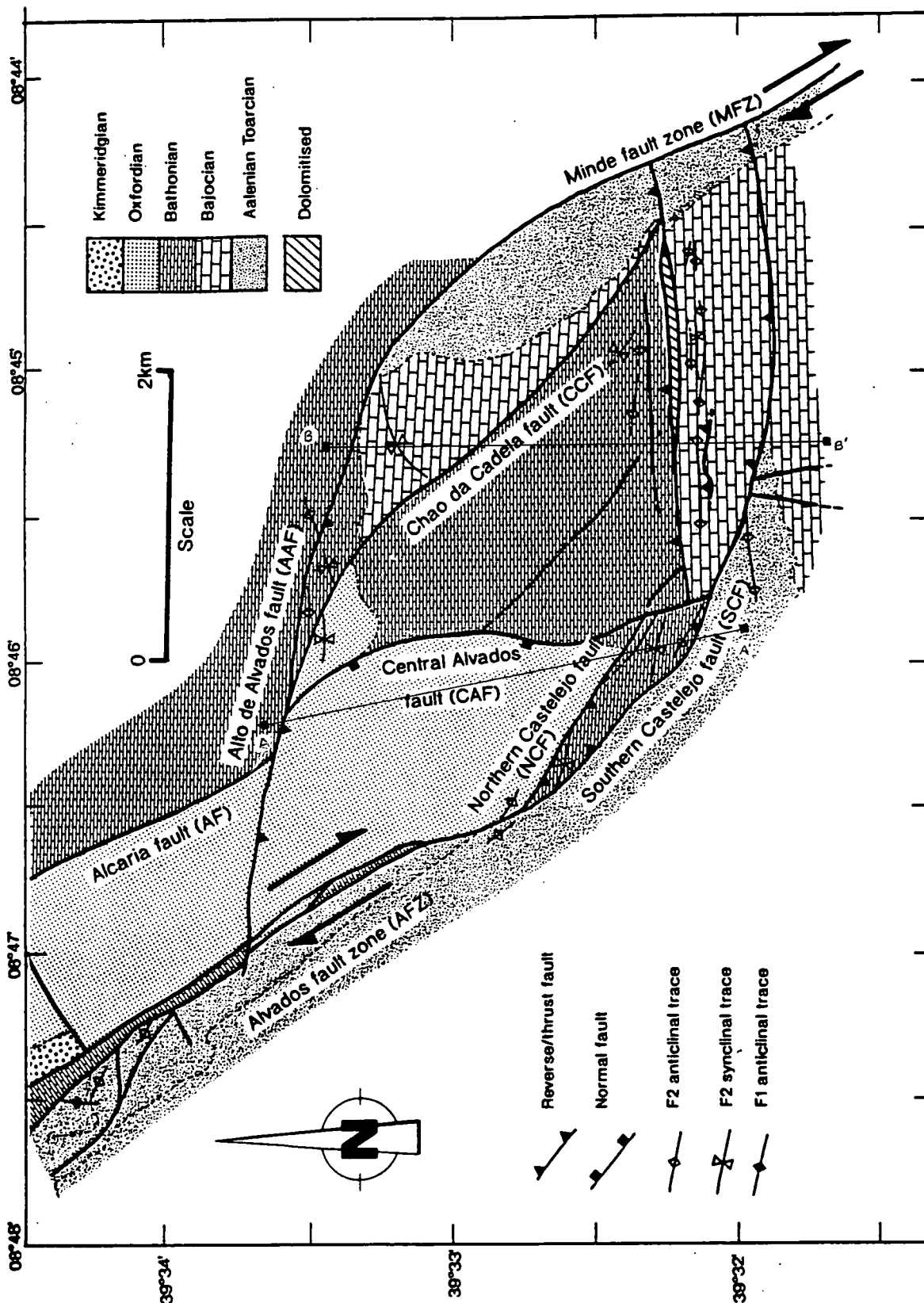


Figure 3.6 General geological and structural map of the inverted Alvados pull-apart basin. The kinematics associated with each fault refers to the most recent identifiable sense of motion.

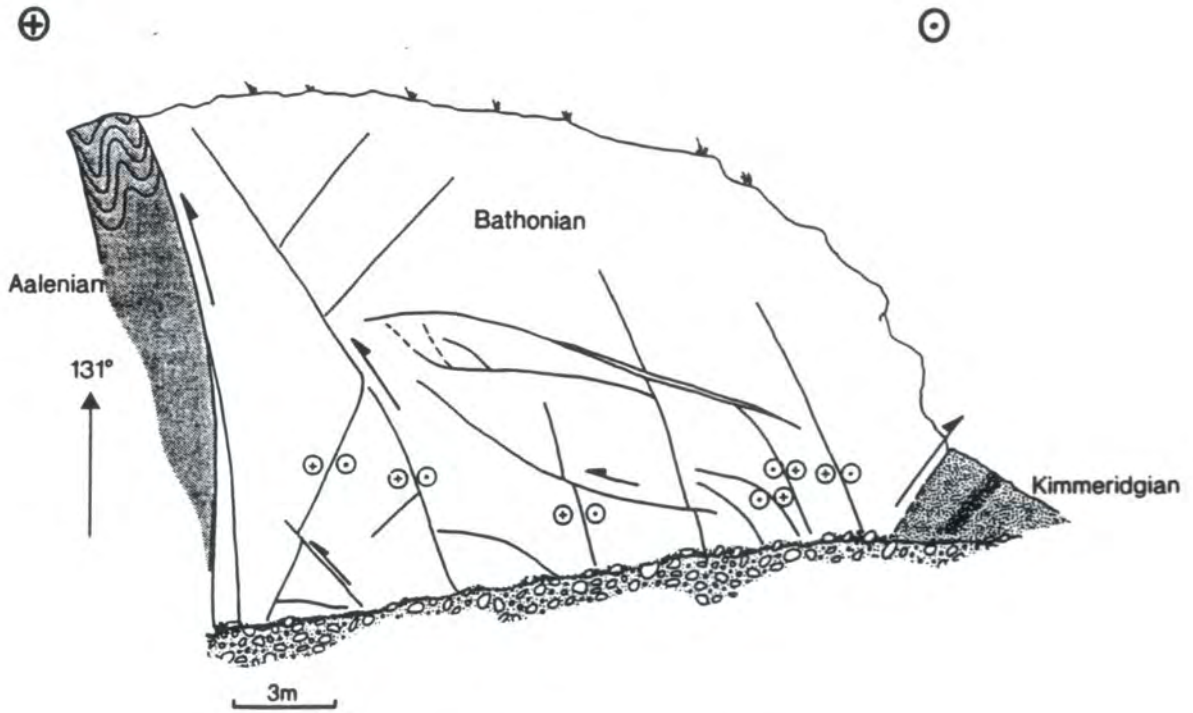


Figure 3.7 Traverse across the Alvados fault zone, immediately behind the Bela Vista Restaurante, Alcaria. Note the downward convergent nature of the boundary faults, and the shallowing upwards of the Bathonian/Aalenian boundary fault.



Plate 3.3 View looking due south from the triangulation point (423m) on Pragosa, towards the Alvados fault zone visible in the mid-ground. The uplifted block of Bathonian micrite (middle right) has 100m of relief. The fault trace continues to the left where it is marked by two small pressure ridges (P.R.). The 300m+ Costa de Alvados scarp (background left) marks the topographic boundary of the basin.

zone form a mean 7° anti-clockwise transection angle to these folds. In contrast, the Bathonian micrites that form the tectonic sliver are gently folded with a horizontal fold axes parallel to the Alvados fault zone. Kinematic analysis of fault plane slickensides reveal a similar proportion of reverse and thrust faults verging to the SSW-SW, and a dominant set of dextral faults, which represent Y shears, the mean strike of which is 144° . Minor numbers of secondary strike-slip faults are present forming three spatial / kinematic sets: a synthetic dextral set forming a 38° clockwise angle with the main fault (R shears), an antithetic sinistral set describing a 116° clockwise angle (R' shears), and an anomalous sinistral set parallel to the dextral Riedel faults.

The southwestern boundary of the Alvados fault zone forms an extremely sharp contact between the micritic Bathonian aged, Candeeiros formation, and shale dominated Aalenian aged, Brenha Formation. A strong sub-vertical fabric, parallel to the fault is seen within the shales. Slivers and blocks of micrite up to 40cm long are enclosed by the anastomosing fabric, which is most intense around the margins of the blocks and poorly developed in shale dominated areas. In places the shale is seen to infill fractures in the large micrite clasts, and commonly acts as detachment surfaces for mesoscopic faults. Internally the isolated clasts of micrite are only weakly deformed by the development of calcite extensional veining. In contrast the Bathonian micrites of the hanging wall display a spectacular stylobreccia up to 20cm wide, along this faulted contact. The clasts are composed of micrite, calcite and veined micrite varying in length from 1mm to 6cm. Clast shapes are generally elongate along a horizontal axis, with a correlation between increasing roundness and decreasing size. The clasts are bounded to a varying degree by stylolitic sutures, the smaller clasts are commonly entirely sutured possibly indicating the freedom to rotate. Transfer shears within the breccia cause the pressure solution to compartmentalize, producing domains of high residue to clast proportions, adjacent to domains of relatively low amounts of solution (plate 3.4a,b). The amount of residue present increases toward the fault plane, where a narrow zone of red fault gouge is present. It appears from observations of this fault rock that pressure solution has played an important role in strain softening the fault zone, by the production of clay rich residue.

3.3.1.1 Kinematics and deformation style

Fault plane kinematics and the sense of fold obliquity indicate a component of dextral motion along the Alvados fault zone. In addition, the geometric relationships of these structures consistently indicate a transpressive deformation style. A comparison of the fold axis orientation and interlimb angle of the oblique folds within the Aalenian, and

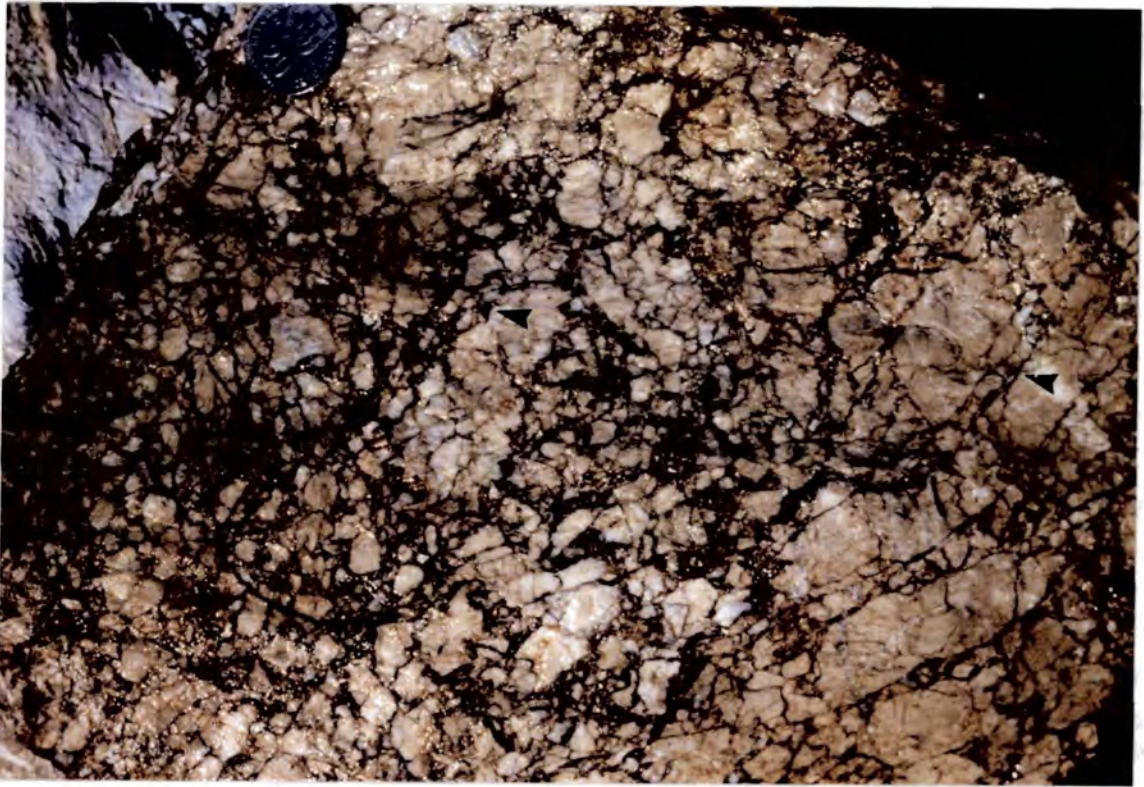


Plate 3.4a Stylobreccia within the Bathonian aged micrites of the Alvados fault zone. Note clast size decrease, and residual increase towards the fault plane (right to left in this view). A dominant oblique fracture/shear set is present (see arrows). Coin diameter 2.6cm.



Plate 3.4b Close up of compartmental shears within the stylobreccia, resulting in differential amounts of solution. Note more rounded nature of clasts within the residual rich areas. 20 Escudos coin 2.6cm.

the predicted relationship of these features for simple transpression (Little, 1992) are in very close agreement. Likewise, a low angle of anti-clockwise cleavage transection has been suggested by Murphy (1985) to be a common relationship in a dextral transpressive system (Figure 3.8). Mesoscopic and macroscopic fault orientations also suggest a dextral simple transpressive shear along the Alvarados fault zone (Sanderson & Marchini, 1984). The mesoscopic secondary faults display larger angles to the Y shears than are observed for simple shear fault zones, indicating they formed in a simple transpressive regime. As mentioned earlier the Alvarados fault zone displays a gross flower or palm tree structure, such structural geometries are commonly associated with transpressional fault segments e.g. Mecca and Durmid hills of southern California.

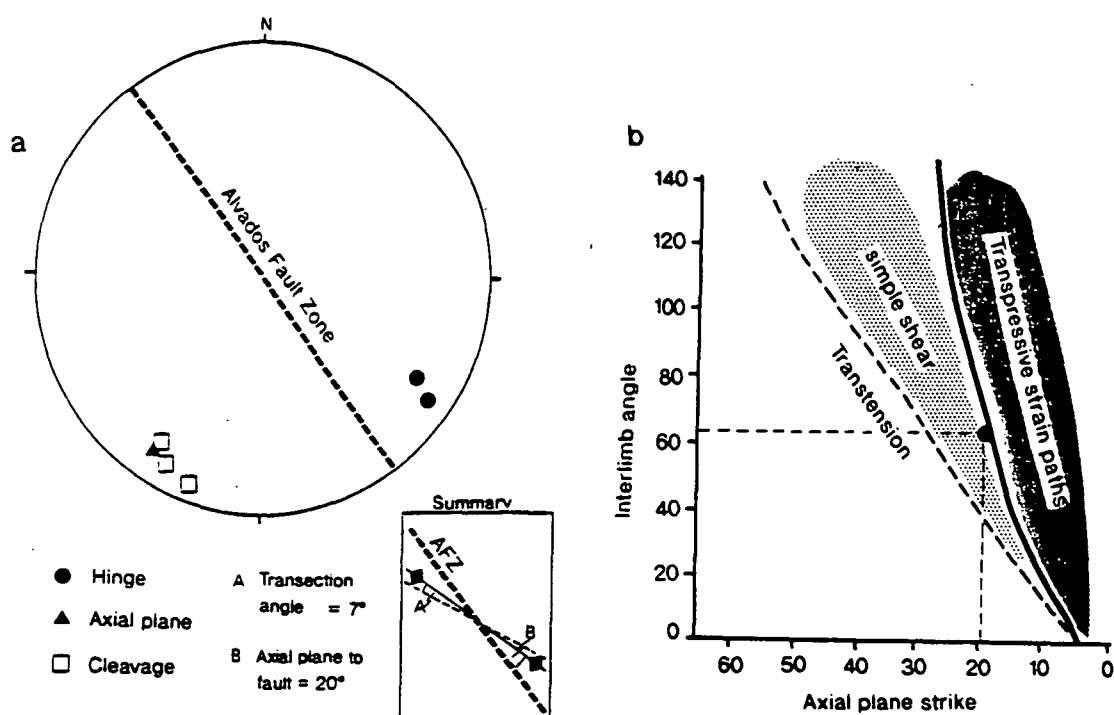


Figure 3.8 A) Equal area stereonet displaying fold axial plane and cleavage transection relationships (Cleavage and axial plane are represented as poles, hinge data as lines). B) Fold appression plot (after Little, 1992) for the Bela Vista data suggests a simple transpressive deformation path (solid line) for fold formation.

The Alvarados fault zone does not conform entirely with the simple transpressive model. The gentle folding within the competent Bathonian micrites is parallel to the fault zone, indicating an orthogonal maximum shortening axis. Clearly this is inconsistent with the predicted and observed simple transpressive structures. Due to the large rheological contrasts present between the competent micrites, the shale rich Aalenian and poorly consolidated Kimmeridgian sandstones, partitioning of strain may

be likely. Mount & Suppe (1987) describe a strain partitioned system along the San Andreas fault in central California, where the competent wall rocks deformed with folds and thrusts orthogonal to the main wrench fault, and strike-slip motion partitioned along the lower shear stress fault zone. A similar scenario could be invoked for the Alvados fault zone, but this would require a change in the style of strain to account for the mesoscopic faulting previously described. The Alvados fault zone may have suffered an early component of compression perpendicular to the zone which produced fault zone parallel folds, followed by the superimposition of simple transpressive strain as the fault zone evolved.

3.3.2 The Minde Fault

The Minde fault forms a spectacular fault scarp of up to 300 metres high, trending northwest-southeast past the villages of Mira D'Aire and Minde, and onto Moitas Venda (Figure 3.9a and plate 3.5). Although the fault has produced this strong topographic expression, exposure of the fault zone is poor due to Quaternary deposition and agricultural working. However, the fault was studied at the northwest end of its trace, due west of Mira D'Aire, and at its southeastern end between Minde and Moitas Venda.



Plate 3.5 View looking SE along Coasta de Mira towards Minde. The Minde fault lies at the base of the scarp. Relief of the scarp is approx. 300 metres.

3.3.2.1 Fault Kinematics

The Mira D'Aire section of the Minde fault zone has a trace bearing 144° and is marked on its eastern side by a minor fault scarp beneath the main Costa de Mira scarp, where micritic and oolitic Bathonian rocks are juxtaposed against Aalenian limestone and shales. This juxtaposition is a relict normal throw from its extensional origins in the Late Jurassic (Willis, 1988). A small exposure of the fault zone is present along a minor agricultural track, beneath the memorial erected on Cabeco de Mira. Kinematic analysis of the fault surfaces reveal a set of high angle fault-zone-parallel, dextral faults, with several lower angle faults of varying obliquity to the Minde fault trace, displaying reverse movements with top-to-the NNE/NE and S/SW (Figure 3.9a). This thrust transport direction is consistent with minor thrust fault transport directions measured to the west and northwest of Mira D'Aire.

3.3.2.2 En-echelon folding

En-echelon folding is present along the Minde fault zone southeast of Cabeco de Mira, forming an oblique anti-clockwise angle to the fault zone, indicating dextral shear. The folds are upright and have gentle to open interlimb angles. An analysis of the interlimb angle to angle of axial plane obliquity with the fault zone (θ') was conducted, based on the fold appression graph of Little (1992). The fold axis azimuth was substituted for the axial planar strike, as axial plane measurements were not possible given the exposure. Due to the upright nature of these folds and their low angle of plunge, the fold axis azimuth is considered to be a very good approximation for the axial planar strike, hence making this substitution acceptable. Figure 3.10b shows the plot of interlimb angle verses approximated axial plane strike, for individual folds and the total fold data set. The plot of individual folds produces a confused scatter between a transpressional and transtensional origin. This scatter may be the result of the inclusion of subjectivity in the data caused by field mapping of the fold axis. To counter this problem all the fold limb data was collated and a best fit π -girdle calculated using the geological software package ROCKWARE. The result was a statistical mean fold axis (π pole) of $07^\circ/120$, with a mean interlimb angle of 120° . When plotted on the fold appression graph, it coincides with the predicted curve for simple transpression. The Minde fault zone is therefore similar in both shear sense and deformation style to the left stepping Alvados fault zone.

On a larger scale a prominent strike swing can be mapped between the Minde fault and the Mira D'Aire fault (Figure 3.9a). The strike swing defines an 'S' shape in plan view, striking sub-perpendicular between the faults and swinging into sub-parallelism adjacent to the fault traces. This strike swing is suggestive of fault drag on originally non-parallel bedding during dextral motion.

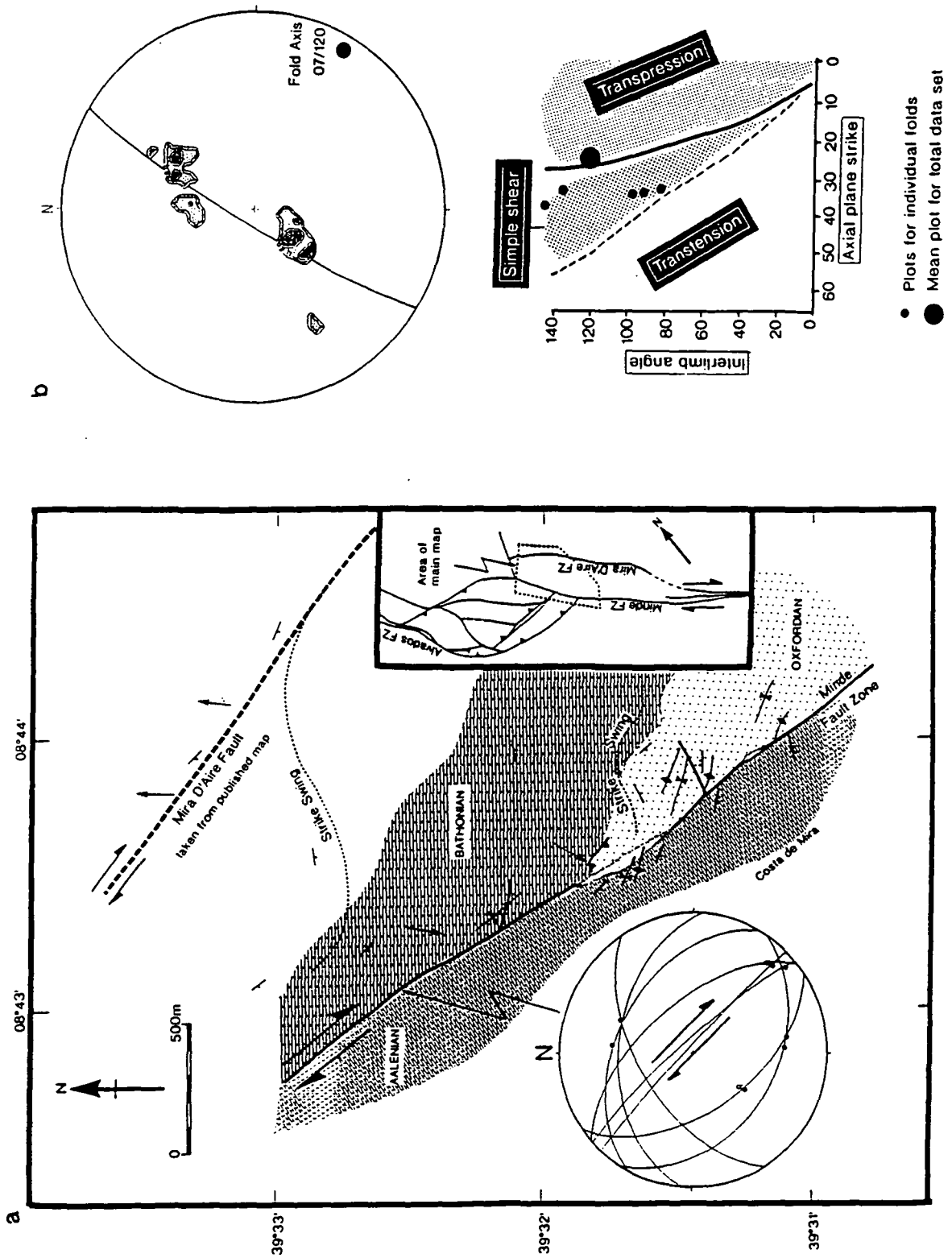


Figure 3.9 a) Structural map of the northwest end of the Minde fault. b) Equal area stereonet of fold limb data for en echelon folds, plus π -diagram construction for the mean fold axis. Fold appression graph displaying data derived from Costa de Mira.

Locally, the fault trace is marked by the development of a zone of dolomitisation up to 40 metres wide and 300 metres long. In places, the extent of the dolomitisation obliterates the original bedding orientation, although anti-clockwise oblique folds are seen partially dolomitised within these zones. A traverse through one of these zones of dolomitisation reveals an increase in tectonic fabrics and brittle structures related to a dextral shear, some apparently syn-dolomitisation and other structures obviously post-dolomitisation. Therefore, the dolomitisation process is probably related to localised syntectonic fault zone fluid movements.

The southeastern end of the Minde fault zone, between Minde and Moitas Venda, is more complex and marks the confluence of several faults, including the Mira D'Aire fault. The Minde fault zone trace trends at 125° and is marked by a zone of steep to sub-vertical bedding, which is dolomitised up to 50 metres across. The dolomitisation does not prevent recognition of bedding because of the variable interbedded shale content of the Aalenian sequence.

Kinematic evidence along this section of the fault is sparse. A limited number of synthetic secondary shears were observed in the dolomitised zone that form a $45-65^\circ$ clockwise angle to the fault trace, a much greater angle than R shears of a simple shear system. Mesoscopic thrust transport directions indicate a 025° axis of maximum incremental shortening (Z axis). This is supported by the orientation of en-echelon folds mapped at Casais Robustos, whose fold axes are oriented $02^\circ/118$ (Figure 3.10), orthogonal to the Z axis. The configuration of structures along the southeast segment of the Minde fault zone suggest a maximum shortening direction 80° anti-clockwise of the fault trace, indicating a dominant pure shear component of deformation across this segment. However, the sense of obliquity and the formation of the Serra D'Aire thrust zone at the eastern termination of the Minde fault zone implies that a significant component of dextral motion must be present along the fault zone. Dextral motions can be demonstrated on several of the faults parallel to the Minde fault zone (figure 3.10). The presence of both dextral slip and shortening across the fault zone suggest that the Minde fault zone is transpressive in nature. Using the graphical construction method of McCoss (1986) it is possible to determine the relative displacement vector between the S. dos Candeeiros and Serra D'Aire blocks. Using the fold axis orientation of the en echelon folds at Casais Robustos as the axis of maximum infinitesimal strain, a displacement vector (S) oriented toward 190° was derived. The angle between the displacement vector S and the perpendicular to the deformation zone (angle A), is 35° . This indicates a transpressive strain that is generally contractional with an oblate strain ellipsoid.

In summary, the Minde fault can be considered as segmented in its deformation style. The northwest segment is transpressive with fault zone localised

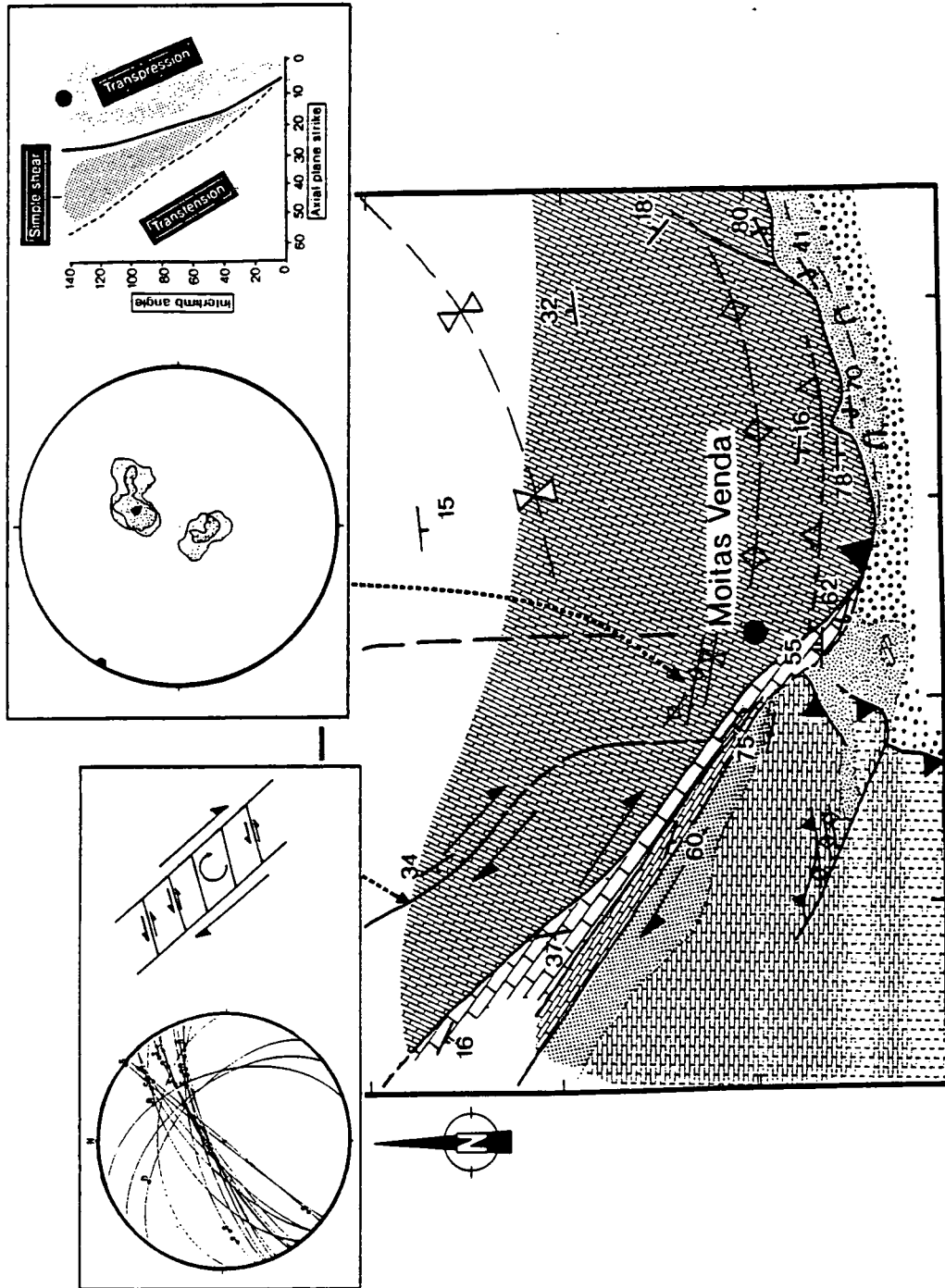


Figure 3.10 General structural map of the southeastern end of the Minde fault. (Top left) Equal area stereonet of antithetic cross faults that form clockwise rotating blocks within the Mira D'Aire fault zone. (Top right) contoured poles to fold limb data, and π -pole reconstruction of the mean fold axis, for the en echelon folds at Casais Robustos. Fold appression graph indicates a pure shear dominated transpressive deformation path (solid circle)

folding and fault development. The southeastern segment is transpressive but dominated by the pure shear component, resulting in considerable steepening of the adjacent bedding and a greater complexity in the form of the localisation of many faults. This segmented nature is due to the change in Minde fault zone strike, 144° in the northwest to 125° in the southeast, therefore increasing the amount of oblique convergence between the fault walls. It was suggested by Willis (1988) that the Minde fault has been reactivated by reverse motion during the Miocene, but it would appear that the fault zone is transpressive in nature displaying an increasing component of pure shear toward the southeast end of its trace.

3.3.3 The inverted Alvados pull-apart basin

The Alvados pull-apart basin is located between the dextral transpressive left stepping Alvados fault zone and Minde fault zone. It forms a rhombohedral configuration of faults, bounded on its southwest and northeast sides by the Alvados fault zone and Minde fault zone, respectively. The structure is closed by east-west to east-southeast striking transverse faults. Linking these extensions across the graben are northwest-southeast trending faults. The Alvados pull-apart basin is 7km by 3.3km with an aspect ratio (length:width) of 2.12, smaller than the commonly observed aspect ratio of 3 (Aydin and Nur, 1982). The centre of the structure contains the Oxfordian interbedded limestones and shales that comprise the youngest part of the sedimentary sequence, which is in turn, surrounded by large bounding fault scarps and tectonic ridges (e.g. the Castelejo ridge, see Plate 3.6).



Plate 3.6 View looking due west from the Grutas de Alvados towards the Castelejo ridge (middle distance), and Costa de Alvados, the Alvados fault scarp (far distance).

3.3.3.1 Structure and kinematics of the Alvados pull-apart basin

The structure of the Alvados pull-apart basin is domainal with a concentration of deformation at the northern and, in particular, the southern boundaries. The southern boundary is dominated topographically by the fault bounded Castelejo ridge, that runs from the southeastern termination of the Alvados fault zone to the regional high at Pedra do Altar, adjacent to the Minde fault zone (Figure 3.6).

The southern boundary - the Castelejo ridge

The Castelejo ridge is formed from Bathonian micrites and oolites of the Candeeiros fm., that are fault bounded to the north and south by downward convergent moderate to high angled faults, which are thrust onto Oxfordian and Aalenian aged sediments, respectively. The Southern Castelejo fault zone is well exposed and accessible in many places, striking between 135-118° and dipping between 56-78° to the north. The fault zone consists of several fault planes that coalesce along strike. The fault planes display dip-slip to oblique-slip reverse lineations with a component of dextral motion. Each plane has an associated breccia zone up to 30cm wide with dolomite mineralisation causing yellow staining. Well-developed oblique anti-clockwise sigmoidal platey fabrics are present within some breccia zones, indicating reverse shear with a component of dextral motion. The adjacent wall rocks show contrasting deformation styles: the competent Bathonian micrites of the hanging wall are gently to openly folded, whereas the less competent Aalenian shales of the Brenha fm., form a prominent footwall syncline, with localised tight synclines isolated by the progressive propagation of northwards verging thrusts (plate 3.7). The relationship of Bathonian and Aalenian age strata in the hanging wall and footwall respectively indicates a net normal throw on the fault zone.

The northern fault zone is composed of several discrete faults that anastomose along strike with a mean orientation 117/22-53° S. The fault planes display reverse dip-slip motion, although minor strike-slip lineations are present. The main fault, between the hanging wall Bathonian and footwall Oxfordian, shallows upwards, and is marked by a thick breccia zone that is dissected by numerous small scale faults. In contrast to the southern fault zone, the northern fault has a reverse throw.

The micrites and oolites of the Candeeiros fm. are bounded by these faults, and define an array of en-echelon folds with a mean fold axis oriented 04°/112, which forms an anti-clockwise θ' angle varying between 05-22°. Coaxial mesoscopic reverse faults are also present, that together with the folds indicate a principal axis of shortening (Z axis) that is sub-horizontal and trending N22°E. Minor faults striking parallel to the reverse faults and displaying strike-slip movements are present, although not common. On the mesoscopic scale, tectonic pressure solution stylolites



Plate 3.7 (Above) View looking east along the Southern Castelejo fault (SCF). Sub-vertical bedding of the footwall syncline can be seen immediately beneath the SCF (marked by an arrow). **(Below)** Looking west along the SCF, gentle folding and flexure of the Bathonian micrites contrasts with the well developed folds of the footwall Aalenian aged lsts. and shales, above.



occur adjacent to the main faults forming a dense (1.1 to 1.6 stylolites/cm) sub-vertical anastomosing cleavage, that is contemporaneous with sub-horizontal calcite veins.

The 67° clockwise oblique angle between the Castelejo ridge and the maximum shortening direction suggests the ridge underwent dextral transpression with a dominant pure shear component. Its gross geometry is that of a flower structure, consistent with a transpressive strain model (Figure 3.11 a).

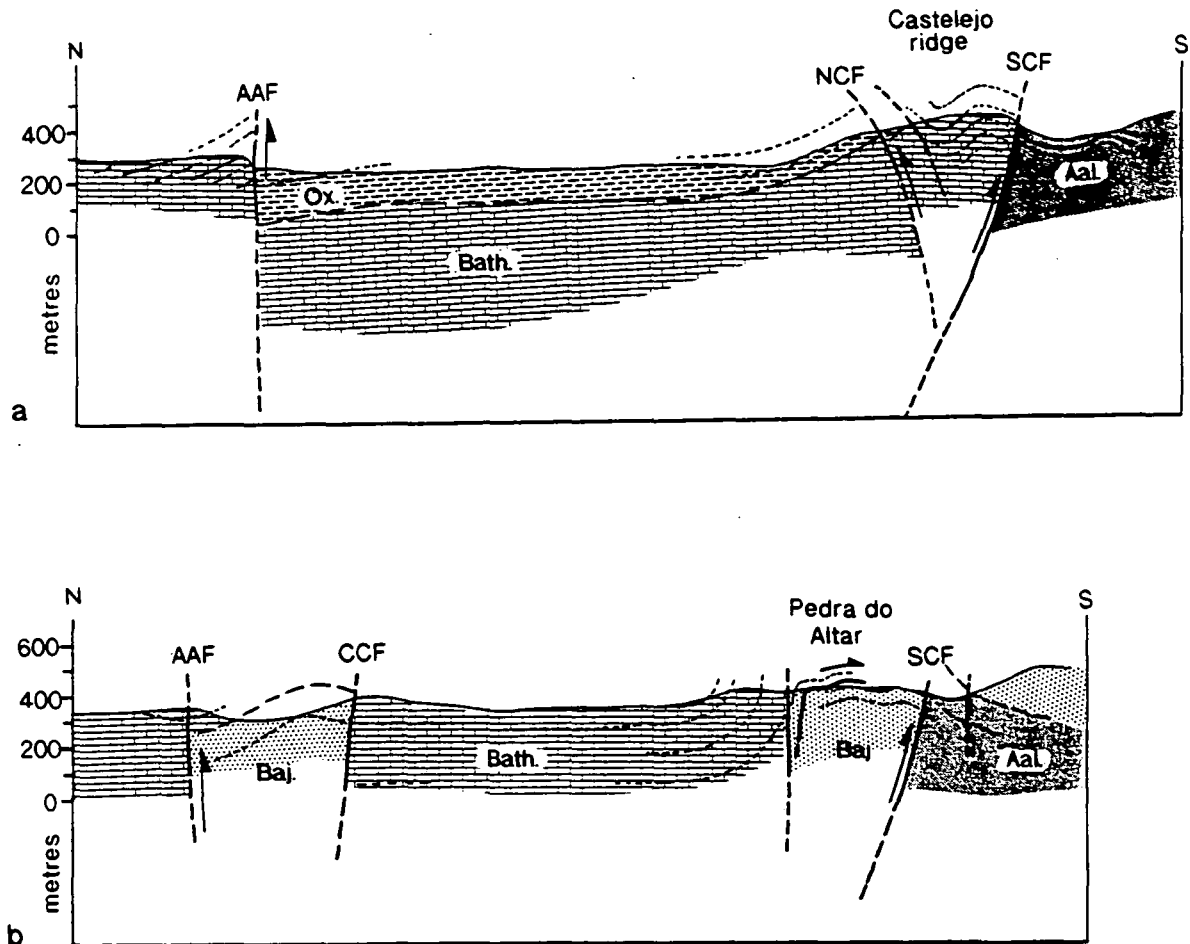


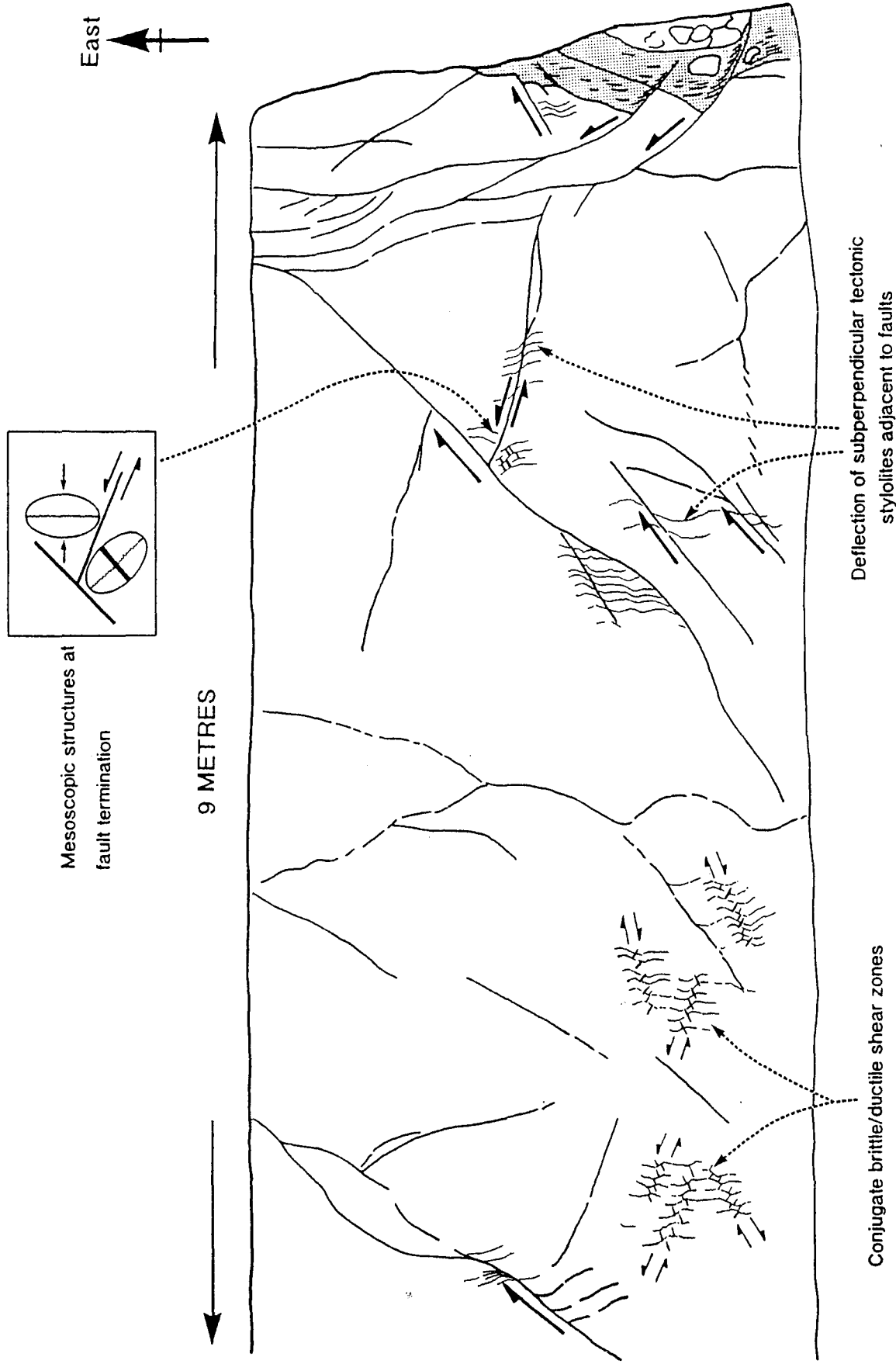
Figure 3.11 a) N-S cross section through the Castelejo ridge. b) N-S cross section through the Pedra do Altar region, revealing its contrasting structural geometry relative to the Castelejo ridge. (Aal., Aalenian; Baj., Bajocian; Bath., Bathonian; Ox., Oxfordian) Fault names the same as fig.3.6

Pedra do Altar region

The Castelejo ridge is structurally divided by a low angle fault striking approximately north-south, separating the flower structure to the west from a dominantly pure shear domain in the east. Across this fault the structural geometry is fundamentally different (Figure 3.6). The en-echelon folding to the west has been replaced by a large faulted monoclinical structure with minor folding superimposed upon the low angle limbs. A π -diagram analysis of bedding indicates a mean fold axis oriented at 08°/091, with a steep

sub-vertical limb dipping to the north (figure 3.11b). The sub-vertical limb of the monocline is dissected by a strike parallel fault, which juxtaposes Bathonian aged carbonates in the north, against Bajocian aged carbonates to the south. The fault trace is marked by a zone of dolomitisation, displaying a prominent low angled fabric on a variety of scales, from centimetres to several metres. Thin section analysis indicates that some of the discrete planes are shears, however the fabric appears to be predominantly an original bedding feature. It appears that the dolomitised zone represents a narrow sliver of low angled bedding faulted between the steep monocline limbs.

A second less prominent strike parallel fault is present 150 metres north of the main fault discussed above. This fault can be traced for approximately 1.5km between three disused quarries. At its western exposure, in a quarry east of Grutas de Alvarados, the fault is sub-parallel to the regional tectonic stylolites, and truncated near the top of the quarry face by a low angle thrust that steepens downwards into a bedding parallel sub-vertical fault. The fault zone is marked by a thick copper-blue clay zone containing disseminated pyrite and chalcopyrite cubes that display calcite pressure shadows formed parallel to the fault zone (plate 3.8). The clay has an intense planar fabric which is commonly sigmoidal in geometry due to the propagation of conjugate reverse faults out of the fault zone, and offset the fault walls (figure 3.12). The clay zone contains numerous rounded to sub-rounded clasts of wall rock <1mm to 60cm in diameter. The clasts are commonly unbrecciated, displaying solution pits on surfaces parallel to the regional cleavage (i.e. the XY plane of the strain ellipsoid) and slickolites on surfaces oblique to XY plane, indicating that dissolution processes have taken place over the entire surface of the clast. The intensity of stylolites within the wall rocks, and the presence of isolated clasts, increase towards the clay rich fault zone. In areas of moderate strain, anastomosing stylolites isolate elongate, multi-allochem clasts up to several centimetres in size. In the higher strain fault zone margins, the stylolites anastomose around individual oncoliths producing rounded clasts contained in a soft residual matrix (plate 3.9). The large clasts appear to become isolated by a combination of concentrated pressure solution and mesoscopic faulting (figure 3.12). The eastern exposure of the fault is located due south of Pedra do Altar. The fault zone has the same characteristics as the western end, although a more closely spaced pressure solution cleavage has formed adjacent to the fault. The fault again displays dominantly reverse faults propagating out of the fault zone, but oblique-slip and even strike-slip sinistral slickenlines were observed along the main fault plane.



QUARRY DUE EAST OF GRUTAS DE ALVADOS

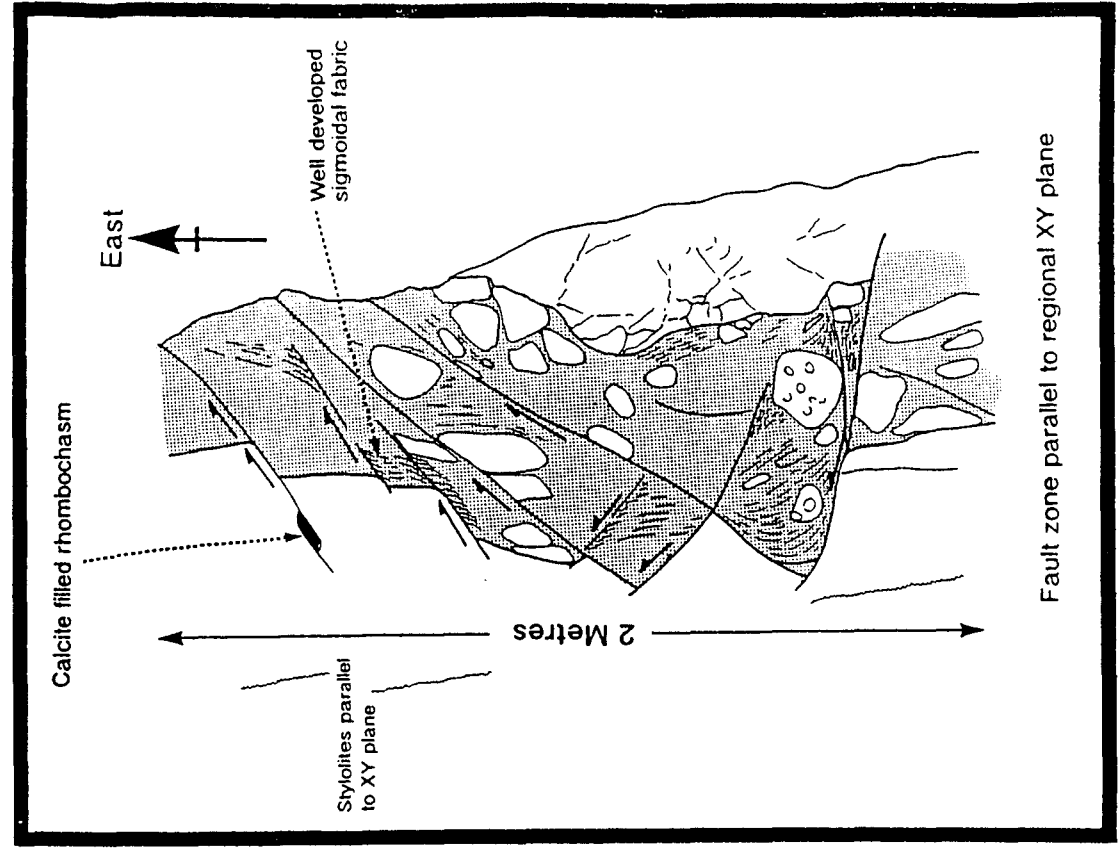
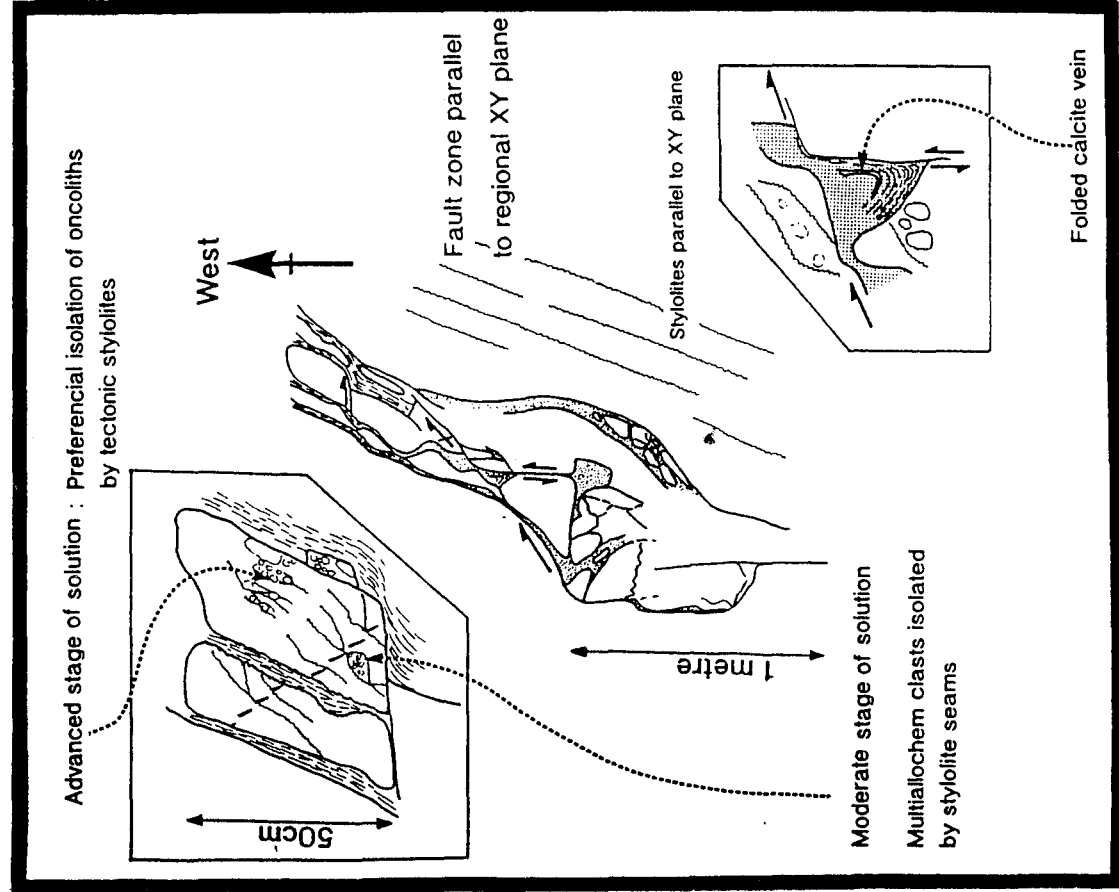


Figure 3.12 A) Fault zone observed in quarries SE of Grutas de Alvados. Quarry face displaying conjugate brittle/ductile shear zones, and high angle reverse faults. Selected mesoscale structural relationships are shown. B) Detailed structure of the clay rich fault zone. See text for details.



Plate 3.8 Micrograph displaying calcite pressure shadows formed between stretched and boudinaged pyrite cubes. Field of view 1.9mm.

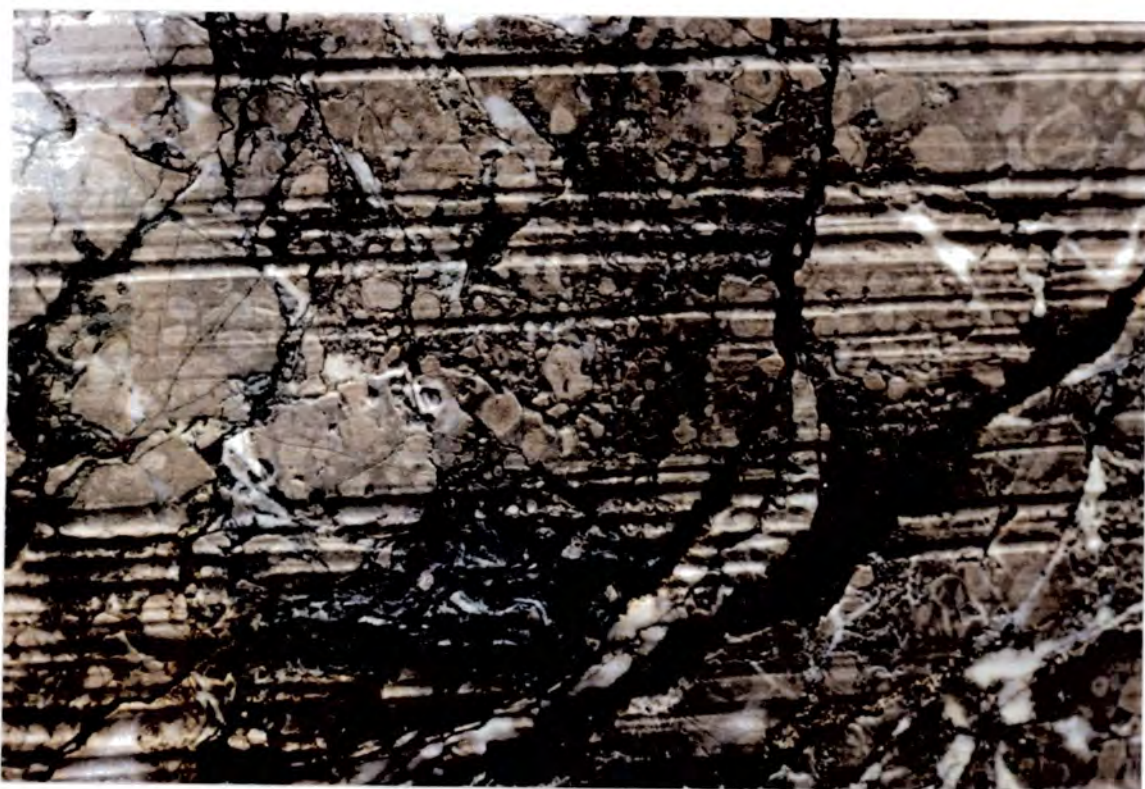


Plate 3.9 Differential pressure solution of micritic matrix relative to Oncoliths, resulting in the isolation of single or multi-allochem clasts within a soft residual matrix.

The parallelism of the fault zone to the regional tectonic stylolites indicates that it has formed parallel to the XY plane of the finite regional strain ellipsoid in a pure shear regime. Therefore, the fault zone does not conform with an Andersonian model for fault geometry and formation. The absence of fault breccia and fault gouge also indicates that the fault zone did not evolve via typical cataclastic processes. As the faulting present appears to post date the formation of the clay rich zone another process for fault formation must be invoked. The intimate relationship between stylolitic sutures and fault zone clasts suggests that pressure solution may have had an important role in concentrating strain along a heterogeneous stratigraphic horizon within the sub-vertical monocline limb. A good candidate for such a horizon may be a coarse oncolithic horizon similar to the oncolithic rock that constitutes the fault zone clasts. The differential solution of the micritic matrix not only has a role in the formation of clasts, but also in the production of pressure solution residual which has resulted in strain weakening. With increased dissolution the residual rich zone becomes the site for strain concentration and the formation of mesoscopic reverse faults. The large amount of clay material along the fault zone produces a 'free surface' (a plane of low coefficient of friction) which probably acts as an accommodation structure for minor movement within the region, explaining the anomalous kinematic interruptions observed on the fault planes.

Geometry and kinematics of the mesoscopic faults

Mesoscopic faulting coaxial to regional folding is abundant throughout the area (Figure 3.13a) with two dominant fault sets; a low angle southward verging thrust set, and a sub-vertical reactivation of bedding planes within the steep limb of the monocline.

The thrusts are commonly simple low angle planar faults exploiting bedding planes. However, in the steep monocline limb the spatial relationship of the thrusts to other structures is more clearly defined. Two relationships appear common: thrusts becoming discordant to bedding at the monocline hinge, and thrusts propagating from sub-vertical reactivated bedding planes. Slickenlines along the low angle thrusts have a mean vector azimuth 015° , while slickenlines along the sub-vertical reactivated bedding planes are more complex. A dominant dip-slip lineation is present, parallel to the mean thrust vector of 015° , however, these dip-slip lineations are regularly interrupted by oblique and strike-slip fault movements (plate 3.10). These disruptions in the dip-slip lineation have varying plunge but a consistent azimuth towards the east (Figure 3.13b). Where shear sense is unambiguous, the oblique and strike-slip component has a sinistral sense of motion. The presence of sinistral interruptions along the high angle faults may be due to the accommodation of a slight sinistral

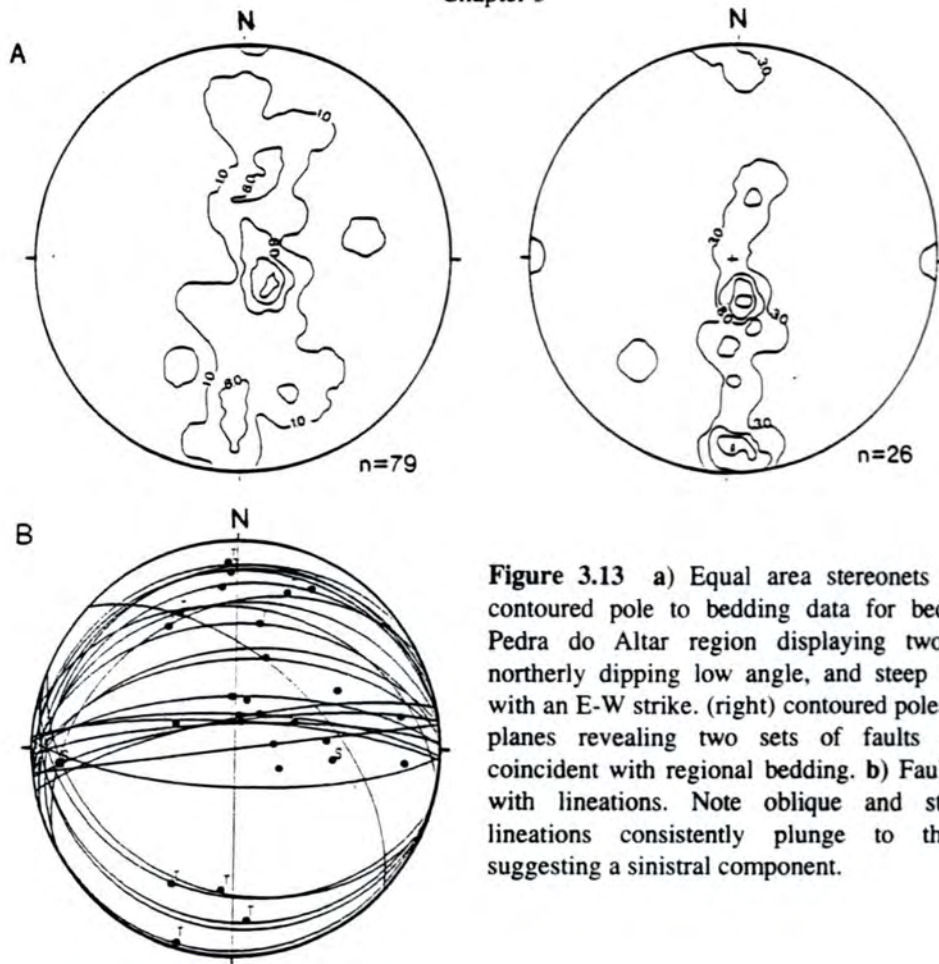


Plate 3.10 Short sinistral interruption in the dominantly reverse slickenlines on a steep fault plane, near the Grutas de Alvados. 2.5 Escudos coin 2cm in diameter. (Grid reference: 08°45'01" 39°32'02")

component introduced into the Pedra do Altar system due to the slight obliquity of the Z axis to the area's structural grain.

Mesoscopic structures

The Pedra do Altar region is exceptionally good for observing detailed mesoscopic structures since the steep zone has been extensively quarried for decorative stone. Thrust plane parallel brittle/ductile shear zones are common throughout this region and form a 48° conjugate set with reverse shear sense. The shear zones display a variety of relationships between pressure solution stripes or stylolites and en-echelon tension gash veins. A common relationship is the presence of both pressure solution effects and veins in the same shear zones, with intensely sigmoidal stylolites approximately at right angles to the veins. The two structures must be contemporaneous as veins can be seen cutting stylolites and stylolites seen removing vein material. The stylolitic solution planes form at angles slightly less than 45° to the shear zone walls, and are commonly interconnected, possibly forming the channel ways required for the removal of carbonate material in solution. A second relationship is the superimposition of a regional tectonic stylolitic cleavage over a conjugate array of tension gashes. The cleavage is not deflected within the shear zone, but it does become modified by extensional veining. The brittle shear zones display a cyclic strain pattern of regional cleavage overprinting brittle shears and vice versa. The sub-vertical cleavage also overprints the brittle/ductile shears.

Ramsay & Huber (1987) produced a model based on the concept of shearing acting together with dilation, this links the shear zone orientations with the orientation and type of regional bulk strain inducing the shear zones. Figure 3.14 shows the complete spectrum of bulk two-dimensional deformation between uniaxial bulk shortening and uniaxial bulk stretching. Furthermore, the authors relate overall positive dilation with any system that forms primarily extensional veins, and overall negative dilation where pressure solution seams remove material out of the system.

What is immediately apparent from an examination of the structures present in the quarry face is that two differing styles of strain are present. The 48° 2θ angle of the brittle tension gash arrays, and the lack of pressure solution effects within the shear zones, suggests a bulk strain involving positive dilation with the development of shear zones similar in strain and orientation to the positive dilational model B, figure 3.14. However, as mentioned sub-vertical stylolites overprint this system and vice versa, suggesting that bulk shortening (the pure negative dilation model E, fig 3.14) along a sub-horizontal axis is intermittently occurring. These two conflicting systems indicate that there has been a cyclic change between sub-horizontal bulk shortening and vertical stretching combined with shortening. The presence of brittle/ductile shear

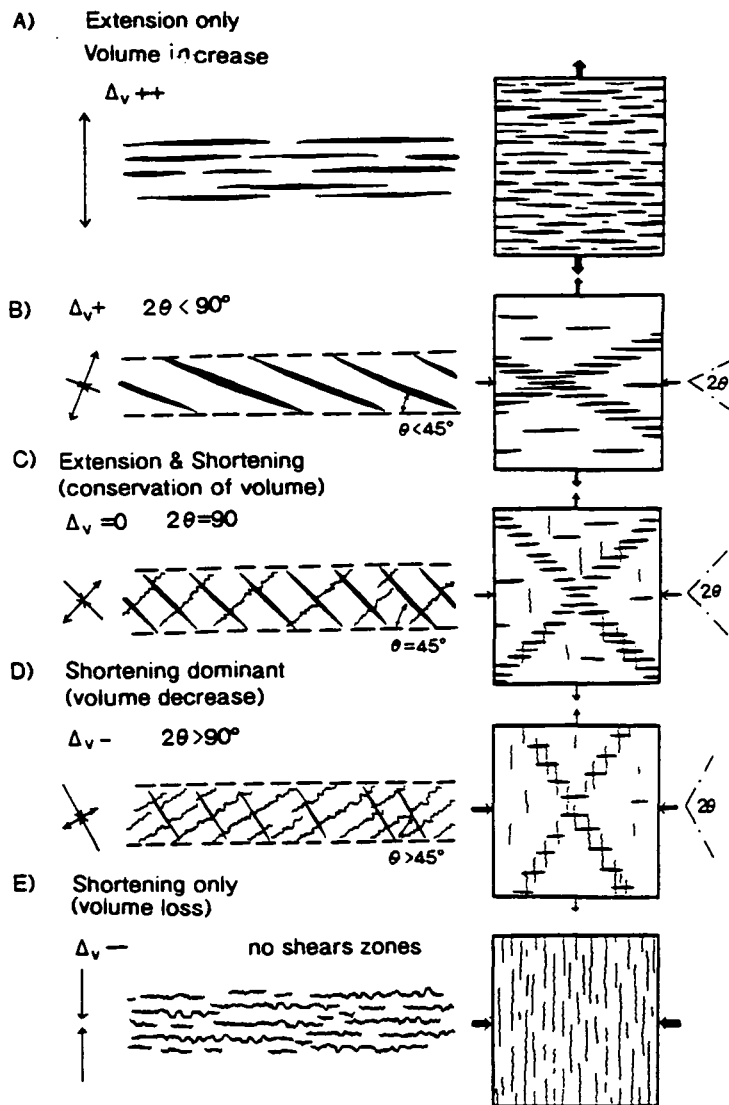


Figure 3.14 Model spectrum for relating the geometric features of conjugate en echelon vein arrays to the overall bulk shape changes and dilation taking place. Vein and stylolite surfaces are located in their initiation orientations. (Re-drawn from Ramsay & Huber, 1987 fig.26.42)

zones suggest that the change in strain may have been progressive, from negative dilation, through constant volume (model C, fig 3.14), to the positive dilation model.

It is suggested that the strain system observed is related to increases in the applied tectonic stress due to stress cycling in the seismogenic regime. Temporal variations in the shear stress (τ) fluctuate in a crude saw tooth oscillation (figure 3.15), the cycle of which is subdivided into four phases: the α -phase, during which mainly elastic strain accumulation takes place, the β -phase which is possibly pre-seismic anelastic deformation, the coseismic γ -phase of mainshock rupturing, and a post-seismic δ -phase of decelerating aftershocks. These oscillations of shear stress have been shown to extend considerable distances into the surrounding crust of seismically active faults (Sibson, 1989). The structures preserved within the quarry appear to be

related to the earthquake stress cycle. Due to the susceptibility of limestones to undergo low strain rate pressure solution processes, the sub-vertical stylolitic cleavage that forms a uniaxial bulk shortening strain, probably occurred during the β -phase of the cycle when *mainly* elastic strain was accumulating. The heterogeneous deformation in the form of conjugate vein arrays probably formed during the γ -phase, perhaps representing microseismic foreshocks. Following the main rupture event along one of the adjacent faults, the stress is dissipated and the process repeated.

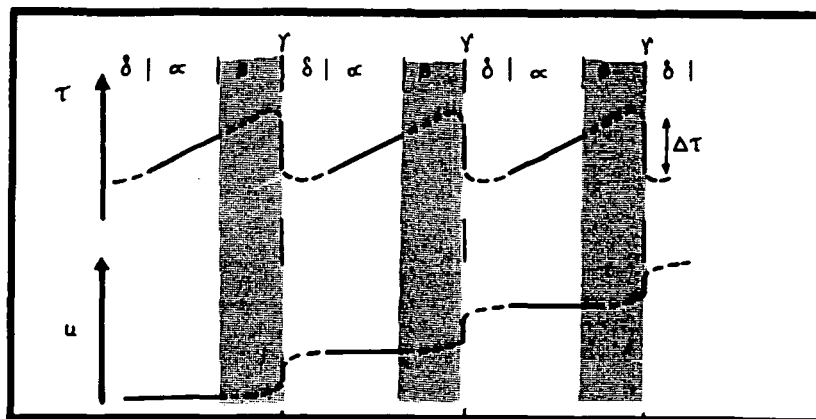


Figure 3.15 Temporal variations in the shear stress (τ) and displacement (u) for seismically slipping crustal fault zones (modified from Sibson, 1989). The anelastic β phase has been extended to take into account the low strain-rate pressure solution processes.

The strain systems observed in the Pedra do Alto region represent a complex relationship between wall-rock rheology, the earthquake stress cycle, and bulk strain. In this region, the seismic cycle exerts a control over the temporal variation in bulk strain, with initial sub-horizontal, uniaxial bulk shortening, followed by biaxial strain resulting in extension along a vertical axis with associated continued shortening along the Z axis. It appears that lithologies susceptible to pressure solution processes in the upper seismogenic zone, preserve an oscillating strain path that alternates between k -values of 0 and 1, relative to the earthquake cycle. Such cyclic strains at this crustal level, are dependant on lithologies that permit low strain rate/low shear stress deformation mechanisms, such as pressure solution within limestones. Hence, care must be taken when attempting to describe the bulk deformation controlling these structures, as they are subjected to temporal variations in stress and its resultant incremental strain.

The steeply bedded zone also has a well developed sub-vertical anastomosing stylolitic cleavage. As observed within the Castelejo ridge, the stylolites are contemporaneous with sub-horizontal calcite veins indicating that the strain varied during the deformation cycle i.e. anelastic pressure solution processes take up strain,

possibly during the β -phase of the earthquake stress cycle. An increase in shear stress will eventually result in preseismic strains and the release of stress. The cycle will then begin again with aseismic diffusional mass transfer processes. Estimates can be made for the amount of shortening along the Z axis using the cross cutting relationships of the stylolites and veins. Using a thin section micrograph the amount of solution for a single stylolite can be calculated applying simple trigonometry on the offsets created by the solution of non perpendicular calcite veins. The results indicate a mean shortening across each stylolite of 1.26mm. When this figure is projected for the entire thin section these calculations indicate a possible 25% shortening parallel to the Z axis. The corresponding vertical extension in the X direction can be calculated by restoring the extensional calcite veins. This method gives a mean vertical extension of 7%. Extensional veining perpendicular to the Y axis is minimal, and can therefore be ignored for these purposes. The disparity in the Z and X axes indicates that there has been an approximate net volume decrease of 18% (max.). The studied sample is representative of the deformation along the steep zone. The data set is admittedly limited but it provides an estimate for the finite strain, being dominantly oblate. As there has been a net loss of carbonate material by dissolution, it indicates that the extensional veining is not synchronous with stylolite formation, as in such a system the amount of material in dissolution would equal the amount of precipitate in the extensional veins (i.e. conservation of volume).

The incremental strain at any moment in time is essentially a uniaxial strain (only one principal axis length is changing), for the stylolites the Z axis shortens, for the sub-horizontal fracturing the X axis increases. The result of the cyclic superimposition of these incremental strains is a biaxial (plane strain) finite strain, with sub-horizontal Z and Y axes and a vertical X axis. This situation is complicated where conjugate vein arrays form an intermediate strain state, which is biaxial (figure 3.16a). The orientations of the principal strain axes can be derived from the mesoscopic faults. The Z axis is derived from the mean slickenline vector on the thrusts faults combined with the acute bisectrix of the conjugate brittle/ductile shears, producing an orientation of 06/015. The Y axis can be calculated by constructing a β -plot for mesoscopic fault planes (assuming Andersonian faulting), this gives a Y axis oriented 03/270. The X axis, being orthogonal to Z and Y can be constructed on a Lambert equal area stereo net, orientation 82°/159 (figure 3.16b). However, as can be seen in figure 3.16b, the strain axes are not exactly mutually perpendicular, which when taken with the evidence for a minor component of sinistral motion within the Pedra do Altar region, suggests the strain is slightly non-coaxial.

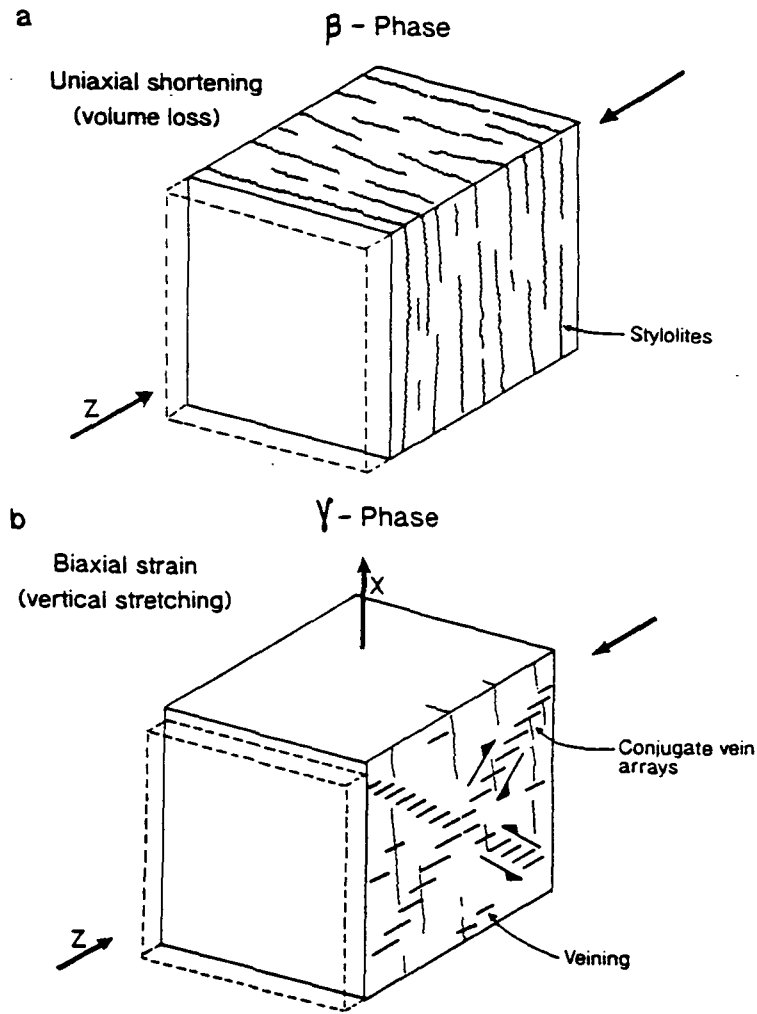
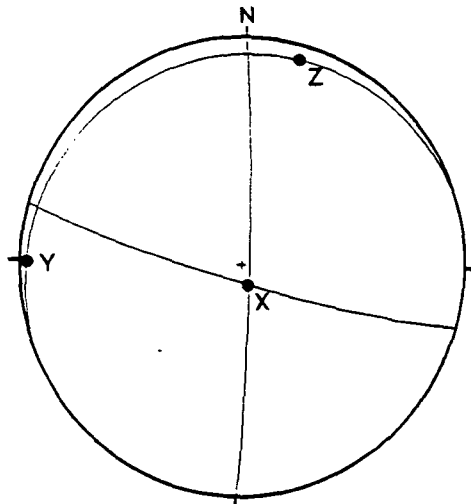


Figure 3.16 A) Cyclic strain related to the seismic cycle. (Top) β -phase anelastic strain in the form of pressure solution stylolites results in pure shear and volume loss (uniaxial strain). (Bottom) Complicated deformation associated with the γ -phase, sub-horizontal veining produces uniaxial stretching along the X-axis, however, this is commonly combined with a stretching dominated biaxial strain resulting in *model B* vein arrays. **B)** Reconstruction of principal strain axes for the Pedra do Altar region, see text for details.



Northern boundary of the pull-apart basin

The northern boundary of the Alvados pull-apart basin is defined by the Alto de Alvados fault, a reactivated normal fault striking approximately 100° , which displays reverse motion. The Alto de Alvados fault trace can be followed from the Alvados fault zone 1km south of the village of Alcaria, along a prominent fault scarp to the northern end of the Minde fault zone. The fault scarp coincides with the confluence of several faults: the Alcaria fault joining from the north, and two splays joining from the south. The western splay splits the Castelejo ridge, the Central Alvados fault, and the easterly splay (Chao da Cadela fault) striking southeast joining the eastern limit of the Pedra do Altar region. In general these fault zones are poorly exposed (figure 3.6).

The Alcaria fault divides the northern side of the Alto de Alvados fault zone into two structural domains. On the western side of the Alcaria fault, Oxfordian limestones and shales increase in dip towards the Alto de Alvados fault zone becoming parallel to it, with a maximum southerly dip of 70° . In contrast the Bathonian micrites on the eastern side have only moderate northerly dips against the Alto de Alvados fault zone (maximum 38°). Oblique anti-clockwise folds have developed adjacent to the northwest end of the Chao da Cadela fault near its confluence with the Alto de Alvados fault zone indicating a component of dextral motion is present. At the junction of the southeastern end of the Chao da Cadela fault and the main Pedra do Altar fault, a fanned array of folds has developed.

The Central Alvados fault was not observed at any point along its trace, however, its relationship to topographic contours indicates the fault plane has a low to moderate westerly dip. Given the most recent and possibly the current dextral sense of motion on the master faults, the Central Alvados fault is oriented in a position favourable for extensional movement, as indicated by its net normal throw. As mentioned before the Central Alvados fault exerts a structural control on the Castelejo ridge indicating that it must have evolved early in the history of pull-apart basin development.

Evolution of the inverted Alvados pull-apart basin

The complex fault system at Alvados is formed by two left stepping, NW-SE, dextral transpressive faults (Alvados and Minde faults), with approximately E-W transverse reverse faults closing the structure to the north and south. As mentioned many of the individual faults display normal stratigraphic throws, with the structure as a whole displaying the youngest stratigraphic levels at its centre (figure 3.11). Based on the stratigraphic relationships the structure can be termed a rhomb-shaped graben or pull-apart basin. Pull-apart basin formation occurs when the direction of stepover and lateral offset of the master faults have the same sense, i.e. left stepping sinistral faults

or right stepping dextral faults. If the stepover relationships are the opposite, the result is a compressional structure or pressure ridge. As described, the master faults are presently left stepping and have a dextral component of motion producing the transpressive and pure shear strains observed along the Castelejo ridge and the Pedra do Altar and Alto de Alvados faults. These observations indicate that the Alvados pull-apart basin has undergone an inversion event which has not fully recovered the extensional throw on the faults. The presence of the pull-apart basin, albeit partially inverted, necessitates an initial sinistral phase of motion along the Alvados and Minde master faults. Kinematic evidence for an initial period of sinistral motion is scant, a solitary oblique clockwise fold adjacent to the Alvados fault zone is present and labelled F_1 in figure 3.6. However, the preponderance of net extensional throws on most of the major faults provides strong evidence of this sinistral phase.

It is therefore clear that the Alvados pull-apart basin has a complex evolution involving multiple reactivation and inversion. Wilson et al., (1990) suggest that the Alvados and Minde faults formed during extensional faulting east of the S. dos Candeeiros fault during the Late Jurassic. Some of these extensional structures are intruded by penecontemporaneous basic dykes that yield dates of 140 Ma (Willis, 1988), base Cretaceous. In the early Miocene, sinistral reactivation of the Alvados and Minde faults took place, initiating pull-apart basin formation. Based on structural and stratigraphic relationships, a fault chronology can be constructed. The Southern Castelejo fault and Alto de Alvados fault zone formed in response to fault tip stresses, and define the boundaries of the basin. As previously mentioned, the Central Alvados fault exerts a control over the structure of Castelejo and the Pedra do Altar region, indicating it initiated early in the basin development. As the Central Alvados fault is a low angle sub-bedding parallel structure, and that during the period of basin development it was oriented in a position favourable for contractional movement, it is proposed that the Central Alvados fault was initially a thrust. Figure 3.17 shows a proposed method for the formation of Central Alvados fault. The model depends on the Alvados fault zone forming a continuous fault with the Southern Castelejo fault, therefore allowing the subsidence of the basin floor down the Southern Castelejo fault and along the Alvados fault zone which would act as a lateral ramp. In this scenario the bend in the Alvados fault zone at Lagoa de Alvados would act as a restraining bend, creating a compressional stress build-up around it. The Central Alvados fault is seen as a necessary response to this, if continued movement along the Alvados fault, and basin subsidence is to be allowed. Continued basin extension resulted in the formation of the Pedra do Altar fault as an extensional rider on the Southern Castelejo fault, although it was confined to the east of the Central Alvados fault.

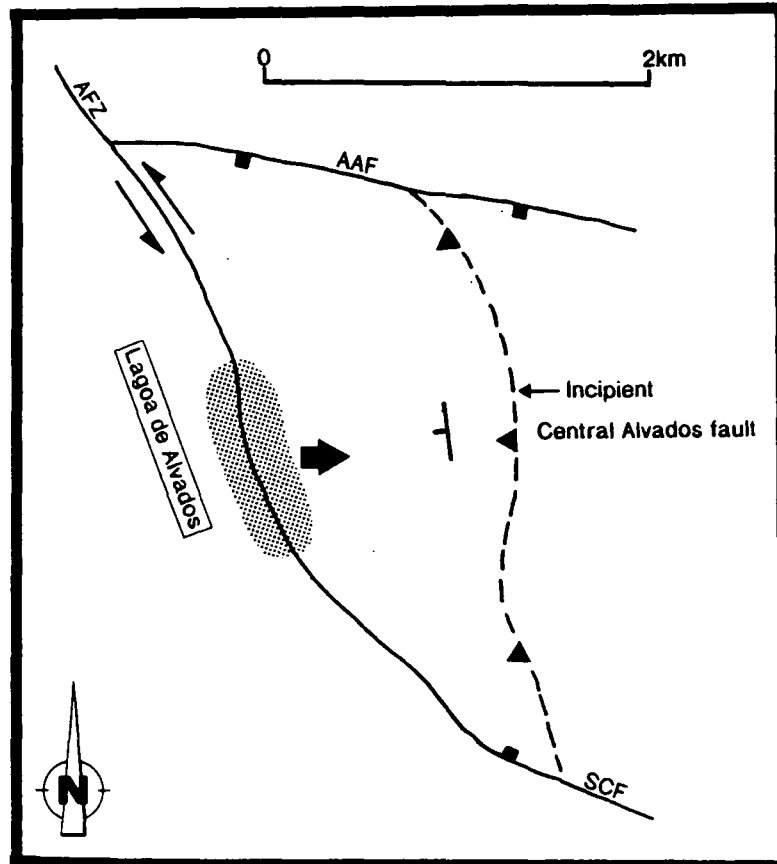


Figure 3.17 Formation of the Central Alvados fault. Initial sinistral motion along the Alvados fault (AFZ) during the Middle Miocene, creates localised transpressional stresses along a restraining bend at Lagoa de Alvados (thick arrow), resulting in the formation of the Central Alvados fault as a bedding parallel thrust. (SCF., Southern Castelejo fault; AAF., Alto de Alvados fault).

Inversion of the basin occurred due to the dextral transpressive reactivation of the Alvados and Minde faults, and the production of a pressure ridge or 'push-up'. The Northern Castelejo fault formed during this inversion event to complete the fault bounded, transpressive Castelejo ridge. Also initiated during this period was the Chao da Cadela fault. The Central Alvados fault, now oriented in an extensional field, was probably reactivated with a normal sense of motion to give the extensional throw seen at present. The fact that net extensional throws are present within the basin suggest that either the amount of dextral offset was not as great as the sinistral phase, or that the partitioning of strain between fault slip and bulk deformation was sufficient to leave a remnant throw. Given the more pervasive nature of the compressive structures in the southern region, i.e. the tightening of extensional drag folds into a steep monocline against the Pedra do Altar fault, large numbers of mesoscopic thrusts, and net shortening and volume loss by pressure solution, suggest that strain partitioning between fault slip and bulk deformation may be important.

Estimates for the amount of shortening, and hence the amount of dextral motion along the Alvados and Minde faults, were made by comparing the aspect ratio of the present structure and that predicted by Aydin and Nur (1982), who suggested

that the aspect ratio of pull-apart basins is scale independent, and has a value of 3. Comparing these ratios suggests that 32% shortening has occurred along the basin, which in turn, suggests 2.9km of right lateral movement on the Alvados-Minde fault system. Folding accounts for ~12% of the shortening within the basin, allowing for volume loss via concentrated pressure solution (estimated maximum of 5% relative to the whole basin), leaves a minimum of 15% shortening to be taken up on basin faults. If distributed equally among the three main basin faults, 15% shortening represents 450m on hade by reverse slip. This figure seems unrealistic, even allowing for unaccounted movement out of the plane of section. This estimate has not taken into account the cumulative displacements along the abundant mesoscopic faults, and may underestimate the amount of pressure solution. However, the afore mentioned structures seem unlikely to account for the additional shortening predicted by the model of Aydin & Nur. In addition, no evidence of an increase in the separation of the Alvados and Minde faults was seen, as is required by the model, on the contrary, the fault separation appears to be fixed. Therefore, this model of basin formation appears to be inappropriate for the Alvados pull-apart, hence the displacement estimates are erroneous. Therefore, the dextral displacement is likely to be less than 2.9 km.

3.4 The Alcanede fault zone

The Alcanede fault zone trends 124° forming the southwestern boundary of the Candeeiros block. The fault zone joins the southern end of the Mendiga fault with the Amiais de Baixo thrust, and is marked by a pronounced topographic feature. The fault juxtaposes Jurassic and Cretaceous rocks of the Candeeiros block over Cretaceous to Tertiary sediments on the southern side. The fault zone has two distinct segments: a northwestern segment displaying a discrete fault zone separating Oxfordian limestones in the hanging wall from footwall Kimmeridgian and Portlandian siliciclastics, and a southeastern segment marked by a fault parallel monocline that translates into an over thrust footwall syncline marking the beginning of the Amiais de Baixo thrust zone. The segments are separated by a transfer fault trending 160° immediately northeast of the village of Mosteiros (Map 1).

3.4.1 Southeastern segment

The trace of the southeastern segment is marked by a conspicuous topographic ridge running adjacent to the village of Alcanede, produced by a steeply inclined Oligocene limestone horizon dipping toward the southwest. Deformation along the fault segment is represented by a broad monocline with a steep limb up to 1km wide, displaying a fault parallel, sub-horizontal fold axis and distributed mesoscopic faulting. A weak, roughly axial planar, pressure solution cleavage is present within the competent

limestones of the monocline limb. Bedding plane reactivation has occurred along the steep limb with movement striae indicating an oblique dextral/extensional sense of shear. The extensional component probably results from flexural slip along the limb as the Candeeiros block uplifted relative to the southeast side of the fault zone. At the southeastern termination of the Alcanede fault zone lithological truncations were mapped indicating a change in deformation style from monoclinical folding to faulting. Along the same section of the deformation zone the monocline transforms gradationally via a strike swing from NW-SE to E-W, into an overthrust footwall syncline located beneath the Amiais de Baixo thrust.

3.4.1.1 Mesoscopic faulting along the southeast fault segment

The mesoscopic faults within the deformation zone define an almost orthogonal conjugate set of strike-slip faults, formed dominantly by a set of fault zone parallel dextral oblique faults, and to a lesser extent, a sinistral set, oriented NNE-SSW (figure 3.18). The acute bisectrix of this conjugate angle suggests a NNW-SSE oriented axis

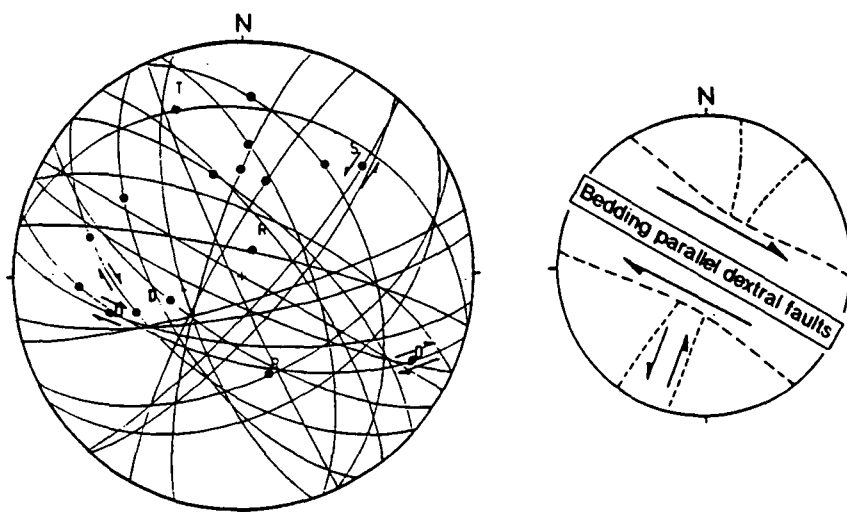


Figure 3.18 Equal area stereonet displaying secondary faults located along the southeastern segment of the Alcanede fault.

of principal shortening (Z axis). Slickenlines observed on high angle reverse faults are not coincident with the conjugate acute bisectrix, and indicate an approximately N-S oriented Z axis. The faults sets have small displacements, which probably approximate to incremental strains, and are presumed to be coeval. Therefore, the faults are expected to be coaxial. However, as pointed out the orientation of the dextral fault set exploits the steeply dipping bedding of the monocline limb, therefore increasing the conjugate angle of the fault sets from that expected to form in a homogeneous rock. Hence, the azimuth of the acute bisectrix for the fault set does not lie parallel to the azimuth of the incremental Z axis derived from thrust fault slickenside striae.

3.4.2 The northwestern segment

The northwest segment of the Alcanede fault zone displays a contrasting structural style to the southeastern segment. Lithological truncations, and/or abrupt changes in strike, can be mapped along the length of fault segment. A marked topographic lineament is present where Oxfordian limestones and shales are juxtaposed against younger, poorly consolidated, clastic sediments. Deformation along the northeastern side wall varies due to the presence of a NE-SW oriented compartment fault. Southeast of this compartment fault the bedding strikes parallel to the fault trace with a regional dip of 15° towards the fault. Within 150 metres of the fault the bedding steepens rapidly becoming locally overturned. Northwest of the compartment fault the Jurassic limestones strike approximately N-S dipping 30° to the east, adjacent to the fault trace the strike swings from N-S to ENE-WSW indicating possible fault drag folding by a dextral component of slip.

Several oblique, ^{ant:}clockwise fold traces were mapped along the southwestern side wall within the incompetent Kimmeridgian and Portlandian coarse sandstones. The sense of obliquity is again suggestive of a dextral component of slip along the northwest segment (figure 3.19a).

3.4.2.1 Shear sense evidence along the northwest fault segment

As mentioned above, oblique fold axes and fault drag, adjacent to the northwest fault segment, suggests a dextral component of motion is present along the northwestern segment. Where exposed the fault commonly manifests itself as zones of anastomosing breccias, within which asymmetric clasts or 'bull-nose' clasts are common. The asymmetry of these clasts is commonly accentuated by the development of debris trails from the long axis of the clast. In rare examples asymmetric growths of calcite pressure shadows can be seen. These asymmetries again suggest a dextral component of motion within the fault zone, a sense of motion that is corroborated by observed mesoscale lithological offsets and mesoscopic fault geometries. Examination of slip surfaces along the fault zone reveals a spectrum of slip directions from reverse dip-slip, through oblique-slip to strike-slip. The best exposure of the fault zone is found directly north of the village of Mosteiros

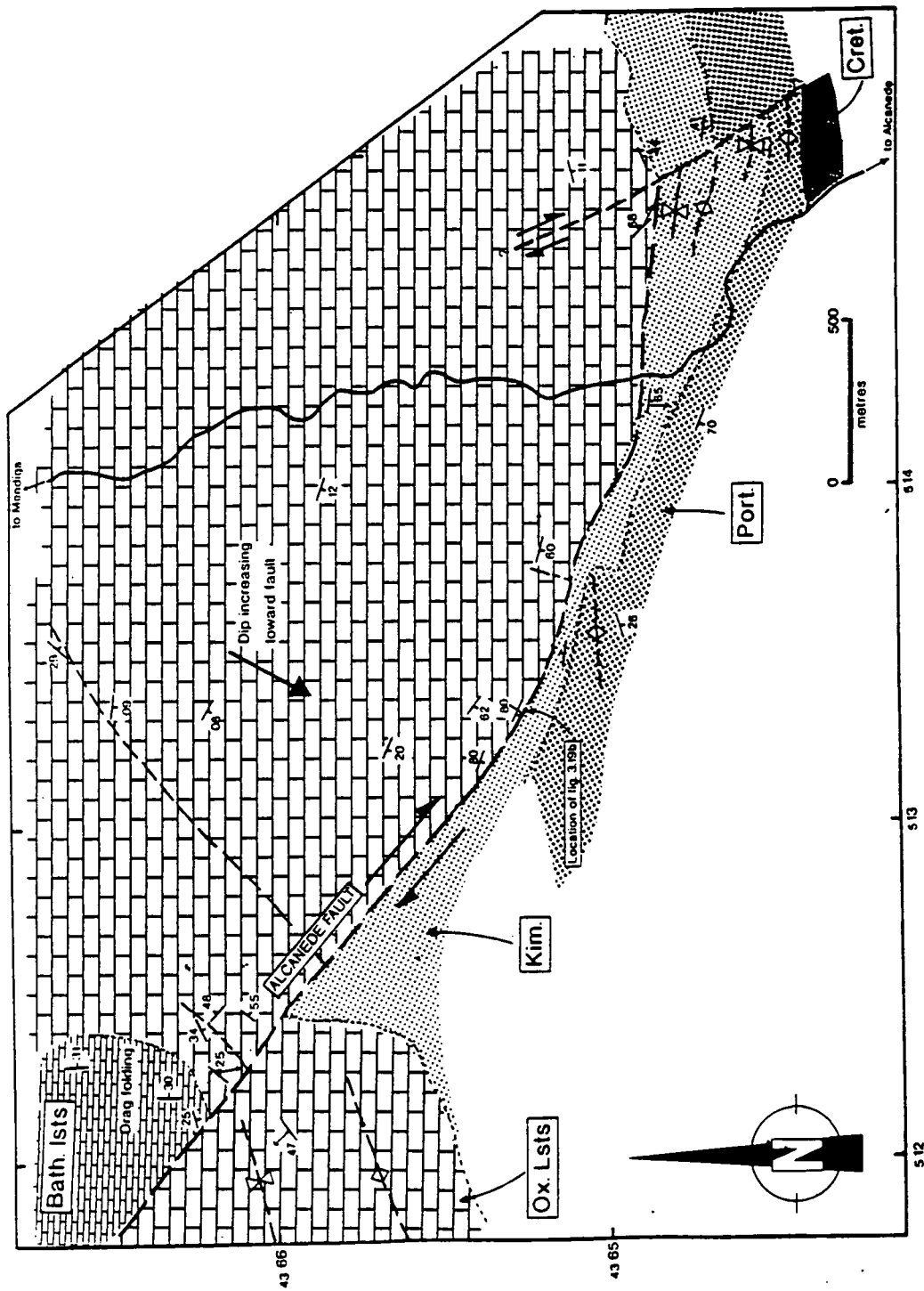


Figure 3.19a Structural map of the northwestern segment of the Alcanede fault. (*Bath. lsts.*, Bathonian aged limestones; *Ox. Lsts.*, Oxfordian aged lacustrine carbonates; *Kim.*, Kimmeridgian Ssts. and marls; *Port.*, Portlandian aged red beds; *Cret.*, Early Cretaceous yellow ssts.)

in a road section running parallel to Vale das Fontes Regueiras (grid ref. 50°72' 25'80"*)). The fault zone is 15-20 metres wide at this location, and is characterised by a strong fabric produced by numerous cross cutting mesoscopic faults. The faults form two sets, a high angle set (dipping up to 85° N), and a lower angle set (dipping at 70° N), suggesting that the northwest segment of the Alcanede fault dips at a high angle to the north. Visible offsets and slickenlines along these mesoscopic faults indicate that the lower angle faults have a reverse sense of shear and appear to post-date the higher angle set. The steep faults define platey slivers of rock forming bundles, that are bound on upper and lower sides by reverse faults. Slickenlines observed along these steep faults reveal a dominant strike-slip component. These mesoscopic faults form an 18° oblique clockwise angle to the main fault trace. The strong presence of oblique clockwise reverse faults together with a strike-slip component suggests a dextral transpressional strain along the fault zone.

Fault geometries and kinematics observed within the sub-vertical bedding adjacent to the northwest segment is also suggestive of a transpressive nature for the Alcanede fault. A flower or palm-tree structure is present displaying partitioned strain. The central 'stem' is formed by steep oblique or strike-slip faults, with numerous convex upward reverse faults splaying out from it. The thrust transport directions are away from the central fault and change across the 'stem'. The flower structure truncates sub-vertical to overturned bedding therefore indicating it was a late stage structure (Figure 3.19b).

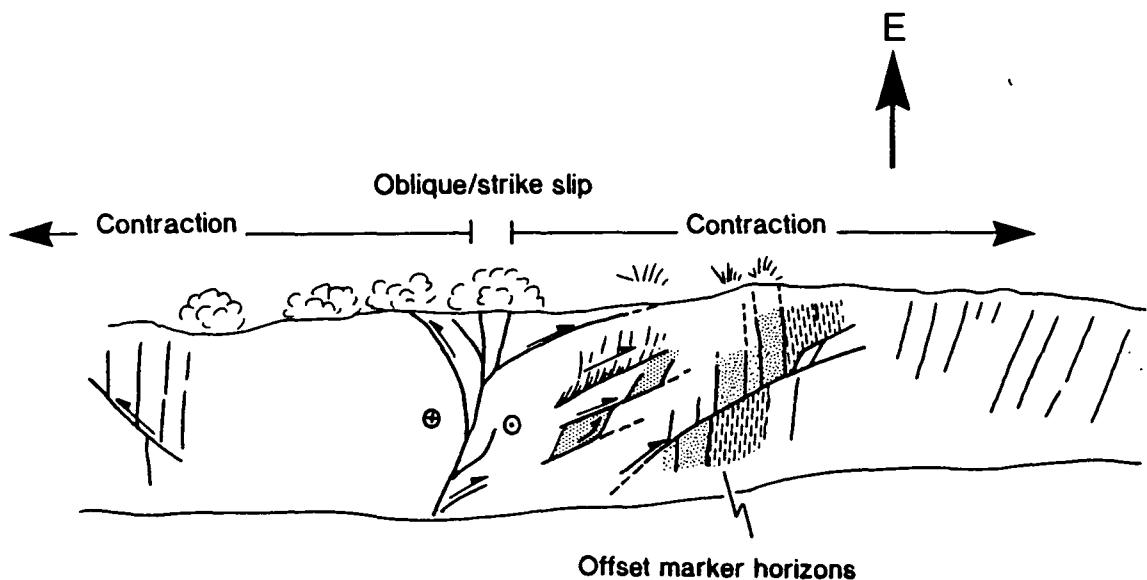


Figure 3.19b Transpressional fault system displaying a flower structure geometry and spatial strain partitioning of the strike-slip and shortening components. Location highlighted in fig. 3.19a

* All grid references for the S. dos Candeeiros region are prefixed by 08° (Lat.) and 39° (Long.).

3.4.3 The deformation style and kinematics of the Alcanede fault

Considering the data presented in sections 3.4.1 to 3.4.2, the Alcanede fault appears to have a complex deformation style. In both the southeastern and northwestern segments of the fault, dextral and reverse components of shear are evident, and where thrust transport directions are found the strain appears to be transpressional. However, the strain in the southeast segment cannot be modelled by simple transpression, and appears to display temporally partitioned strain. The formation of the fault-parallel monocline along the southeastern segment indicates that initial deformation occurred via fault perpendicular contraction, producing a high angle fault-parallel anisotropy that has been reactivated by the dextral component of slip. The presence of a dextral component within the extensional flexural shear suggests that a component of dextral slip was occurring during the latter stages of monocline formation. Therefore, the progressive formation of a sub-vertical anisotropy (steep bedding) appears to have exerted a fundamental control on the temporal partitioning of strain in the southeastern segment.

The variation in deformation style along the northwestern segment also suggests that the initial orientation of bedding with respect to the fault zone at the onset of deformation is important. A similar style of deformation to that observed along the southeast segment is found along the northwest segment, with fault-parallel folding of presumed originally fault parallel bedding. However, the timing of the two strain components is not clear. The presence of flower structure geometries demonstrating spatial strain partitioning, and zones of contemporaneous strike-slip and reverse slip suggest that the two components were coeval.

3.5 The Mendiga fault zone

The Mendiga fault zone trends NNE-SSW, sub-parallel to the S. dos Candeeiros fault zone, and forms the northwestern boundary of the Candeeiros block. The fault trace coincides with a large fault scarp running southwest from the quarry overlooking Porto de Mós towards the village of Mendiga, from which it derives its name. Jurassic aged fault scarp talus deposits are found along its trace, indicating that it initiated during the Jurassic rifting episode. Since the Jurassic the fault has undergone a period of reactivation with two distinctly different structural and kinematic styles present at its northeastern and southwestern ends.

3.5.1 The northeastern segment

The northeastern segment of the Mendiga fault is exposed in a large quarry overlooking the town of Porto de Mós. The quarry is currently being worked for road stone therefore it provides superb unobscured exposures of the structures. The quarry

has been cut into an Aalenian aged limestone and shale sequence approximately 300m wide, and is bounded on two sides by the steep northwesterly dipping Mendiga fault on the northwest, and a large extensional fault on the southeastern side. In the hanging wall of the Mendiga fault is the black pebbled conglomerate horizon that represents the base of the Oxfordian sequence, indicating that the fault has an extensional stratigraphic throw. The limestone and shale sequence contained between these main faults is intensely faulted, with numerous steep extensional faults producing an intricate fault system. Where offsets are discernible, they are commonly only a few metres to less than a metre in magnitude. Some of the more continuous faults have large throws that are greater than the height of the excavation face (i.e. greater than 10m), and are presumed to be first order faults, onto which numerous smaller extensional faults ride. These relatively large throws are suggested by: the presence of subtle roll-over anticlines, formed where fault planes shallow slightly, and the distribution of deformation in the adjacent fault walls by small rotated fault blocks. The fault blocks accommodate extensional motion via a network of faults that extend the thickness of individual limestone units becoming listric along shale horizons (plate 3.11).



Plate 3.11 Distributed faulting adjacent to an extensional fault with a relatively large displacement. Distributed deformation is manifest as listric faults within competent Lst. beds that detach along shale horizons producing equi-dimensional (in profile) rotated fault blocks.

A plot of extensional fault plane orientations on an equal area stereonet reveals that the faults generally strike northeast to southwest, however, the poles to fault planes cluster into three distinct sets. Such multi-modal fault sets indicate that a triaxial strain has occurred, in this particular case the three sets of faults accommodated a three-dimensional, coaxial, extensional strain, as non-coaxial rotational strain fields produce quadrimodal fault systems (Reches, 1978).

Examination of the extensional fault planes reveals a sub-horizontal corrugation due to the differential abrasion of the truncated limestone and shale beds. These corrugations produce elongate depressions that behave as erosional shelters allowing the accumulation of fault breccias, while the crests of the corrugations become polished due to the precipitation of clear calcite, which are in turn striated and deeply grooved by plough marks produced by asperities along the fault walls. These striations indicate a dip-slip extensional movement along the faults. The fault planes are commonly reactivated, displaying sub-horizontal calcite fibres, striated accretionary calcite steps and thin zones of striated red fault gouge. Shear sense indicators suggest a consistent sinistral motion, although occasional dip-slip reverse slickenside striae were also observed.

Late dextral faults are also seen offsetting many of the structures within the quarry. They possess a NNW to SSE orientation, and form a conjugate set with the sinistral reactivation faults. The reverse slickenside striae lie within the acute bisectrix of this conjugate set, suggesting they are coeval. These dextral fault planes are covered with slickolites indicating that the strain rate and amount of displacement along the faults was low (figure 3.20).

The bedding within the quarry faces defines a monoclinial fold adjacent to the main Mendiga fault plane, with reverse faulting present within its hinge zone, suggesting that the monocline is a result of compression, and is not a relic drag fold formed during the Jurassic when the Mendiga fault was extensional. The main Mendiga fault plane trends NNE-SSW and dips steeply to the northwest. Slickenside striations vary from dip-slip to strike-slip, which in all cases display components of dextral and reverse slip. This shear sense is confirmed by a wide variety of shear sense criteria; 'T' fractures, 'R' fractures, and accretionary calcite steps.

The faulting in the quarry indicates that two phases of deformation have occurred within this region, an early probably Late Jurassic extensional phase of faulting that produced three sets of coeval extensional faults indicating a triaxial strain, and a later compressional phase, resulting in the reactivation of the extensional faults as sinistral strike-slip faults, and the formation of dextral faults to form a conjugate set, with occasional coaxial reverse faults present. The component of dextral motion along the Mendiga fault suggests that the reactivation may be related to the late transpressive

phase of motion along the Alcanede and Alvados/Minde faults, with the generally late compressive structures related to the contractional strain at the termination of the Alvados fault during its dextral phase of motion.

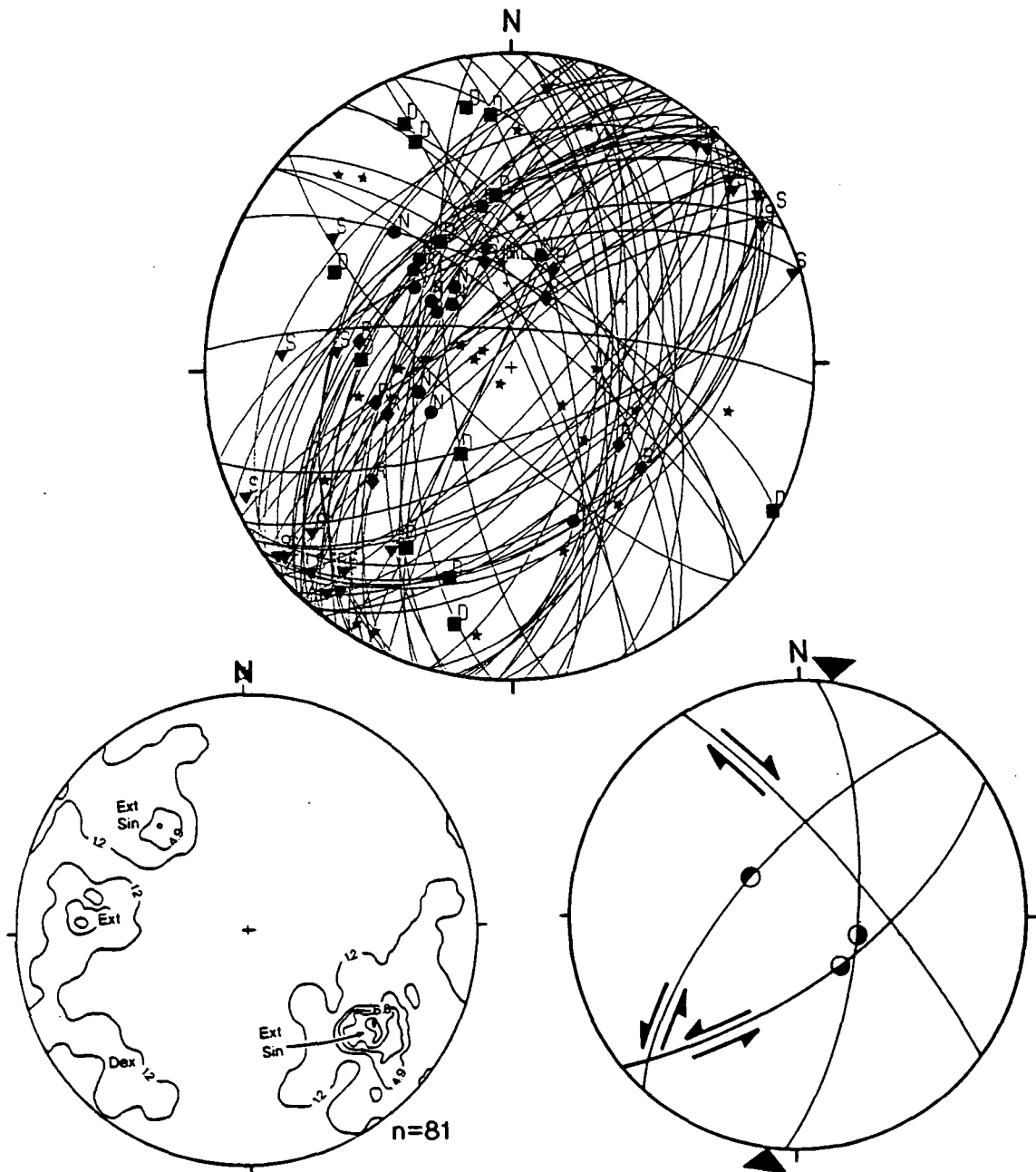


Figure 3.20 (Top) Equal area stereonet displaying fault planes and slickenlines. Triangle=sinistral, square=dextral, circle=extensional, diamond=reverse, and star=unknown shear sense. (Bottom left) Contoured poles to fault planes for same data set. Ext=extensional faults, Sin=sinistral faults, and Dex=dextral faults. Reactivation shear sense indicated by lower abbreviation. (Bottom right) Schematic representation of the fault sets. (solid semi-circle indicates downthrow side)

3.5.2 The southwestern segment

The southwestern segment of the Mendiga fault is marked by a thick zone (3-4 metres wide) of composite extensional calcite veining (plate 3.12). The fault zone has been

locally excavated along its length, presumably for the calcite mineralisation. The excavated sections provide excellent exposures revealing slickenside surfaces. These surfaces have a corrugated nature with secondary extensional fractures or 'comb structures' developed orthogonal to the crests and troughs of the corrugation. These structures clearly indicate an oblique sense of slip in the fault zone, with components of dextral and extensional motion. Extensional veining elsewhere along the fault trace displays oblique mineral growth, suggesting that constant, low strain rate, dextral slip was occurring across the vein during extension and calcite precipitation. Slickensides on the vein walls have an oblique striation consistent with dextral oblique extension. Examination of rarely exposed mesoscopic faults along the main fault trace reveal the presence of a dextral 'horsetail' fault system (Segall and Pollard, 1983), sub-parallel to the main Mendiga fault, again confirming a dextral component of motion along the main fault zone.



Plate 3.12 View looking SSE along the Mendiga fault, showing the composite extensional calcite veining common along its southeastern end. Hammer shaft 35cm.

The southwest segment is further complicated by the development of a first-order, right stepping, en-echelon fault geometry. The faults have a relay zone 3km long, and are separated by a fault bridge 1.25km wide. The fault bridge appears to be partially breached by a connecting splay, (nomenclature from Ramsay & Huber, 1987). The northwesterly stepover can be traced to the northwestern termination of the Alcanede fault. The fault zone is very poorly exposed, but anastomosing breccia zones can occasionally be seen along its trace. The breccias do not possess a cataclastic

texture, instead they display asymmetric 'bullnose' clasts with cataclastic debris trails and rare calcite pressure shadows developed from their long axes. This suggests that these narrow zones are small splays associated with the main fault that have not accommodated large displacements. However, the clasts consistently indicate a dextral extensional shear sense within the zones, confirming their structural and kinematic relationship to the main trace of the southwest Mendiga fault segment.

As shown above, the southwestern segment of the Mendiga fault possesses a consistent oblique sense of slip with components of both dextral and extensional movement. Like the northeastern segment of the fault, the kinematics of the southwestern segment appear to be the result of extensional strains associated with the northwest termination of a dextral strike-slip/transpressive fault, i.e. the Alcanede fault.

The variation in the normal component of strain across the Mendiga fault from contractional in the northeast to extensional in the southwest, suggests that it is due to tip line stresses at the termination of dextral strike-slip faults (Sanderson & Marchini, 1984; and Rispoli, 1981). The dextral component of motion along the fault is presumably the result of relative motion between the rotation of the Candeeiros fault block (see section 3.8) and the 'sheet' of Oxfordian aged strata that sits between the S. dos Candeeiros fault and the Mendiga fault zone.

3.6 The southeastern thrust zone of the Candeeiros block

The southeast boundary of the Candeeiros block is formed by a continuous thrust fault (Amiais de Baixo thrust zone) connecting the termination of the Alcanede fault zone to the southeast termination of the Minde fault zone. The thrust sheet carries Middle Jurassic to Upper Cretaceous age strata over Oligocene to Miocene clastics of the Lower Tagus sub-basin. A second thrust sheet (the Monsanto thrust) is present forming a diverging splay above the Amiais de Baixo thrust, the branch point of which is located approximately 2km northeast of the village of Monsanto. The Monsanto thrust transports Bathonian limestones over Cretaceous and Oligocene sediments that form a nested basin on the back of the Amiais de Baixo thrust sheet.

3.6.1 The Amiais de Baixo thrust zone

As mentioned the Amiais de Baixo thrust zone joins the southeast terminations of the Alcanede and Minde faults. The strike and geometry of deformation associated with the Alcanede fault gradually transforms into the adjacent thrust zone. In contrast, the junction of the thrust zone with the Minde fault zone displays abrupt truncations and changes in structural geometry.

The thrust zone produces a dominant fault scarp in the southwest which diminishes toward the northeast where poorly consolidated Cretaceous clastics overlie

the Upper Cretaceous and Oligo-Miocene clastics. This decrease in throw suggests a northeasterly propagating thrust, alternatively it may be the effect of a superimposed anti-clockwise block rotation upon southerly directed thrusting (section 3.8), resulting in differential amounts of thrust transport. The thrust sheet can be divided into three sub-areas: the area southwest of the village of Abra, the area to the east of Abra (Relvinhas sub-area), and the perched Oligocene clastic basin north of Abra. (Map 1).

3.6.1.1 Southwestern sub-area

The southwestern sub-area is formed of Bathonian and Oxfordian aged limestones, bounded on its eastern side by a NNW-SSE oriented compartment fault (the Prado fault), the Amiais de Baixo thrust to the south, and an upper Jurassic unconformity to the north. The area is dominated by a periclinal anticline cored by Bathonian micrites, the fold axis of which swings from NW-SE to E-W following the local trace of the Amiais de Baixo thrust. The anticline initiates parallel to the Alcanede fault and its associated monocline. However, unlike the Alcanede monocline, which straddles its deformation zone, the Amiais de Baixo anticline has formed in the hanging wall of the fault and is southwest verging. Discrete stratigraphic truncations are present in the footwall of the thrust zone with a NW-SE oriented overturned footwall syncline present which verges to the southwest. Following the thrust zone east, the structural grain changes to an east-west orientation, with approximately southerly directed thrust transport. A poorly developed axial planar pressure solution cleavage is associated with the Mesozoic carbonates.

The thrust zone is exposed immediately north of the village of Prado (grid ref. 46'37" 24'10"), where it forms a 1 metre thick breccia zone separating Oxfordian limestones of the hanging wall, from Lower Cretaceous coarse yellow sandstones of the footwall. The thrust zone consists of sub-rounded to sub-angular, commonly rhomboidal shaped clasts, up to 20cm in length, set in a coarse grained sandstone matrix. A strong planar fabric is present within the breccia zone, along which many of the elongate clasts lie. No slickenline lineations were observed due probably to the distributed nature of the deformation and the poor cohesion of the fault rock. At the upper limit of the thrust zone the rhomboidal or 'bullnose' clast formation process can be observed. Large clasts are formed by the intersection of two discrete fracture sets, R and P shears, which form anastomosing shear lenses or 'bullnose' clasts (figure 3.21 and plate 3.13). The shear sense derived from these bullnose clasts indicate a top to the south thrust transport direction. The orientation of the planar fabric suggests that the Amiais de Baixo thrust strikes 080° at this point along its trace.



Plate 3.13 Anastomosing shear lenses or 'bullnose' clasts along the Amiais de Baixo thrust, indicating top to the right (south) thrust transport direction.

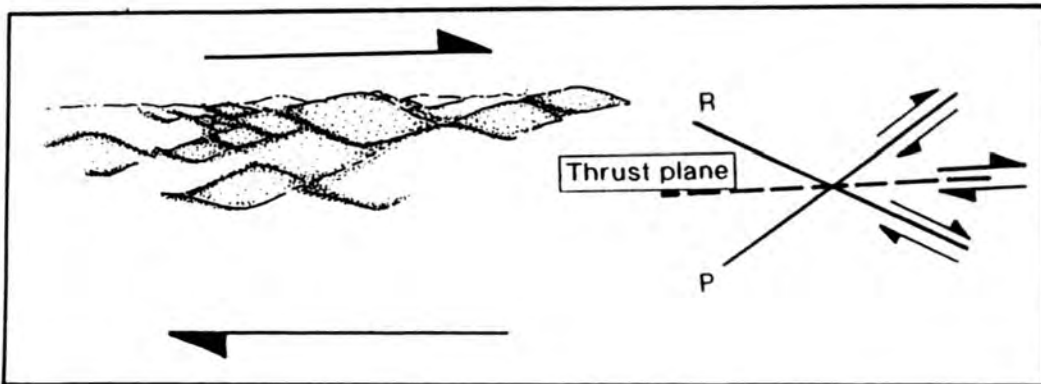


Figure 3.21 Geometry of shear lenses relative to the fracture sets. R, Riedel shears; P, P-shears.

3.6.1.2 The Relvinhas sub-area

The Relvinhas sub-area is composed of Aalenian to Bathonian age micrites unconformably overlain by Lower Cretaceous clastics. Together they form a southeast verging hanging wall anticline within the thrust sheet. The thrust sheet sequence overlies Cretaceous and Oligocene aged rocks of the footwall, that form an overturned syncline. π -diagram analysis of hanging wall bedding indicates a consistent orientation for the hanging wall anticline fold axis of $20^{\circ}/071$ within the vicinity of the Prado fault, to $14^{\circ}/067$ around Relvinhas hill top (figure 3.22).

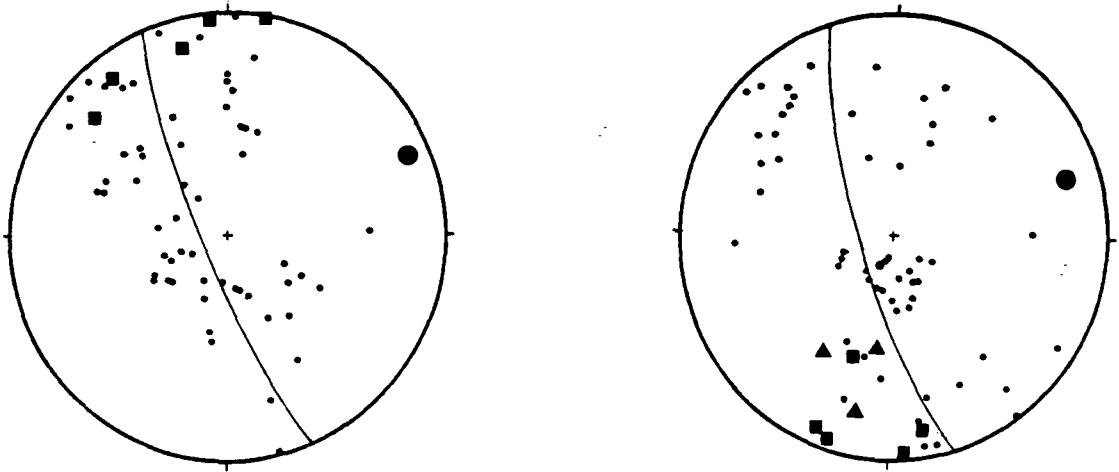


Figure 3.22 Equal area stereonets displaying π -diagrams for bedding in the Amiais de Baixo thrust sheet near the Relvinhas region (left), and the area east of the Prado fault (right). Cleavage transects the fold axes in a clockwise sense. Dots = poles to bedding; squares = poles to cleavage; triangles = lineations on bedding surfaces.

Cleavage

A weakly developed pressure solution cleavage is present throughout the sub-area, commonly manifesting itself as isolated stylolitic seams observable only in freshly hammered surfaces. The cleavage is sub-perpendicular to bedding and dominantly east-west striking, forming a clockwise transection angle with the hanging wall anticline of approximately 23° . Axial planar cleavage is also present. The chronological relationship between the cleavage sets indicates that the transecting cleavage post-dates the axial planar cleavage (see 3.6.2.1).

Mesoscopic faulting and bedding plane reactivation along the Relvinhas thrust segment

The main thrust plane is not exposed along this segment of the fault trace, consequently there is a paucity of data for this section. The data obtained represents mesoscopic thrust faults that display a SSE direction of transport which coincides with the fold profile plane for the hanging wall anticline, indicating they have a coaxial relationship. The thrust sheet is dissected by a north-south oriented dextral fault that forms a roughly transport parallel compartment fault. The deformation style varies abruptly across this fault suggesting it has a controlling influence on the developing structures (see Map 1).

By far the most common mesoscopic faults observed are bedding parallel reactivation faults formed along the steep southern forelimb of the hanging wall anticline. These faults are discrete planes and do not possess breccia zones or gouge. The fault planes display short calcite accretion steps and pressure solution slickolites, bearing testimony to the minor displacements which have occurred. The slickenline lineations derived from the calcite slickenlines and slickolites, display a very consistent sinistral sense of shear with a minor component of reverse motion (figure 3.23). Good

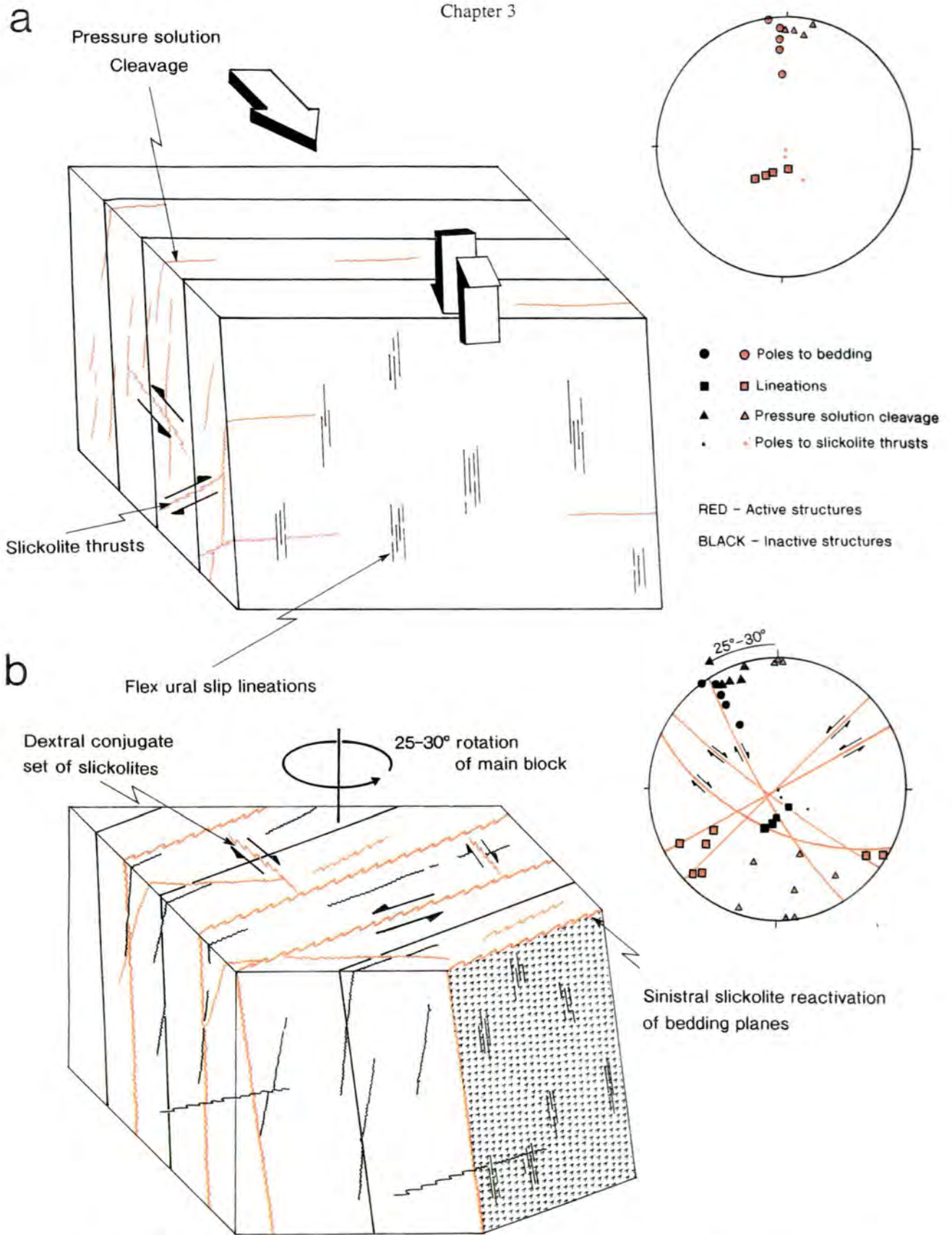


Figure 3.24 a) Mesoscale structures associated with the formation of the hanging wall anticline. b) Late non-coaxial structures overprinting initial set by 25-30°. See text for detail.

The strain preserved in the hanging wall rocks at Penas de Prado, allows a detailed insight into the evolution of the Amiais de Baixo thrust zone. The last structures to form indicate an almost due south direction of thrust transport, and are superimposed upon structures associated with an apparent south southeasterly thrust transport direction. This scenario can be interpreted in two ways: either the regional principal shortening direction responsible for the thrust development rotated from a SSE-NNW orientation to a N-S configuration, or the rock body was rotated about a vertical axis in an anti-clockwise sense relative to a stable shortening axis. As mentioned in section 2.2, the relative orientation of the regional shortening direction to the Lusitanian basin changes in an anti-clockwise sense between the Late Miocene and Recent. This is opposite to the relative sense of strain rotation in the quarry, therefore, it appears that the rock body must have rotated relative to the shortening direction, suggesting a 25-30° anti-clockwise rotation of the S. dos Candeeiros block. Figure 3.24 is a schematic block diagram showing the evolution of strain within the hanging wall incorporating the block rotation. The detailed structural relationships, so well preserved in the fresh exposures of the Penas de Prado quarry, are not found in such completeness elsewhere due to the poor exposure. However, sinistral reactivated bedding planes plus transecting cleavages were observed along the length of the Relvinhas sub-area suggesting that the rotation occurred on a regional scale.

3.6.1.4 The perched Oligocene basin

The Oligocene sediments form an elongate 6.5km x 1.5km basin which trends parallel to the thrust zone, and lies to the north of the towns of Amiais de Baixo and Canal. The Oligocene sediments lie unconformably on Cretaceous sediments which in turn are unconformable on Middle to Upper Jurassic carbonates.

Stratigraphic relationships, based on the Serviços Geológicos De Portugal 1:50,000 geological map, reveal that the base Aptian-Albian unconformity has a varying relationship to the underlying Jurassic stratigraphy indicating that tectonic disruption had taken place during the Late Jurassic. The relationships show that the Prado fault is post-Portlandian and pre-Cretaceous in age and therefore is most probably a Late Jurassic to base Cretaceous extensional fault. The Cretaceous sequence displays a straight succession from Albian to Turonian, that has been gently folded into a syncline parallel to the Amiais de Baixo thrust. The overlying Oligocene forms a northwestward over-stepping relationship with the Cretaceous.

The structural and stratigraphic relationships seen in the Amiais de Baixo region, may be explained by a thrust top model. This model involves the formation of an elongate, thrust parallel depositional basin on the back of a developing thrust sheet behind the thrust front. During hanging wall anticline development and uplift at the

thrust front, the deposition centre of the perched basin will move toward the hinterland resulting in the syntectonic sedimentary sequence forming an over stepping unconformity. If this interpretation is correct, it suggests that the initiation of thrusting in this region occurred in the Oligocene. Alternatively, these stratigraphic relationships may simply relate to localised uplift relative to the present day position of the Amiais de Baixo thrust (Figure 3.25). Evidence supporting a localised early phase of uplift was recognised by Wilson et al., (1990) who speculate that uplift may have begun as early as the uppermost Cretaceous within the Lusitanian basin. Therefore, it seems likely that regional uplift in the Amiais de Baixo region may be related to Betic tectonics to the south of Portugal, during early Oligocene subduction (Leblanc and Oliver, 1984), which was the precursor to the main Miocene inversion event in the Lusitanian basin. However, detailed stratigraphic and sedimentological studies are required to validate this hypothesis.

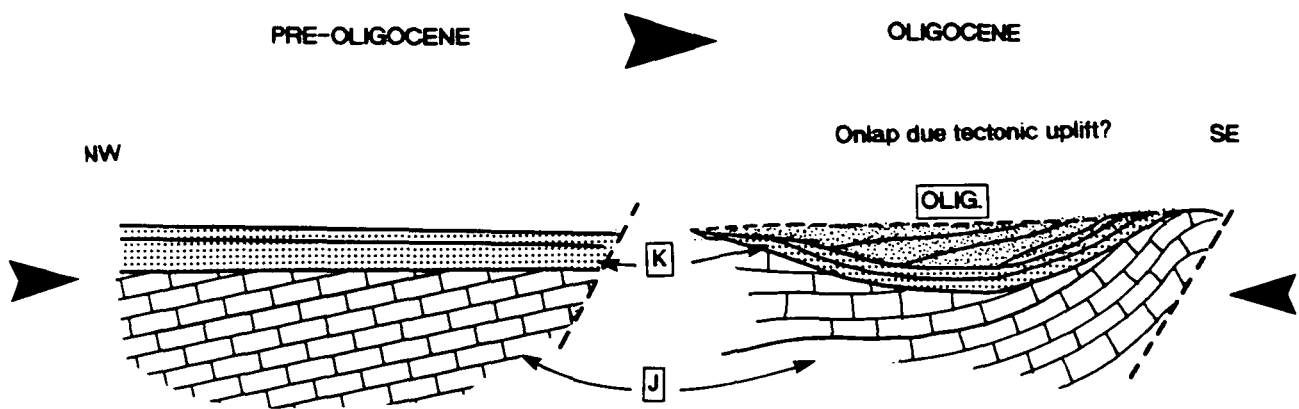


Figure 3.25 Possible origins of the Oligocene basin northwest of Amiais de Baixo.

3.6.2 Monsanto Thrust Zone

As mentioned in the introduction to section 3.6 the Monsanto thrust forms a diverging splay above the Amiais de Baixo thrust sheet, placing Bathonian micrites over the Cretaceous and Oligocene clastics of the Amiais de Baixo perched basin. The thrust trace can be followed for approximately 14km, from Moitas Venda in the northeast, to its lateral thrust tip near the village of Estudante in the southwest.

Deformation in the hanging wall is confined to a zone up to 2km wide along the thrust front, the structure of which is dominated by a hanging wall anticline and a gentle hinterland syncline, that overlie a truncated footwall syncline. The geometry of this hanging wall anticline varies quite dramatically along the fault trace from an open inclined fold to a tight overfold. The tightness of the interlimb angle and hence the

amount of strain does not adhere to a pattern of increasing strain away from the lateral tip, instead the most developed folds coincide with compartment faults that lie parallel to the thrust transport direction. These compartment faults also coincide with systematic strike swings, and therefore appear to exhibit an important control on the structural development of the thrust sheet (Map 2).

The complexity of the thrust zone increases towards its northeast termination, where a number of spectacular thrusts have developed which are confined between the Moitas Venda fault and a compartment fault approximately 700 metres to the southeast. The lateral relationship between these faults is unclear, however they appear to die out laterally with a small overlap.

3.6.2.1 Thrust zone kinematics

The main thrust plane was not exposed, but numerous mesoscopic reverse and thrust faults were encountered. The dominant set of faults, by far, are ENE-WSW striking back thrusts. The best exposure of which, was observed in a road cut along a single track road at Penas dos Corvos, (grid ref. 43'89" 27'90"). The exposure is dominated by post-folding back thrusts that reactivate bedding surfaces in the forelimb of the hanging wall anticline. Numerous thrust geometries are present including a bedding parallel duplex zone, and 'extensional' back thrusts (figure 3.26a). These 'extensional' thrusts are formed where back thrust faults cut down sequence in previously tilted strata so that the contractional faults carry younger rocks over older therefore displaying 'extensional' stratigraphic throws (see figure 3.27). The fault planes are commonly coated with fault precipitated calcite accretionary steps or slickolite striae, which allow for easy shear sense determination. Figure 3.26b displays a equal area stereographic projection for thrust and reverse fault slickenside striae, the vector mean thrust transport direction derived from this data set being 172° . When considering only the late back thrusts a transport direction of $359-179^\circ$ is derived. This direction of thrust transport is very similar with that derived from the Penas de Prado quarry, namely a north-south orientation.

3.6.2.2 Large scale fold geometry and associated structures

As mentioned, the thrust sheet is dominated by a well developed hanging wall anticline and a complimentary, gentle to open, hinterland syncline. Although systematic strike swings are present along these structures, they are not of a large magnitude and therefore do not affect the large scale analysis of the fold. A π -diagram of total bedding from the Monsanto thrust sheet and underlying footwall syncline reveals a fold axis oriented 03/073 (Figure 3.28a). The data points represented by poles form a tight scatter along the constructed π -circle. Using

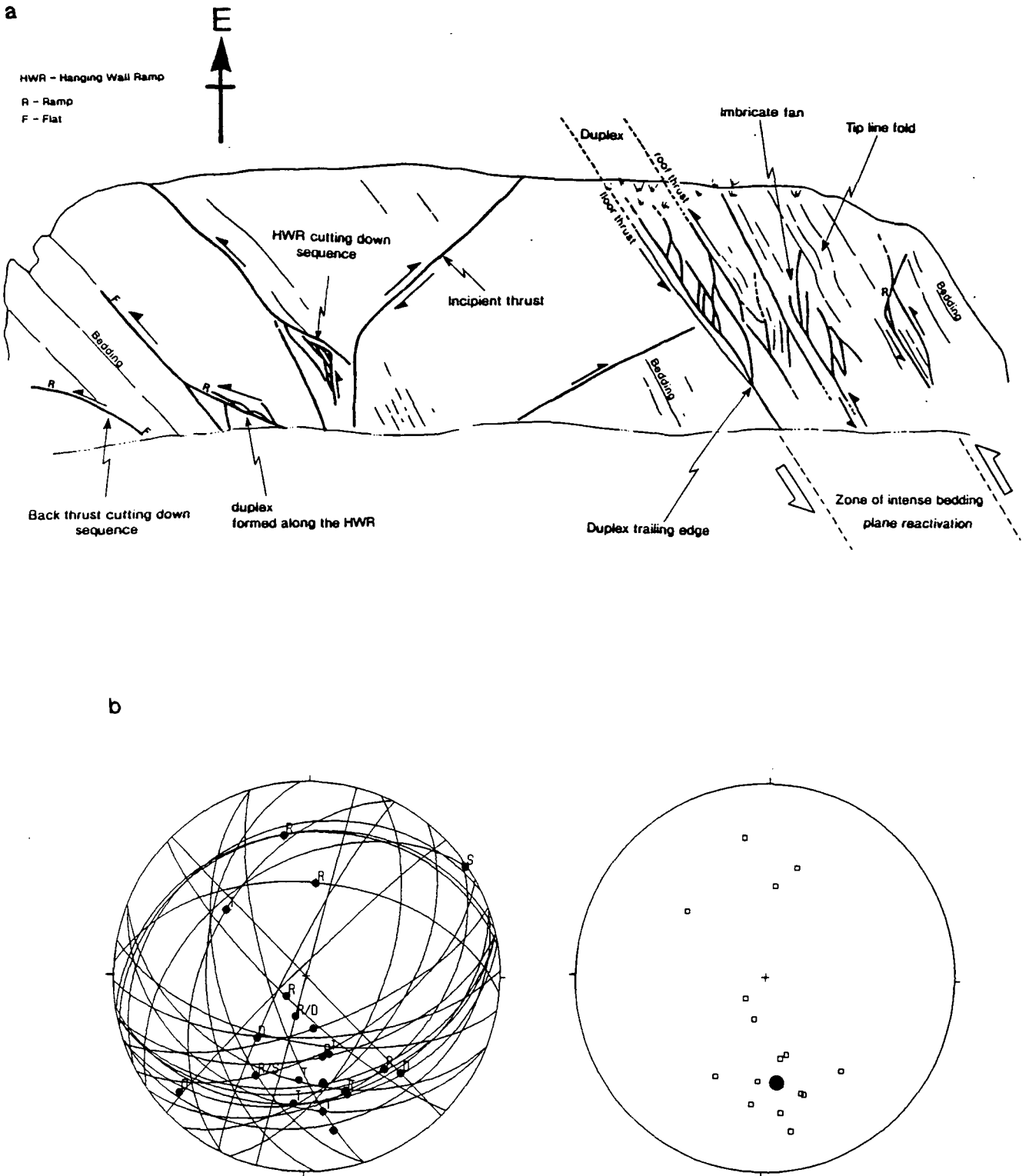


Figure 3.26 a) Sketch of road cut at Penas dos Corvos displaying the exploitation of bedding by late back thrusts which frequently cut down section. b) Equal area stereonet of fault planes and lineations measured along the Monsanto thrust zone (left), and (right) thrust and reverse fault transport directions, indicating a mean transport direction of 172-352°

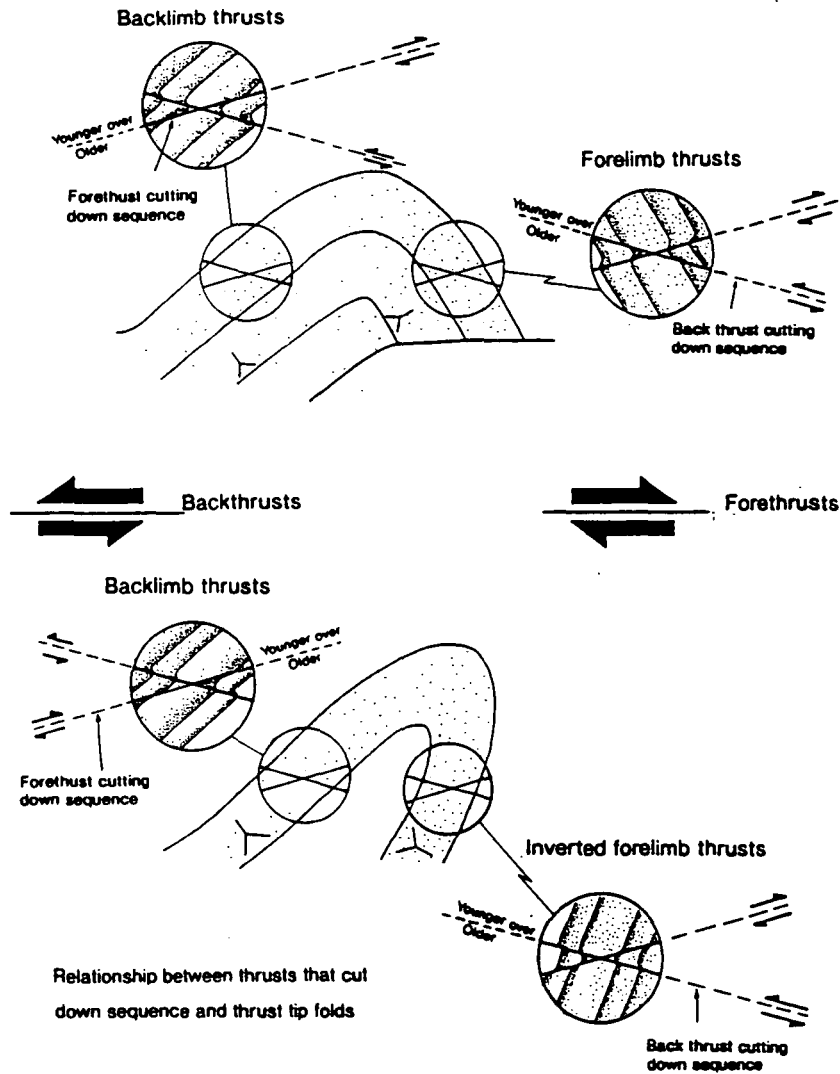


figure 3.27 Schematic diagram showing the relationship between thrusts that cut down sequence and thrust tip fold limbs.

Ramsay and Huber's (1987) classification the fold can be considered as sub-cylindrical since approximately 90% of the data points lie within 20° of the π -circle.

Bedding planes throughout the deformation zone commonly display reverse shear sense slickenside striae, that have an approximate pitch of 90° . An equal area stereographic projection of slickenlines measured on bedding surfaces show that their mean lineation and mean vector lie along the π -circle or fold profile plane (Figure 3.28b), suggesting that they are related to flexural slip during fold generation.

A well developed and frequently intense pressure solution cleavage, in the form of normal stylolite seams, is present throughout the deformation front. When plotted on an equal area stereonet, the poles to cleavage form a rough scatter along the π -circle

indicating an axial planar relationship to the folds (Figure 3.28a). Unlike the Amiais de Baixo thrust zone there is no transecting cleavage post dating the anticline formation.

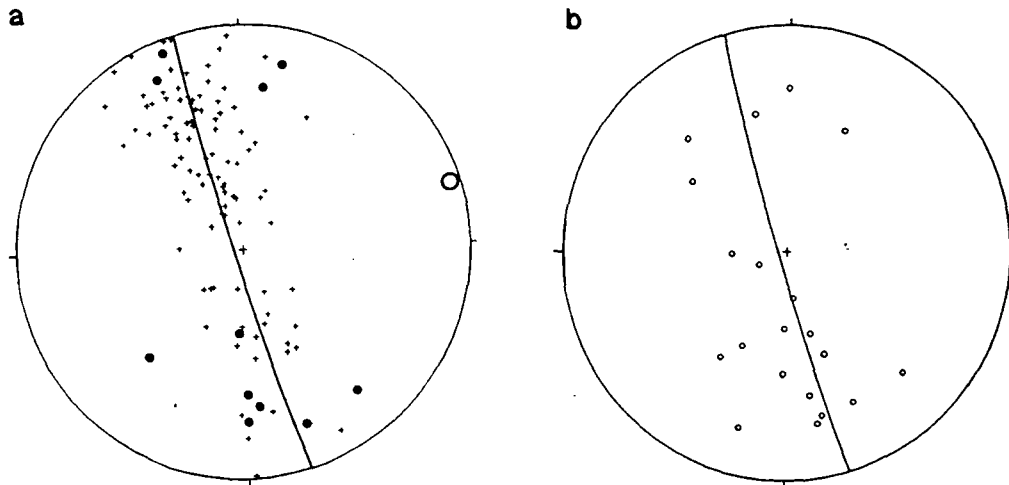


Figure 3.28 Equal area stereonets of **a**) poles to bedding (crosses), and cleavage solid (circles). π -diagram analysis reveals a mean fold axis oriented $03^{\circ}/073$, and **b**) bedding plane slickenlines with fold profile plane for reference.

Localised fold variations

In general there is an increase in the degree of fold development, from the lateral thrust tip in the southwest to the complex zone of thrusts and folds adjacent to Moitas Venda in the northeast. However, this trend is punctuated by the localised development of a tight overfolded anticline and an associated hinterland synclinal and anticlinal pair to the immediate northwest of the village of Monsanto. These folds can be traced westwards for a short distance where they merge to become the regional hanging wall anticline. To the east, the folds end abruptly against a north-south oriented compartment fault, beyond which the structural style differs considerably. The marked variation in fold style on either side of this fault may be related to a basic difference in the basal thrust plane geometry: to the west, a localised flat-ramp geometry thrust plane is envisaged to generate the complex fold geometries in the overlying thrust sheet and, to the east, a much simpler uniformly dipping thrust plane (figure 3.29). The relationship between localised fold geometry variations and compartment faults is common along the Monsanto thrust zone, as well as the Amiais de Baixo thrust zone, suggesting that the faults have had a fundamental influence on the adjacent thrust plane geometry and thrust zone development. This fundamental control suggests the faults may pre-date the Monsanto thrust. Given the similar orientation and structural relationships of these faults to the Prado fault (discussed in 3.6.1) they may be of similar age and origin, i.e. reactivated Late Jurassic extensional structures.

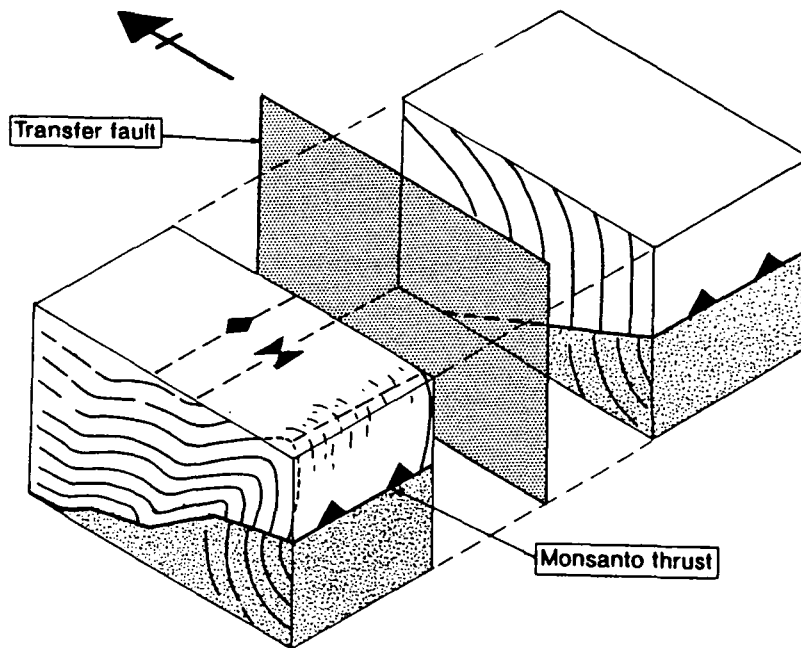


Figure 3.29 Schematic diagram displaying inferred thrust plane geometries and their effect on thrust sheet structure, either side of N-S oriented transfer fault.

3.6.2.3 Strain and small scale structures associated with folding

Due to the relatively low strain states within the Monsanto thrust sheet it is possible to identify a varied development of small scale structural features within different regions of the folds. These structures can be related to the large scale fold geometry by considering the incremental and finite strain models for flexural folds and tangential longitudinal strain, plus the consideration of prefold strains arising from initial compaction, layer parallel shortening and oblique early tectonic strains. Definite chronologies can be established for these strains from cross cutting relationships and a strain model for the progressive development of the folds established.

Prefold Strains

The strain produced by either flexural folding or *BUCKLING* is commonly superimposed on a pre-existing strain. There are three common types of prefold strain that can occur before the active folding of a layer. They are: *layer parallel shortening* and bed thickening, some *earlier period of tectonic deformation* that produces ellipses with their principal strain axes oriented obliquely to the layer surfaces, and *diagenetic compaction* or shortening perpendicular to bedding. Layer parallel shortening and early tectonic deformation will be treated together as in this case some of their effects produce coaxial structures that effectively shortened the rock parallel to bedding.

Pure layer parallel shortening strains are common throughout the Monsanto region. They are homogeneous and manifest themselves as bedding perpendicular stylolite seams and contemporaneous bedding parallel extensional calcite veining. Heterogeneous layer parallel shortening strains or pure shear tectonic deformation

parallel to bedding, is represented by the development of conjugate brittle/ductile tension gash arrays whose Y-axes are perpendicular to bedding surfaces. By stereographically rotating the tension gash data to correct for the effects of folding, it is seen that they form two strike-slip sets, a NE-SW oriented sinistral set and a dextral WNW-ESE set. The principal strain axes for these conjugate shears can be calculated by hand using the method of Hobbs et al., (1976) and Ramsay & Huber (1987), (see Appendix 1) This reconstruction produces a mean Z axis oriented $10^{\circ}/340$, indicating that the prefold strain is coaxial with the large scale fold structures (Figure 3.30).

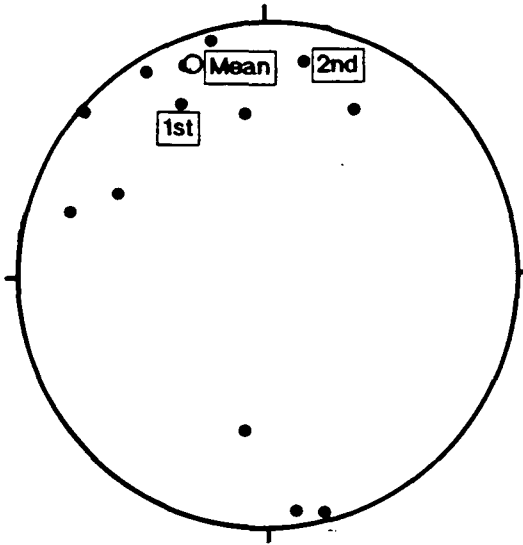


Figure 3.30 Equal area stereonet of reconstructed principal shortening directions (Z axes) of prefold strains in the Monsanto thrust sheet.

Early tectonic deformation, in the form of layer parallel simple shear, is difficult to distinguish as its effects are similar to those generated by flexural fold strains. However, unlike flexural fold strains, prefold strains develop independent of their position within the later fold. Therefore, early increments of tectonic strain can be distinguished due to their inconsistent strain pattern relative to the overprinting flexural fold or tangential longitudinal strain.

Flexural fold strain

In well bedded rocks, the strains set up during the folding process are often controlled by simple shear parallel to bedding. If the simple shear is distributed continuously through the structure the fold formed is termed a flexural flow fold, whereas if the shear is discontinuous (confined to bedding planes) the fold is termed a flexural slip fold (Ramsay and Huber, 1987). The sense of shear associated with flexural slip displacements have a systematic relationship to the fold with the structurally uppermost layer always displaying movement towards the antiformal hinge, relative to the lowermost structural layer. Slickensides and the precipitation of overlapping fibrous calcite along the bedding surfaces, with a lineation perpendicular to the fold hinge is also typical of flexural slip. Such relationships are found throughout the

Monsanto region, especially within the forelimb, indicating that the flexural slip process is a dominant fold mechanism.

In flexural flow folds, the evenly distributed simple shear strains which occur throughout a layer, sometimes produce extensional vein systems. The geometry of these vein systems follows the same principals as tension gash array formation, with the veins commonly initiating at angles of about 45 and 135° to the bedding surfaces. As the fold develops the vein systems become modified by later strain increments, figure 3.31 displays a common progression in the geometrical modification of the

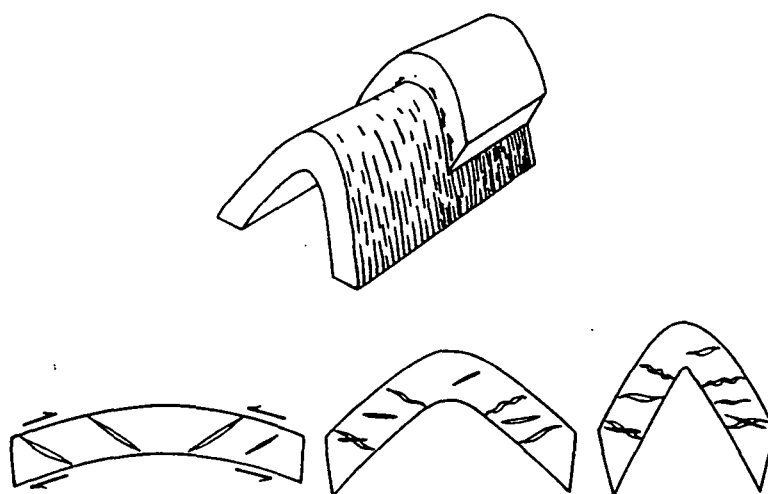


Figure 3.31 a) flexural slip model, b) formation and modification of 'ideal' extensional veins produced by flexural shear (Re-drawn from Ramsay & Huber, 1987).

vein system. However, in nature, these ideals are rarely realised and a complex relationship between extensional veins, cleavage and the incremental and finite strains exist. Figure 3.32 shows a simplified line drawing of the relationship between small scale structures from two localities within the southeast forelimb of the main anticline immediately north of Monsanto village. Figure 3.32a displays the relationship between cleavage and veins in a flexural flow strain system. The extensional veining has been localised into bedding parallel tension gash arrays within the layer. Overprinting these vein arrays, at an angle slightly less than 90°, is an intense pressure solution cleavage. The removal of vein material in solution along these oblique cleavage planes has resulted in the formation of 'bowtie' veins. In this situation the vein arrays represent the first increments of simple shear strain that have not undergone further increments of growth and rotation. Instead, with continued fold development, the vein systems have been overprinted by a solution cleavage which has formed parallel to the maximum finite longitudinal strain trajectory $(1+e_1)$. A

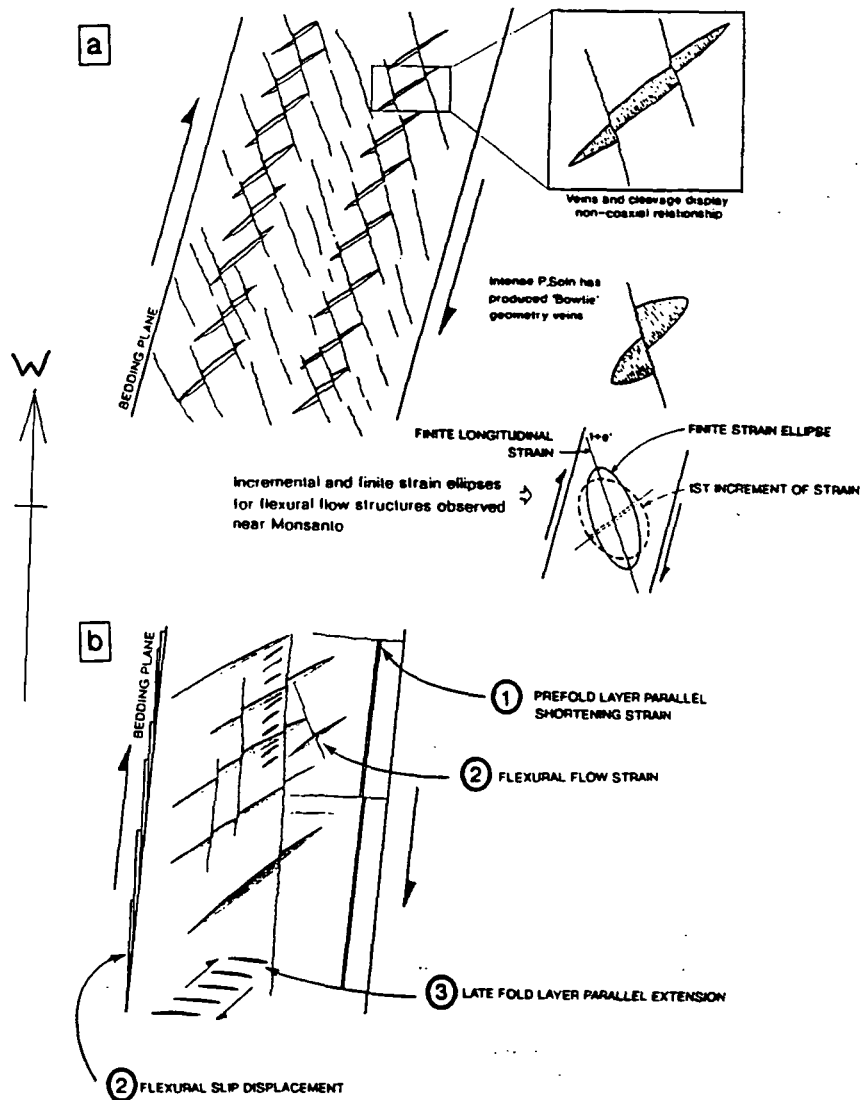


Figure 3.32 a) Flexural flow strain within the Monsanto thrust sheet. The structures formed are commonly non-coaxial, with pressure solution cleavage rotating faster than extensional veins. b) Complex strain history: 1) prefold strains, layer parallel shortening; 2) flexural shear, and flexural slip strain; 3) layer parallel extension.

more complex relationship is shown in figure 3.32b. Within the micritic beds an initial layer parallel shortening strain is overprinted by flexural flow strain, in the form of oblique extensional veins. This in turn is superimposed by a layer parallel extensional strain and related vein arrays. Evidence for flexural slip folding is present with abundant slickensides developed on the bedding surfaces, therefore the fold mechanism is a combination of both flexural fold models and produces an inhomogeneous strain. The strain history of prefold layer parallel shortening, flexural flow/slip folding and late-fold layer parallel extension is common, but it does not fully explain the strain accommodation during folding.

Tangential longitudinal strain

In sequences of varying lithology and hence rheology, strains other than those of simple shear must be incorporated to allow for strain compatibilities. The principal axes of these additional strains act sub-perpendicular and sub-parallel to the bedding surfaces and are termed tangential longitudinal strains. This type of strain tends to dominate thick competent units in interlayered sequences. To maintain geometric compatibility when folding a competent bed the outer arc of the layer must undergo layer parallel extension, while the inner arc undergoes layer parallel compression. At a point between the inner and outer arc is a surface of no finite strain, known as the finite neutral surface (figure 3.33). The geometric features of the small scale structures that form under conditions of tangential longitudinal strain are summarised in figure 3.33 b to d. Strain within the outer arc is characterised by layer parallel cleavage and layer perpendicular veining, that commonly tapers toward the base of the bed, while the inner arc is dominated by a layer perpendicular convergent cleavage fan and layer parallel veining. However, in natural rocks, small scale structures commonly superimpose upon one another, producing apparent strain reversals where the sense of shortening implied by one structure may be perpendicular to the maximum shortening implied by another. These structural relationships are the result of the migration of the finite neutral surface toward the inner arc. Finite neutral surface migration is a geometric necessity, enabling layer parallel extension in the outer arc to more or less equal the layer parallel shortening in the inner arc. Figure 3.33e & f show the progressive development of folds by tangential longitudinal strain processes indicating the strains developed with fixed (3.33e) and migrating (3.33f) finite neutral surfaces (Ramsay and Huber, 1987). In natural rocks the pure tangential longitudinal strain model briefly discussed above, is rarely developed in its ideal form and is generally combined with layer parallel simple shear strains.

Within the gentle mesoscale folds found along the Monsanto anticline the fold hinges are dominated by outer arc extension 'style' strain with the development of radial, downward-tapering, perpendicular extensional veins, and layer parallel pressure solution cleavage. Rare examples of neutral surface folding can be found with apparent 'strain reversals' present between the inner and outer arcs suggesting migration of the finite neutral surface. Commonly, however, the strain observed can not be completely explained by the tangential longitudinal model. Outer and inner arc strain is rarely observed within a single layer or bed, instead the strain is dominated by perpendicular veins and parallel cleavage, suggesting that individual layers have

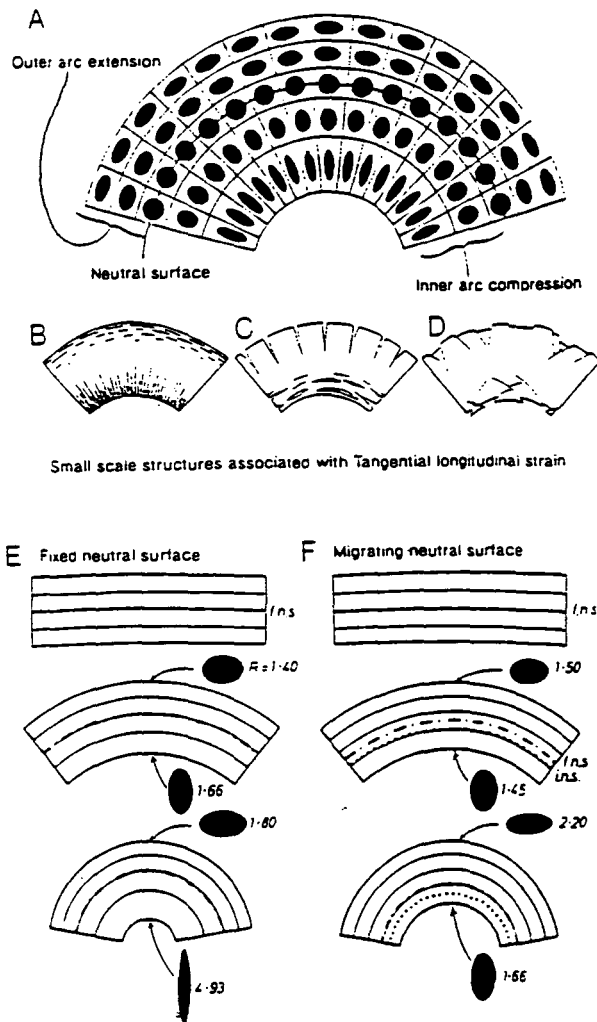


Figure 3.33 a) Tangential longitudinal strains (T.L.S.) associated with neutral surface folding. b) Cleavage, c) Extensional veining, and d) shears, associated with T.L.S. e) and f) strain compatibilities for fixed and migrating neutral surface folds. (Taken from Ramsay & Huber, 1987, figs 21.18, 21.21).

undergone layer parallel extension. This scenario may be due to the fact that the tangential longitudinal strains are not acting on the scale of individual beds, but on packages of rheologically similar beds within the sequence, with the studied outcrops located in the outer arc of the deforming package. The bedding surfaces exposed along the hinge zones of these folds do not display slickenside striae, therefore indicating that hinge zone migration has not occurred.

Strain and kinematics within the Monsanto thrust sheet

As presented above, the type of strain preserved within the Monsanto thrust sheet, particularly in the Monsanto anticline, does not conform to any one particular model or mechanism of fold formation, but is commonly a combination of several models. A more actualistic model is presented below, based on the observed relationships.

Initial deformation began in the prefold stage with the initiation of tectonic compression and the formation of a layer parallel shortening strain, commonly

accompanied by the formation of a coaxial set of conjugate strike-slip tension gash arrays. Progressive deformation and fold development was facilitated by a combination of flexural slip and flow folding within the fold limbs. This strain was inhomogeneous with a concentration of strain along the bedding surfaces producing interlayer slip. Layer parallel extension took place within the hinge zones, possibly as part of the neutral surface folding of rheologically similar rock packages. Layer parallel extension also occurred within the steep limb as it rotated to an angle of approximately 90° with the incremental tectonic strain.

This distribution of deformation, as represented by the mesoscopic structures, indicates that insignificant fold hinge migration has occurred. The concentration of tangential longitudinal strains and the absence of slickenlines along the hinge suggest that the folds have formed by fixed hinge kinking or buckling, with further deformation occurring by the passive rotation of the limbs. These fold kinematics suggest that the folds are break-thrust folds (Fischer et al., 1992).

3.6.2.4 Evidence within the Monsanto thrust zone for the rotation of the Candeeiros block

Structural studies on both meso and macro scales within the Monsanto thrust sheet reveal that the early pre-fold strain and the large scale folds are coaxial in nature, with a mean azimuth of maximum shortening oriented 160° . A thrust transport direction of 179° was derived from the movement striae on post-fold fault surfaces, suggesting that thrust movement and fold formation were non-coaxial. This relationship is remarkably similar to the Amiais de Baixo thrust zone (3.6.1.3). Both zones display an early strain that corresponds to an axis of principal shortening that is oblique and anti-clockwise of the principal direction of shortening suggested by the later thrust faults. In the Monsanto thrust sheet this relationship suggests that 18° of anti-clockwise rotation has occurred since the initiation and development of folding, and the late stage thrusting.

3.7 Serra D'Aire thrust zone

The Serra D'Aire thrust carries Middle Jurassic Bajocian and Bathonian micritic limestones of the Candeeiros formation onto, and over Cretaceous and Oligocene clastics. The fault trace is marked by a pronounced fault scarp, northwest of which is the 668m Serra D'Aire summit. This is the highest mountain in southern and central Portugal, and coincides with the large Serra D'Aire anticline that runs parallel to the thrust zone.

The exposure southeast of Serra D'Aire is generally poor and often restricted to the fault scarp. The best exposures were found along several road cuttings that intermittently cross the thrust zone. From these limited exposures it is possible to

appreciate the increased structural complexity of the thrust zone, relative to the Monsanto or Amiais de Baixo thrust zones. The large scale structures of this thrust front are commonly discontinuous along strike due to the presence of several NW-SE oriented compartment faults, and north-south trending reverse faults. At the northeastern end of the studied fault segment the thrust sheet is intensely faulted by anomalous strike-slip faults that have complex kinematic relationships with the thrust faults. At the southwestern termination of the thrust zone, near Moitas Venda, a well defined strike swing from northeast-southwest to an east-west orientation is present. This strike swing coincides with a complex kinematic fault system. (Map 3).

3.7.1 Moitas Venda region

The main fault scarp of the Serra D'Aire thrust can be seen immediately to the southeast of the village of Moitas Venda. At the time of study, a large civil engineering project was blasting a road cutting through the thrust front to accommodate a new motorway link between Lisbon and Leiria. During this period of construction before the walls of the road cut had been stabilised, a superb view of the geometry of the main Serra D'Aire thrust plane and associated structures was available.

The thrust zone strikes east-west dipping at approximately 40° to the north and truncates the footwall syncline. The zone is formed by two discrete parallel thrust faults between which is a 2-3 metre thick fault zone. This zone separates the steeply bedded Candeeiros formation in the hanging wall, from overturned Aptian-Albian age terrestrial clastic deposits in the footwall. The fault zone is formed of elongate rhombic 'horse' shaped clasts of micrite up to 10cm in length, that have an imbricate geometry. The clasts display extensional calcite veins perpendicular to their long axes and occasionally pressure shadows, formed by calcite fibre growths parallel to their elongate axis. The possession of structural continuity between the clasts suggest that they are 'insitu' or unrotated and hence were formed by systematic faulting in response to simple shear and not the process of cataclasis where the multiple mechanical fracturing of rock particles is combined with rotation and mechanical mixing. The surfaces of these micrite clasts are smeared with a dark grey clay that forms the matrix to the thrust zone. The clay itself possesses a scaly fabric formed by the interaction of two surfaces: a closely spaced penetrative fabric that is sheared and rotated into a sigmoidal geometry by a later set of discrete anastomosing shear planes, producing a similar geometry to the micrite clasts. The shear plane surfaces display a lustrous sheen and are strongly lineated by plough marks. Such scaly clay fabrics have been described in many soft sediments deformed experimentally by Maltman (1987), and Will & Wilson (1989), and are characteristic of deformation in weakly lithified sediment (Knipe, 1986). It therefore seems probable that during thrust zone formation there was

a large influx of wet unlithified clays along the thrust plane, possibly derived from the underlying Lower Jurassic shales and mudstones of the Brenha fm. Immediately below the thrust zone are overturned Cretaceous clastics that form the northern inverted limb of a large footwall syncline. Folding has been accommodated by flexural shear and grain boundary slip. Possible sheared rootlets appear to be present in the Cretaceous. They are manifest as anoxic green 'streaks' within the coarse red sandstone and form a consistent oblique angle from perpendicular of 38°. If these are indeed rootlets they would have originally been perpendicular to bedding, therefore their present attitude allows a calculation of the amount of shear strain (γ) within the fold limb

$$\gamma = \text{Tan}\psi$$

where ψ the angular shear strain, is the angular deflection of the rootlets from the perpendicular. Therefore,

$$\gamma = \text{Tan}38^\circ$$

$$\text{Shear strain } (\gamma) = 0.781$$

This value is not representative of the footwall as a whole as the strain is a flexural flow strain, and hence decreases near the fold hinge. However, due to the homogeneous nature of the Cretaceous sandstones it is a representative strain for that section of the synclinal limb.

The footwall rocks also preserve evidence of footwall collapse, as a thrust duplex is seen beneath the main thrust zone offsetting sub-vertical to overturned footwall bedding. Due to the steep overturned nature of the bedding, the steep imbricate faults are in fact thrust flats 'sensu stricto' as they are parallel to bedding, the sub-horizontal faults represent thrust ramps (plate 3.15).

The steep southerly limb of the hanging wall anticline is separated from the hinge by a strike parallel reverse fault. High angle mesoscopic reverse faults are prevalent within this steep limb, they are commonly the origin of low angle thrusts that shallow upwards and away from these mesoscopic reverse faults. North of the large reverse fault the bedding is sub-horizontal with a slight dip to the south. Some bedding planes display tectonic reactivation with various small scale fault geometries common to thrust systems. The development of footwall rip-outs, geometrically identical to the side-wall rip-outs of Swanson (1989), and extensional down dip rhombochasms (Aydin and Nur, 1985), indicate a southerly direction of thrust transport (Figure 3.34).

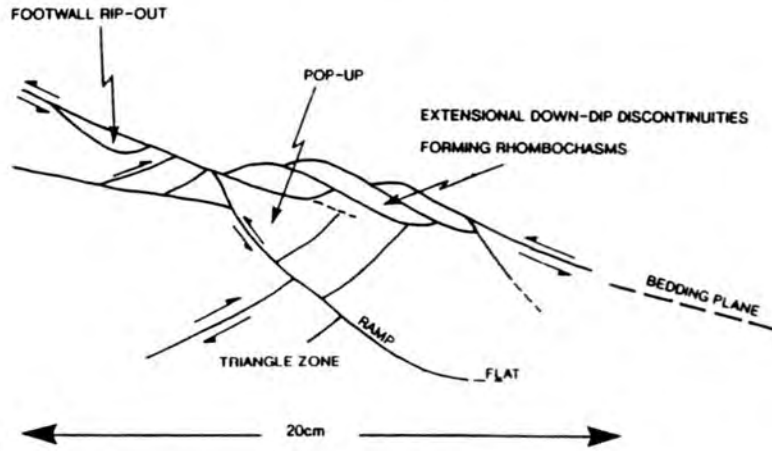


Figure 3.34 Small scale thrust geometries indicating southerly vergent thrust reactivation of bedding plane, Moitas Venda.



Plate 3.15 Footwall collapse beneath the Serra D'Aire thrust plane, producing a thrust duplex. M1 roadcut at Moitas Venda.

3.7.2 Northern region

In contrast to the Moitas Venda region, the north easterly end of the thrust zone displays a NNE-SSW structural grain. A best fit π -circle to bedding for folding along the thrust front indicates a fold axis oriented $04^{\circ}/214$. This constructed fold axis plots closely to bedding/extensional vein intersection lineations on an equal area stereonet, suggesting that these veins were formed by tangential longitudinal strains. A second set

of bedding/vein intersections plot orthogonally to the fold axis along the π -circle, suggesting that fold axis parallel extension has taken place, probably due to the non-cylindrical nature of the fold. Cleavage is poorly developed within the thrust sheet, but where present it is axial planar (figure 3.35).

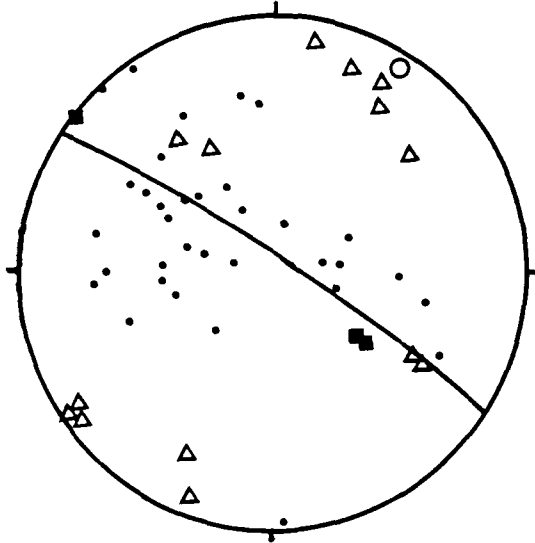


Figure 3.35 Equal area stereonet of poles to bedding (dots), and cleavage (squares). Open triangles represent bedding/vein intersection lineations. Open circle equal to fold axis. See text for details.

A localised zone of complex thrusting is present west of the village of Alqueidão, consisting of three thrust faults that coalesce along strike, with the middle thrust carrying younger Cretaceous clastics over older Bathonian micrites. This zone has been interpreted as a foreland propagating thrust sequence, within which the frontal fault has cut up through the initial thrust to produce the observed structural and stratigraphic relationships (see figure 3.36).

The structure of the thrust sheet is divided into two domains by a NW-SE oriented dextral compartment fault. The northern side of the fault is dominated by a steep back-thrust that cuts obliquely across strike and separates the forelimb and the backlimb of the hanging wall culmination. Early prefold thrust structures can be seen in the forelimb which have since been passively rotated during folding (Figure 3.37). The majority of the mesoscale faulting within the thrust sheet is post folding, with a dominance of backthrusts which exploit the tilted bedding planes. The structure is further complicated by the presence of anomalous sets of dextral and sinistral faults commonly orthogonal to the thrust front.

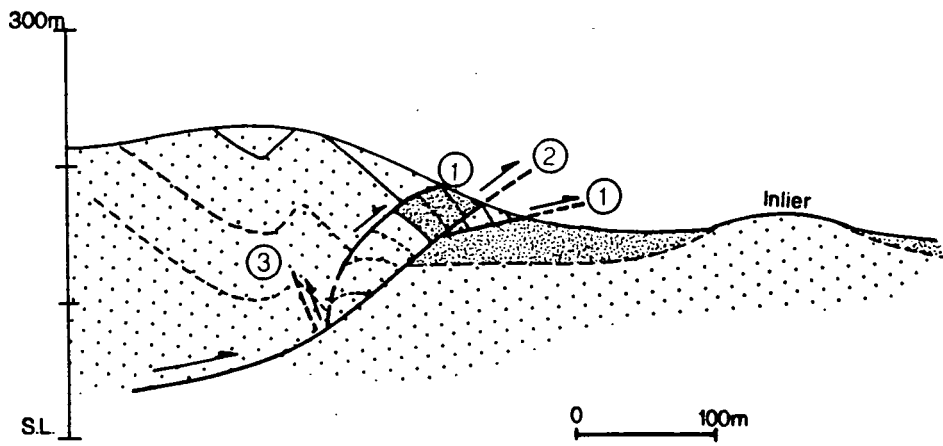


Figure 3.36 Interpretation of thrust sequence exposed to the west of the village of Alqueidão, see text for details.

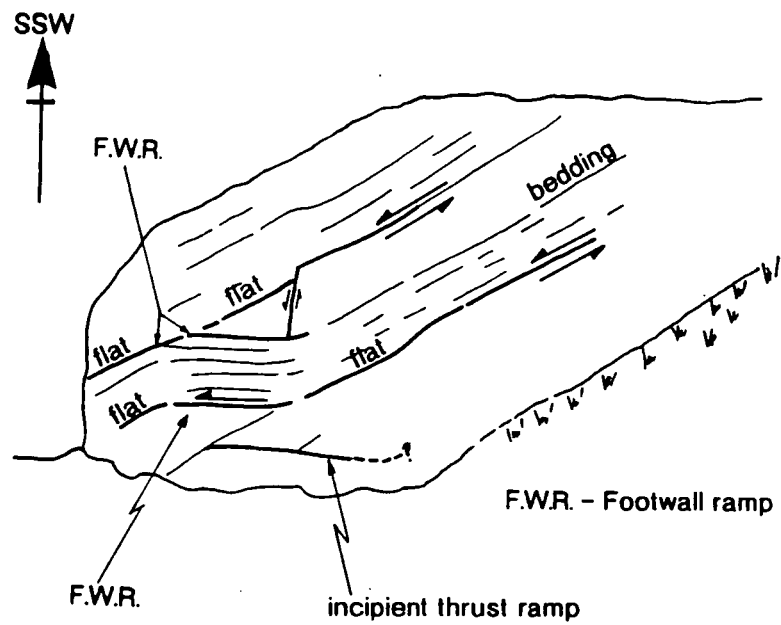


Figure 3.37 Rotated early formed thrusts within the forelimb of the Serra D'Aire thrust sheet, overlooking the village of Pafarrão.

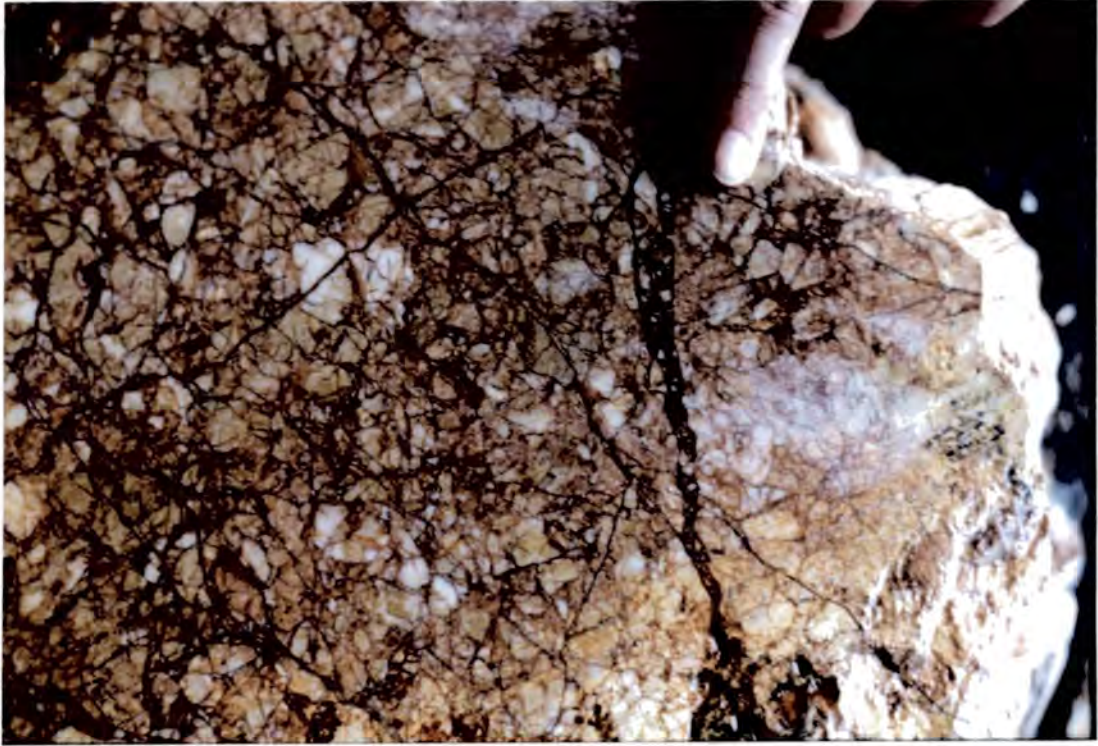


Plate 3.17 View of thrust plane displaying the fault stylobreccia, which consists of multiply fractured micrite (dominant) and calcite clasts, Extensional veins filled by red fault gouge and cataclasite lie approx. orthogonal to the fault plane striations (top right of finger)

3.7.3 Fault kinematics

3.7.3.1 Moitas Venda region

Thrust and reverse faults observed along the road section east of Moitas Venda display a consistent east-west strike with a top to the SSW direction of transport, consistent with thrust transport directions seen along the Monsanto and Amiais de Baixo thrusts. An anomalous set of steep NNE-SSW oriented faults displaying sinistral oblique extensional movement striae are present along the road cutting. The fault set is parallel to the direction of thrust transport and hence is parallel to the local plane of finite extension suggesting they are related to the exhumation of the thrust sheet and the associated reduction in confining stresses. This change in stress conditions may have been sufficient to allow extension parallel to the thrust strike. However, the origin of the sinistral component remains unclear.

3.7.3.2 Northern region

As mentioned above, the northern region possesses a complex fault system associated with the south-southeast movement along the basal thrust. A plot of total thrust and

reverse fault lineations for the area indicates a mean transport azimuth of 148° . Roughly parallel to this transport direction is a set of closely spaced mesoscopic dextral strike-slip faults. Rare sinistral faults were observed sharing this orientation, but they are more commonly parallel to the thrust zone.

A comparison of thrust transport directions observed along the main thrust plane in both the northern and Moitas Venda regions suggests a mean southerly direction of transport. This suggests that oblique thrusting has occurred along the Serra D'Aire thrust zone. Using the simple graphical construction presented by McCoss (1986), the principal axes of the infinitesimal or incremental strain ellipse can be determined (figure 3.38). Using the north-south thrust direction as the displacement vector S , an axis of minimum incremental strain, Z axis, oriented to 148° degrees, was derived. The model predicts precisely the observed thrust transport direction, therefore suggesting that the mean displacement vector for the Serra D'Aire block is correct. The relative magnitudes of the principal infinitesimal strain axes and ellipsoid shapes are a function of the angle A , which is the angle between S and the fault zone normal, these relationships are shown in figure 3.38. In this case $A=65^\circ$, indicating that the tectonic regime is transpressive but dominantly compressive. However, A is very close to the critical angle of 70.5° (the ASTP, or axially symmetric transpression angle), which has important consequences for the kinematics of the deformation zone (see section 1.2.3, p.40). When A is very close to the ASTP angle, the relative magnitudes of principal axes of incremental strain can vary due to minor variations in the displacement vector S , relative to the deformation zone. This in effect allows lineations to switch from dip-slip to strike-slip.

This theory has important implications for the kinematics of the Serra D'Aire thrust zone. As mentioned the model already predicts the thrust transport direction observed, it also predicts that the zone has a transpressive incremental strain and has an A value close to the ASTP angle, suggesting that lineation switching may be possible (Figure 3.39b). This may explain the occurrence of thrust faults and sinistral strike-slip faults sharing the same strike (Figure 3.39c). The anomalous dextral wrench faults are interpreted as being the result of distributed sinistral shear along the deformation zone with the dextral faults acting as antithetic cross faults that accommodate anti-clockwise domino style block rotations (Figure 3.39a).

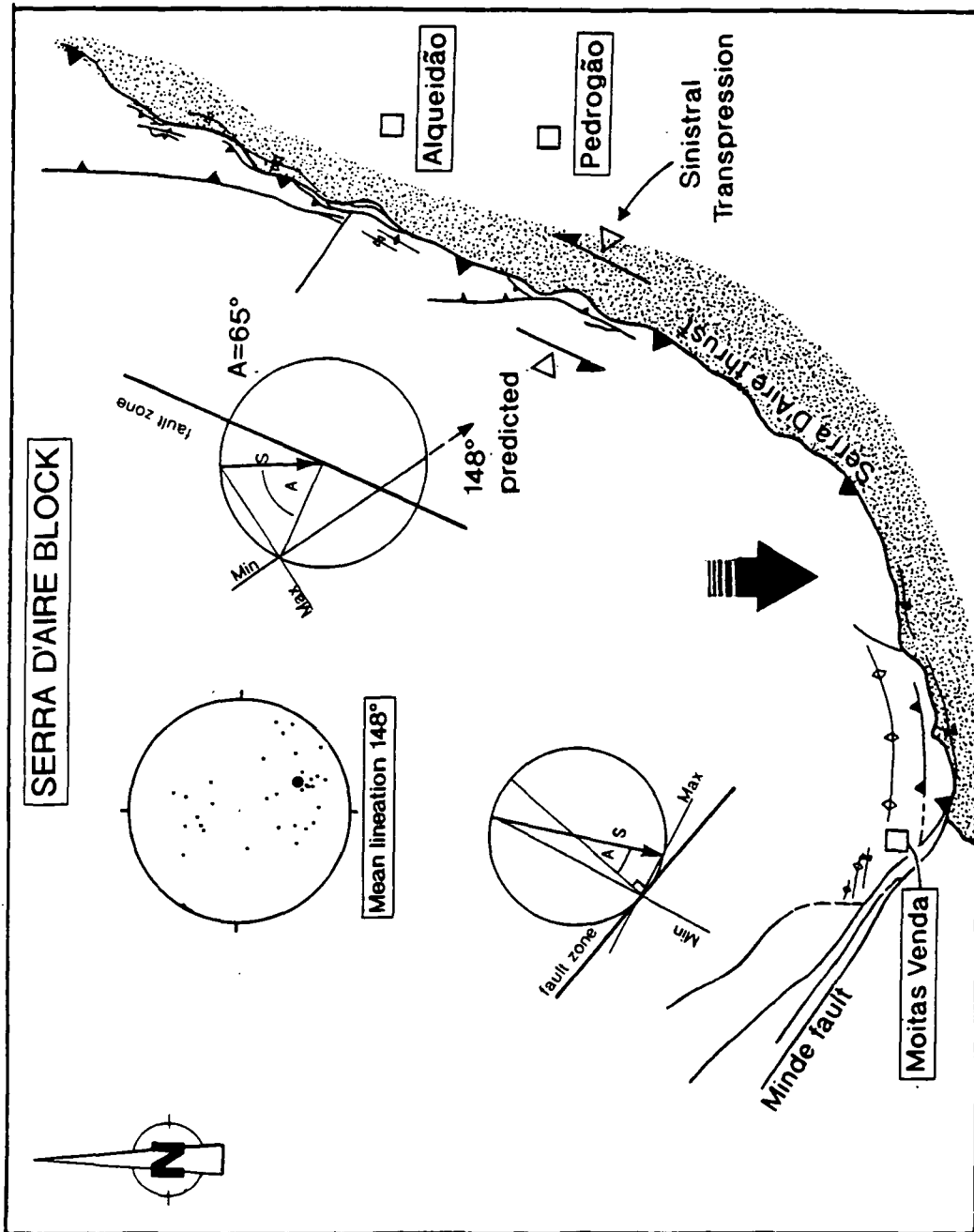


Figure 3.38 McCoss constructions (1986) for the Serra D'Aire thrust zone. The graphical construction predicts a thrust transport direction for small displacement faults (small displacements approximate to the increment strain direction), of 148° . The observed mean thrust or reverse lineation vector is 148° , suggesting the proposed N-S thrust sheet displacement direction is correct. (See text for details) S=thrust sheet displacement direction, Large arrow = proposed thrust displacement direction.

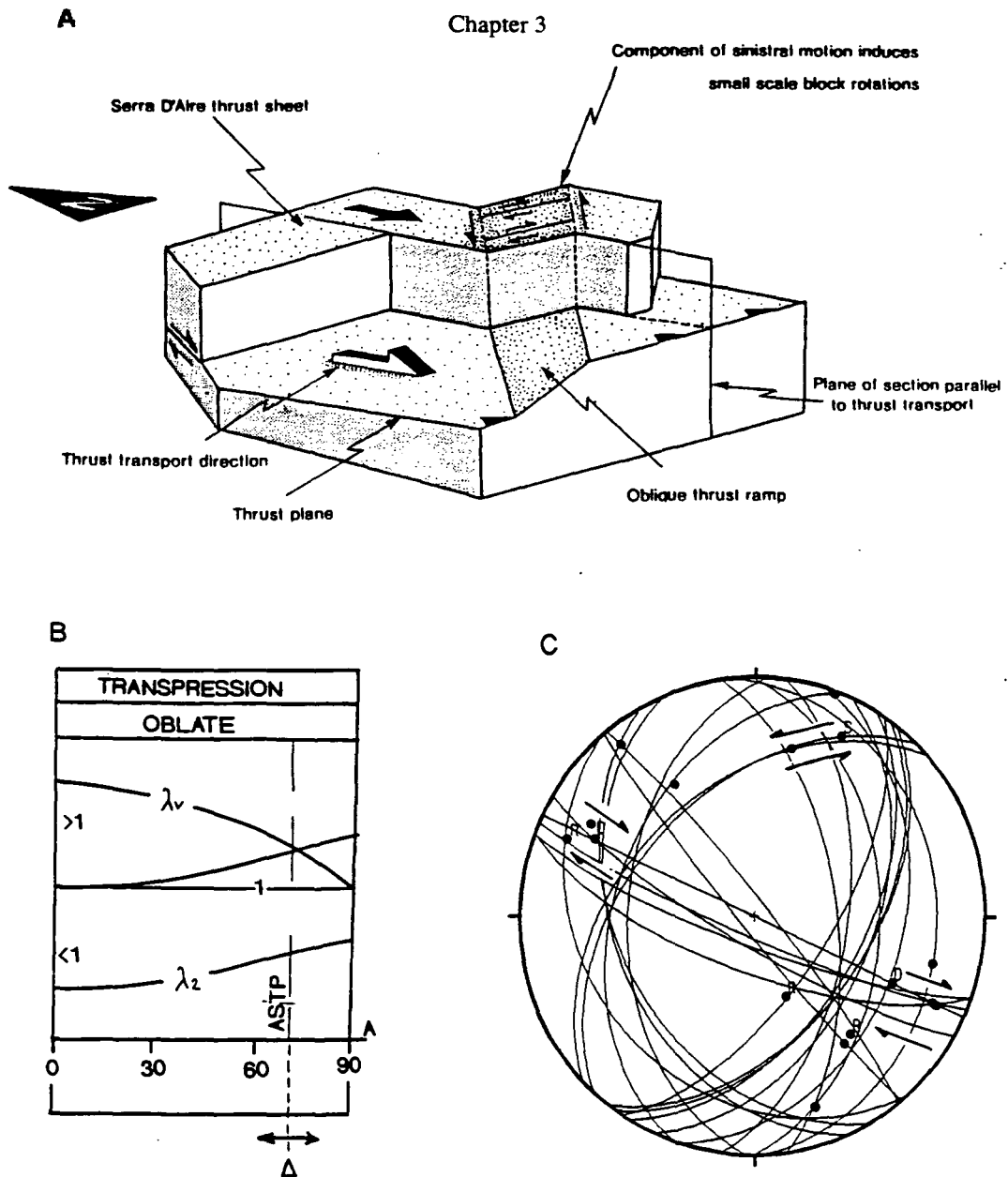


Figure 3.39 a) Schematic block diagram of the Serra D'Aire thrust zone. Sinistral transpression along the oblique ramp induces small scale anti-clockwise block rotation. b) Transpressive strain field from the McCoss (1986) graph of angle A against the axes of principal quadratic elongation (see fig. 1.26, p41, this thesis). Δ indicates how minor variations in A about the critical ASTP angle (70.5°) may induce switching between strike-slip and reverse slip motion. c) Equal area stereonet of faults and slickenlines from the northern Serra D'Aire thrust zone. Note sinistral faults and thrusts share the same strike. Dextral faults are orthogonal and are related to small scale block rotations.

3.8 Structural and kinematic evolution of the Candeeiros block

The basic geometry of the Candeeiros block was defined by the end of the Jurassic period by several extensional faults: the S. dos Candeeiros fault, Alvaldos-Minde faults, Mendiga fault, and the northwest end of the Alcanede fault (Figure 3.40/1). These faults exerted a fundamental control on the tectonic style and evolution of the Candeeiros region.

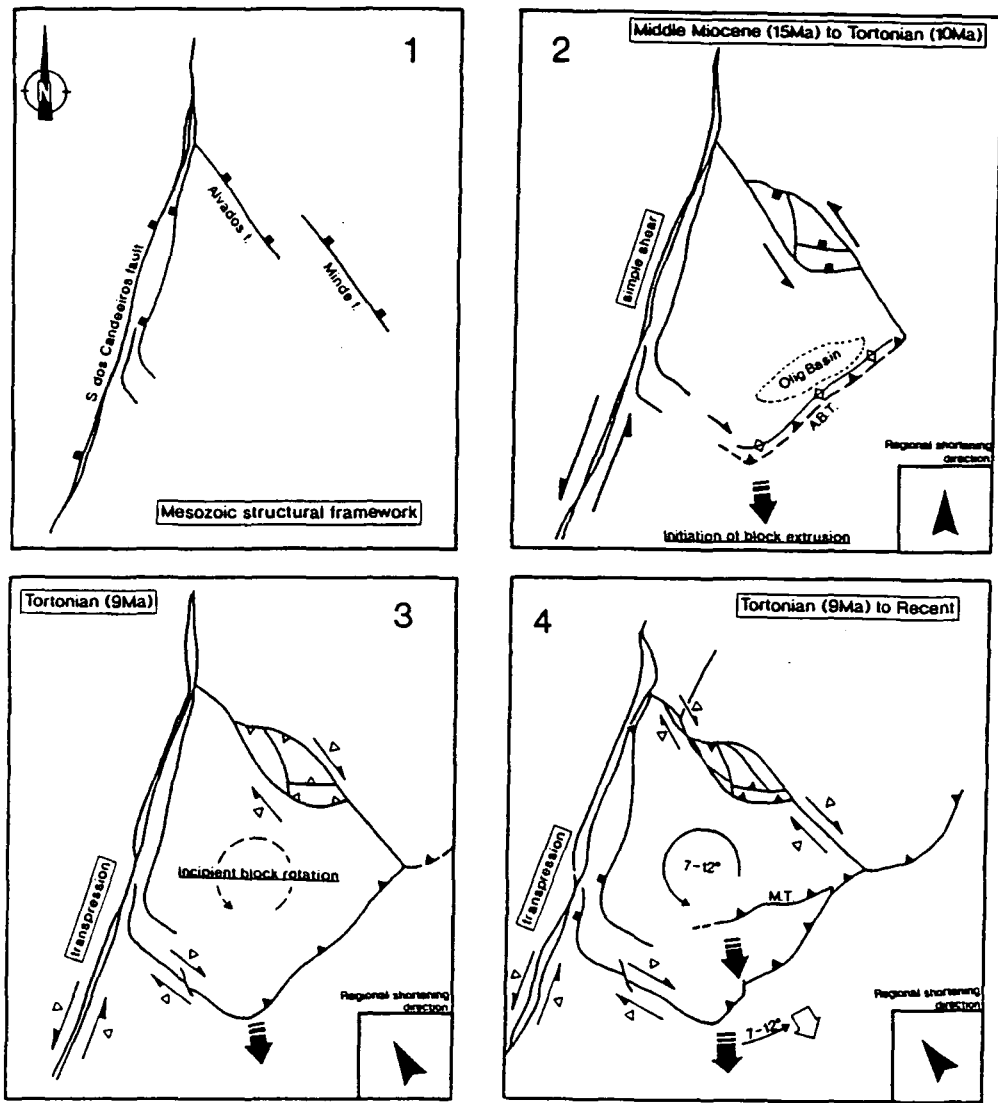


Figure 3.40 Kinematic evolution of the Candeeiros block: 1) Pre-Middle Miocene structural framework; 2) Synthetic reactivation of the Alvados/Minde fault system, and late formation of the Amiais de Baixo thrust (A.B.T.); 3) Rotation of regional shortening direction induces sinistral transpression along the S.dos Candeeiros fault, and block rotation; 4) After 7-12° of block rotation the Monsanto thrust (M.T.) forms. See text for more detail.

The earliest record of Cenozoic deformation within the region is possibly of Oligocene age. Stratigraphic relationships within the Canal and Amiais de Baixo region suggests that the perched basin developed adjacent to a structure, which later became the site of the Amiais de Baixo thrust. This early deformation was possibly related to Oligocene age subduction beneath the Betics, south of Portugal (Leblanc & Oliver, 1984). More detailed stratigraphic field studies are required to resolve the true relationship, if any, of the Oligocene sequence to the present day Amiais de Baixo thrust. The main phase of deformation, including the initiation of thrusting within the Lusitanian Basin (Ribeiro et al., 1990), occurred during the Miocene period due to the superimposition of a north-south oriented shortening direction across the Lusitanian

Basin. The result of this shortening was the reactivation of NNE-SSW and NE-SW oriented faults, causing basin inversion (Wilson et al., 1990). The presence of evaporites along the S. dos Candeeiros fault made the fault zone susceptible to slip and it was probably reactivated as a sinistral strike-slip fault during the initiation of the north-south compression. The orientation of the S. dos Candeeiros fault to the regional compression direction suggests that a simple shear system would have existed during this initial phase of reactivation. However, a sinistral transpressive strain has been demonstrated along the S. dos Candeeiros fault, suggesting a change from simple shear to transpressive strain, probably due to the rotation of the regional shortening direction from north-south to a northwest/southeast orientation during the Miocene to Recent. Penecontemporaneous sinistral strike-slip motion occurred along the left-stepping Alvados and Minde faults, suggest they behaved as synthetic fault splays to the main S. dos Candeeiros fault. The synthetic reactivation of the Alvados-Minde system produced the Alvados pull-apart basin in the stepover between the faults. Along the southeast boundary of the Candeeiros block, the perched Oligocene basin implies that initiation of fault movement in the Amiais de Baixo region may have begun during the Oligocene. Detailed studies of superimposed strain systems suggest that the large scale structure of the Amiais de Baixo thrust formed in response to north-south directed shortening, and may have occurred as a prelude to the drastic change in tectonic style, and the initiation of block rotation (Figure 3.40.2).

Following the formation of these major structural features a significant change in the kinematic and tectonic style of the Candeeiros region occurred. The sense of motion along the Alvados-Minde fault system reversed producing a dextral pair of left stepping strike-slip faults. This reversal of motion initiated a pressure ridge, or push up between the faults, resulting in the inversion of the Alvados pull-apart basin. Detailed structural studies suggest that the strain along the Alvados-Minde faults was dextrally transpressive. Assumed coeval dextral transpressive motion also occurred along the southwest boundary of the Candeeiros block, producing the Alcanede fault zone, therefore, completing the fault boundaries of the Candeeiros fault block as observed today.(Figure 3.40.3). The dextral shear couple associated with these kinematic changes implies that anti-clockwise block rotation about a vertical axis occurred. Estimates for the amount of rotation based on detailed mesoscopic and macroscopic structural relationships consistently indicate an anti-clockwise rotation of the Candeeiros block relative to its thrust transport direction of up to 25-30°. Similar detailed structural studies within the Monsanto thrust zone reveal an 18° anti-clockwise rotation of early formed structures has occurred. The relative values of the amount of rotation between the Amiais de Baixo thrust and the Monsanto thrust suggests that the Amiais de Baixo thrust zone formed first and underwent 7-12° of

anti-clockwise block rotation before the initiation of the Monsanto thrust. Another 18° rotation occurred after the initiation of the Monsanto thrust zone to produce the observed structural relationships within the two fault zones.

The anti-clockwise rotation of the Candeeiros block caused the northwest corner of the block to impinge on the S. dos Candeeiros fault producing a localised region of shortening that is reflected in the structures present in the large quarry overlooking Porto de Mós. At the southwestern end of the Mendiga fault extensional faulting dominates, suggesting that this corner of the block has 'pulled' away from the S. dos Candeeiros fault (Figure 3.40.4). The consistent southerly direction of thrust transport along the Amiais de Baixo and Monsanto thrust zones during their evolution suggests that the anti-clockwise rotation was superimposed upon the general southerly extrusion of the Candeeiros block.

3.8.1 Model for the rotation of the Candeeiros fault block

As shown earlier in this chapter, transpressional strains occur at a late stage within the Candeeiros fault system. The S. dos Candeeiros fault is presumed to have initiated as a sinistral strike-slip fault which underwent a progressive change in strain regime from sinistral simple shear to sinistral transpressive shear. Likewise, transpressive strain occurred at a late stage along the Alcanede and Alvados/Minde faults, with the dextral component of shear associated with anti-clockwise rotation of the Candeeiros block. It seems quite probable that the transpressive strains within the fault system were coeval, which therefore suggests that the introduction of a component of shortening across the deformation zone was fundamental in the completion of the fault boundaries to the Candeeiros block and its anti-clockwise rotation. The role of transpression and transtension in the distribution of deformation was discussed by McKenzie & Jackson (1986), who state that for distributed continental deformation (block formation and rotation) to occur, a component of shortening or extension across the deformation zone must exist, otherwise the simple shear is likely to be taken up by a simple strike-slip system. The 'pinned' block model proposed by McKenzie & Jackson (1986) to explain block rotations and distributed continental deformation possesses some important structural and kinematic characteristics that are seen along the boundaries of the Candeeiros block, the most important being the necessity for a component of shortening or extension across the deformation zone. The model also predicts that the cross faults will be antithetic and possess a component of fault normal strain that is complimentary to that occurring across the main deformation zone, in the case of the Candeeiros region, this would be a component of shortening. However, the pinned model is based on the blocks remaining rigid with only the instantaneous motion occurring along the cross faults, which prevents finite block rotations. It was noted

that in reality the blocks undergo minor amounts of internal deformation to accommodate finite motion along the fault block boundaries. This internal deformation is quite evident along the Alvados/Minde and Alcanede faults where a considerable amount of shortening has occurred locally across the fault zones. Therefore, the evolution and style of deformation within the Candeeiros region appears to mimic that predicted by the 'pinned' model of McKenzie and Jackson (1986).

During the early phase of Cenozoic deformation the regional shortening direction, which probably equates to the regional σ_1 , was oriented roughly north-south (Dewey et al., 1989; and Ribeiro et al., 1988). The relative orientation of the regional σ_1 to the S. dos Candeeiros fault zone during this period suggests that a simple shear strain reactivated the fault zone. The presence of the Jurassic aged Alvados/Minde fault zone was exploited as a synthetic splay fault, otherwise the strain would probably have concentrated along a narrow zone of deformation. The regional σ_1 across the Lusitanian basin rotated from its roughly north/south orientation to a northwest/southeast position during the late Tortonian (9Ma, Dewey et al., 1989), introducing a component of shortening across the deformation zone due to the increased angle between the regional σ_1 and the S. dos Candeeiros fault zone. As the development and rotation of the Candeeiros block appears to be linked with transpressional strains, it is suggested that transpression and block rotation occurred at the end of the Tortonian, and continued possibly into the Quaternary, as suggested by the neotectonic nature of several of the faults in the Candeeiros region.

The presence of a rotated block raises an important subsidiary question, that of décollements, as the block must be allowed to rotate on some sub-horizontal surface of detachment. In many areas of southern California these surfaces are low angle extensional detachment faults (Luyendyk, 1991), or low angled thrusts emanating from flower structures. However, large rheological contrasts between rigid and incompetent layers can behave equally well as detachment horizons (Horns, 1991). In the Lusitanian basin, the Jurassic carbonate sequence sits above a base Jurassic Hettangian age evaporite sequence that is found basin wide. This layer appears to be the best candidate for an intraformational décollement horizon, allowing the Candeeiros block to 'float' on a well-lubricated surface. The role of this evaporite horizon, and its influence on basin tectonics will be discussed in chapter six, and partially in chapter five.

CHAPTER 4

Structure and kinematics of the Serra de Montejunto range

4.1 Introduction

The Serra de Montejunto range forms a NE-SW trending range of mountains between Cercal in the northeast and Torres Vedras in the southwest. At 666 metres, the summit of Montejunto represents the highest elevation in southern Portugal. The Torres Vedras-Montejunto anticline, hereafter referred to as the Montejunto anticline, dominates the structure of the range. This anticlinal structure initiated during the Toarcian (Early Jurassic) as a salt pillow structure that probably formed over a Triassic fault scarp (Leinfelder and Wilson, 1989). As with other halokinetic structures in the Lusitanian basin, the salt extrusion has followed the trends of the major faults: in this case the west southwest trending Torres Vedras fault. Therefore, main structural architecture of the Montejunto region was established as early as the Oxfordian to Kimmeridgian with the formation of the Pragança, Cercal, and Montejunto faults. These faults delineated the sub-basins of the Estremadura trough, and were, therefore, major basin features. The first manifestation of the Pragança fault, during the Middle Jurassic, is suggested by the presence of large synsedimentary slides, and repeated, sudden episodes of subsidence recorded within the sediments. Continued activity along the Pragança fault during the late Oxfordian is recorded by a submarine scarp (Montenat et al. 1988). During the middle to late Kimmeridgian, halokinesis and fault activity progressively decreased leading to the burial of the fault scarp and halokinetic structures by a regressive sequence of littoral carbonates and terrigenous deposits.

The major structural development of the Montejunto area occurred during the Miocene to Recent tectonic inversion event (Ellis et al. 1990). The basic structure of the Serra de Montejunto range is a crude anticline which has been extensively faulted. The core of the structure is formed by Middle Jurassic carbonates that coincide with the summit of Montejunto. At this point the anticline is highly asymmetric, with vertical to overturned bedding in the southern limb, and a gentle to moderate northwesterly dipping northern limb. The central area immediately to the west of the Montejunto summit is intricately faulted and folded, and roughly coincides with the

axis of the Montejunto anticline. Along the southern and northern external zones of the structure spectacular fault scarps are present in association with steep to sub-vertical bedding of the hanging walls. (Figure 4.1). (Map 4)

Exposure is good within the areas of Bathonian and Oxfordian aged carbonate outcrops, which form the areas of highest relief. These Middle to Upper Jurassic carbonates preserve excellent kinematic indicators and incremental strain features. For these reasons the structural and kinematic analysis was concentrated within the immediate vicinity of the summit of Montejunto, therefore, affording an excellent opportunity to document the detailed kinematics of a flower structure, and hence the Miocene to Recent inversion tectonics of the region.

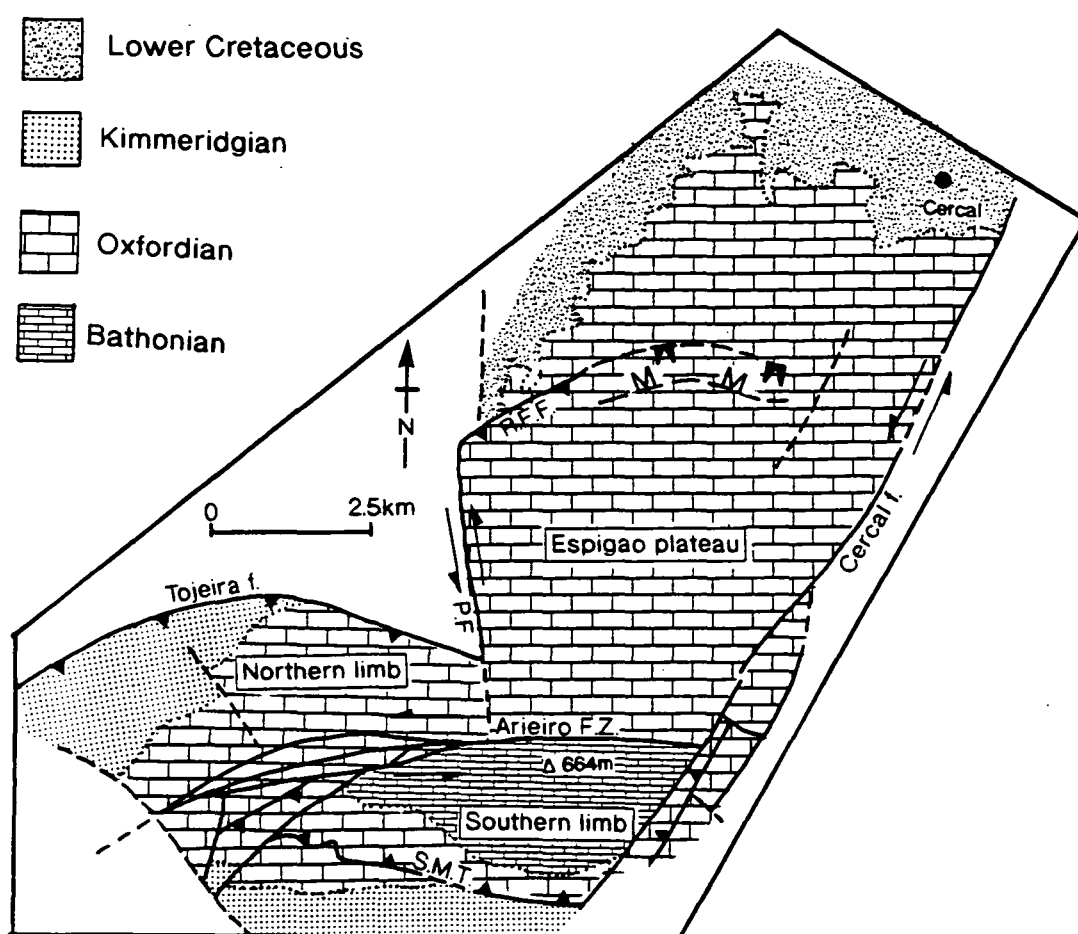


figure 4.1 Generalised geological map of the Montejunto massif and the Espigão plateau. S.M.T., Serra de Montejunto thrust; P.F., Pragança fault; R.F.F., Rocha Forte fault. M, M indicate upper, and lower hinge of monocline, respectively. More detail is available in Map 4 in the back of this thesis.

4.2 Structural domains of the Montejunto anticline

The Montejunto anticline is a general name for the structure that forms the long, narrow, structurally complex region of Jurassic aged carbonates and terrigenous sediments, uplifted along a restraining bend in what is believed to be the southern manifestation of the S. dos Candeeiros fault. The main fault trace swings from 022° near Cercal (the Cercal fault), to 080° immediately south of the Montejunto summit (the Montejunto fault system), with uplift occurring on the northwestern side of the fault system (figure 4.1). The structural style of the Montejunto range reflects the change in orientation of the main boundary fault system. The region adjacent to the NNE-SSW Cercal fault is structurally simple with Oxfordian platform carbonates juxtaposed against the Miocene to the southeast, and partially thrust onto Early Cretaceous sediments in the northwest. This region forms a plateau between 250-400 metres high which will be referred to as the Espigão plateau. In contrast to the Espigão plateau the Montejunto massif is structurally complex. It is dissected by numerous faults of a dominant ENE orientation which are associated with large scale folds. The massif displays the oldest rocks in the region (Middle Jurassic, Bathonian and Callovian aged limestones), whose outcrop coincides with the highest point in the Montejunto range, indicating that the maximum amount of uplift occurred at the bend in the main fault system.

4.2.1 The Espigão plateau

The Espigão plateau is a fault bounded block 3.5km wide, by 6 km long, with a 250-400 metre elevation. It is tectonically bounded on three sides by the NNE striking Cercal fault to the east, the Pragança and Arieiro faults to the southwest, and the Rocha Forte thrust and monocline to the northwest. The northern margin of the plateau is marked by an Early Cretaceous (Albian-Aptian) unconformity.

The structural geometry of the plateau is dominated by a gentle to moderate northwesterly dip, with a mean bedding orientation of 068/26°NW (figure 4.2). However, the regional dip and strike becomes modified adjacent to the tectonic boundaries. The dip increases toward the Rocha Forte fault, where it varies between sub-vertical and 56°, being steepest at the southwest termination of the fault. The regional strike of the plateaux swings from NE-SW to a N-S orientation adjacent to the Pragança fault, with a gentle easterly plunging anticline developed adjacent to the Arieiro fault

4.2.1.1 The Rocha Forte fault

The NE-SW trending Rocha Forte fault forms a prominent scarp running northeast, from the northern end of the Pragança fault, to the village of Rocha Forte. The

footwall and hanging wall strata display steep to sub-vertical bedding within the immediate vicinity of the fault plane, however, as the direction of dip does not differ from the regional dip they do not form footwall synclines and hanging wall anticlines, *sensu stricto*. The Rocha Forte fault thrusts Oxfordian carbonates of the Montejunto formation, over Early Cretaceous terrigenous sediments at its southwestern end, but the throw dies off to the northeast, where the thrust carries lower Oxfordian over upper Oxfordian carbonates. The fault cannot be traced beyond the village of Rocha Forte where it appears to transform into a monoclinical structure that gradually swings from NE-SW to an E-W strike (figure 4.1).

Fault geometry and kinematics

The fault zone is spectacularly exposed in a large quarry face near Rocha Forte village (grid ref. 20'60" 12'58")*. The main fault plane is oriented 056/54°SE, with slickenside striations indicating a thrust transport direction toward 005°. The thrust truncates the moderate to sub-vertical bedding of the footwall, and the moderately inclined bedding of the hanging wall. The fault zone is asymmetric, with numerous incipient and small displacement (<10cm) faults forming an anastomosing array of low angle oblique shears in the hanging wall to the main fault plane. These secondary faults form two sets that have low oblique clockwise (+ve), and anti-clockwise (-ve) angles to the main fault, (+ve and -ve terminology used in the same sense as Chester and Logan, 1987; see figure 4.3). The faults of the +ve fault set are predominantly long (up to 20 metres in length) with a mean angle to the main fault of +15°, and comprise 60% of the total fault population. The -ve fault set commonly form short, interconnecting splays between the +ve set, and possess a mean angle to the main fault of -8°. These faults sets resemble extensional Riedel shears, and contractional P-shears, respectively, in both geometry, and relative abundance (Naylor et al. 1986).

Footwall ripout structures are present immediately beneath the main fault plane, where they occur are asymmetric fault bounded 'scallop' shaped lenses (figure 4.3). The tapered ends of these structures consist of a contractional P-type ramp formed at a low angle to the main Rocha Forte fault, and a trailing extensional R-type shear at a higher angle to the fault plane. These footwall ripouts are very similar to the side wall ripouts described by Swanson (1989), and hence by association, suggest that transient variations in the coefficient of friction occurred along the main fault plane. The asymmetry of these structures allows them to be used as kinematic indicators, that together with the secondary fault geometries, confirm that the Rocha Forte fault has undergone thrust motion.

* Within the Montejunto region all grid references are prefixed by 09°(long.) and 39°(lat.).

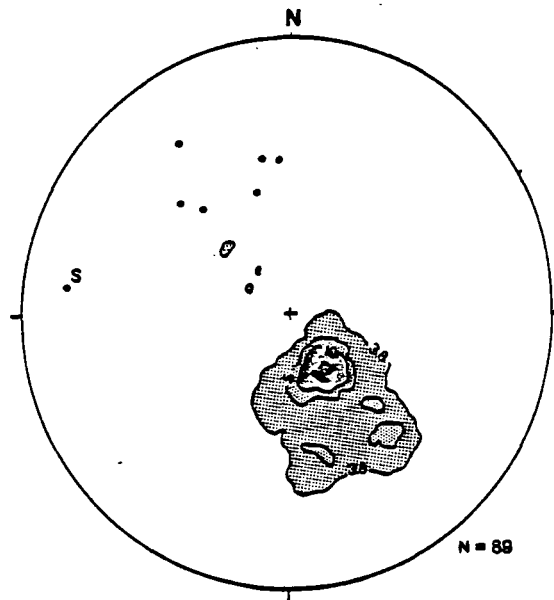


Figure 4.2 Contoured equal area stereonet of poles to bedding from the Espigão plateau. Mean bedding orientation 068/26°NW. Solid circles represent flexural slip slickenlines on bedding planes. Contour intervals 3.8, 5, 10, 13%.

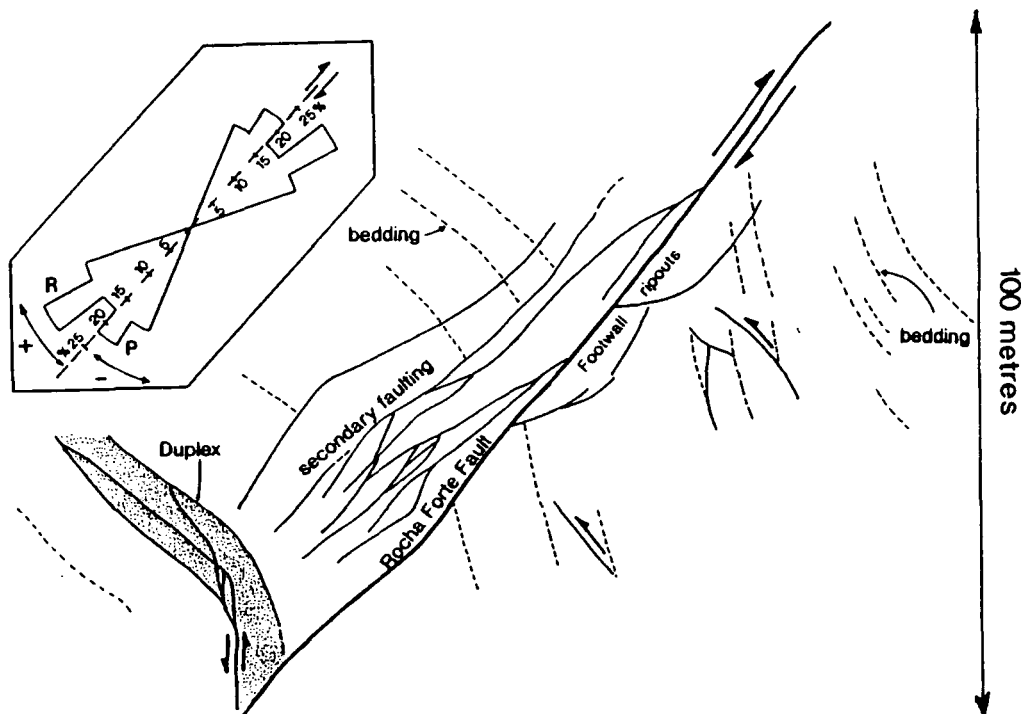


Figure 4.3 Tracing taken from a photo-mosaic of the Rocha Forte fault, displaying the asymmetric development of secondary faults. (Insert) A rose-diagram of secondary fault orientations dispersed about the main fault plane. View looking towards the southwest

Antithetic backthrusts are present within the footwall, where they are seen propagating out of moderately dipping bedding planes into the steep to sub-vertical beds that lie immediately beneath the fault plane. These faults are effectively cutting down sequence, producing contractional faults with extensional stratigraphic throws. Backthrusts are also present within the hanging wall, where they exploit the bedding planes. However, due to the result of flexural shear between the beds it is difficult to distinguish the former from the latter. Unambiguous proof of bedding parallel thrusting can be seen where a single bedding unit has undergone layer parallel shortening via thrust duplexing. By area balancing the duplex, it can be shown that 58% shortening has occurred along the structure (figure 4.4).

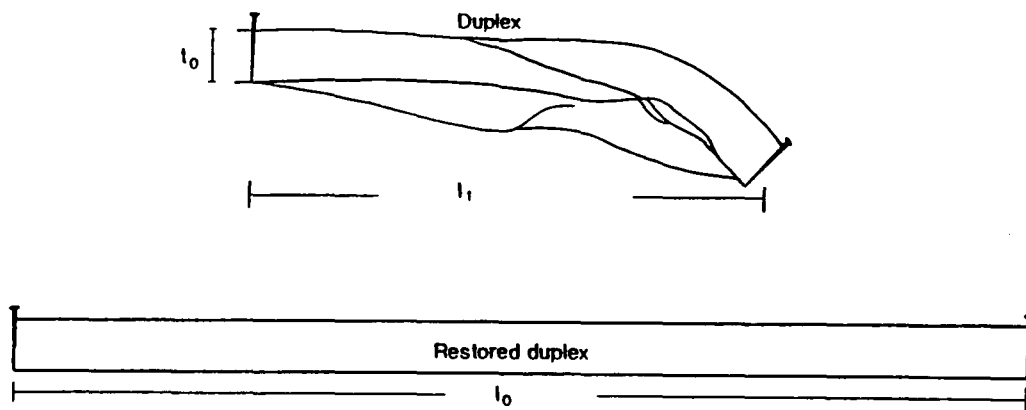


Figure 4.4 Duplexed bed (top), highlighted by stipple in fig.4.3. (Below) area balanced restoration of the bedding unit, indicating 58% shortening along the duplex.

Small scale kinematic indicators and fault rocks

A sample of fault rock was taken from the footwall of the main Rocha Forte fault, and was cut parallel to the fault plane striations, and polished to allow the fault rock textures to be observed (plate 4.1). Fault rock formation extends to greater than 7cm from the fault plane (the maximum thickness of the sample), and possesses three zones of differing fault rock type. These zones show a gradual increase in cataclastic deformation from the external to internal zones.

The external zone consists of a poorly formed cohesive fault breccia, that gradually transforms into a well developed breccia. This in turn grades into a pale cream cataclasite zone (Ramsay & Huber's classification 1987), 2-3cm thick, with rounded to angular clasts up to 5mm in length. The clast size reduces with proximity to the fault plane. The boundary between the breccia and cataclasite is well pronounced, and is offset by numerous secondary faults that are marked by visible offsets and narrow zones of pale fault gouge. The dominant fault set has a mean +ve 44° oblique angle to the mean fault, the subordinate set forms a +ve 85° angle, that together form a

conjugate pair. The asymmetry of the shears, and obliquity of their acute bisectrix, indicates that they formed in response to fault plane shear and not layer parallel extension or contraction, hence they represent R and R' shears. However, these shears have formed at higher angles than normally observed, suggesting that a localised component of shortening may have been present across the immediate wall rocks. Late tensile 'T' fractures (Petit 1987) are present within the immediate vicinity of the fault plane cutting the cataclasite. They taper down from the fault plane with a listric geometry and form a high +ve angle with fault plane.



Plate 4.1 Polished slab cut perpendicular to the Rocha Forte fault plane and parallel to the slickenlines. The boundary between the cream cataclasite and fault breccia is clearly seen. The overlay 'picks' the main micro fractures which form a conjugate Riedel and Antiriedel fault set. Note late extension 'T' fractures adjacent to the fault plane.

Lying along the fault plane, and immediately above the specimen collected, is a 1.5cm thick red clay gouge possessing an oblique flattening fabric. The gouge contains clasts of veined and fractured micrite up to 5mm in length, that are aligned parallel to the fabric. This oblique flattening fabric is consistent with the 'T' fractures, and secondary shears, indicating a reverse sense of shear along the Rocha Forte fault.

The thrust transport direction derived from the slickenlines on the fault plane is not coaxial with the folding and flexural slip lineations within the hanging wall, suggesting that it may represent a late change in thrust transport direction from NW to NNE.

4.2.1.2 The Pragança fault

The Pragança fault is marked by a large scarp, which represents a palaeo-fault scarp from the Upper Jurassic (Montenat et al. 1988), that has since been reactivated during the Miocene and possibly the Recent. The fault runs due north from the eastern end of the Tojeira fault, to the western termination of the Rocha Forte fault (figure 4.1). The Pragança fault juxtaposes Oxfordian limestones to the east, against upper Oxfordian limestones and Kimmeridgian clastics on the western side.

No exposure of the main fault plane was observed, although numerous secondary faults were encountered along the fault trace. Deformation related to movement along the Pragança fault seems to be distributed over a wide area, as broad parallel fault zones are present up to 200 metres east of the fault scarp. These secondary faults appear as prominent, planar fractures, displaying movement striae. Brecciation was only seen where the faulting was particularly intense, suggesting that the amount of displacement along individual faults is small. The relative lack of disruption of the adjacent bedding also suggests that displacements are small. The faults form a dip bimodal, north-south striking set, the mean of which is $177/81^{\circ}\text{E}$. The associated slickenlines are almost exclusively strike-slip, and plunge slightly about the horizontal, displaying a consistent sinistral shear sense. The mean orientation of these slickenlines is $03^{\circ}/356$ (figure 4.5). The sinistral sense of motion along the Pragança fault agrees with the expected relative motion, based on the need for an accommodation structure to allow thrusting to occur along the Rocha Forte fault. Therefore, the Pragança fault zone behaved as a transfer fault between the two northern thrust zones of the northern margin of the Montejunto anticline.

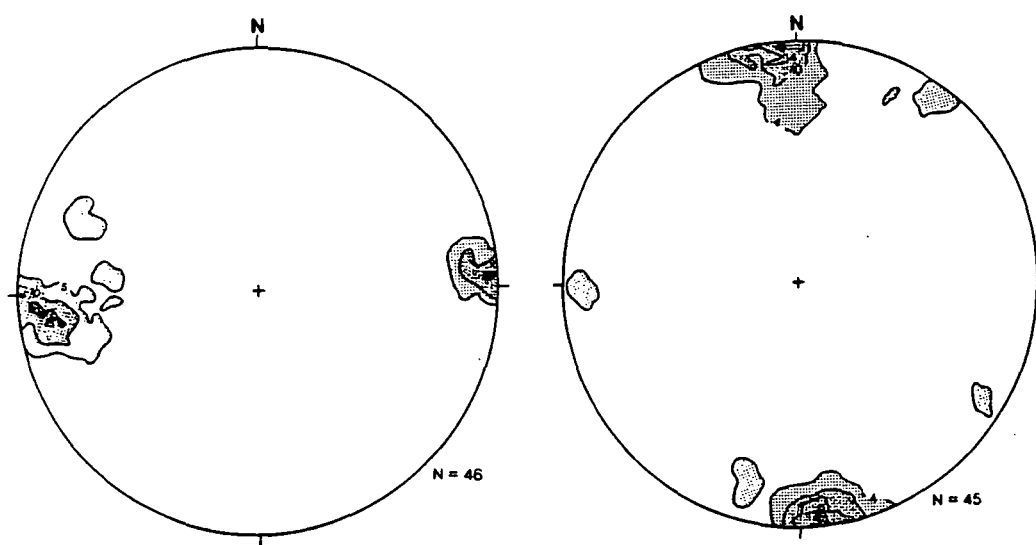


Figure 4.5 Contoured equal area stereonets of (left) poles to fault planes, mean $177/81^{\circ}\text{E}$; (right) Slickenlines on fault surfaces, mean $03^{\circ}/356$. Contour intervals at 4, 10, 14, 17%.

4.2.1.3 The Cercal fault

The Cercal fault can be traced from Montejunto, in the southwest, 16.5 km northeast to Alvaris, where its trace becomes uncertain within the Lower to Middle Miocene Alcoentre formation. The fault lies directly along strike from the southern end of the S. dos Candeeiros fault trace, at Rio Maior, and is believed to be related to this fault system.

The fault produces an obvious scarp where the competent Oxfordian carbonates are juxtaposed against Oligocene and Miocene aged terrigenous sediments. At the northern end of the Cercal fault, a strong linear topographic expression is present to the east of the village of Cercal. According to the Serviços Geológicos De Portugal 1:50,000 geological map of Bombarral, the fault trace near Cercal is offset by several late oblique sinistral faults. However, the southern trace of the fault is relatively planar where the competent Oxfordian limestones are present in the northwestern sidewall.

Fault geometry and kinematics

The Cercal fault is exposed along a length of 1km between San Salvador and the intersection of the fault with the N1 road to Cercal village. In general, the fault is marked by a thick zone of calcite mineralisation up to 5 metres in thickness. Differential weathering of this material reveals that the mineralised zone is made up of multiply fractured calcite clasts contained within a later calcite matrix, which is in turn cross cut by late extensional veining. Mesoscopic faults along the zone possess a NNE-SSW strike, and dip steeply to the northwest, displaying strike-slip movement. Slickolite striae and accretionary calcite steps along these faults indicate they have a sinistral sense of motion.

The main fault plane is superbly exposed near its intersection with the N1, where the fault plane forms a 10-15 metre high scarp (plate 4.2)*. The fault surface is extremely planar with an orientation of 016/80°NW, and is commonly covered by colluvium deposits. Where clean surfaces are present sinistral slickolite lineations are found possessing a 15° northerly pitch, indicating a small component of reverse motion is present. The fault plane is dominated by a sub-vertical lineation produced by the intersection of extensional veins and pressure solution cleavage with the plane. The lineation anastomoses around fault zone clasts to produce a fault stylobreccia. The sub-vertical nature of these structures is again suggestive of strike-slip motion. Synthetic, low angle, oblique, anti-clockwise faults are present, which probably represent Riedel fractures (plate 4.3)

* Plate 4.2 does not exist



Plate 4.4 Polished slab of fault rock from the Cercal fault plane. Clast size decreases toward the fault plane (towards the left), where red cataclasite is present. Note the oblique, low angle, spaced pressure solution cleavage (marked with an arrow), sense of obliquity suggests sinistral shear.

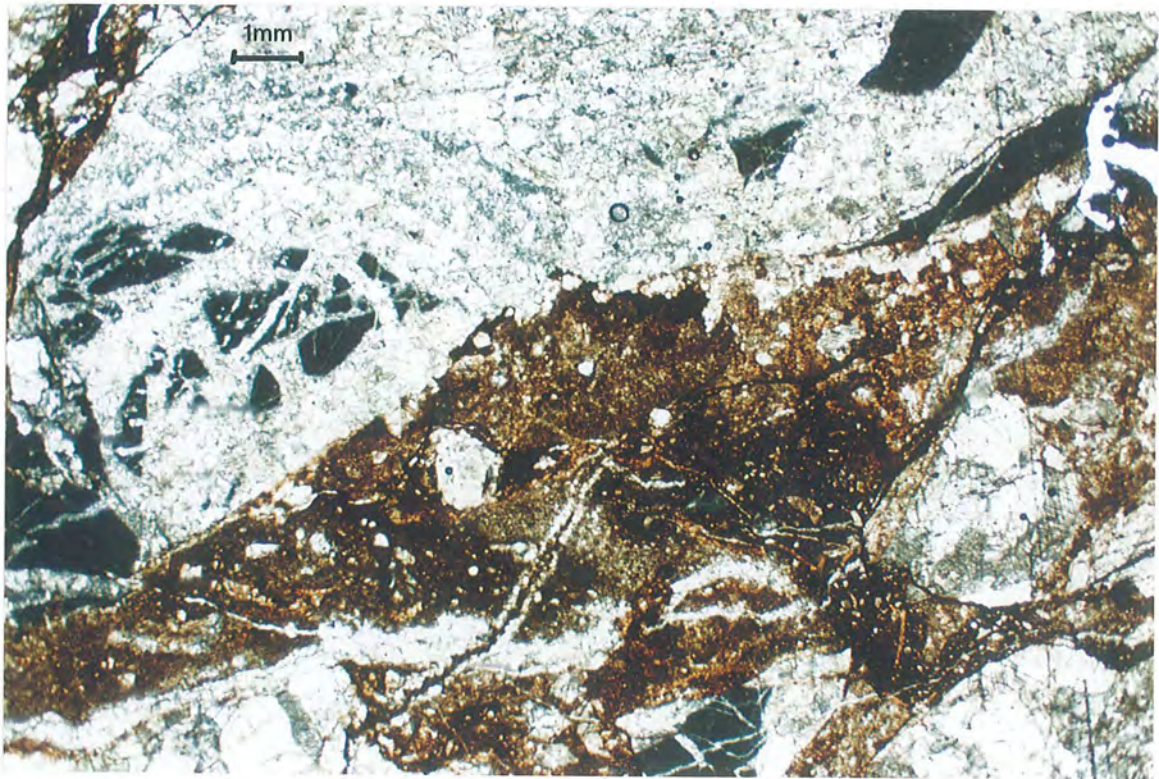


Plate 4.5 Photomicrograph of calcite clast with an asymmetric development of gouge tails, contained within a cataclasite matrix. Resemblance of this clast to a σ -porphyroclasts suggests sinistral shear.

contacts, and short constant amplitude sutures within the cataclasite (plate 4.4).

A thin section reveals that the clasts within the cataclasite and breccia have been multiply fractured. The clasts are predominantly blocky calcite, commonly containing highly angular clasts of micrite wallrock, which are occasionally totally desegregated, but are more commonly restorable to their pre-fractured state. This suggests that the wallrock was pervasively fractured by narrow extensional veins preceding their brecciation and inclusion in the fault gouge. Within the gouge an equant clast of calcite has developed asymmetric tails of dark brown, presumably clay rich gouge, forming a structure similar to the σ -structure of Passchier and Simpson (1986), see plate 4.5.

Taken together, the: slickenside lineations, Riedel faults, overprinting solution cleavage, and σ -structure, consistently indicate a sinistral sense of shear along the Cercal fault, therefore, further suggesting a relationship between it and the sinistral S. dos Candeeiros fault.

4.2.1.4 Arieiro anticline

The Arieiro anticline forms an open fold, lying to the immediate north of the Main Arieiro fault trace, beneath the summit of Serra de Montejunto. The fold axial trace trends east-west, parallel to the fault strike, and possesses an easterly plunge of ~20-25°. Close to tight, coaxial parasitic folds are found on the southern limb, within the immediate 50m of the Main Arieiro fault.

4.2.2 The Main Montejunto massif

The Montejunto massif is a fault bounded region of complex structure that displays the oldest rocks within the Montejunto range. The massif has a general asymmetric antiformal geometry, the southern limb of which is short and steep relative to the northern limb, making the structure southerly verging. However, this gross generalisation is complicated by the presence of faulting within the hinge zone of the antiform (the Arieiro fault system), and along the external margins of the massif, the Tojeira fault to the north, and the more complex Montejunto fault system to the south. These external faults form a downward convergent pair, that appear to coalesce at depth along a steep basement fault (see section 5.3). Structural traverses across the antiform show that the degree of asymmetry increases from east to west (see figure 4.6a & b).

4.2.2.1 The Northern limb

The following subsection describes the structure of the northern limb of the Montejunto antiform around the villages of Tojeira and Pereiro, from the Tojeira fault in the north, to the Arieiro fault system in the south.

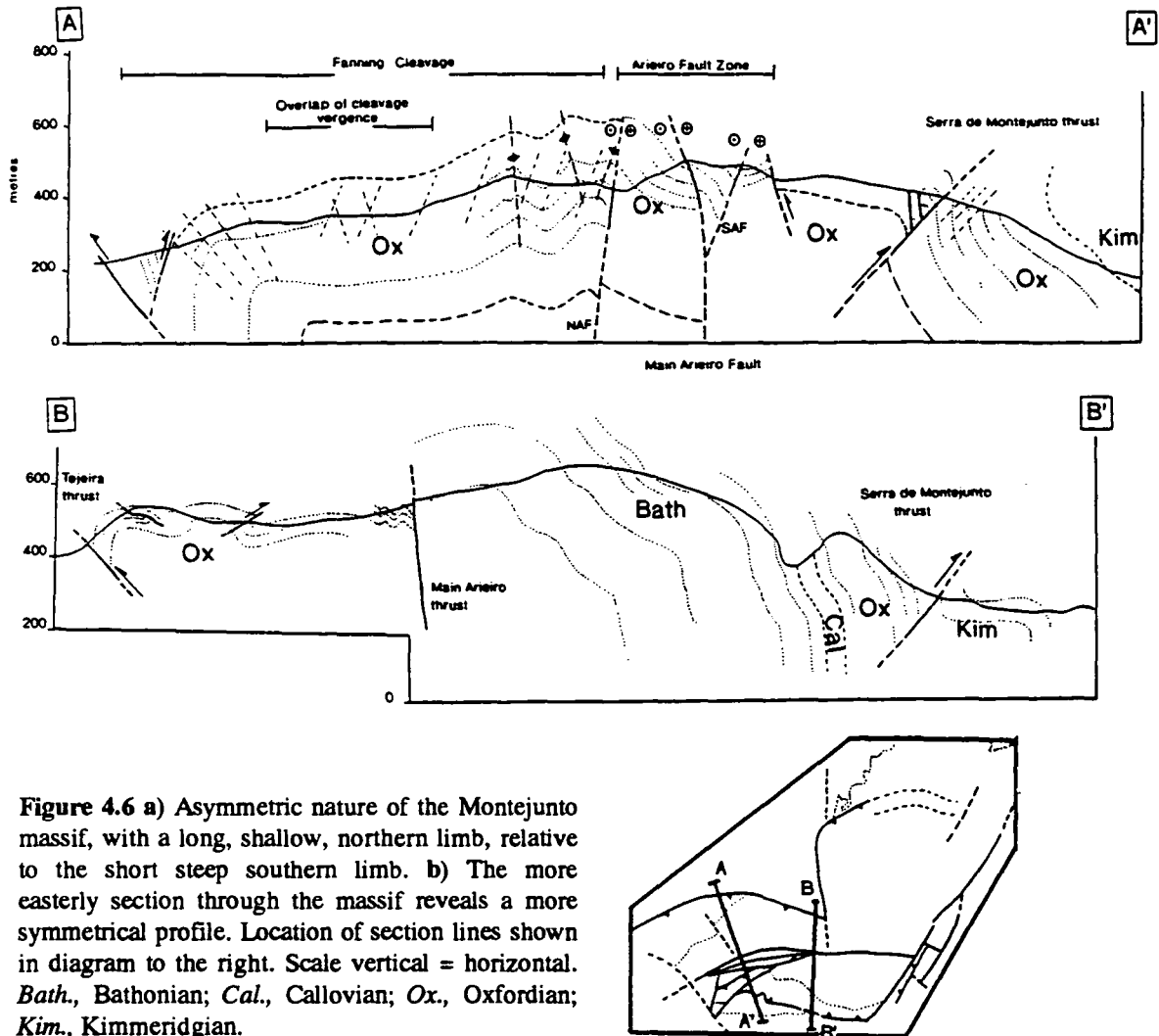


Figure 4.6 a) Asymmetric nature of the Montejunto massif, with a long, shallow, northern limb, relative to the short steep southern limb. b) The more easterly section through the massif reveals a more symmetrical profile. Location of section lines shown in diagram to the right. Scale vertical = horizontal. *Bath.*, Bathonian; *Cal.*, Callovian; *Ox.*, Oxfordian; *Kim.*, Kimmeridgian.

4.2.2.1.1 Tojeira fault

The northern boundary of the Montejunto massif is marked by the Tojeira fault, which emplaces Upper Jurassic Oxfordian and Kimmeridgian aged carbonates and siliciclastics of the Montejunto and Abadia formations, respectively, onto Portlandian aged red terrigenous sediments (the Lourinhã fm.). The fault trace is marked by a pronounced scarp where competent Oxfordian limestones are juxtaposed against younger, poorly cemented, sandstones. The adjacent hanging wall bedding is steeply inclined to overturned along the length of the fault. Together, the fold limb vergence, and stratigraphic throw along the fault, indicates a northerly direction of thrust transport.

4.2.2.1.2 Folding

In general, the northern limb possesses a low to moderate angle dip towards the north, and a roughly east-west strike. The fold limb is dissected by a fault trending 150° , the trace of which, runs between the villages of Pereiro and Tojeira. The fault appears to compartmentalise the deformation, with generally steeper bedding present on the Pereiro side of the fault (southwestern side), relative to the Tojeira side (northeastern side), the result of which, is an apparent dextral offset along the fault.

The bedding within the northern limb commonly displays monoclinial flexures, the hinges of which are parallel to strike, and give way to well developed folds adjacent to the Tojeira and Arieiro fault zones. As mentioned earlier, the hanging wall of the Tojeira thrust displays steep to overturned bedding, which forms a simple hanging wall anticline. Adjacent to the Arieiro fault system the folds generally define asymmetric antiformal polyclines or box folds, that verge to the south. A π -diagram of total bedding reveals a general fold axis oriented $11^\circ/256$, which corresponds closely with measured parasitic fold axes (figure 4.7). These parasitic folds complicate the geometry of the box fold adjacent to the Northern Arieiro fault, to the northeast of the compartment fault. The folds vary in style from symmetrical gentle to open folds between the axial planes of the box fold, to close asymmetric folds that possess straight limbs and sharp hinge zones. The hinges of these close to tight folds display an intense anastomosing pressure solution cleavage, that becomes more regularly spaced away from the hinge. Several of the parasitic structures seen are related to thrust or reverse faulting, suggesting that thrust tip folding and breach thrusts play an important role in the modification of the polyclines. Such structures are present to the immediate east of Moinho do Céu (grid ref. 04'18" 10'89"), where a northward vergent thrust fault has produced locally overturned footwall bedding. The thrust can be followed west along its trace to its lateral tip, where an unbreached overturned fold is present. Similar fault-fold relationships are present to the west of Moinho do Céu, and along the hairpin bends of the Vila Verde dos Francos to Montejunto road (see figure 4.8)

Cleavage commonly manifests itself as well spaced, pressure solution stylolites within the limestones, and a planar, penetrative cleavage within the thin interbedded marls and mudstones, that together form the Montejunto formation. Cleavage is difficult to see within the Kimmeridgian as the poorly lithified sandstones are not prone to cleavage formation, and the marls are very badly weathered. Where clean exposures of the Kimmeridgian marls are seen a planar, penetrative cleavage is present. The cleavage is axial planar to the folding within the northern limb, generally forming a convergent cleavage fan, with southerly dipping cleavage planes in the

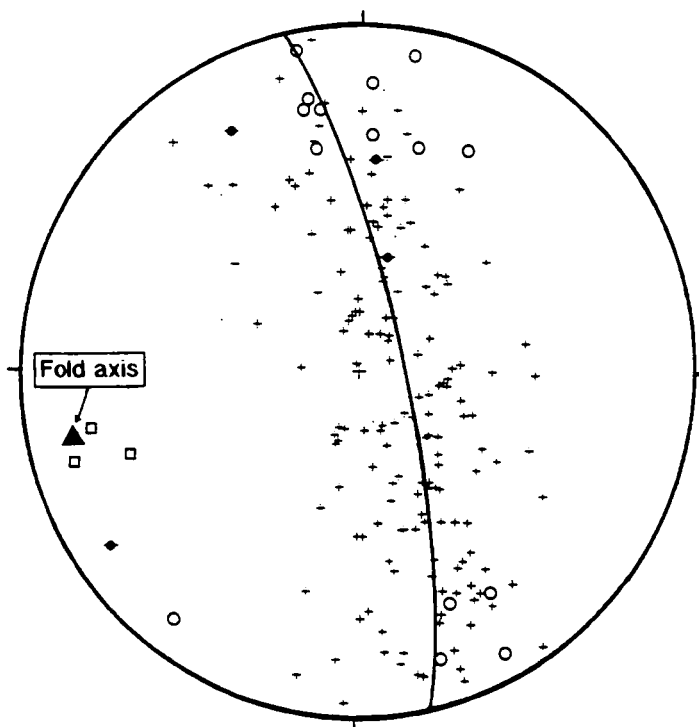


Figure 4.7 Equal area stereonet of data from the northern limb of the Montejunto massif. Crosses - poles to bedding; *Open circles* - poles to cleavage; *Squares* - parasitic fold hinges, *Solid circles* - lineations on bedding surfaces; *Solid triangle* - π -pole (fold axis) to bedding girdle, calculated fold axis - $11^\circ/256$. See text for details.

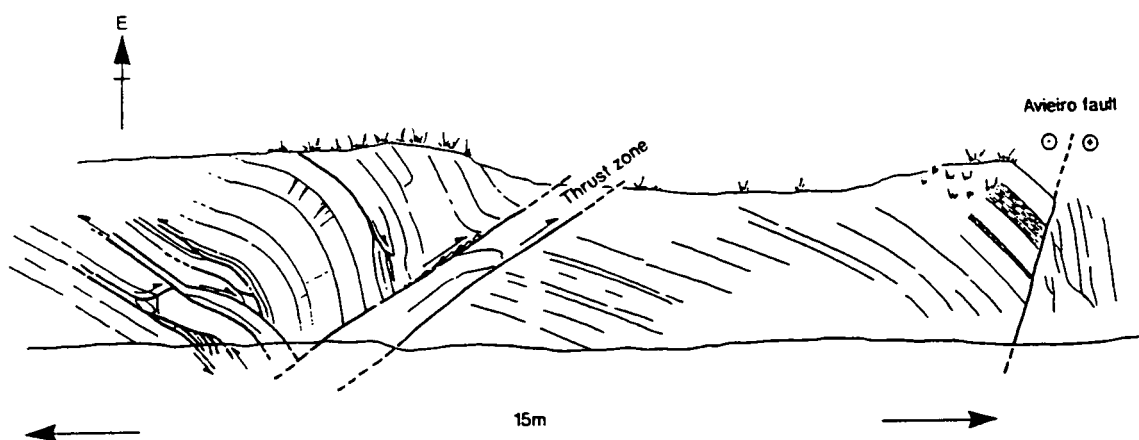


Figure 4.8 Breached fold with rotated bedding parallel thrusts in the hanging wall anticline. Road cut along the hair-pin bend of the Vila Verde dos Francos to Montejunto road.

north, adjacent to the Tojeira thrust, and northerly dipping cleavage in the south, adjacent to the Arieiro fault zone. However, this general geometric distribution has been modified to the east of Moinho do Céu, where localised southerly dipping cleavage has formed in relation to the northward verging thrust fault mentioned earlier. There is no discrete line along which cleavage vergence switches from north to south, instead there is a zone of overlap where cleavage verges both north and south (figure 4.6 & 4.9). No relative chronology between the cleavage was observed within this zone.

The cleavage fan is presumably related to the opposing directions of tectonic transport and fold vergence that are present along the Tojeira and Arieiro fault zones, as opposed to cleavage fans that are formed in single folds, due to flexural shear or tangential longitudinal strains. The zone of variable cleavage orientation may be due to transient variations in the dominant incremental strain fields related to deformation at the northern and southern margins of the region, or to a gradual switch in deformation from one zone to another. Without the relative chronology of the cleavage in this zone, neither hypothesis can be validated.

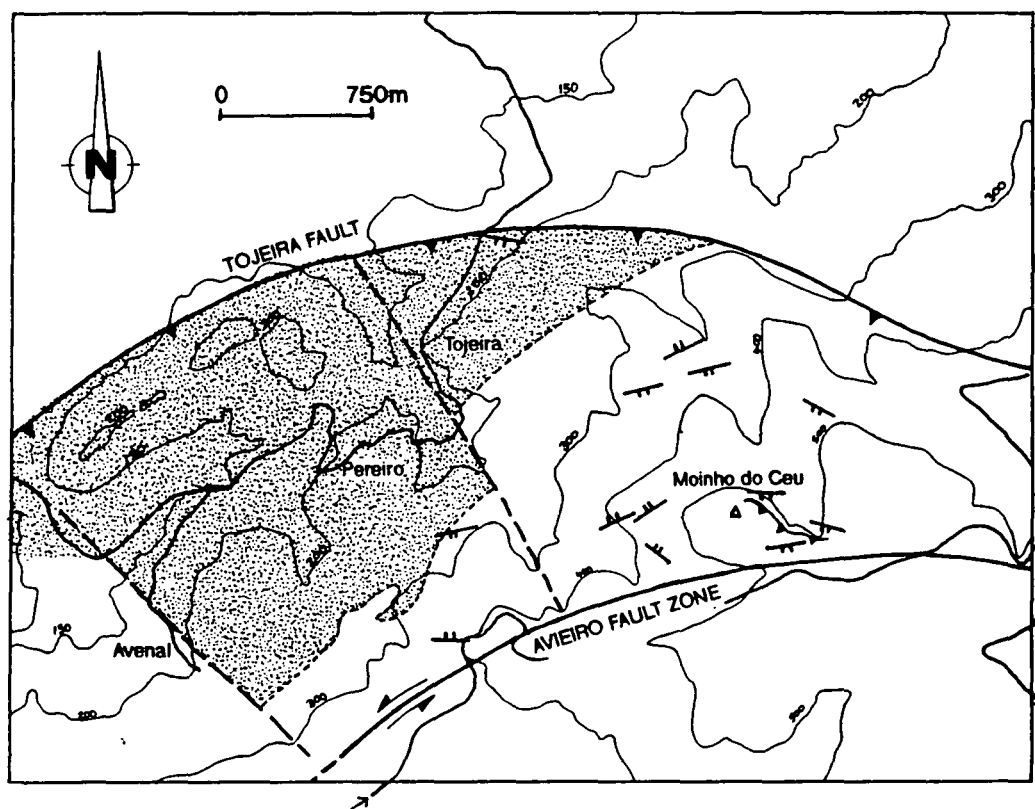


Figure 4.9 Generalised map of the northern limb of the Montejunto anticline revealing the spatial distribution of cleavage orientation. Localised development of northerly vergent cleavage near Moinho do Céu due to thrust fault. Contours in metres.

4.2.2.1.3 Faulting

Thrust faults

Thrust faults are common throughout the Tojeira and Pereiro region. The faults form two discrete sets based on their geometry and kinematics; 1) a NE-SW striking set, and 2) a NW-SE striking set.

- 1) The NE-SW striking set form a dip bimodal, conjugate set (figure 4.10a), displaying a mean slickenline lineation vector of $10^{\circ}/160$.
- 2) The NW-SE striking set form a more symmetric dip bimodal, conjugate set, with a mean thrust transport direction of $12^{\circ}/020$ (figure 4.10b).

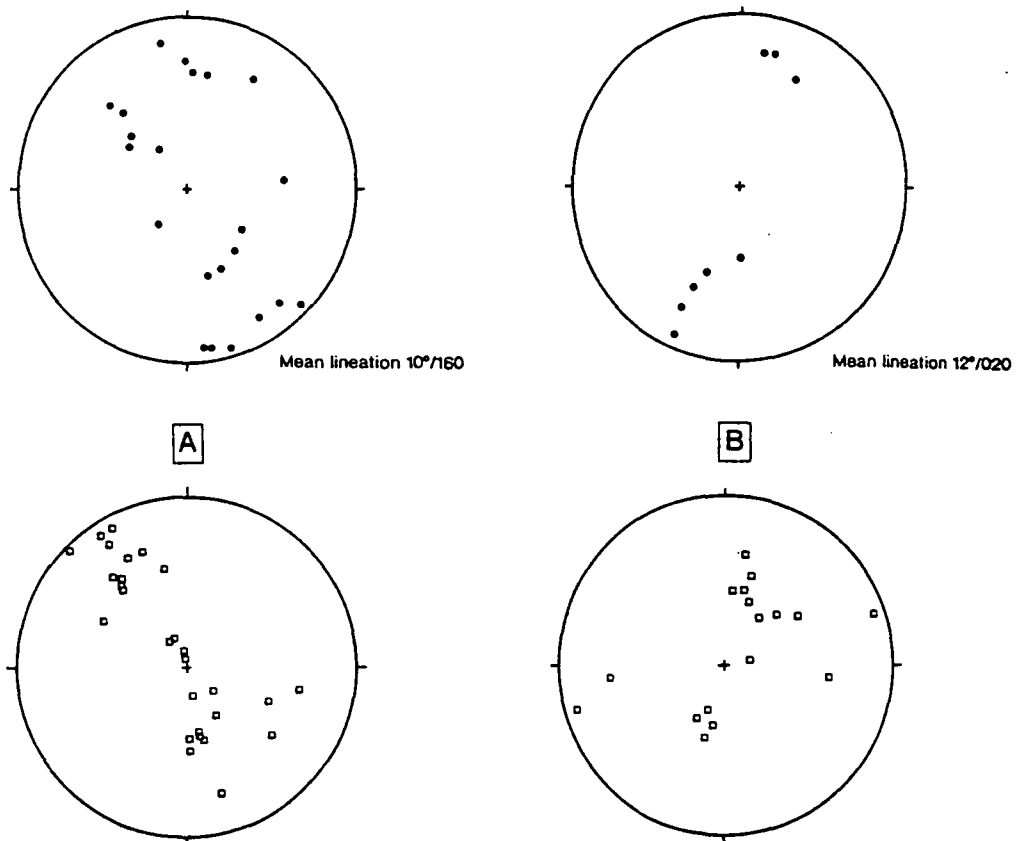


Figure 4.10 Equal area stereonets of a) slickenlines on NE-SW striking thrust planes (top), mean lineation $10^{\circ}/160$; and poles to the fault planes (lower diagram). b) slickenlines on later NW-SE striking thrust planes (top), mean lineation $12^{\circ}/020$; and poles to the late thrust planes (lower diagram).

These distinct fault sets are found throughout the northern limb, although generally, only one set is present in an exposure. However, the two fault sets are found coexisting within the same exposure along the road cut east of the monument at Cruz da Salvé Rainha, overlooking the village of Pragança (Grid Ref. 03'57" 11'17") The fault sets possess a consistent relative chronology, with the NE-SW striking faults forming as thrust flats along the bedding planes, that are commonly rotated into an apparent extensional orientation. These faults are offset by NW-SE thrusts that cut up section forming forelimb thrusts, which display associated lateral splays, and oblique

ramps. Most of these faults have small displacements, and display little or no wallrock deformation. However, to the southeast of the monument, along the road to Montejunto, is a complex thrust structure that has been interpreted as a backthrust hanging wall anticline, that formed along a prominent forelimb thrust. The thick fault zone, and the complex associated structure, suggests that this thrust zone has witnessed a much greater amount of displacement relative to the discrete planar thrusts (figure 4.11). The majority of early thrusts found near Cruz da Salvé Rainha, represent prefold thrust flats exploiting bedding planes, which become rotated during progressive fold formation and are superseded by the development of the larger, more complex thrust zone illustrated below.

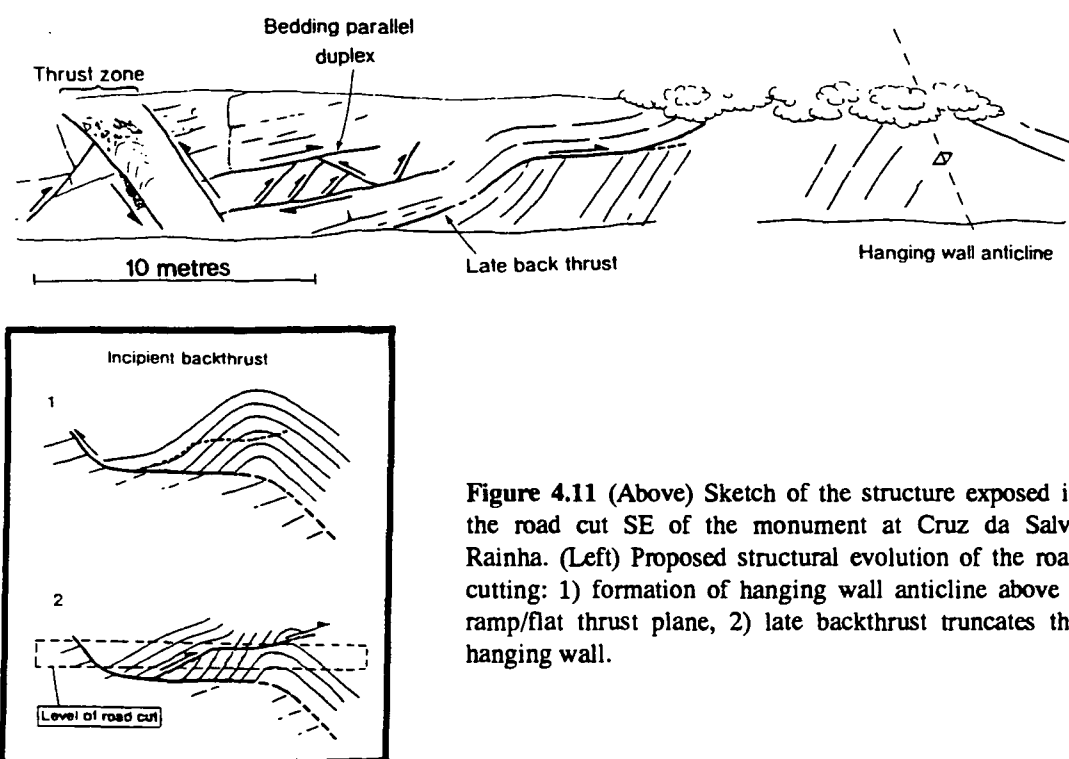


Figure 4.11 (Above) Sketch of the structure exposed in the road cut SE of the monument at Cruz da Salvé Rainha. (Left) Proposed structural evolution of the road cutting: 1) formation of hanging wall anticline above a ramp/flat thrust plane, 2) late backthrust truncates the hanging wall.

The spatial and chronological relationships of these two fault sets suggest that the NE-SW oriented set formed first. The approximately orthogonal relationship between the mean thrust transport direction of this early thrust set, and the mean fold axis of the northern limb of the Montejunto anticline suggests they are penecontemporaneous. This progressive north-northwest vergent thrust deformation became superimposed by the late NW-SE striking thrust set, suggesting a significant change in the deformation style.

Strike-slip faults and slickolites

Both dextral and sinistral faults, and slickolites, are seen in the region. They form an unusually high mean conjugate angle of 104° , however, conjugate fault sets were not seen in the same exposure. Using the mean orientations of the dextral and sinistral fault sets, the direction of maximum shortening can be determined (see figure 4.12a), the orientation of which is $30^\circ/177$. Conjugate strike-slip faults with large conjugate angles, although rare, have been described by Marshak et al. (1982) who proposed several reasons for their formation: (1) The faults initiated with a smaller conjugate angle, but became rotated during shortening, therefore, increasing the observed angle; (2) pressure solution processes may permit the initiation of orthogonal fault sets; and (3) the faults may in fact be reactivated joints.

(1) Cloos (1955) and Duby (1980) demonstrated experimentally that conjugate shear planes initiate with a dihedral angle of 55° - 60° , and that with continued shortening, the sinistral faults rotate clockwise, and the dextral faults rotate anti-clockwise, therefore, increasing the apparent dihedral angle. However, the magnitude of displacement along the observed faults, and related country rock shortening, appears to be too small to allow significant rotation of the faults.

(2) Rutter and Mainprice (1978) suggest that pressure solution slip follows a linear viscous flow, where the strain rate is proportional to the shear stress along the sliding plane. As shear stress is at its maximum on planes oriented at 45° to σ_1 , solution shears, or slickolites are likely to form most rapidly along this orientation (Marshak et al. 1982). Although the data base is small, slickolites appear to form at similar angles to faults displaying precipitated calcite steps, suggesting that the geometry of these faults may also be controlled by pressure solution slip processes (figure 4.12b)

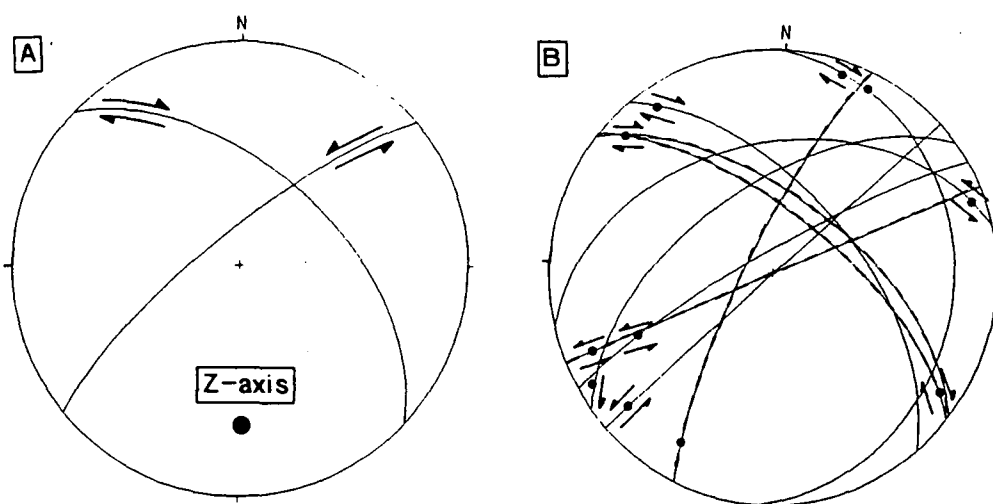


Figure 4.12 Equal area stereonets showing: a) Reconstruction of the shortening axis for the mean sinistral and dextral faults recorded in the northern limb. b) Cyclographic projection of sinistral and dextral fault planes, with respective slickenlines (dots, arrows show shear sense). Dashed cyclographic traces represent slickolite planes.

(3) It is important not to rule out the role of pre-existing fractures such as joints and veins, as it takes less work to cause slip along pre-existing fractures, than to initiate new faults.

Jointing and veining within the region forms a relatively random scatter without an obvious correlation between the faults and joints. Marshak et al. (ibid.) discuss the effects of the superimposition of a compressive stress system upon randomly oriented pre-existing planes, and concluded that such a system was unlikely to produce the observed orthogonal relationship.

The observed geometries of the fault sets appear to be compatible with a pressure solution slip mechanism having a major influence on their formation. This is further suggested by the presence of an orthogonal, conjugate set of slickolites in the unjointed, homogeneous micrites at Penas de Prado quarry, along the southeastern edge of the Candeeiros block (see section 3.6.1.3).

4.2.2.2 Arieiro fault zone

The Arieiro fault zone separates the northern and southern limbs of the Montejunto massif. The Main Arieiro fault (MAF) can be traced from the Cercal fault, near Bom Santo, due west for approximately 2.4km, to the hairpin bend southeast of the tiny village of Arieiro. Here a confluence of splay faults is present, with the Main Arieiro fault continuing along its trace which gradually bends to a WSW-ENE strike. Two main splays originate from the Main Arieiro fault, a southerly splay, which rejoins with the main fault 2.5km further west along its strike, and a northerly splay, that likewise rejoins the main fault approximately 3km west of the original confluence. These faults will be referred to as the Southern Arieiro fault (SAF), and the Northern Arieiro fault (NAF), respectively. The Southern Arieiro fault in turn gives rise to three NE-SW oriented splays (see figure 4.13).

4.2.2.2.1 Main Arieiro fault

The Main Arieiro fault is marked by an obvious scarp that forms the topographic spine of the Montejunto massif. Exposure along the scarp is good, but it is generally poor along its base to the north of the fault trace. Therefore, the apparent asymmetry of structures mapped along the fault zone is a product of this poor northerly exposure.

Geometry and kinematics

The fault zone is seen at two exposures along the fault trace, the best of which is a road cutting near Arieiro village (grid ref. 03'39" 10'78" or 9512 3790 in fig.4.13). Numerous fault planes were observed, the predominant orientation of which strike

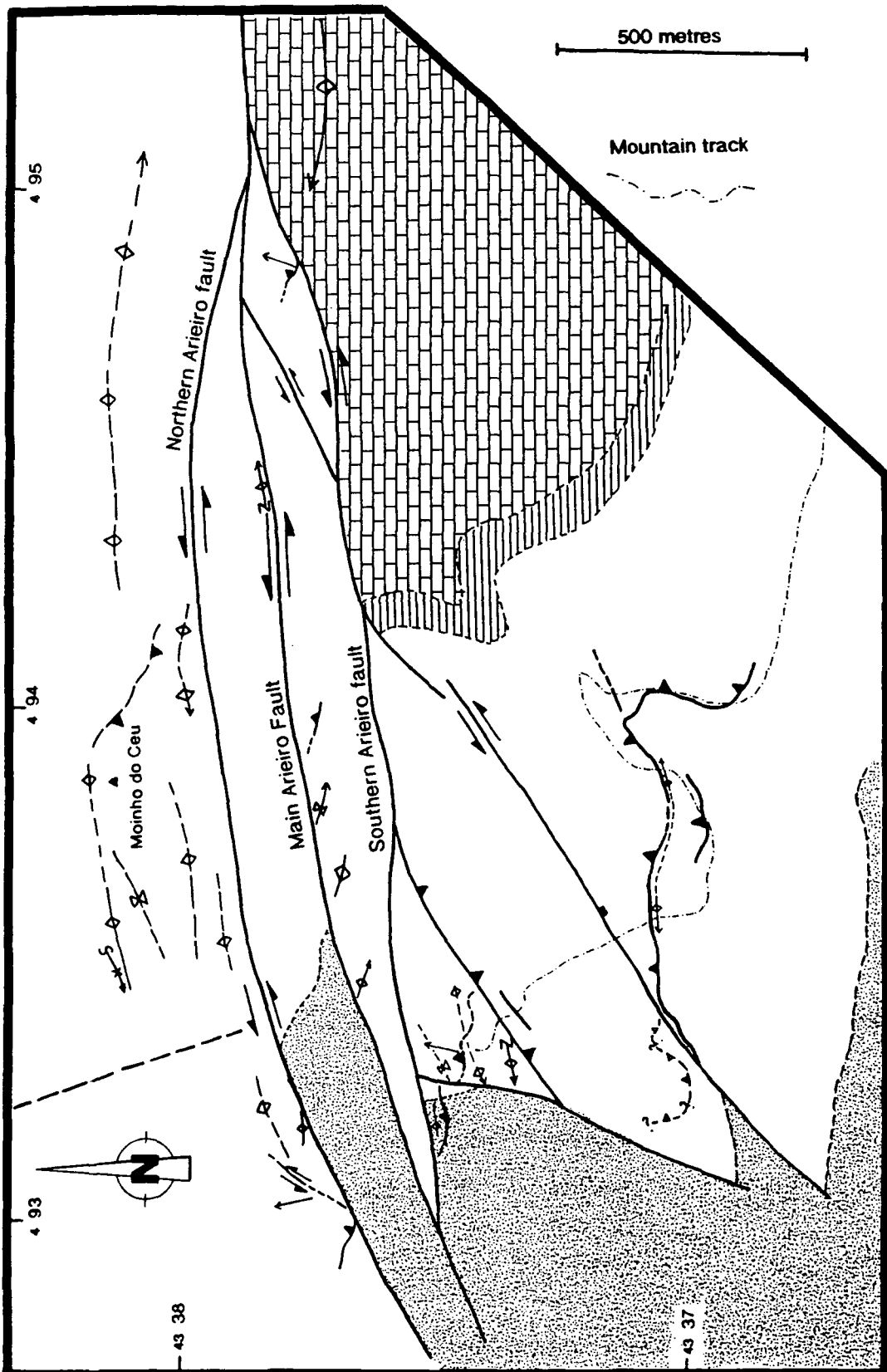


Figure 4.13 Structural map of the Arieiro fault system. Brick ornament = Bathonian, horizontal lines = Callovian, of the Candeeiros fm.; unornamented = Oxfordian, Montejunto fm.; stippled = Kimmeridgian, Abadia fm.

ENE-WSW, and dip steeply to the SSE, therefore, suggesting that the Main Arieiro fault has a similar orientation. The fault surfaces are commonly coated with overlapping accretionary calcite steps that display a complex kinematic style, with equal proportions of strike-slip, and reverse-slip slickenlines on fault planes of the same orientation (figure 4.14). The strike-slip lineations have a consistent pitch to the east of less than 10° , possibly indicating a minor component of extension along the fault plane. The reverse lineations are found on faults of the same orientation as those that display sinistral slickenlines, and in one instance, reverse movement is present on the footwall contact of a fault zone, that in turn, displays sinistral motion along its hanging wall contact. The reverse slickenlines have a mean pitch of 70° to the SW, indicating a slight component of sinistral motion is present. The lineations form two distinct sets with no intermediate oblique lineations between them. No relative age relationships were seen between the two slickenline sets, suggesting that their formation may possibly be contemporaneous. If this is so, it suggests that the changes in the fault motion from strike-slip to reverse movement occurred abruptly, and may have flipped between the two.

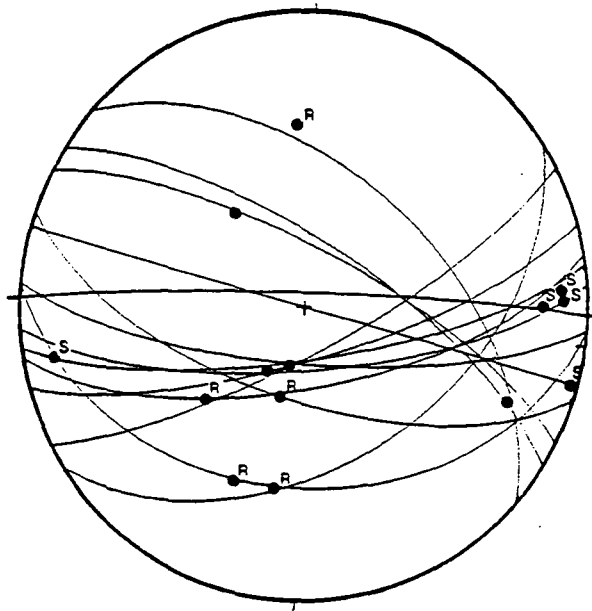


Figure 4.14 Equal area stereonet of mesoscale faults and slickenlines from the Main Arieiro fault zone. Note orthogonal lineations on several of the steep ENE-WSW faults. *S*, sinistral movement; *R*, reverse movement.

Folding

Folding adjacent to the fault trace displays two geometric relationships: (1) fold axes parallel to the fault trace, and (2) oblique en echelon folds.

(1) Folding parallel to the fault trace is present on a variety of scales, from the mesoscopic scale to regional folds (e.g. the Arieiro anticline section 4.2.1.4). Mesoscale folds form close to tight, southward verging, folds immediately adjacent to the fault trace.

(2) Several clockwise oblique folds are present along the trace of the fault. These folds possess a mean fold axis oriented $03^\circ/275$, and a harmonic mean interlimb angle of 79° . A plot of the mean fold axis to fault angle (θ) of 23° , against the mean interlimb angle, indicates a simple transpressive relationship (figure 4.15). The orientation of bedding between the Main Arieiro fault, and Northern Arieiro fault, is generally strike parallel to the fault trace, but localised oblique clockwise folds are present along a road cut south of Moinho do Céu.

The dominant folds and flexures adjacent to the Main Arieiro fault are fault parallel, and probably related to a contraction strain. However, the en echelon folds and strike-slip slickenlines indicate that late sinistral motion has occurred along the Main Arieiro fault. They also suggest that this sinistral motion was transpressional.

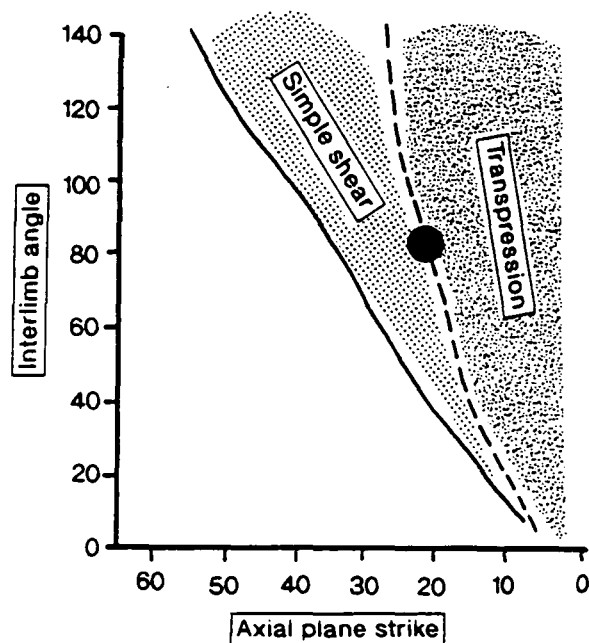


Figure 4.15 Fold appression graph for en echelon folds adjacent to the Main Arieiro fault. Dashed line separates fields of transpressive deformation paths from simple shear deformation paths, solid line separates simple shear from transensional deformation paths. Solid dot represents the plot of mean axial plane/fold axis angle against mean interlimb angle, suggesting a simple transpressive strain path. (Graph modified from Little, 1992)

4.2.2.2.2 Northern Arieiro fault

The Northern Arieiro fault is exposed along two road cuttings, at grid ref. $04'10'' 10'76''$, and $04'88'' 10'60''$. The fault is marked by a zone of calcite mineralisation displaying slickensides oriented $096/69^\circ\text{N}$, adjacent to the zone of fault confluence,

and $057/82^{\circ}\text{NW}$, at the western end of the study area. Slickenlines along the fault planes indicate a dominantly sinistral sense of motion, with a component of extensional movement present at the southwestern end of the fault trace (figure 4.16a). This extensional component may be due to the change in fault orientation, effectively producing a releasing bend geometry. As mentioned in section 4.2.2.1, and above, the folding present on either side of the Northern Arieiro fault is sub-parallel to the fault trace, no oblique folds were observed.

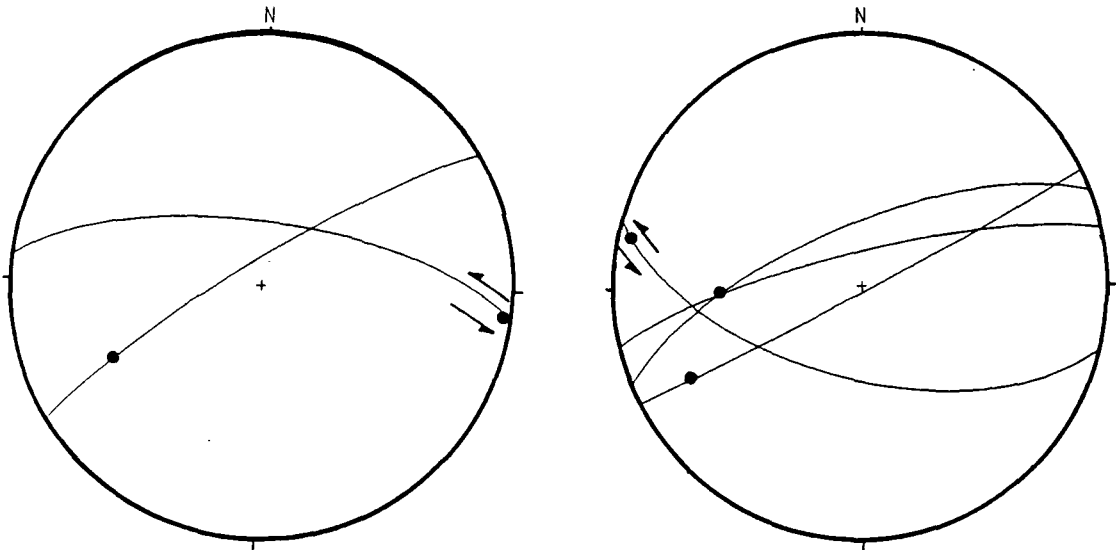


Figure 4.16 Equal area stereonets of: a) Main fault plane exposures of the Northern Arieiro fault (NAF) revealing the 'porpoise nature' of the slickenlines, probably due to the change in fault orientation. b) Mesoscale faults from the Southern Arieiro fault zone (SAF).

4.2.2.2.3 Southern Arieiro fault

The Southern Arieiro fault zone is poorly exposed along its length, and is commonly marked by a thick zone of calcite mineralisation that displays various textures. The calcite often possesses a drusy fill texture, displaying multiple phases of extension and mineralisation. These infilling textures become deformed by discrete zones of deformation that produce fault breccias consisting entirely of calcite clasts. The clasts are abraided and subrounded, up to 8mm in length, with occasional large euhedral crystals present. These clasts appear to be supported by a matrix of small (>2mm) angular clasts. Discrete fractures parallel to, and approximately 21° clockwise oblique to the fault trace, are present. Slight sinistral offsets of euhedral crystals are seen along some fault parallel fractures, suggesting that the oblique fracture set may correspond to Riedel shears.

Elsewhere, the zone of deformation is up to 10 metres wide, with discrete, well developed, fault zones approximately 6cm thick. The external surface of one of these individual fault zones has pronounced calcite accretionary steps displaying sinistral motion. The fault rock itself is formed of a protocataclasite, formed dominantly of

angular clasts of calcite varying from 8mm to microscopic in size. The matrix to these clasts is a dark fault gouge, with localised dolomite cements developed. Very few limestone clasts are present within the protocataclasite, suggesting that the protolith was a calcite mineralised zone. A well developed pressure solution cleavage, clockwise-oblique to the fault plane has resulted in penetrative suture contacts between the large clasts. This has also modified the smaller clasts by the removal of carbonate material in solution to produce a general elongation of the clasts parallel to the cleavage (plate 4.6). Several of the large calcite clasts have kinked and offset twin planes which give conflicting senses of shear. This is probably because the individual clasts have become rotated during the cataclastic process.

Mesoscopic deformation styles and textures similar to the above are common along the fault trace, although the rocks containing these features are poorly exposed along the western end of the fault.

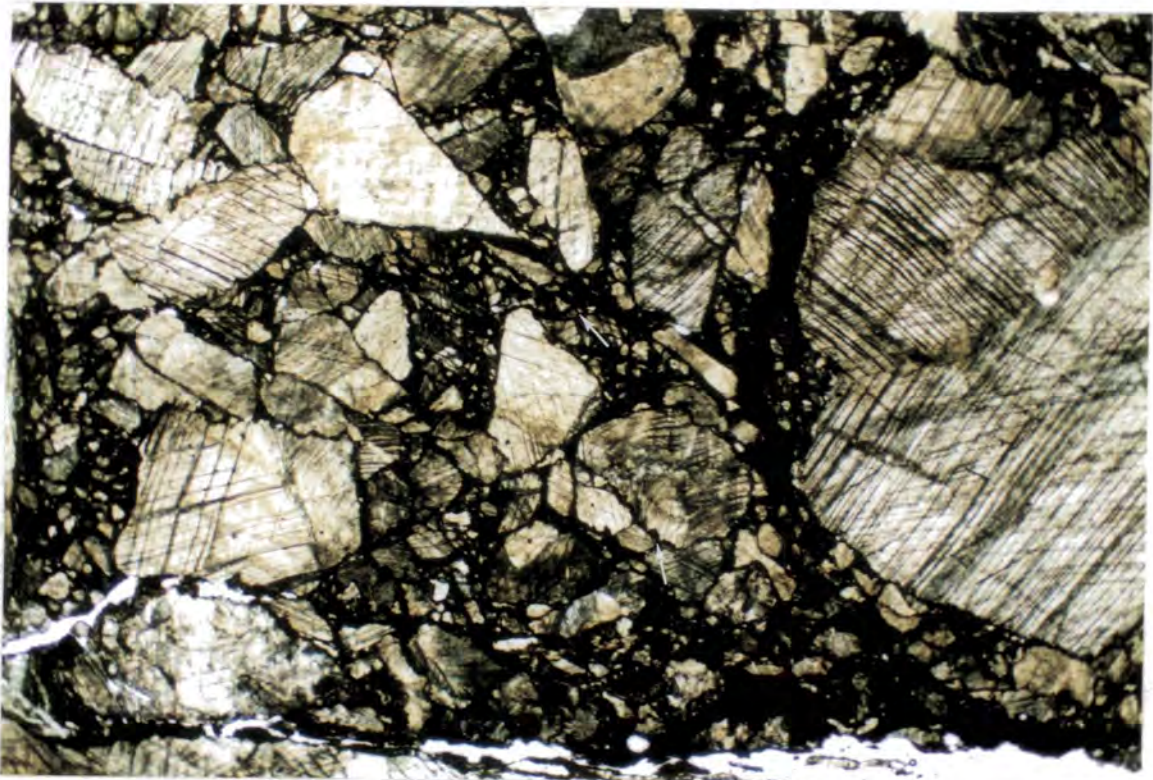


Plate 4.6 Protocataclasite displaying a preferred orientation of elongate clasts due to the removal of CaCO_3 in solution along a well developed pressure solution cleavage (marked by arrows). Evidence of suturing between larger clasts is common.

Fault geometry and kinematics

The fault zone has a dominant trend of approximately 075° , but its direction of dip is somewhat uncertain. As the fault zone appears to be characterised by calcite

mineralisation, a measurement of the undeformed composite veining along the fault trace may give an indication of the fault zone dip. However, the calcite veining does not display a constant orientation changing from a southerly dip, east of the confluence between the Southern Arieiro fault and a NE-SW oriented splay fault, to a northerly dip west of this confluence. To complicate the issue, the few minor fault planes observed display variable directions of dip along the length of the major fault trace (figure 4.16b). This latter fact may not be important as second order splays in strike-slip fault zones commonly display variable dip directions (Tchelenko, 1972; and Naylor et al., 1986). It appears that the Southern Arieiro fault may change its direction of dip at the point of confluence with the splay, which shares a southeasterly dip with the eastern end of the Southern Arieiro fault. Therefore, it appears that the Southern Arieiro fault may be segmented.

The kinematics of the Southern Arieiro fault zone display a consistent sinistral sense of shear, as derived from the following structures: accretionary calcite steps along fault planes; an oblique, clockwise, pressure solution cleavage within the fault zone; short offsets of fault zone clasts; oblique extensional veining similar to T criteria tensile fractures of Petit (1987); and synthetic antitaxial veins. The slickenlines observed along the fault planes have a westerly pitch which increase towards the western end, indicating that a component of reverse motion is present along the eastern segment, and a minor component extensional motion along the western segment. The stratigraphic throw and structural geometry associated with the western segment suggests a net reverse motion, therefore, this minor extensional component may post-date an early contractional displacement.

4.2.2.2.4 Southern fault splays

As mentioned earlier, three main fault splays initiate from the Southern Arieiro fault. These comprise two parallel NE-SW striking faults that terminate at their southwestern ends against a NNE trending splay, which marks the boundary of the studied area (see figure 4.13). Deformation within the area delineated by the fault splays has a complex structural geometry and kinematic style. The northerly splay, along with the NNE trending splay, define a fault block adjacent to the Southern Arieiro fault. This block possesses a fold pair, with a syncline in the footwall of the Southern Arieiro fault suggesting the fault had a component of reverse movement, and an asymmetric anticline present in the footwall of the northern fault splay, which possesses a reverse sense of motion (figure 4.17). The southern limb of the anticline dips steeply to the south, displaying a tight, Z geometry, parasitic fold. The geometry, and spatial relationship of the anticline to the adjacent splay fault, suggests that the two are not genetically linked via fault tip fold processes. Instead their geometry is

reminiscent of deformation against a pre-existing buttress, suggesting that the northern splay may possibly be the site of a previous structure. The orientation of bedding on either side of this fault have perpendicular strikes, with localised coaxial deformation overprinting the bedding orientations adjacent to the fault. This structural difference also appears to be non compatible with deformation of an initially homogeneous rock body, further suggesting that the northern splay represents the site of an older structure.

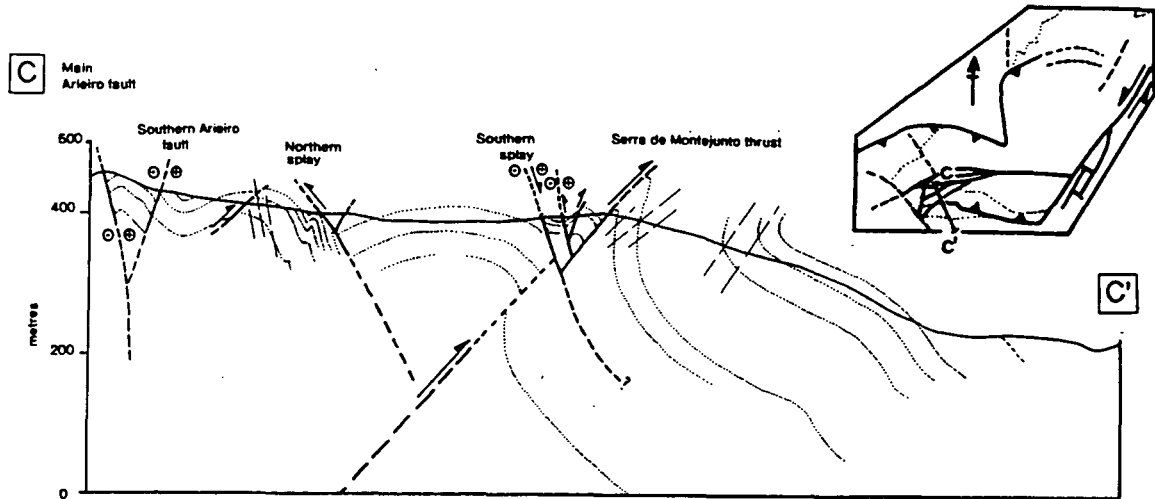


Figure 4.17 Structural cross section through the Northern and Southern Splay faults. Location of section is shown in the inset.

The region between the two parallel splay faults is relatively undeformed, possessing a dominant southwesterly dip, which as mentioned above, strikes perpendicular to the structures in the northern block. However, the orientation of bedding becomes modified against the fault zones, with bedding locally dipping towards the faults. This is most dramatically seen against the southern splay, where steep drag folding is present.

An extensional fault zone is present immediately south of the northerly splay, which is marked by an extensive zone of calcite mineralisation. The calcite veining forms a zone between 1.25 and 1.5 metres wide, displaying several discrete zones of differing calcite textures. The centre of the zone possesses a medial trail of wallrock clasts, bordered on either side by rosettes of druzey calcite that have nucleated on isolated clasts of wall rock, and are presumably related to hydraulic fracturing. The edges of the zone are marked by thick, planar, veins displaying druzey fill textures (plate 4.9). These textures indicate a change in the style of extensional mechanisms, from initial hydraulic fracturing and brecciation of the original rock, to late planar extensional veining, resulting in the formation of a druzey fabric, indicating growth into a fluid filled cavity. The surfaces of the planar veins display dip-slip slickenlines. Due to the



Plate 4.8 Sinistral transensional fault zone. Sigmoidal calcite crystal growth records the changing incremental strain (see below). Note cataclastic deformation has removed approximately half of the calcite mineralisation. Length of hammer shaft, 35cm.

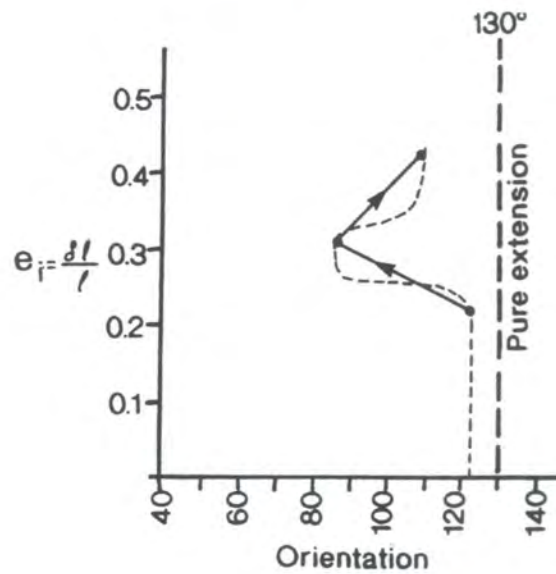


Figure 4.18 Plot of maximum incremental longitudinal strain (e_i) against the orientation of crystal growth for the sigmoidal calcite growth in plate 4.8. Dashed line represents a smoothed curve for the evolution of e_i . The consistent plot of the data to the left of the pure extension direction indicates that the mineralisation has been subjected to a component of sinistral shear throughout its extensional phase.

obvious extensional nature of the zone, and the lack of overprinting contractional structures, the movement sense along the slickensides is presumed to be a normal, making the zone a late extensional fault.

The southern fault splay is marked by a dominantly extensional fault zone, which does not display a change in the strike of the bedding on either side. However, the fault does coincide with a change from a simple structural geometry to more complex fault and fold relationships to the south. The fault is marked by a wide zone of calcite mineralisation between 20-32cm thick. Near its northeastern end the fault zone displays a thick syntaxial calcite vein exhibiting sigmoidal crystal growth. These curved patterns show how the incremental longitudinal strains changed during progressive deformation. Figure 4.18 shows the change in the maximum principal incremental strain (e_i) against the orientation of the crystals. The deformation path clearly shows that the vein was effected by varying degrees of sinistral motion relative to extension, and that throughout its formation, it has displayed transtensional motion. The values of δ / λ and λ / δ used in the calculation of e_i were based on half the width of the sigmoidal vein, as the northwestern half of the vein has been removed by later faulting. This late cataclastic period of faulting was possibly sinistral as small scale sinistral fractures offset the sigmoidal calcite crystals (plate 4.8).

The fault zone is also exposed along a mountain track (grid ref. 04'58" 10'25"), where extensional drag folding is seen (plate 4.10). The fault zone displays a 15-20cm druzey filled calcite vein, but the presence of a sigmoidal geometry could not be ascertained as the view afforded of the fault was in profile only. A cataclastic zone up to 5cm thick is present along the footwall of the fault zone. The fault rock is composed of a narrow zone, (<1cm), of cataclasite immediately adjacent to the fault plane, containing predominantly micrite, and some calcite clasts, up to 2mm in length. The asymmetries of several of these clasts suggest a sinistral component of motion was present within the fault zone. The remainder of the fault rock consists of a hydraulically fractured protocataclasite, with clasts of protocataclasite displaying a druzey calcite mineral precipitation along their edges. The calcite veining is predominantly parallel to the fault plane, and is commonly separated by thin zones of fault gouge. No unambiguous shear sense evidence is present for a dip-slip component of movement. As the thick druzey texture vein is not fractured and included within the cataclastic zone, it must represent late extension on what was possibly an original sinistral fault.

From the discussions presented above, it is clear that the southern splay fault has a varying style of deformation, from early strike-slip to late extension / transtension, with a consistent component of sinistral motion throughout its discernible history. Similar late extensional, and transtensional structures are



Plate 4.9 Thick extensional veining displaying varying styles of mineralisation, see text for details. Lens cap (50mm) for scale.



Plate 4.10 View looking NE at the Southern Splay fault, drag folding indicates an extensional sense of motion. Note thick zone of calcite mineralisation. Hammer for scale (shaft 35cm).

abundant throughout the Montejunto massif (see section 4.3).

4.2.2.3 Southern limb of the Montejunto massif

The southern limb of the Montejunto massif is located to the south of the Arieiro fault, and includes the area defined by the splay faults, described above. A complete study of the southern limb was prohibited by the presence of a large military installation on the summit of Montejunto. However, transects were conducted through the western and eastern ends of the structure, with along-strike observations between the transects possible below the 'line of sight' of the airbase.

4.2.2.3.1 Folding

In general, the southern limb consists of dominantly E-W striking bedding that steepens towards the south where it becomes locally overturned adjacent to the main faults (Cercal and Serra de Montejunto faults). However, the bedding orientation is rotated to a NE-SW strike adjacent to the Cercal fault at the eastern edge of the massif. The hinge zone of the Montejunto anticline can be traced over a short distance, to the south of the Montejunto airforce-base, where it is truncated by the Arieiro fault (figure 4.13). The hinge is seen to plunge to the west, which is confirmed by a π -diagram analysis of total bedding data which predicts the fold axis orientation to be $17^\circ/268$ (figure 4.19).

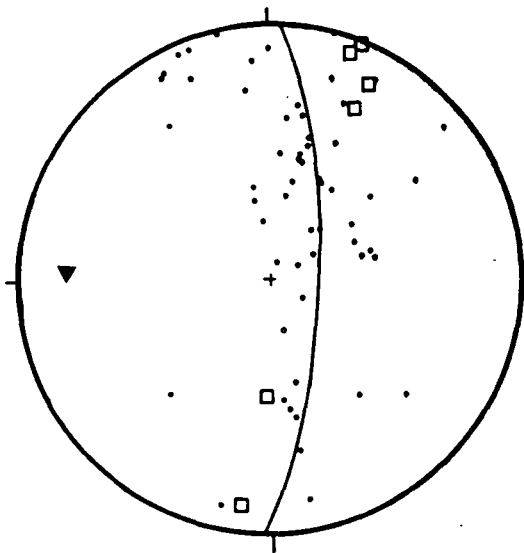


Figure 4.19 Equal area stereonet of poles to bedding (dots) and poles to cleavage (open squares). π -diagram analysis indicates a fold axis orientation $17^\circ/268$ (solid triangle).

As with the northern limb, the southern limb possesses parasitic monoclines, the fold limb vergence of which, are consistent with the position of the regional fold hinge. These parasitic folds are developed on a variety of scales, from rare centimetre

scale folds, to flexures possessing limbs tens and hundreds of metres in length (see figure 4.6b). The dominance of monoclinial folds is virtually complete except for a single parasitic fold pair displaying an easterly plunging fold axis, and northerly fold vergence (plate 4.13).



Plate 4.11 Looking NE towards a parasitic fold pair on the southern limb of the Montejunto anticline. Fold verges up the topographic slope, toward the regional anticlinal fold axis. Single track dirt-road in the foreground for scale.

Internal structures

In the following section internal structures are classified as those structures that occur within the bedding units, such as: extensional veining, jointing, and cleavage. For this study the extensional veins will be classified using the same nomenclature as that proposed for describing joint sets.

Extensional veining - Syntaxial calcite extensional veins are common within the southern limb. Although a thorough survey of the vein relationships was not conducted, the reconnaissance sampling of their orientations reveals an orthogonal set of dip bimodal veins (figure 4.20a). They form a roughly NNE-SSW striking set of cross veins or *ac* veins, based on the terminology of Cloos (1922)* and Sander (1926,

1930)* respectively (*in Ramsay & Huber, 1987), and an E-W set of longitudinal veins or *bc* veins. As expected the *bc* veins display the widest scatter of poles on the stereonet, as their orientation is perpendicular to bedding. A set of wide extensional veins (>10cm) are present parallel to the *ac* veins, but they may not be associated with the large scale folding, as is otherwise inferred by their parallelism with the *ac* veins (see section 4.3).

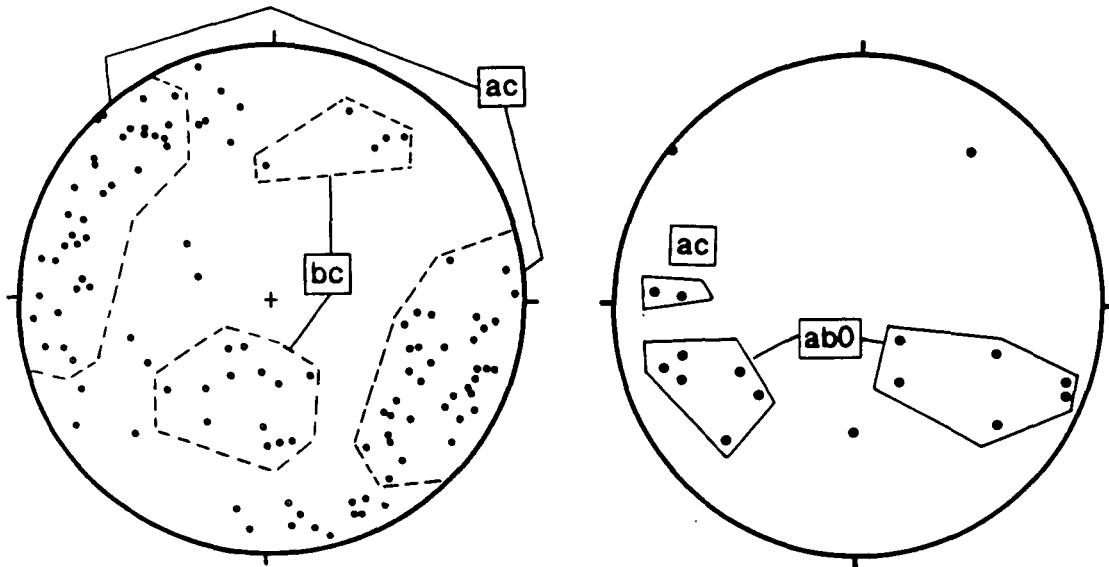


Figure 4.20 a) Equal area stereonet of poles to extensional veins from the southern limb of the Montejunto anticline. Boundaries are generalised to highlight the major vein sets. b) Equal area stereonet of poles to joint planes. Joints dominantly form oblique to the fold axis, and the fold profile plane.

Longitudinal or *bc* veins are dominant within the sub-vertical bedding of the lower southern limb, with concentrations of outer arc extensional veins and joints in the hinges of the monoclinical flexures. These outer arc structures are obviously related to tangential longitudinal strains, hence their intersection with bedding surfaces (V/S_0 lineation) produce a lineation equivalent to a bedding/cleavage intersection lineation. However, their usefulness as a method of predicting the fold axis orientation is dependent on the vein being produced by neutral surface folding, which due to exposure restrictions, is often not possible to determine. Therefore, very few V/S_0 lineation data were recorded. Those that were measured give a relatively ambiguous result, but when supplemented with the observed fold axis of a parasitic fold pair, they suggest that a localised easterly plunge occurs within the regional structure around the Penha da Cruz area (grid ref. 03'00" -09'97").

Joints-Jointing is crudely distributed into two sets, an *ac* set of cross joints, and an oblique set of *ab0* joints (figure 4.20b).

Cleavage- In general, cleavage is not observable on weathered surfaces. However, where fresh surfaces are available a widely spaced stylolitic cleavage is present within the limestones, with a more obvious narrowly spaced planar cleavage occurring in the

marly horizons. The poles to the cleavage planes consistently plot clockwise of the mean fold profile plane (figure 4.19), possibly suggesting a sinistral non-coaxial relationship, however, the small data set necessitates caution in this interpretation.

External structures

For the purposes of this section external structures will be structural elements developed along the bedding planes, but does not include intersections of other planar structures.

The bedding planes are commonly weathered and reveal very little detail, but along fresher exposures slickenlines are seen forming two distinct sets. The most dominant set consists of westerly plunging sinistral slickenlines (plate 4.12), the



Plate 4.12 Minor sinistral strike-slip reactivation (via crack-seal mechanism) of a steep bedding plane along the southern limb of the Montejunto anticline.

second set consists of reverse slickenlines. The latter plot along the fold profile plane suggesting they are related to flexural slip. Evidently, the sinistral lineations can not be related to flexural fold processes, and, therefore, must represent fault reactivation of the bedding surfaces. The relative amount of sinistral displacement along these bedding planes, based on the amount of cataclastic deformation, was probably very small, as no brecciation or gouge is present.

These late strike-slip movements suggest that the steep beds within the southern limb have undergone temporal kinematic partitioning. This scenario describes the change from contractional deformation, and its associated dip-slip flexural slip, to a later, separate period of sinistral reactivation. This change in kinematic style is probably due to the production of sub-vertical bedding by the progressive folding of the southern limb, which provides a favourably oriented anisotropy that can be exploited by synthetic shears from the southern end of the Cercal fault.

4.2.2.3.2 The Serra de Montejunto thrust

The large scale geometry of the southern limb is dominated by a roughly east-west oriented, southerly vergent thrust fault, the Serra de Montejunto thrust. The thrust has produced a region of steep to overturned bedding, forming a truncated overturned footwall syncline. The thrust can be traced westwards from the Cercal fault, through the Oxfordian carbonate sequence, where it becomes offset by the southern splay fault (figure 4.13). Structural cross-sections by Guery (1984), imply that the thrust affects locally deposited Quaternary age deposits, that in turn, lie unconformably upon the Kimmeridgian marls and clastics at the eastern end of the thrust trace. However, no such relationship was observed during this study.

No exposure of the thrust zone was observed in the east, but it may be traced by the structural geometry and stratigraphic relationships of the footwall and hanging wall rocks. In contrast, the thrust zone is well exposed along a mountain track to the north of Ramada, where the track follows a topographic spur, allowing three traverses through the thrust zone. These traverses reveal approximately 500 metres of along-strike geometry, which changes quite significantly from west to east.

Western traverse - The basic geometry of the thrust is quite simple, consisting of a hanging wall anticline thrust over a truncated overturned footwall syncline (figure 4.21). However, the geometry of the hanging wall has been modified by steep reverse backlimb faults, that possess a component of sinistral slip. The main fault zone has a moderate dip of 50° to the north, and is located immediately above the normal limb of a tight footwall anticline (plate 4.13). The zone is approximately 1.5 metres thick, and is dominated by large fault bounded blocks that represent fault reactivated bedding



Plate 4.13 Tight anticlinal fold hinge found immediately beneath the Serra de Montejunto thrust plane along the western traverse. The thrust zone is highlighted by arrows. Compass/clinometer (10cm) for scale. View looking east.



Plate 4.14 Exposure of the Serra de Montejunto thrust zone along the eastern traverse. View looking east. 30 litre rucsac for scale.

Eastern traverse - The mountain track appears to follow the exposure of the thrust zone, suggesting that the angle of dip has reduced significantly. The hanging wall displays steep to sub-vertical southerly dipping bedding, that has been juxtaposed onto low angle footwall bedding. The thrust plane dips to the north at a lower angle than the fold axial plane, resulting in the thrust plane cutting the steep backlimb of the footwall syncline at successively lower levels to produce the observed structural geometry (figure 4.21). The narrow exposures of the thrust plane in the track give a tantalising glimpse of the complex fault geometries within the zone, with several footwall ramp structures and possible thrust duplexes present. The fault zone is well exposed where it ramps up through the mountain track (grid ref. 05'19" 10'12"), displaying a 50° northerly dip. At this point the hanging wall possesses sub-vertical bedding, separated from low angle footwall bedding by a 40cm thick zone of brecciation, that is internally structured into an upper and lower zone. The upper part is formed by roughly rhomboidal shaped clasts, up to 3cm in length. The lower zone consists of large, fault bounded, sigmoidal-shaped clasts up to 15cm in length, forming a thrust duplex (plate 4.14). From the large scale relationships seen along the eastern traverse, the S. de Montejunto thrust fault can be classified as a forelimb thrust.

The changes in structural geometry along the strike of the thrust zone indicates that a fundamental change in the geometry of the thrust plane has occurred. The planar 50° northerly dipping backlimb thrust in the west, translates into a ramp/flat geometry forelimb thrust in the east. It is proposed that the change from one geometry to the other is achieved via an oblique ramp (see figure 4.21).

Geometry and Kinematics of Mesoscale faulting

Mesoscale faulting measured along the Serra de Montejunto thrust forms a conjugate set of reverse faults, the mean intersection of which plunges at 34°/264. Reverse sense slickenlines along these secondary faults have mean vector azimuth of 184°, indicating that the faults have an oblique sense of slip (figure 4.22). The intersection lineation of a conjugate set of faults on a dip-slip thrust plane would be expected to be sub-horizontal and parallel to strike, but as clearly seen, the intersection lineation has a definite plunge which has been interpreted to be the result of an oblique ramp with a northwesterly direction of dip as shown in figure 4.21. The presence of consistent oblique motion on these faults is further evidence to support the possible oblique geometry of the main thrust plane between the two traverses.

Faulting outside of the Serra de Montejunto thrust zone is dominated by moderate to low angle, ESE striking backthrusts, the mean thrust transport azimuth of which is 031° (figure 4.23). This transport direction is orthogonal to the local strike of the

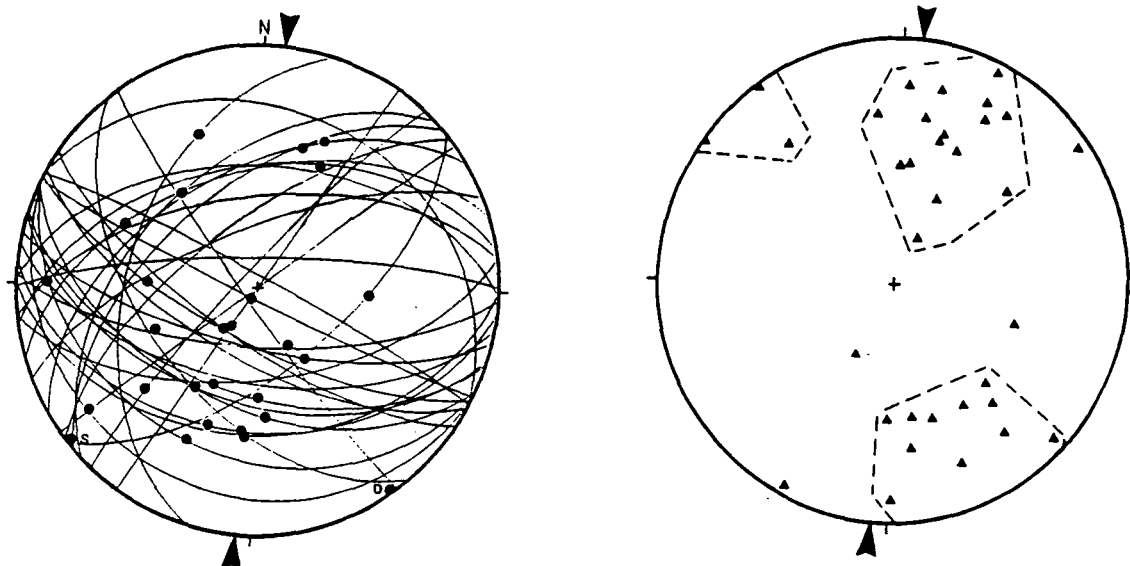


Figure 4.22 Equal area stereonets of (left) secondary thrust faults and slickenlines from the Serra de Montejunto thrust. The fault planes form two sets, which have a mean β intersection of $34^\circ/264$. (Right) poles to fault planes highlighting strong bimodal nature of the fault population. Mean thrust transport lineation 184° .

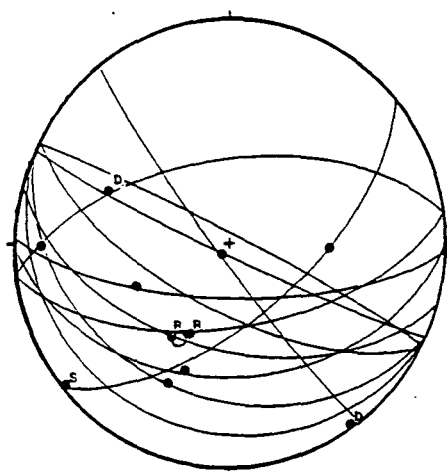


Figure 4.23 Equal area stereonet of backthrust fault planes and lineations (dots) from the southern limb of the Montejunto anticline. Mean thrust transport direction of which is 031° .

steep hanging wall forelimb, suggesting that the faulting may be the result of localised strain within the fold limb. However, this transport direction is oblique to the main fold axis, which appears to be related to N-S motion along the S. de Montejunto thrust.

Observations of strike-slip faulting from the main thrust zone, and the forelimb, reveal two sets of faults: a sinistral set oriented 040° , and a dextral set oriented 120 - 140° . Together they form a conjugate angle of approximately 90° the bisectrix of which has a north-south orientation (figure 4.24). The significance of orthogonal conjugate fault sets is discussed in section 4.2.2.1 (Faulting). In this instance, the strike-slip faults are commonly parallel to strong anisotropies. Sinistral faulting is

commonly parallel to oblique thrusts within the Serra de Montejunto thrust zone, while dextral faults are commonly bedding parallel within the steep forelimb. Therefore, it is probable that the orthogonal conjugate angle is a result of pre-existing structures.

The coincidence of the strike-slip conjugate bisectrix to the transport direction along the Serra de Montejunto thrust, suggests they are coeval and are related to north-south contraction. Folding along the southern margin of the Montejunto anticline, therefore, appears to be related to tip fold processes. Continued coaxial shortening after the development of the fold limb is suggested by the conjugate strike-slip faults that exploit the steep bedding.

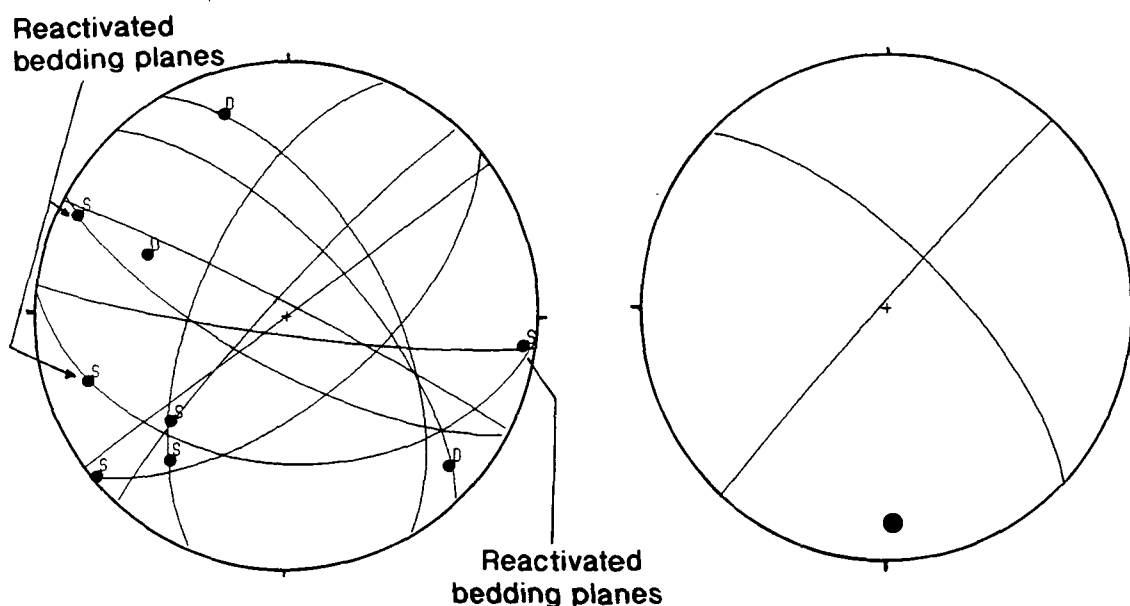


Figure 4.24 Equal area stereonets of (left) conjugate strike-slip fault planes, and slickenlines from the southern limb of the Montejunto anticline, *D*, Dextral; *S*, Sinistral. Note anomalous late bedding plane reactivation. (Right) Mean conjugate fault planes, solid circle represents the reconstructed Z-axis for the conjugate set.

Footwall geometry

Along the western end of the Serra de Montejunto thrust, a well exposed overfold syncline is present in the footwall (figure 4.6a). At the eastern end of the thrust trace the footwall is composed of poorly exposed Kimmeridgian marls and clastics of the Abadia formation, therefore, the structure is poorly constrained. However, steep zones within the Kimmeridgian sequence are marked by resistant sandstone units that are differentially weather to form prominent topographic features, as seen to the north of Carvalhos (grid ref. 03'32" 09'61"). Exposure of the resistant Kimmeridgian units is lost after this steep zone possibly because the bedding becomes sub-horizontal, hence, no prominent units are exposed. This interpretation is backed-up by the work of Guery

(1984), who indicates that the steep bedding flattens out before becoming overturned against the thrust plane (figure 4.6b).

4.3 Late extensional veining and faulting within the Espigão plateau and Montejunto massif

Both the Espigão plateau and the Main Montejunto massif are dissected by thick extensional calcite veins, that display a very consistent orientation across the area, the mean orientation of which is $029/77^{\circ}\text{NW}$ (figure 4.25). The veins are distinguished by their sheer thickness (between 10cm and up to 20 metres), and their planar geometry. The veins display a variety of textures that are generally dependant on the vein thickness. Veins up to 60cm thick display dominantly single fill druzey textures, the mineral growth of which, is occasionally oblique to the vein walls indicating a component of sinistral motion. The wider mineralised zones up to 20 metres thick have a composite nature. They are occasionally composed of multiple druzey fill events, with individual veins up to 30cm thick, but they more commonly display zones of different calcite textures, such as: rosette druzey calcite textures around clasts of brecciated wall rock, and medial trails of wall rock probably formed by a crack-seal mechanism. Multiply fractured and sealed veins are present displaying clasts of wall rock, and earlier generations of calcite fills, cemented by later calcite precipitation, indicating that hydraulic brecciation has occurred.

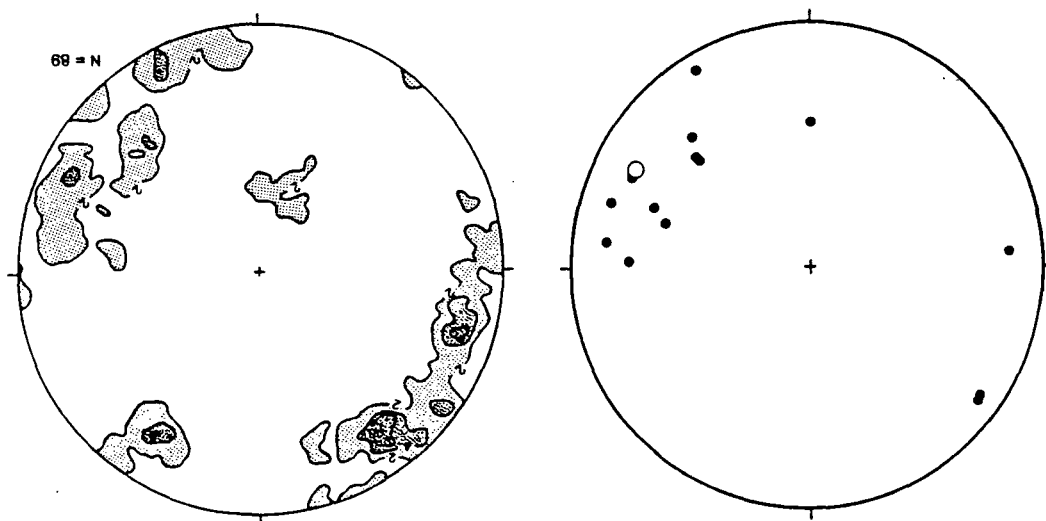


Figure 4.25 a) Equal area stereonet of poles to thick extensional veins from the Montejunto massif (open circle = mean vein orientation $029/77^{\circ}$). b) Contoured poles to thin extensional veins from the Montejunto massif. Mean extension direction of 127° . Contour intervals: 2, 4, 6%.

It is clear from the discussion of the southern splay fault, earlier (section 4.2.2.2.4), that a component of sinistral motion was present during the formation of the calcite mineralisation, and was also present post mineralisation. This kinematic

style is not uncommon within the area, although these veins generally have a higher angle of strike relative to the pure extensional veins which strike at 030° . These thick veins and mineralised zones appear to be very late structures in the formation of the Montejunto region, as they cross cut most of the structure within the Montejunto massif, e.g. the southern splay fault which offsets the Serra de Montejunto thrust.

4.4 Strain orientations within the Montejunto anticline

The orientation of the principal strain axes within the Montejunto and Espigão region were calculated from the observation of en echelon tension gash arrays, and to a much lesser extent, late extensional veins (see methodology below). Due to the very late nature of the extension veining within the massif, the latter method provides a constraint on the late incremental strain occurring across the Montejunto range, whereas, the data derived from the vein arrays has to be scrutinised carefully before it can be considered to represent the true incremental regional strain.



Plate 4.15 Well developed en echelon sigmoidal tension gash array dissected by a late fault. Montejunto massif.

4.4.1 Methodology

En echelon vein arrays - Many authors have attempted to describe conjugate vein arrays in terms of stress orientations, however, it has to be remembered that the

geometry of a vein in an array is a record of strain (Beach, 1975). Therefore, in this section principal strain axes will be employed where commonly stress axes are inferred. The arrays are of a primary en echelon vein type, that do not display pressure solution effects, and possess a low conjugate angle. Highly sheared examples have developed late shears through them (plate 4.15), therefore, the vein arrays fall into classification 2b of Beach (1975).

Calculation of principal strain axes from single and conjugate arrays - To calculate the strain axes orientations, the array and incremental vein orientations were measured. In the case of conjugate arrays, the principal shortening direction was taken as being the bisector of the conjugate set (Rothery, 1988), and the construction of the X and Y axes followed a similar technique used by Hobbs et al. (1976) for the construction of stress axes from conjugate faults. To construct the strain axes for single arrays a modified version of the method proposed by both Hobbs et al. (1976), and Ramsay & Huber (1987), for single faults was used. With only a single vein array, the θ angle used in the construction is based on observed θ angles from conjugate sets. However, the θ angles observed vary relative to the angle (δ), the angle between the vein and the array orientation (ϕ), hence, the θ angle used during the construction is relative to the δ angle (Appendix 1). The low conjugate angles observed indicate that the arrays have a component of extension across the zone of shear, perpendicular to the direction of principal shortening (Beach, 1976, Ramsay & Huber, 1987 pg.629, and Rothery, 1988). Although the results derived are based on the incremental geometries of the vein arrays, they may not necessarily represent the incremental strain ellipse, as passive rotation may have occurred due to folding, i.e. prefold strains, which may, therefore, have an important bearing on the interpretation of the structural evolution.

Azimuth of principal extension - Where thin irregular extensional veins are seen the direction of opening can be deduced by matching irregularities on either side of the vein. This provides the azimuth of extension, but not the X -axis, as the measured direction is not a vector. The extension direction can also be estimated from the mean orientation of other extensional structures, such as the thick veining, and the regional extensional veining (figure 4.25a & b). As these structures are believed to be late extensional veins, the orientation derived provides an approximate direction for the late incremental X -axis.

4.4.2 Strain distribution and orientation

The orientations of the principal strain axes derived from the en echelon vein arrays describe a complex spatial distribution (figure 4.26). Three types of strain were

interpreted from the derived data: 1) Strains that exploit rock anisotropy, 2) Localised strain, or strains that are complimentary to local kinematics, and 3) regional strains, that are relatively consistent over a large area, and coincide with known regional deformation.

1) Rock anisotropies, such as bedding in the case of the Montejunto region, may become exploited by shear to produce anomalously oriented vein arrays. Therefore, construction of the principal strain axes to such arrays also display an anomalous orientation, e.g. locality 600 (figure 4.26). Hence, the direct correlation between the principal strain axes and the principal stress axes, σ_1 , σ_2 , and σ_3 , is not always valid.

2) Localised strains are found along the Main Arieiro, and Northern Arieiro faults, at localities: 150, 151, and 173. They display differing relationships to the structural geometry of the fault zones. The conjugate array at locality 173 is coaxial with the en echelon folding adjacent to the Main Arieiro fault, where as, the arrays observed at localities 150 & 151, in the northern wall of the Northern Arieiro fault are superimposed over fault parallel folds. This indicates a change in the localised strain due to the superimposition of sinistral shear along the Arieiro fault system.

3) Regional strains have been interpreted as strain systems that display a relatively consistent orientation of maximum principal strain axes over a large area, and can be related to regional structural styles or stress systems. In the Montejunto massif, the most consistent spatially distributed strain system possesses a roughly NW-SE oriented Z-axis, which is probably related to the Tortonian to Recent regional stress system across the Lusitanian basin (Ribeiro et al., 1988; and Dewey et al., 1989, see section 2.2). The orientation of these regional Z-axes display a general northerly plunge in the northern limb, and a southerly plunge in the southern limb of the Montejunto anticline. This relatively consistent distribution of shortening directions between the northern and southern limbs possibly suggests that the vein array populations have been tectonically rotated, probably by the steepening and tightening of the limbs of the developing Montejunto anticline. This observation has important consequences for the tectonic evolution of the Montejunto region, as it suggests that the large scale folding of the Montejunto anticline continued at least into the Tortonian (later than 9 Ma).

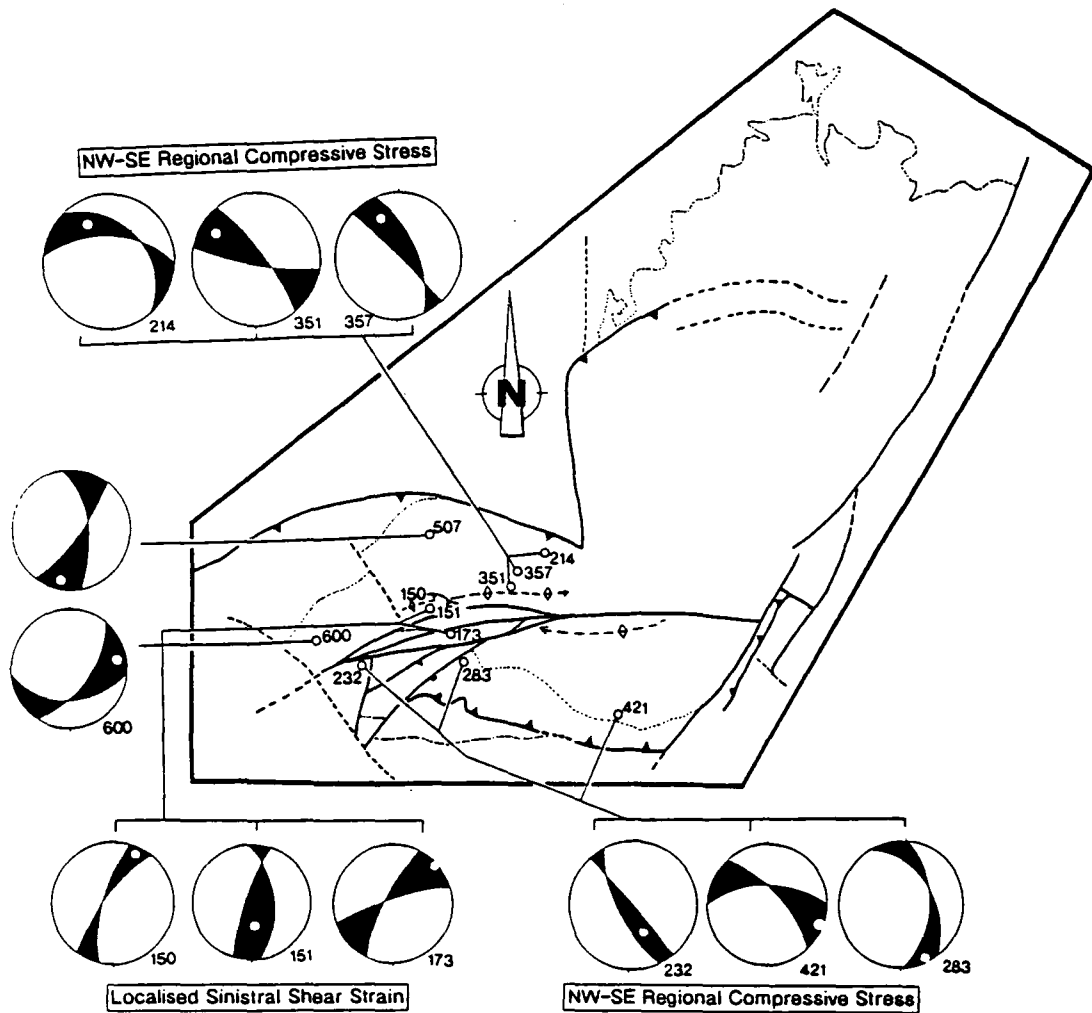


Figure 4.26 Strain distribution within the Montejuntó massif derived from conjugate and singular en echelon vein arrays. Conjugate vein arrays are represented by equal area stereonets, black segments - contractional regimes, white segments - extensional regimes, the boundaries to these regimes are marked by the conjugate shear planes. White dots mark the constructed principal shortening direction (z-axis), numbers refer to map localities during data collection. See text for details.

The late extensional veins discussed earlier (see section 4.3), represent late dilational strains, which commonly approximate to incremental strains. In calculating the extension direction from the vein orientations it has been assumed that they have opened by pure extension, as the component of obliquity observed along a small minority of the veins is relatively minor. This assumption appears to be valid as the observed direction of vein opening, measured by matching up irregularities in the opposing vein walls, lies within the range of mean extension directions derived from the vein orientations. Together, the three sources of data produce a harmonic mean extension direction of 123.5° , see table 4.1. This extension direction implies that a late ESE-WNW oriented dilational incremental strain was superimposed over the regional NW-SE contractional strain.

Data source	Extension direction
Late thick extensional veins n=16	119°
Mean small extensional veins n=89	127°
Extension direction from matching irregular walled veins n=5	125° (Harmonic mean)
	Mean 123.5° (Harmonic)

Table 4.1

4.5 Structural and Kinematic evolution of the Serra de Montejunto region

As with the S. dos Candeeiros region, the basic structural geometry of the Serra de Montejunto range was probably defined as early as the Late Triassic, with the presence of a fault scarp that resulted in the accumulation of Hettangian evaporites. In turn, the formation of a salt pillow above this buried Triassic scarp during the Toarcian, initiated an area of localised uplift and flexure on the site of the present day Montejunto anticline. However, the detailed architecture of the present day structure was not established until the Oxfordian to Kimmeridgian with the formation of the Pragança, Montejunto and Cercal faults. These faults delineate the sub-basins of the Estremadura trough, and are the main structural expressions of the Atlantic rifting event in the Montejunto-Torres Vedras region.

Clearly, from the discussions presented in this chapter, the main period of structural formation in the Montejunto region occurred after the Mesozoic rifting event by a complex interaction of compression, transpression, and dilation, all of which were superimposed upon a pre-existing structural framework. This complex structural history appears to be divisible into two phases of differing tectonic style, that together form a single progressive deformation event. Due to the absence of absolute age constraints on the deformation sequence, the chronology of these events can only be resolved relative to local structures, and known, well constrained, regional events.

4.5.1 Initial phase of North-South shortening

Initial reactivation of the Mesozoic structures probably began during the Lower to Middle Miocene, when a north-south oriented regional shortening direction, probably approximate to σ_1 , was superimposed across the Lusitanian basin. The result of this stress system was contraction across the roughly east-west structural orientation of the Montejunto region, and the development of a narrow zone of fold and thrust formation. The Montejunto anticline appears to have initiated by the reactivation of an originally extensional fault (see section 5.3), forming the Serra de Montejunto thrust which forms the southern boundary of the main massif. The slickenlines along this fault

indicate a due south direction of thrust transport. Clearly, from the tip folding associated with this southern boundary thrust, the development of the Montejunto anticline was at an advanced stage during this initial phase of deformation.

The evolution of the northern thrust zone relative to the southern is less clear. The continuity of geometry, and fold style, between the limbs within the main Montejunto massif, suggests that the formation of the northern and southern thrust zones were contemporaneous. However, early pre-fold thrust faults within the Tojeira thrust zone possess a NNW thrust transport direction, which are superseded by a late set of NNE verging thrusts. Between the Early and Late Miocene there is a documented rotation in the regional σ_1 from N-S to NW-SE, therefore, the observed discrepancy in thrust transport directions between the two thrust zones may be due to a sequential development of the thrusts from north to south, during this period of regional stress rotation. The evolution of the northern thrust front is further complicated by the presence of the Late Jurassic Pragança fault, which acted as a sinistral transfer fault between the Tojeira and Rocha Forte thrust faults. The NE-SW structural orientation of the Rocha Forte thrust zone suggests that it may have formed later than the Tojeira thrust, in response to a more NW-SE oriented regional compressive stress (see below). The parallel relationship between the Montejunto fold axis and parasitic folds, and the Arieiro fault system, especially the Northern Arieiro and Main Arieiro faults, suggest that the hinge zone of the developing Montejunto anticline became dissected by steep reverse faults during this early deformation phase. By comparing the geometry and kinematics of the northern and southern boundaries of the Montejunto massif it appears the main structural geometry of the Montejunto anticline was probably present by the Middle Miocene, with thrust and fold development initiated along the southern, Serra de Montejunto thrust, followed by the formation of the northern Tojeira thrust. The absence of NNW oriented slickenlines along the Serra de Montejunto thrust suggests that motion along this fault ceased before the regional stress rotated, with continued shortening occurring along the Tojeira thrust zone. These thrusts form a downward convergent fault system, that bound the Montejunto anticline to producing a large 'pop-up' structure (figure 4.27/1 and 4.27/2). During this period of dominant N-S shortening, the NNE oriented Cercal fault probably acted as a passive sinistral accommodation structure, or lateral ramp.

4.5.2 Late sinistral transpression

The kinematic and strain history of the Montejunto anticline became further complicated by the progressive superimposition of a deformation event possessing

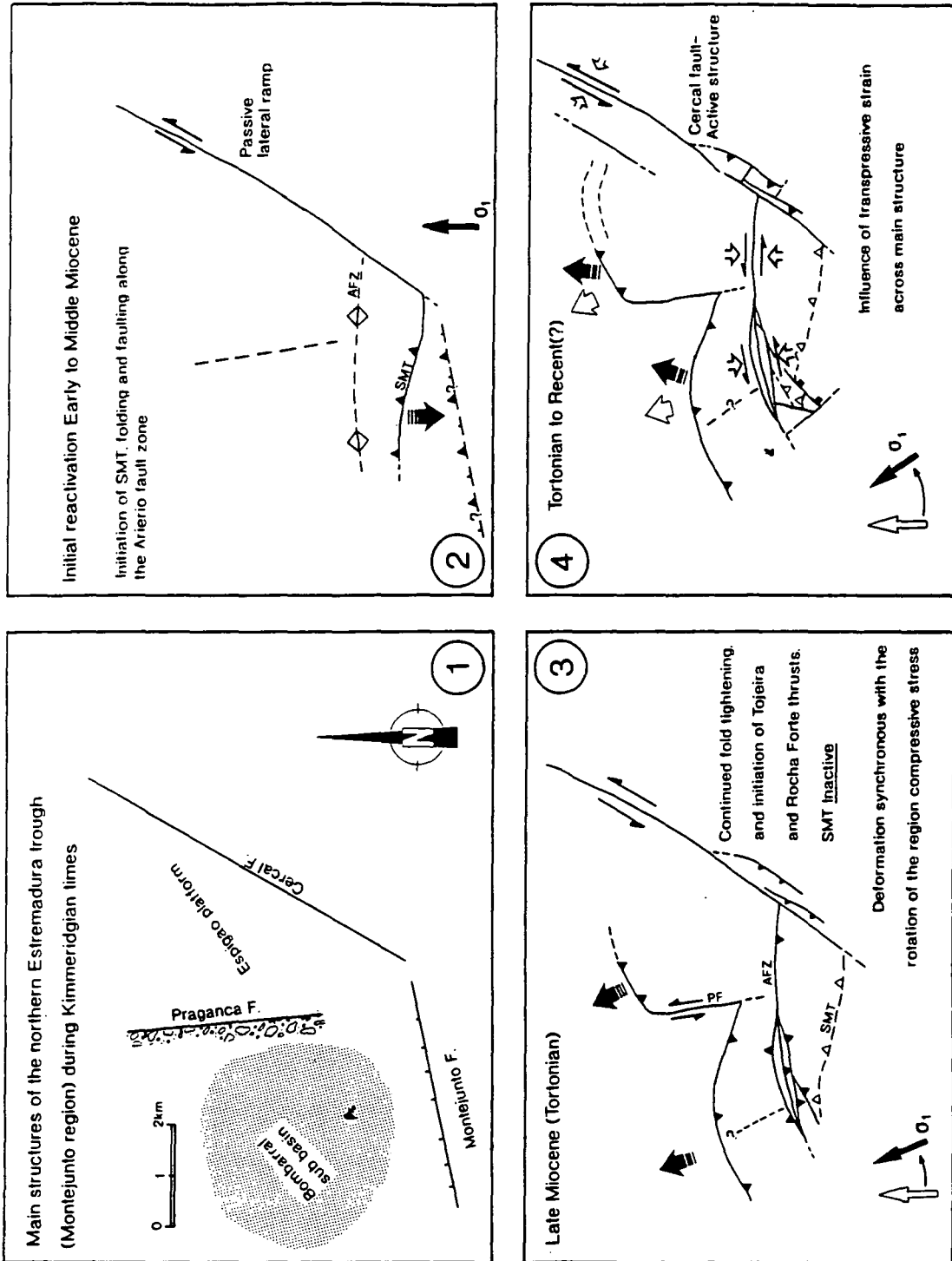


Figure 4.27 Schematic structural and kinematic evolution of the Montejunto massif. 1) Pre-Miocene structural architecture of the Montejunto region. 2) Initial Middle Miocene reactivation of the Montejunto region in relation to a superimposed N-S regional shortening, or σ_1 direction. 3) Late Miocene rotation in the regional shortening/ σ_1 direction. 4) Introduction of sinistral transpression across the Montejunto massif as a result of synthetic active motion along the Cercal fault (Tortonian to Recent).

a strong component of sinistral motion. This dramatic switch in kinematic style was probably related to the rotation of the regional σ_1 , from N-S to NW-SE, by the Late Miocene (Tortonian). The direct result of this regional stress system is recorded as conjugate sets of vein arrays, analysis of which, suggest that the tightening of the Montejunto anticline continued into the Tortonian, probably contemporaneous with sinistral deformation. The orientation of the Tortonian to Recent maximum principal stress direction to the NNE oriented Cercal fault suggests that like the similarly oriented S. dos Candeeiros fault, it had, and still has a transpressive nature. This change to a transpressive style probably resulted in the Cercal fault becoming an active structure which influenced the adjacent deformation occurring in the Montejunto anticline. Therefore, the Montejunto anticline has behaved as a major restraining bend in the sinistral transpressive Serra de Montejunto-Candeeiros (SMC) fault system since the Tortonian. This intuitively suggests that the Montejunto anticline become a late transpressive structure, as observed in many such examples of restraining bends along the San Andreas fault e.g. the Mecca, Indio, and Durmid Hills (Sylvester, 1991). Indeed, the ENE-WSW oriented faults of the Montejunto anticline do display synthetic reactivation from the sinistral Cercal fault, with the central Arieiro fault system accommodating most of the sinistral displacement within the Montejunto massif. The presence of oblique clockwise en echelon folds along the Main Arieiro fault indicates that it must have accommodated the majority of the sinistral motion relative to other faults in the system, which do not display such a broad area of sinistral deformation. A comparison of the θ' angles of these folds to their interlimb angles, indicate that the sinistral displacement along the Main Arieiro fault was a simple transpressive one. Further east along the Main Arieiro fault, abrupt lineation switches between sinistral and reverse slip were observed. Lineation switching can theoretically occur in a transpressive zone where the angle between the displacement vector and the normal to the deformation zone (angle A), is equal to or varies slightly about the critical angle of axially symmetric transpression (ASTP) of 70.5° (McCoss, 1986). This model predicts the orientations of the incremental strains associated with axially symmetric transpression, therefore, this theory and the validity of the interpretation of the lineation switching, can be tested by comparing the predicted incremental strains with the observed data. Figure 4.28 shows the McCoss construction of the incremental strain axes for the Arieiro fault zone, using the theoretical ASTP angle $A=70.5^\circ$. This graphical construction predicts a maximum incremental extension direction trending $120-300^\circ$, and an orthogonal minimum extension direction of $030-210^\circ$. A comparison of the observed field data reveals a very good fit for the maximum extension direction, as derived from late extensional veins. The thick late veins have an almost exact fit with the predicted extension direction. The poorest fit was derived from the small scale

extensional veins, which is probably due to the inclusion of vein data associated with localised strains. The mean of all this data produces an extensional direction that almost lies within the limits of measuring accuracy, therefore, fitting very well with the model's predictions. Isolated small scale distributed thrusts throughout the massif commonly display approximately NNE-SSW transport directions suggesting that they are related to this transpressive incremental strain, indeed, the Rocha Forte thrust has a late NNE oriented transport direction superimposed over a NE-SW structural grain possibly indicating that this transpressive strain locally post-dates NW-SE contraction, which formed as the direct result of the reorientation of the regional compressive stress during the Tortonian. The thrust relationships observed at Cruz da Salvé Rainha confirm that the NNE verging thrusts postdate thrusts with a NNW transport direction. Therefore, it appears that the model of a late-superimposed sinistral transpressional incremental strain is substantiated by the available field data. On a more detailed scale the localised strain distribution appears to respond directly to the local anisotropy: with local lineation switching occurring where the angle (A) approximates to the critical ASTP angle; dominant sinistral simple transpression occurring where angle (A) is slightly greater than 70.5° , corresponding to a decrease in the angle of strike along the Arieiro fault; and in areas with no obvious suitable planes of weakness, the structures form parallel to the regional incremental strain. Minor amounts of bedding plane reactivation occurs along the southern sub-vertical limb where synthetic splays from the Cercal fault exploit the anisotropy formed by the regional folding.

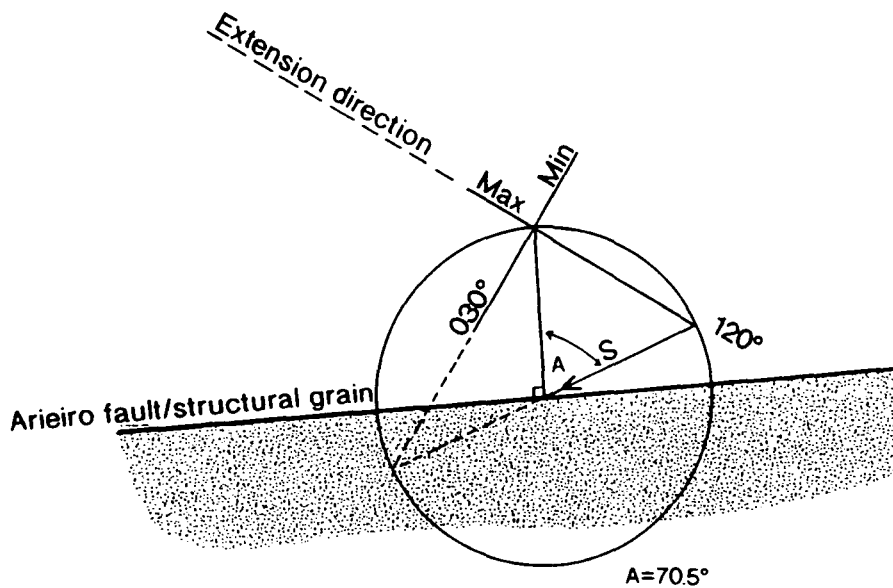


Figure 4.28 McCoss construction for the Main Arieiro fault. Angle $A = 70.5^\circ$ (ASTP), based on the presence of fault lineation switching. The construction predicts incremental extension and shortening directions of 120° , and 030° , respectively. See the above text for details.

The latest stage of deformation appears to be the formation of the thick extensional veins / faults (e.g. the Southern Splay fault). In general, these extensional structures are related to the transpressive incremental strain which has induced a minor amount of clockwise, oblique directed extension, relative to the structural axis of the Montejunto anticline. This important distinction between tectonic and gravity driven extension, suggests that extensional collapse of the uplifted structure has, so far, not occurred.

In summary, this late transpressive phase probably initiated the Rocha Forte thrust due to NW-SE directed compression. The transpressive nature of the once passive Cercal fault induced sinistral transpressive reactivation along the Arieiro fault system, which displays simple and complex transpressive kinematics. The superimposition of this transpressive strain also resulted in the reactivation of the northern thrust zone, producing NNE directed thrusting. No late reactivation was seen along the Serra de Montejunto thrust zone suggesting that it remained inactive, therefore, this late deformation stage has a strong asymmetric nature (figure 4.27/3 and 4.27/4).

The geometry of the Montejunto structure at depth (see chapter 5.3) has been interpreted to display several downward convergent contractional faults, that coalesce along a steep single fault zone (Hutton & Gawthorpe, T.S.G. 1988 unpub. abst.). This interpretation is reminiscent of the flower structures or 'palm-tree' structures observed in seismic section by Harding & Lowell, (1979); Bally, (1983); and Harding, (1985). Therefore, the Montejunto anticline displays a three dimensional geometry and tectonic deformation style consistent with it being a flower structure, formed within a major restraining bend (figure 4.29).

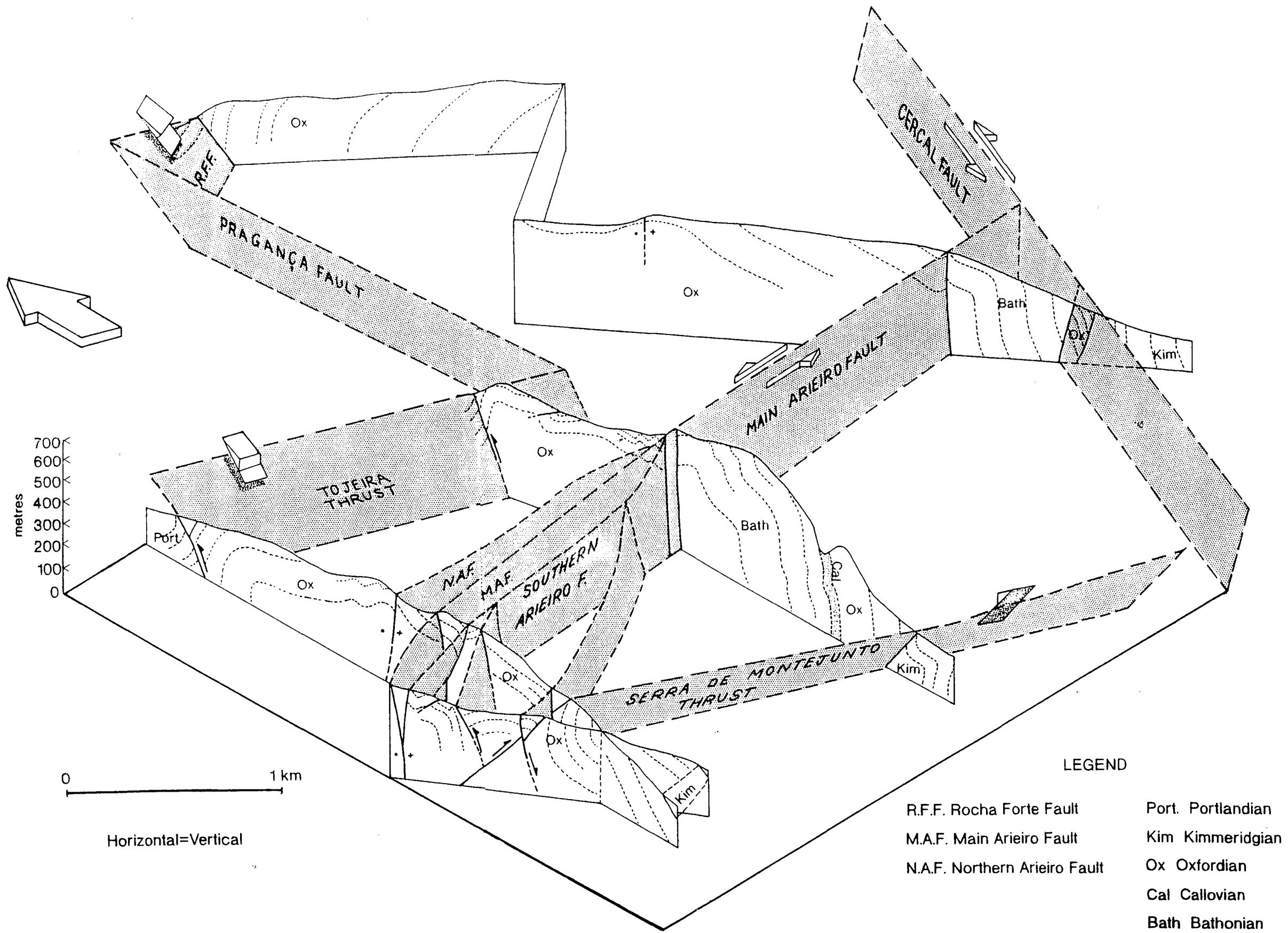


Figure 4.29 Three dimensional structural fence diagram of the Montejunto massif. Stippled planes represent extrapolated fault planes between structural sections.

CHAPTER 5

Neotectonics of the Lusitanian Basin

5.1 Introduction

A study of the neotectonic map of Portugal (Cabral and Ribeiro, 1988) reveals a dominance of NNE-SSW and NE-SW oriented neotectonic faults that are operative in a regional maximum compressive stress field oriented NNW-SSE across the Algarve region in the south, swinging to a NW-SE orientation across the Lusitanian Basin, and finally assuming a WNW-ESE orientation to the west of Portugal (figure 5.1). These neotectonic structures have been identified predominantly by geomorphology, airphotograph analysis, and detailed geological maps and mapping. Objective identification of neotectonic faults in the Lusitanian Basin is rare due to the limited knowledge of Quaternary geology, however, faults affecting Plio-Quaternary deposits have been described (Cabral et al., 1984; Cabral, 1989; and Dias & Cabral, 1989). The dominant mode of neotectonic activity is a regional uplift, which becomes greater toward the north of Portugal where total Quaternary uplift averages 400 to 500 metres (Cabral, 1989). The presence of both historical and instrumental seismicity within the Portuguese region reveals that tectonic activity is continuing, with both interplate and intraplate events measured (Fonseca and Long, 1989a, 1989b).

The link between seismicity and observable geological structures at the surface, has commonly not been attempted due to the absence of focal mechanism data, and uncertainty with regards to the exact epicentre location, this being especially true for onshore Portugal (Moriera, 1985). However, the seismotectonics of the southern Portuguese region was addressed in the Estremadura trough by the inception of the RESTE project 1987-88 (The Temporary Seismic Stations Network of Estremadura). The results of this work in the Lower Tagus Basin (Fonseca et al., 1988; and Fonseca & Long, 1989a, 1989b) will be summarised in the following chapter, with an additional interpretation offered for the Lusitanian Basin *sensu stricto*, based on a re-evaluation of published seismicity and geological constraints on the style of deformation derived from the S. dos Candeeiros fault system.

5.2 Neotectonic surface structures

Neotectonic structures with demonstrative Quaternary deformation are present within onshore Portugal. Unfortunately for this study, however, these structures are located in

the northeast of the country, within the Central Iberian Zone (see figure 5.1). Cabral (1989) demonstrates the sinistral Quaternary nature of the NNE oriented Manteigas-Bragança fault zone, with its associated pull-apart basins (e.g. the Vilarica Basin), and pressure ridges, that together represent a reactivated basement shear zone. Geomorphological features such as the apparent offset of the Douro river, combined with indirect geological evidence, suggest a 1km sinistral displacement during the Quaternary. Estimates of slip rate during this time vary between 0.2-0.5mm \cdot yr⁻¹, indicating moderate to moderately high degrees of fault activity (Slemmons, 1982). In addition to the geomorphological and geological expression of the Manteigas-Bragança fault zone, there is relatively important historical and instrumental seismicity, with shallow (3.1km) focal depth events recorded (INMG, 1983). The Ponsul fault (Dias and Cabral, 1989) presently forms a low angle, ENE striking, Quaternary aged thrust fault, whose segments range from 10 to 30km in length. The fault again represents a reactivated Hercynian basement sinistral strike-slip fault, however it presently displays distinct compressive episodes dated possibly from as early as the Upper Miocene. Computer aided reconstruction of the principal maximum compressive stress axes for striated fault sets located along the Ponsul thrust indicate a dominant sub-horizontal NW-SE orientation, which is consistent with both the kinematics of the structures described above, and the present predicted stress orientations operative across Portugal (Cabral and Ribeiro, 1988).

A study of the Neotectonic map of Portugal (ibid.) reveals several major neotectonic, and 'possibly' neotectonic, faults and structures within the Lusitanian Basin. The NNE oriented S. dos Candeeiros fault is indicated to be a neotectonic sinistral strike-slip fault, with the adjacent Alvados/Minde fault system also suggested to be neotectonic in nature, and possessing a dextral sense of motion. These interpretations agree with the most recent kinematic system described in chapter 3, indicating that the S. dos Candeeiros fault system has probably been active in its present tectonic style since the middle Late Miocene. The neotectonic nature of the Alvados fault is implied by the obvious geomorphological features associated with localised restraining bends along its length (see plate 3.3, p.93). The southeastern thrust zones, which bound the Candeeiros and Aire blocks, are marked as 'possible' neotectonic thrusts. This uncertainty possibly arises due to the disagreement between the observed thrust transport direction and the present day maximum compressive stress field, but as discussed in section 3.8, the intimate tectonic and structural relationship between the bounding faults of the Candeeiros and Aire blocks, and the main S. dos Candeeiros fault zone implies a contemporaneous, and hence, neotectonic nature for this thrust zone. At the southern end of the S. dos Candeeiros fault zone, Quaternary activity is proposed for the Cercal, Rocha Forte, Pragança, and Tojeira

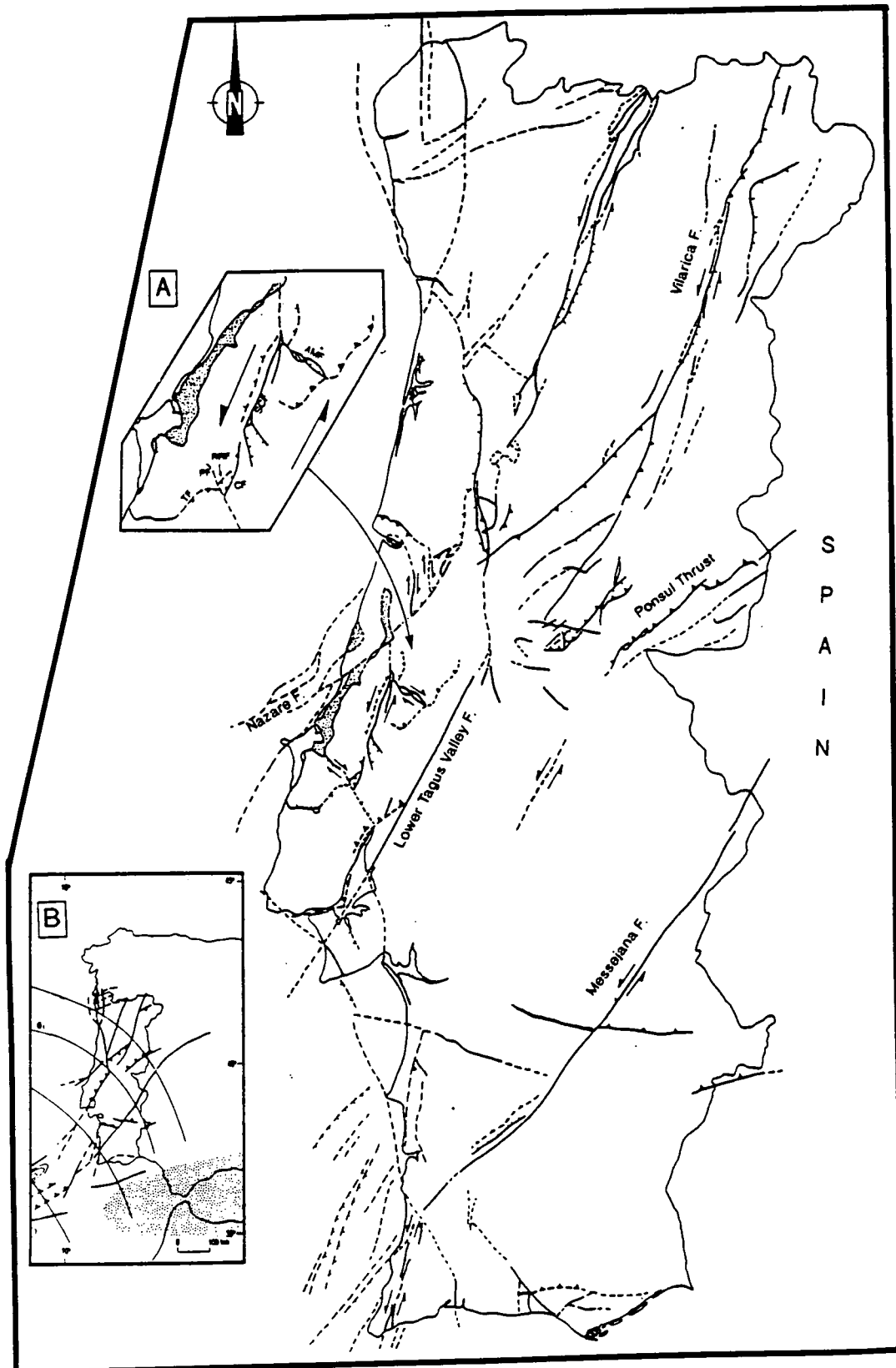


Figure 5.1 Neotectonic map of Portugal, displaying the main faults. *Solid line* - Certain neotectonic fault, *Dashed line* - Possible neotectonic fault. **Inset A:** Lusitanian Basin neotectonics, *AMF*, Alvados / Minde fault; *SCF*, S. dos Candeeiros fault; *RFF*, Rocha Forte fault; *CF*, Cercal fault; *PF*, Pragança fault; *TF*, Tojeira fault. **Inset B** Neotectonic stress field across Portugal. (Re-drafted from Cabral & Ribeiro, 1988).

faults. This is in agreement with the observations of chapter 4, where the aforementioned faults display the latest interrelated movements. However, these observed late stage movements disagree with some of the motions proposed by Cabral and Ribeiro (1988). The Cercal fault clearly displays sinistral strike-slip movement indicators, as opposed to the simple reverse slip of Cabral and Ribeiro (op. cit.), whereas the Pragança fault, shown as a dextral fault which is continuous across the Montejunto massif, is in fact a sinistral transfer fault between the northern thrust zones. No evidence was found in the southern limb of the massif for the existence of the Pragança fault, as implied (this thesis). South of Serra de Montejunto, neotectonic displacements are inferred to be relayed to the Vila Franca de Xira fault via a NNW-SSE trending fault. Cabral and Ribeiro (ibid.) suggest reverse slip motion for the NNE oriented Vila Franca fault, whereas Fonseca and Long (1989b) suggest a component of sinistral motion is present. Apart from the eastern boundary of the inverted zone the most significant onshore neotectonic structure is the Caldas de Rainha salt ridge, which is undergoing active diapirism. Figure 5.2 represents a modified neotectonic map of the central Lusitanian Basin, to include the kinematic information derived from this study.

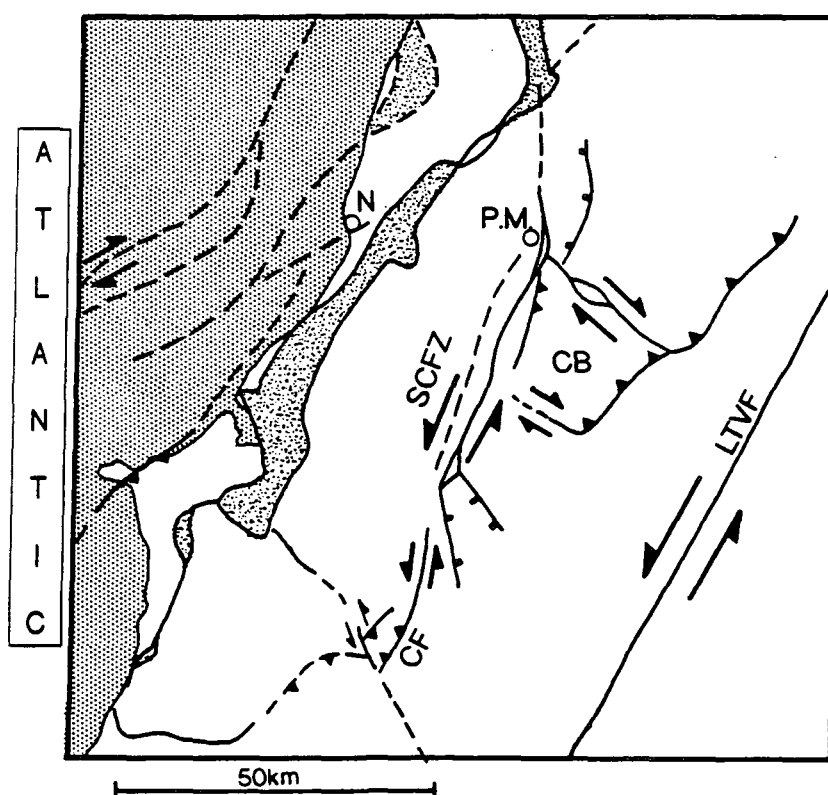


Figure 5.2 Modified neotectonic map of the Lusitanian Basin. Modifications based on observations of last movement indicators, and the interpretations of Fonseca & Long, (1989a,b). *CF*, Cercal fault; *SCFZ*, S. dos Candeeiros fault zone; *LTVF*, Lower Tagus Valley fault; *CB*, Candeeiros Block; *N*, Nazaré; *PM*, Porto de Mós. (Modified from Cabral & Ribeiro, 1988).

5.3 Geometry of Serra dos Candeeiros fault system at depth

The sub-surface structure and geometry of the inverted region of the Lusitanian Basin, and the S. dos Candeeiros fault system in particular, has been addressed by Hutton and Gawthorpe (1988), who interpreted selected seismic reflection profiles and well data supplied by the Gabinete de Exploração e Petróleo, Lisbon (GPEP). Three seismic reflection profiles oriented perpendicular to the structural grain of the basin, and crossing the main fault system, were interpreted (figures 5.3a-c).

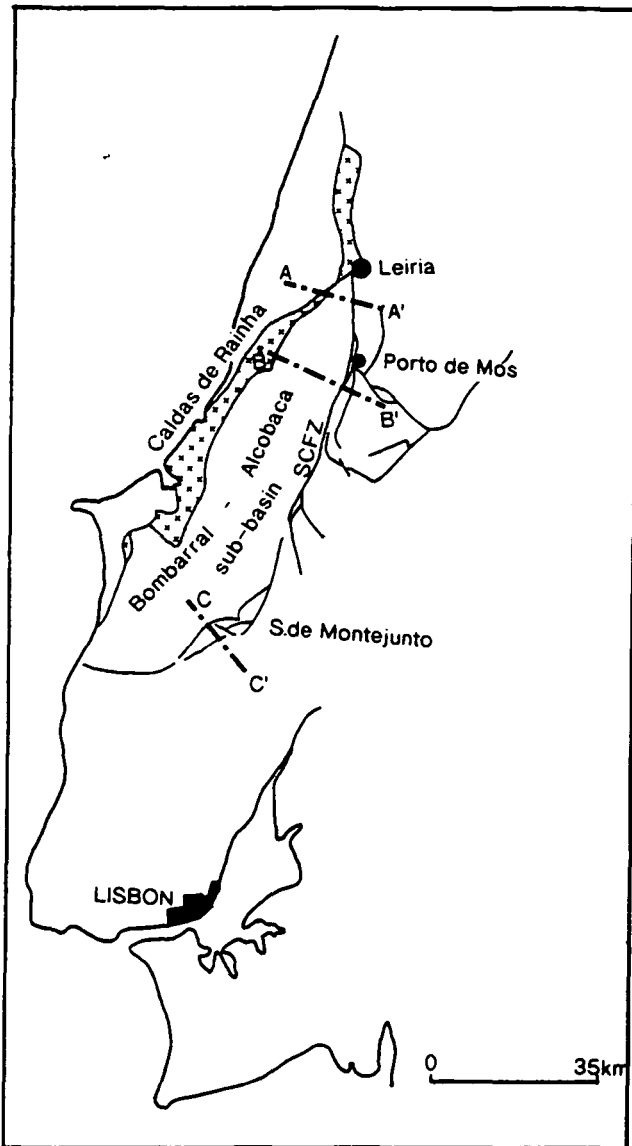


Figure 5.3 Location map of the seismic profiles shown in figures 5.4a-c. (Cross ornamentation indicates exposure of evaporites).

At the northern end of the fault system a WNW-ESE trending seismic line is located crossing the Caldas de Rainha salt ridge and the northern segment of the S. dos Candeeiros fault system (figure 5.4a). The interpretation identifies two sub-vertical zones, which due to their diffuse reflection characteristics, and upward

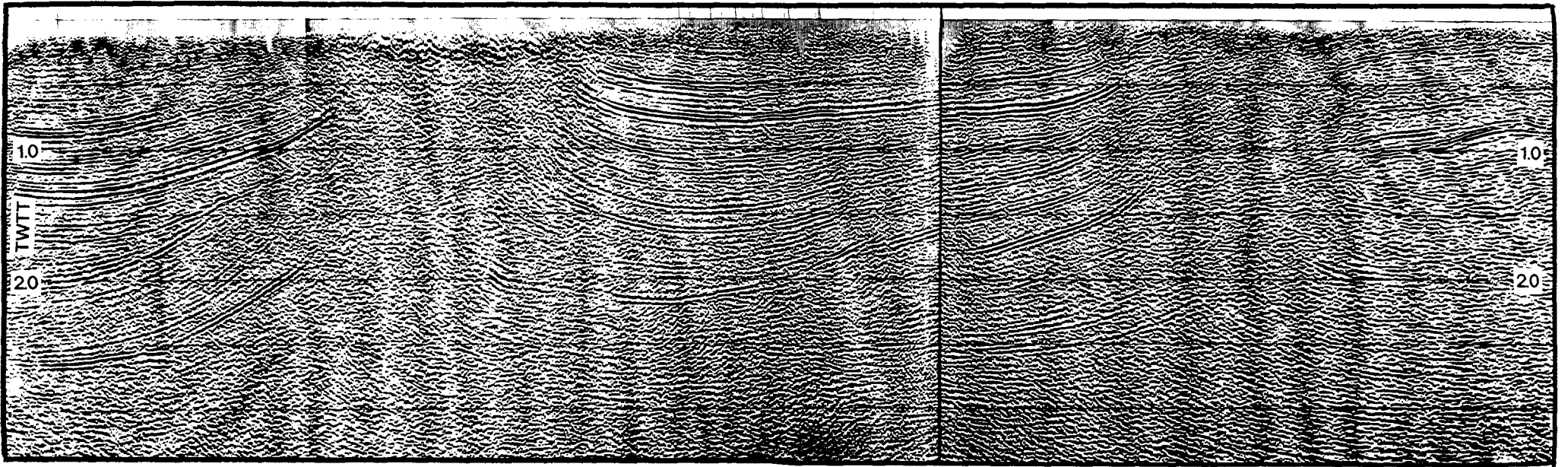
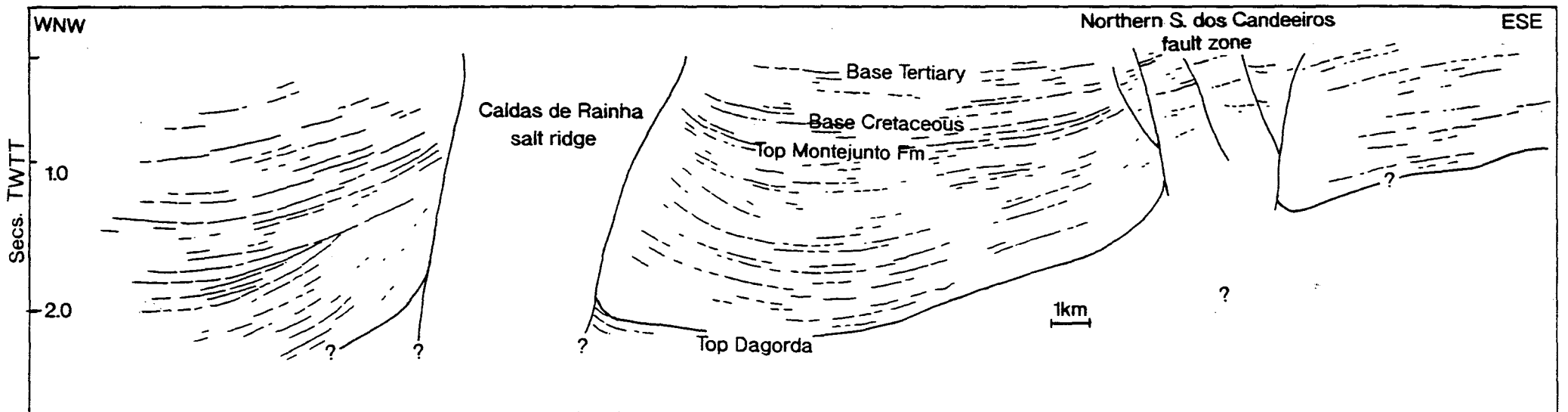


Figure 5.4a Seismic profile A - A'. See text for details.



deflection of the adjacent continuous reflection horizons, plus a surface correlation with exposures of evaporites, have been labelled diapiric salt ridges. These diapirs root in the Hettangian aged Dagorda evaporite formation, the top of which has been picked at 2secs (TWTT) depth, shallowing to approximately 1sec towards the east, in the direction of the S. dos Candeeiros fault, near Leiria. Within the Lusitanian Basin fill sequence there is an obvious truncation and thinning of reflection horizons (which correlate with the Upper Jurassic), towards the Caldas de Rainha salt ridge, suggesting Upper Jurassic aged halokinesis along this diapir. The reflection characteristics within the northern S. dos Candeeiros fault zone suggest the presence of significant amounts of evaporite. However, near surface offsets of reflection horizons have been picked suggesting the presence of discrete faults. Due to the poor imaging of structures beneath the Dagorda formation it is uncertain if the faults cut through the evaporites, and it is in fact suggested that the faults sole into the sub-horizontal evaporite horizon.

Further south, near the town of Porto de Mós, a similar structural style is apparent (figure 5.4b). Again the profile runs partly through the Caldas de Rainha salt ridge and across the S. dos Candeeiros fault zone. The top of the Dagorda formation has been picked at 1.5 secs (TWTT) in the centre of the Alcobaça-Bombarral sub-basin, and is seen to shallow toward the salt ridges of S. dos Candeeiros and Caldas de Rainha, where the onlapping relationship of the Upper Jurassic sequence again testifies to the syn-halokinetic nature of this sequence. The S. dos Candeeiros fault zone images as a steep, northwesterly dipping salt ridge, the bounding faults of which appear to shallow with depth, eventually running along the top of the Dagorda formation. Reflectors in the immediate hanging wall of this fault zone display a subtle change in dip direction from west to east, forming an apparent antiformal structure, which corresponds to a similar geometry mapped in the surface structure. The contact between both the S. dos Candeeiros, and Caldas de Rainha salt ridges, and the Lusitanian Basin sequence appears to coalesce at a steep structure within the Dagorda formation, interpreted by Hutton and Gawthorpe (*ibid.*) to a fault, possibly implying the presence of a basement structure.

The overall interpretation of the structure and geometry of figure 5.4b is very similar to the hypothetical cross section of this region constructed by Zbyszewski (1959), which together, suggest that the Alcobaça-Bombarral sub-basin may be behaving as a crustal flake (Oxburgh, 1972), or 'tile', detaching along a basin-wide evaporite decollement horizon.

Figure 5.4c is a seismic reflection profile across the Montejunto range, running NNW-SSE through the village of Vila Verde dos Francos. The anticlinal nature of the structure is immediately obvious from the unpicked section. However,

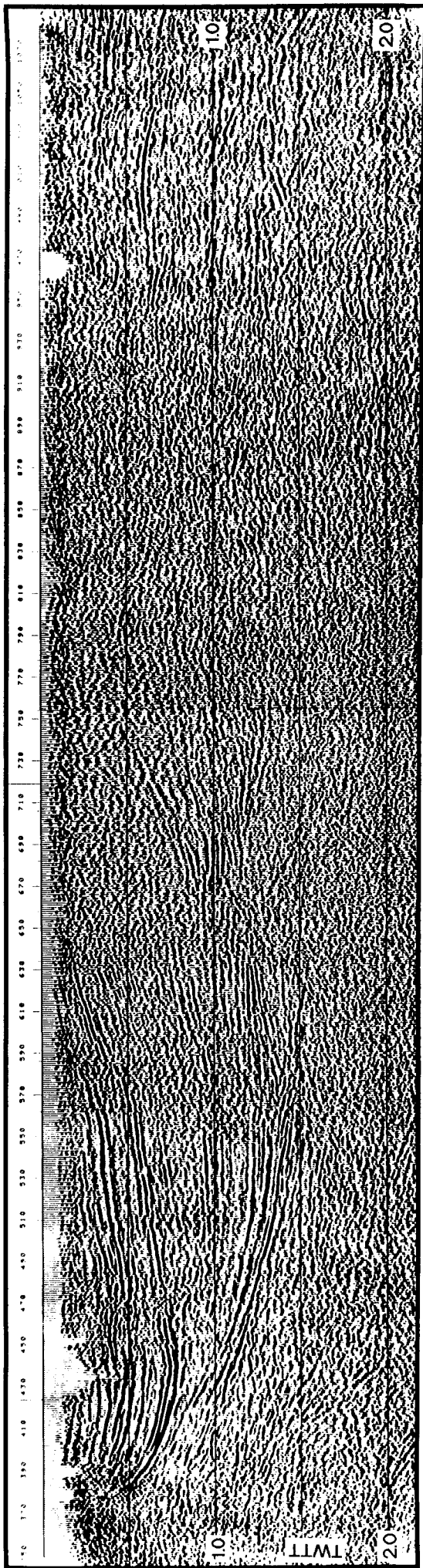
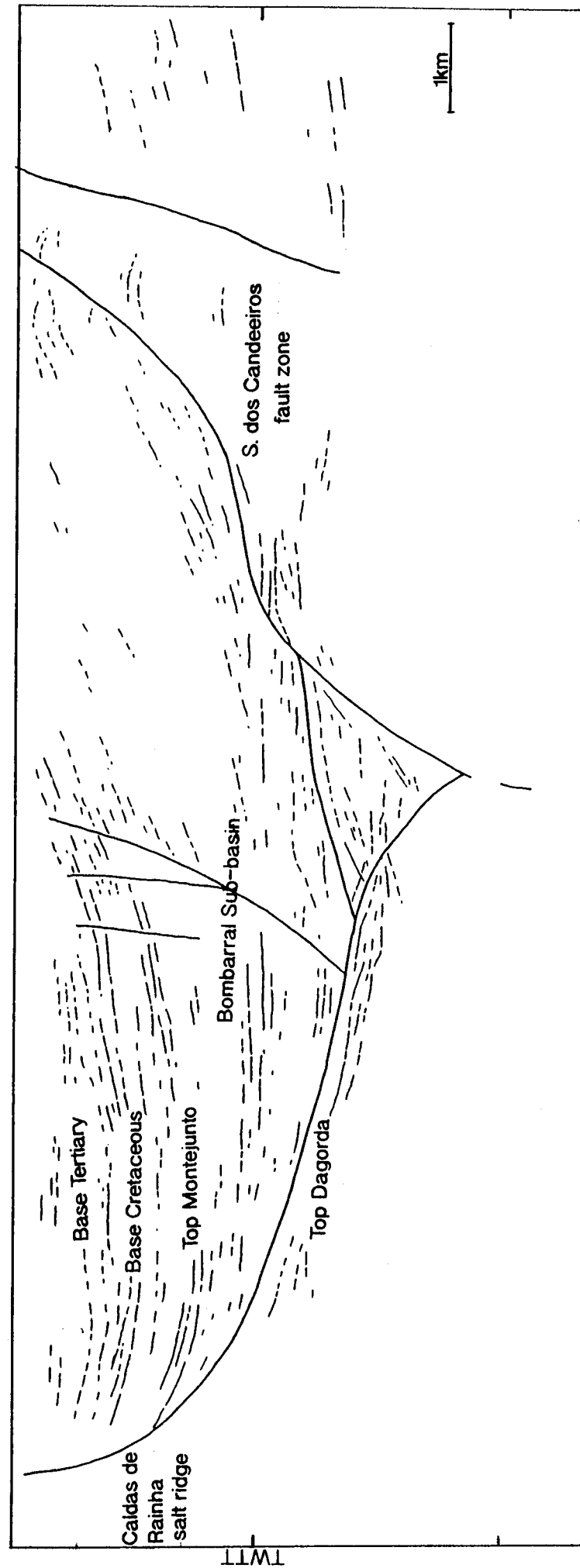


Figure 5.4b Seismic profile B - B'. See text for details.



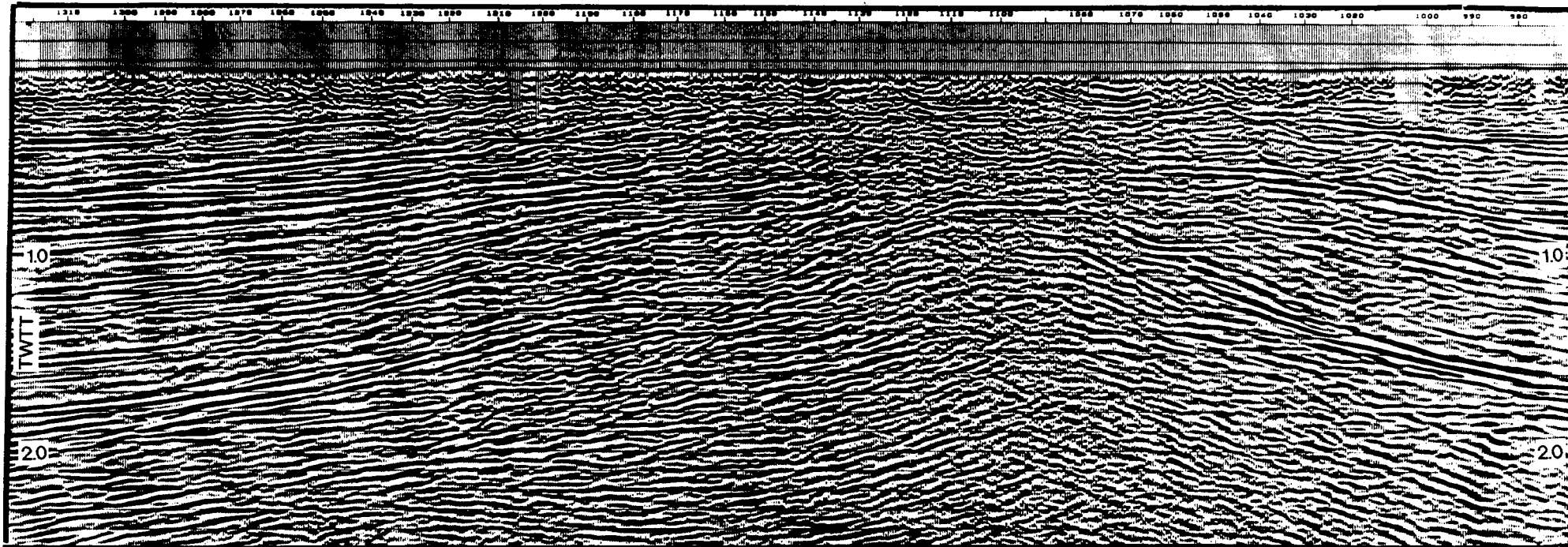
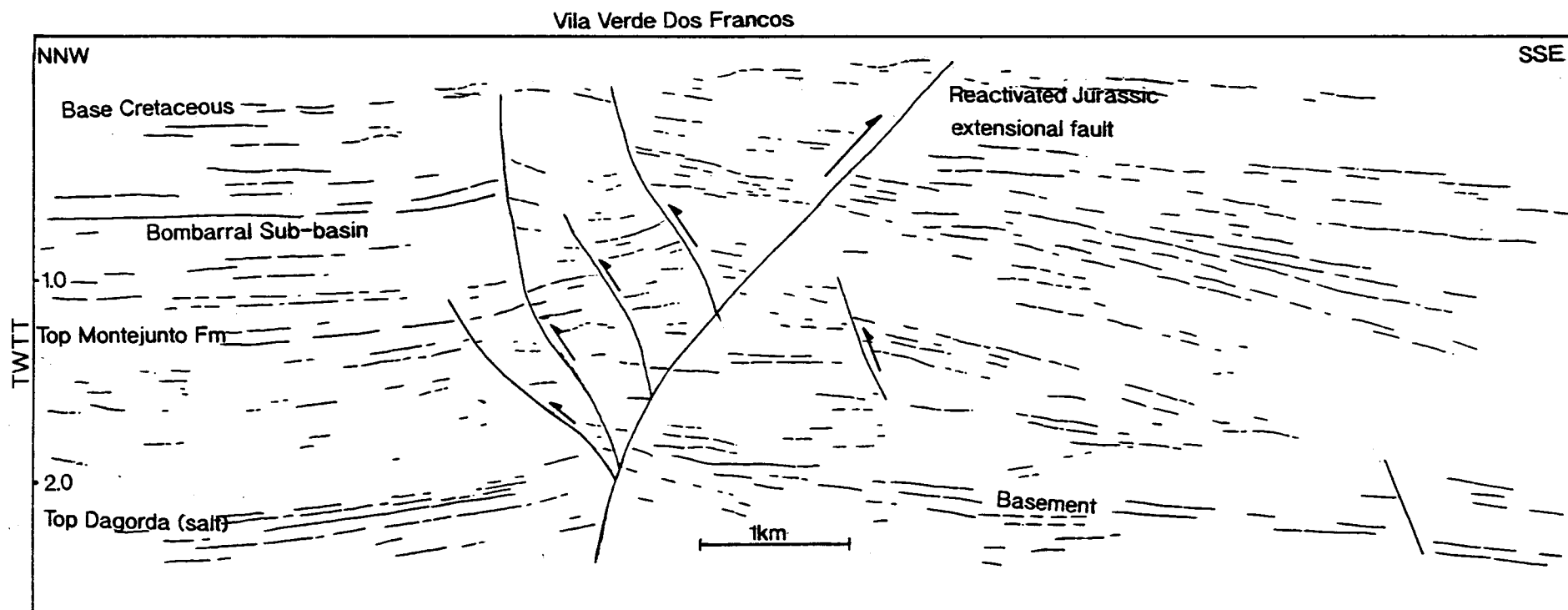


Figure 5.4c Seismic profile C - C' across the Montejunto massif. See text for details.



the structure is complicated by the presence of several SSE dipping faults that appear to splay off a major NW dipping fault which steepens at depth to the sub-vertical, where it is interpreted to offset the basement. The main fault possesses a net extensional throw at basement depths (2 secs/TWTT) even though the overall structure, as interpreted, is obviously a contractional structure. This implies that the structure represents the reactivation and modification of a cover to basement extensional fault, which is probably the Late Jurassic, Montejunto fault of Montenet et al., (1988). A thinning of the Late Jurassic sediments over the Montejunto structure suggests halokinetic movement and the formation of a salt pillow (Wilson, 1988). This early period of diapiric activity is evidenced in figure 5.4c by the top of the Montejunto formation which forms an on-lap surface for the following formations. The general structure of this seismic profile is reminiscent of the flower structures observed in seismic profile by Wilcox et al., (1973). The consistency of the Hutton and Gawthorpe (1988) geometric interpretation with Wilson (1988), plus the detailed strain and kinematic data presented in chapter 4, indicates that a transpressional flower structure satisfactorily explains the structure of the Montejunto range.

5.4 Intraplate seismicity within the Lusitanian and Lower Tagus Basins

The most compelling evidence for neotectonic activity in the Portuguese region is the presence of historical and instrumental seismicity, which has historically resulted in important damage and casualties. Some of the largest earthquakes to affect the Portuguese region were interplate shocks generated at the Gorringe Bank area, on the Azores-Gibraltar fracture zone, examples of which include the 1356, 1755 and 28Feb1969 ($M_L=7.3$) events. Instrumental seismicity from this region appears to occur predominantly within the 20 to 30km depth range (Moreira, 1985).

In addition to the interplate seismicity, there are also important intraplate events, such as the 1909 ($M_L=6.7$) shock which destroyed Benavente (40km northeast of Lisbon), plus a similar magnitude event ($M_L=7.0$) which occurred in the same area in 1531. Destructive events also affected Setúbal ($M_L=7.2$) 1858, the monasteries of Alcabaça 1528, and Batalha in 1716, and 1890 (Moreira, 1984). However, most of the instrumental intraplate earthquakes located on mainland Portugal have small to moderate magnitudes, with uncertainty surrounding their focal depths, and exact epicentre location (Cabral, 1989). The RESTE project was initiated in April 1987 to study intraplate seismicity associated with the lower Tagus river valley, and the Estremadura region. The survey obtained good focal mechanism and hypocentre locations for 10 relatively small earthquakes, between 1.1 and 3.8 (M_L), (Fonseca and Long, 1989b). The epicentre locations produced by this survey were relatively accurate

(within 2km), with calculated hypocentres varying between 8.2-23km, indicating that seismic activity extends through the entire upper crust.

The pattern of historical and instrumental intraplate seismicity within the Lusitanian and Estremadura Basins shows a relatively diffuse dispersion of earthquake epicentres along 3 main trends: A NE-SW trend following the boundary between the Lusitanian and Monte Real Basins, north of Leiria (the Nazaré, Seia-Lousã faults), which appears to extend to the Vilarica region in the northeast of Portugal; the second seismic lineament runs along a NNE orientation up the lower Tagus river valley from Setúbal, south of Lisbon; and the third seismic lineament forms a sub-parallel NNE trending zone, which appears to be associated with the eastern margin of the inverted Mesozoic zone, becoming very dispersed to the immediate north of Lisbon (figure 5.5a). A contoured diagram of the spatial intensity of earthquake epicentres reveals a dominance of activity along the third seismic lineament (figure 5.5b), which appears to converge with the Lower Tagus Valley Fault in the Lisbon region. Where the Nazaré, and Lower Tagus Valley faults intersect the continental shelf, pronounced submarine canyons of parallel trend are seen. This relationship is also seen in the south of Portugal where the seismically active Messejana fault can be traced off-shore by a well developed canyon. Focal mechanisms for this fault suggest reverse movement with a component of sinistral motion (Moreira, 1985).

5.4.1 The Nazaré - Vilarica lineament

The Vilarica (Cabral, 1989) and the Seia-Lousã (Moreira, 1985) faults display Quaternary aged sinistral motion, and are believed to connect to the Nazaré fault which displays dominantly Neogene movement, and is aligned along the off-shore submarine canyon. Epicentre locations along this trend indicate the fault is still active, with a dextral strike-slip sense of motion inferred from the focal mechanism solution for the 26Dec1962 earthquake. However, as mentioned the Vilarica and Seia-Lousã faults are presently sinistral, therefore, suggesting that the seismotectonics of the Nazaré-Vilarica lineament are segmented, with dextral motion occurring west of the boundary fault between the Central Iberian zone and the Ossa-Morena zone, and sinistral dominated displacement to the east. This difference in slip sense appears to be a direct result of the change in orientation of the regional compressive stress between off-shore, and northeast Portugal, as intimated by Moreira (1985).

5.4.2 The Lower Tagus Valley lineament

The Lower Tagus Valley fault is the most significant seismically active fault in central Portugal, as it has been responsible for several important earthquakes such as

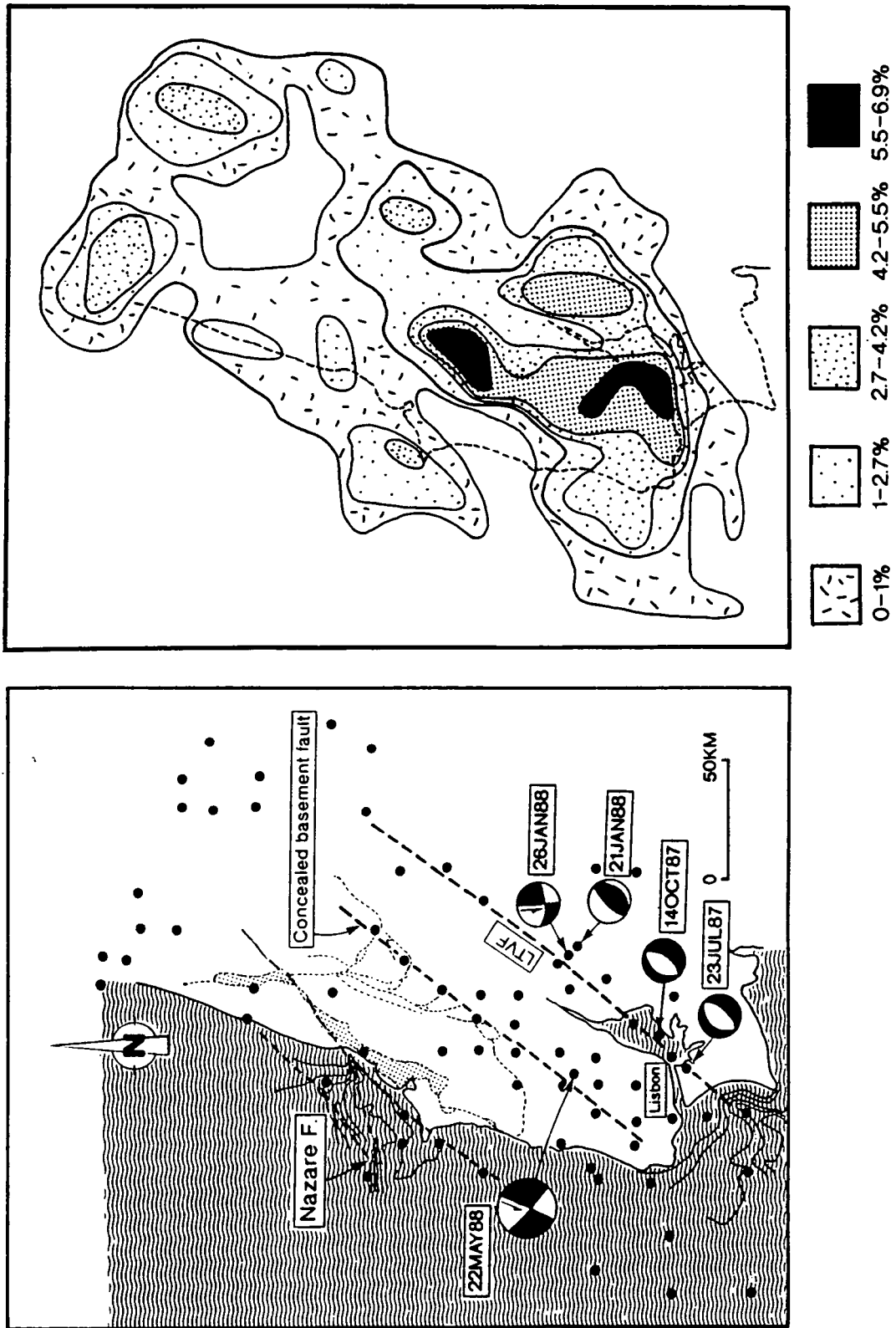


Figure 5.5 a) Map of western Portugal displaying epicentre locations for instrumental seismicity. Data derived from Moreira (1985) and Fonseca & Long, (1989a). Bathymetric contours for the Nazaré, and Lisbon submarine canyons, contour interval 50m. LTVF, Lower Tagus Valley fault. Thin dashed lines represent major surfaces faults within the Lusitanian Basin. b) Contoured map of earthquake epicentres for the Lusitanian, and Estremadura Basins.

the 1531 and 1909 events (intensity IX, Moreira, 1979). The linear dispersal of epicentres associated with this fault zone define a NE to NNE trending array, for which no geological surface evidence is present. However, the proposed trend of the fault is along strike from the Cascais or Lisbon submarine valley, located immediately off-shore Cape Espiche (see figure 5.5). The association between the above facts has been proposed by Arthaud and Matte (1975) to represent a concealed basement fault. Detailed seismological data produced by the RESTE project (Fonseca and Long, 1989a; 1989b) provides the first direct evidence for the existence of a NE-SW fault along the Lower Tagus Valley lineament. These observations are further collaborated by the identification, on seismic reflection profile, of a NNE-SSW strike-slip / transpressional fault along strike from the Lisbon submarine canyon, which displays dominantly middle to late Miocene motion with evidence of later reactivation (Mauffret et al., 1989).

The RESTE data for the Lower Tagus Valley reveals a complex arrangement of focal mechanisms, with reversals in the polarity of the vertical movements along the strike of the fault, plus one event, that of 26Jan1988, for which a strike-slip focal mechanism was derived. Fonseca and Long (1989a, b) have interpreted these events to belong to a single strike-slip fault zone trending NE-SW. The 26Jan1988, and the 22May1988 ($M_L=3.8$) events, the latter located to the west of the Vila Franca fault, have NNE-SSW oriented nodal planes which have been interpreted to represent sinistral strike-slip. These events, together with hypocentres depths varying between 8.2 and 23km, suggest that the Lower Tagus Valley Fault is a concealed, sinistral, basement strike-slip fault (ibid.).

Fonseca and Long (1989b) speculate that the surface faults of the Lower Tagus Valley, namely, the Vila Franca, Alcochete, and Arrábida faults, represent the surface expression of this basement fault which cuts up into the Hettangian evaporite horizon, which lies along the basement / cover interface and acts as a sub-horizontal decollément surface. The displacement associated with the basement fault explores the decollément horizon becoming laterally transferred to pre-existing cover faults, in this case, the Vila Franca-Arrábida fault system (Fonseca, 1989).

5.4.3 Seismicity associated with the Lusitanian Basin

The distribution of earthquake epicentres associated with the outcrop of inverted Mesozoic Lusitanian Basin sediments is rather diffuse especially within the immediate north and northwest of Lisbon. However, a general NNE to NE trend to the epicentre locations is present, especially above a line 39° north of the equator (see figure 5.5). This NE-SW trend becomes more obvious when the 22May1988 focal mechanism (Fonseca and Long, 1989a) is included in the data set. The focal mechanism solution

presents two sub-vertical nodal planes, a NW-SE oriented dextral plane, and a NNE-SSW oriented sinistral plane. The latter solution lies sub-parallel to the inferred Lower Tagus Valley fault, and along an obvious alignment of epicentres, therefore the sinistral interpretation of this event is more consistent with the lineaments identified both onshore and off-shore, as well as the general structural grain of the basin. Fonseca and Long (1989b) suggest this event may represent a concealed basement strike-slip fault parallel to the Lower Tagus lineament, as no surface expression of the fault is present. In addition to this interpretation, Curtis (1991) proposed that the general linear distribution of epicentres represents the trend of a significant basement fault, of which the 22May1988 event is part. The trend of this proposed basement fault does not coincide with surface structures within the Lusitanian Basin. However, it does roughly coincide with the general trend of the eastern limit of Miocene to Recent inversion within the basin. It is therefore suggested that motion is transferred laterally between the basement and cover sequences by the exploitation of the Hettangian evaporites as a decollement surface, linking sinistral basement deformation with sinistral displacement along the S. dos Candeeiros fault system (*ibid.*), (see discussion in chapter 6). Unlike the Lower Tagus Valley, Messejana, and Nazaré faults, no submarine canyon or similar topographic expression exists on the continental margin along strike from this proposed basement fault, implying that it does not extend off-shore and that it may link with the Lower Tagus Valley fault within the Lisbon region. This may possibly account for the diffuse seismic activity in this region.

Additional seismicity, recorded on the west coast of the Lusitanian Basin, is possibly a manifestation of active diapirism occurring along the Caldas de Rainha salt ridge.

5.5 Summary: Neotectonics of the Lusitanian Basin

The Portuguese mainland and continental margin is undergoing important neotectonic activity, as testified by intraplate seismicity and Quaternary deformation. Both the observed surface deformation, and the instrumental seismicity appear to be driven by a predominantly NW-SE oriented regional compressive stress (Cabral and Ribeiro, 1988).

Surface faulting

The Lusitanian Basin, and mainland Portugal in general, is dominated by NNE-SSW sinistral strike-slip faults, and to a lesser extent by NE-SW to ENE-WSW compressional and transpressional structures. The preponderance of sinistral strike-slip structures suggests that the western margin of Portugal represents a region of distributed simple/transpressional shear. The compressive structures generally

represent restraining bends along, or compressive terminations to, the sinistral faults. Estimates for slip rates along the NNE trending Vilarica fault vary between 0.2-0.5 mm^{-yr}, fitting well with the observed levels of seismicity (Cabral, 1989).

Seismic reflection profiles across the S. dos Candeeiros fault system suggest that the faulting observed along the Candeeiros salt ridge detaches along the Dagorda evaporites, which act as a regional decollément horizon. This implies that the Mesozoic sedimentary sequence of the Lusitanian Basin may be behaving as a number of thin (between 2-1.5 secs. TWTT), fault bounded tectonic flakes or tiles, separated from the basement by the Dagorda evaporite sequence.

Instrumental seismicity

Epicentre distributions, hypocentre depths, and focal mechanisms for the Estremadura and Tagus Basin region, suggest that a concealed sinistral basement strike-slip fault, trending NE or NNE, runs beneath the lower Tagus river valley (Fonseca & Long, 1988a,b). This interpretation is justified by the Mauffret et al., (1989) who observed the off-shore extension of this fault, and interpreted it as a strike-slip fault. The lack of surficial evidence for this fault within the Tagus valley suggests that its displacement must become detached along a decollément horizon and transferred laterally before reaching the surface, possible via the Vila Franca-Arrábida fault system. Again the obvious candidate for the decollément is the Dagorda evaporite sequence, as suggested by Fonseca and Long (1988b).

A second parallel, albeit less well defined, linear distribution of epicentres is associated with the eastern margin of the Lusitanian Basin. The focal mechanism interpretation of the 22May88 earthquake, located along this linear trend, indicates sinistral strike-slip motion along a sub-vertical fault plane. It is suggested that this linear array of earthquake epicentres represents a sinistral strike-slip basement fault. The location and trend of surface faults are non-coincident with the proposed basement fault, again suggesting the possibility of displacement decoupling between the basement and cover faults.

Neotectonic style

Both basement and surficial faults appear to be dominated by sinistral strike-slip deformation, indicating that the active deformation of the Lusitanian Basin is probably basement driven. However, the disparity in the spatial distribution of the basement and cover faults suggests that displacement decoupling is occurring, possibly along the Dagorda evaporite horizon, resulting in a lateral transfer of strike-slip motion between the basement and cover.

The relationship of the neotectonics of the Lusitanian Basin, to the evolution of basin tectonics during the entire Alpine deformation event, will be discussed in the following chapter.

CHAPTER 6

The Serra de Montejunto-Candeeiros fault system: Its evolution and implications

"The view is often expressed by geophysicists that the structures in the continental crust are so complex that they cannot be used to determine plate motions....Our aim is to show that, contrary to the pessimistic view of geophysicists, structures in rocks,can give a clear indication of plate motions."

(Shackleton and Ries, 1984)

6.1 Serra de Montejunto-Candeeiros fault system

The S. de Montejunto-Candeeiros fault system consists of two structurally complex regions, the Candeeiros fault block (east of Porto de Mós), and the Montejunto massif (northeast of Torres Vedras), which are linked by the north-northeast oriented Serra dos Candeeiros, and Cercal faults. As discussed in chapters 3 and 4, the S. de Montejunto-Candeeiros fault system displays virtually the full range of structures associated with strike-slip dominated systems: sub-horizontal slickenlines along the master faults, asymmetric development of en-echelon secondary faults, en-echelon folding, pull-apart basins, pressure ridges, rapid reversals of slip sense on faults, localised regions in compression and extension, block rotations, and flower structures.

The quality of exposure and the detailed preservation of superimposed strains found along the S. de Montejunto-Candeeiros fault system, provide an unique opportunity to examine the detailed structural and kinematic evolution of a strike-slip fault system, and its response to a changing regional stress system.

6.1.1 Fault system evolution

The fault system displays distinctly different tectonic styles at its northern and southern ends (chapter 3 and 4, respectively). However, the tectonics of both these regions display two distinct stages in their structural and kinematic evolution; firstly, an initial phase of deformation associated with N-S compression, and secondly, a late period of NNW-SSE/NW-SE oriented regional compression. As described in chapters 3 and 4, this seemingly minor change in the regional compressive stress system had a profound influence on the deformation style.

6.1.1.1 Middle Miocene initialisation of the fault system

The basic geometries of the Serra dos Candeeiros fault, the Candeeiros fault block, and the Montejunto massif were inherited from the North Atlantic extensional tectonics which dominated western Iberia from the earliest Jurassic to Early Cretaceous times. During the Middle Miocene, N-S directed compression affected the Lusitanian Basin, the chronology of which is constrained stratigraphically in the Arrábida region (Choffat, 1908). As demonstrated by the Formosinho anticline, thrusting began during the late Burdigalian (~16Ma). This southerly vergent deformation front is believed to have migrated northwards (Ribeiro et al., 1990), and therefore, the age of thrust initiation within the S. de Montejunto-Candeeiros fault system may be slightly later than 16Ma. This deformation event can be correlated in the Montejunto region with early southward directed thrusting along the Serra de Montejunto thrust, contemporaneous with the large scale folding of the Montejunto massif about an east-west axis. This north-south oriented shortening was accommodated by the Cercal fault (believed to be the southern manifestation of the Serra dos Candeeiros fault), which acted as a sinistral lateral ramp or transfer fault. In the north of the fault system, reduced shear resistance along the Serra dos Candeeiros fault zone, caused by the presence of a salt ridge, suggests that this segment of the S. dos Candeeiros-Cercal master fault was also reactivated as an accommodation structure to east-west striking contractional structures. Late Jurassic age NW-SE trending extensional faults, located to the east of the S. dos Candeeiros fault (the Alvados, and Minde faults), display an initial sinistral strike-slip reactivation, with associated pull-apart basin formation (the Alvados pull-apart), suggesting that the pair of faults behaved as synthetic splay faults to the main S. dos Candeeiros fault.

Continued deformation about this north-south compression direction probably led to the dissection of the Montejunto anticline by fold axis parallel, reverse faults (the Arieiro fault system). In the Candeeiros region, continued north-south shortening resulted in the initiation of thrusting along the southeastern boundary of what is today the Candeeiros fault block. The detailed strain history within the hanging wall of the Amiais de Baixo thrust sheet suggests that this thrusting was southerly vergent (see figure 6.1a)

6.1.1.2 Late transpressional structures

The change from simple, southerly directed thrusting, and associated NNE oriented transfer faults, to more complex fault systems dominated by transpressional structures varies between the study areas. In the northern Candeeiros region, the change in

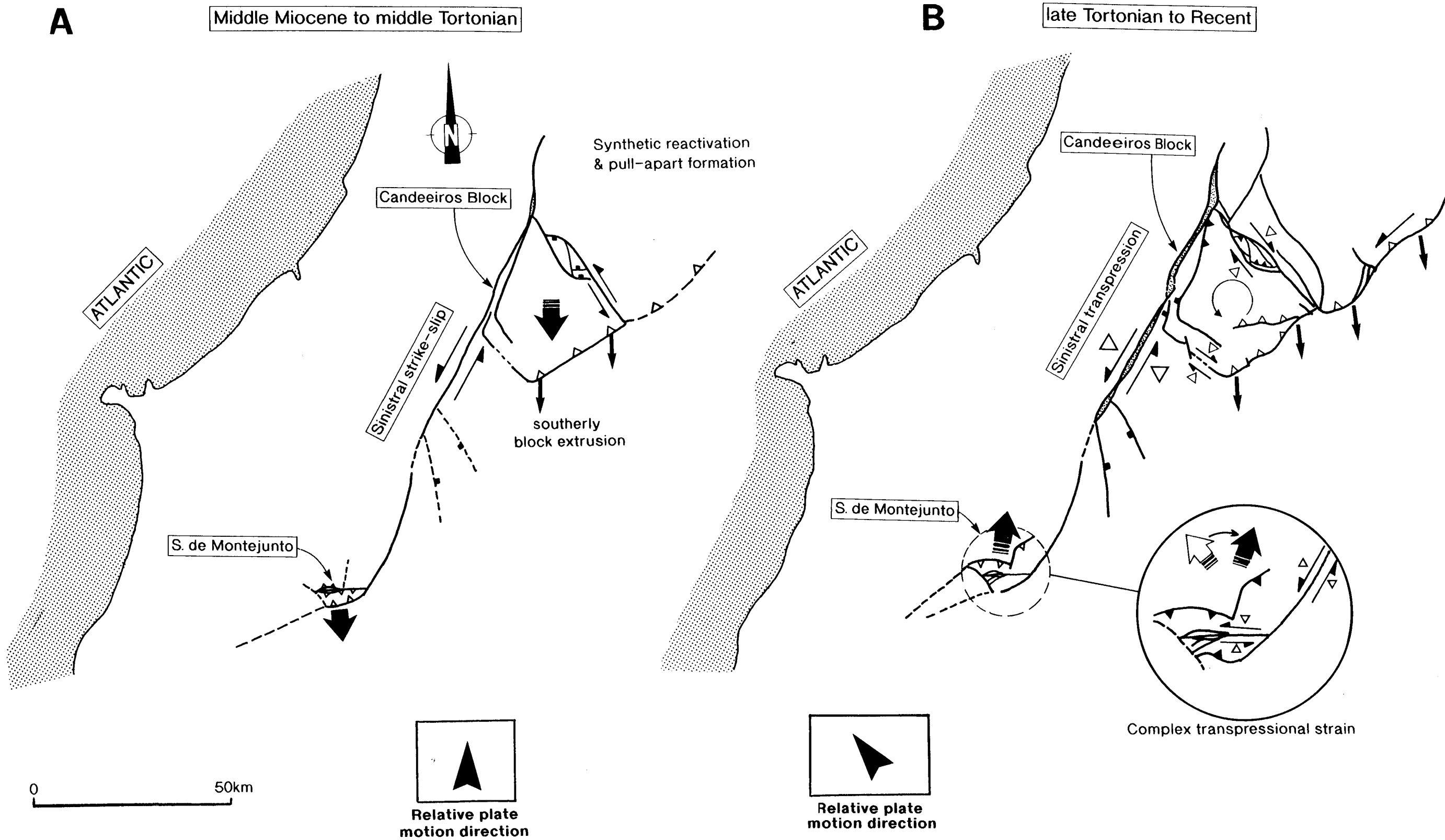


Figure 6.1 Schematic diagram illustrating the structural and kinematic evolution of the Serra de Montejunto - Candeeiros fault system a) Initial reactivation of the fault system in the Middle Miocene, b) Late Tortonian to Recent.

tectonic style appears to be quite abrupt, with the initiation of anti-clockwise rotation of the Candeeiros block presumably coeval with sinistral transpressional strains along the S. dos Candeeiros fault zone. The anti-clockwise rotation was superimposed upon continued southerly extrusion of the block, as evidenced by the rotation and overprinting of early compressional structures by late southerly verging thrusts and associated structures. Rotation of the block resulted in a reversal of slip sense along the block bounding cross faults, (namely the Alvados/Minde fault system, and the Alcanede fault zone), therefore inverting the Alvados pull-apart basin to produce a pressure ridge. These dextral cross faults also display a component of transpression. The geometry and kinematic style of the master fault, and the faults accommodating the rotation, fit well with the predictions of McKenzie and Jackson's (1986) pinned block model. This model suggests that non-plane strain is required to induce block rotations, hence for a transpression dominated system, the angle between the relative movement vector, or the regional compressive stress and the fault walls, must be greater than 45° . Therefore, the transformation to a block rotation appears to be the product of a change in the regional stress system relative to the S. dos Candeeiros fault, i.e. an effective rotation of stress from its Middle Miocene north-south trend to a northwest-southeast orientation (figure 6.1b).

In contrast to the sudden change in tectonic style in the Candeeiros region, the Montejunto massif displays a gradational change from a simple fold thrust system to a transpression dominated structure. This progressive transformation in tectonic style was achieved via a switch in the location of thrusting from the southern to northern side of the massif. These northern thrusts are distinct in that they possess a NE-SW structural grain and a NNW direction of thrust transport. Shortening directions across the massif, derived from conjugate tension gash arrays, commonly display a similar shortening direction (i.e. NNW-SSE) suggesting both sets of structures are related to a regional stress of like orientation.

The NNW verging thrusts are reactivated and offset by a later set of NNE verging thrusts. Contemporaneous with this final change in the direction of thrust transport, is the sinistral transpressive reactivation of the Arieiro fault system. Modelling of this transpressive strain indicates that it is responsible for the late NNE directed thrusting along the northern margin (see figure 6.1b). The introduction of sinistral transpression to the Montejunto massif occurred when the Cercal/S.dos Candeeiros fault changed from its initial role as a passive accommodation structure to the fold and thrust system of the Montejunto massif, to an active transpressive fault that exerted a controlling influence upon the latter deformation events within the adjacent massif. This interpretation of the increasing importance of sinistral transpression is consistent with the observed early deformation sequence, which

displays a transition of the shortening direction across the Montejunto massif from N-S toward NW-SE; the orientation of a compressive stress necessary to induce sinistral transpression along the NNE Serra dos Candeeiros-Cercal fault.

Clearly, as discussed in the conclusions of chapters 3 and 4, and in the brief synopsis of the fault system evolution above, both the Candeeiros and Montejunto regions display a structural and kinematic history consistent with progressive deformation occurring within a crustal shortening regime which rotated from a north-south to a northwest-southeast orientation. The fact that the tectonic interpretations of two distinctly different fault systems, separated by up to 45km, independently predict the same deformation system, suggests that the directions of tectonic shortening resolved from this study are likely to be representative of regional tectonic events (this chapter).

6.1.2 Estimates for the Miocene to Recent displacement along the S. dos Candeeiros-Cercal fault zone

Estimates for the amount of sinistral displacement along the S. dos Candeeiros-Cercal fault zone, are hampered by a lack of identifiable structures that cut across the fault zone. However, at Porto de Mós, the S. dos Candeeiros fault changes orientation, forming a releasing bend (Serviços Geológicos De Portugal, 1:50,000 map). Associated with this releasing bend is a rhomb-shaped exposure of Dagorda evaporites, contained between the fault walls. The known kinematics of the fault system suggests that this rhomb-shaped structure may be a simple pull-apart basin, filled by the halokinetic migration of salt from the Candeeiros salt ridge found along the strike of the fault.

An attempt to restore this fault bend, suggests that the fault walls were probably never an exact fit, possibly due to localised salt diapirism. However, restorations of the fault bend allowing for slight to moderate amounts of fault wall overlap, indicate sinistral displacements of 1.25 to 2.5 km (figure 6.2). The irregular nature of the eastern fault wall results in localised overlap in the restoration. This irregularity of the fault walls maybe the result of post-salt ridge deformation. A test of the validity of this estimate is the Vilarica fault in northeast Portugal. This north-northeast oriented, sinistral, neotectonic fault has calculated slip rates for the Quaternary, of 0.2 to 0.5mm^{-yr}. By extrapolating these slip rates to the known duration of sinistral motion along the S. dos Candeeiros fault, i.e. Middle Miocene to Recent (15Myrs), predicted displacements of 3 to 7.5 km can be derived.

Such comparisons between the strain rate of different fault systems is admittedly crude. However, the lower range of the slip rates derived from the Vilarica fault (0.2mm^{-yr}), presents a comparable figure to the displacement estimates for the

Serra dos Candeeiros-Cercal fault zone, suggesting that these estimates represent realistic figures.

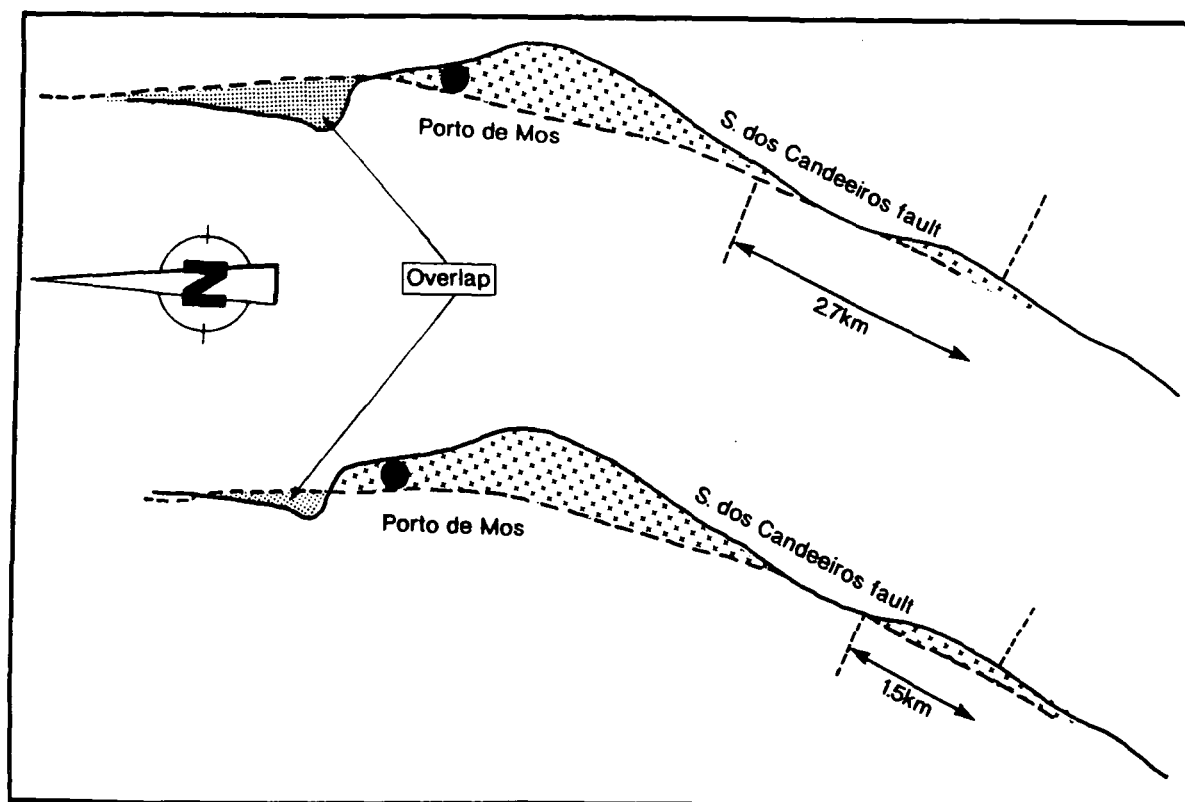


Figure 6.2 Restoration of the releasing bend at Porto de Mós with varying degrees of fault wall overlap.

6.2 Relationship between fault system kinematics and the relative plate motions of Africa-Europe

Since the advent of plate tectonics the aim of many structural and tectonic studies has been to directly relate geological observations to plate motion vectors. This has mainly been attempted by regarding destructive plate boundaries as crustal scale shear zones whose geometry involves extension in or close to the direction of shear, producing mineral stretching lineations (Ramsay and Graham, 1970). When these stretching lineations are regionally consistent, and occur in zones of high strain, they have been equated with the direction of plate motion (Shackleton and Ries, 1984). Such a relationship appears to hold for regions of 'head-on' collision, after allowing for, and removing the affects of later deformation, as demonstrated for the Himalaya-southern Tibet suture (*ibid.*). However, a cautionary note should be sounded for regions of transpressive or oblique convergence, where increasing finite strain can result in temporal strain partitioning, and a switch in the stretching lineation from transverse to boundary parallel (Harland, 1971; Sanderson & Marchini, 1984; and McCoss, 1986).

In such partitioned deformation regimes direct correlation between the stretching lineation and plate motion could lead to erroneous and complex variations in the reconstructed plate motions.

In cases such as the Himalaya-southern Tibet region (Shackleton and Ries, 1984), and that of the Dent Blanche nappe of southwest Switzerland (Baird and Dewey, 1986), the validity of such a plate motion/stretching lineation relationships have been tested by comparisons with plate motion histories determined independently from finite difference magnetic anomaly fitting in adjacent oceans. In both instances the relationship appears to fit well with actual plate motions derived independently. However, such attempts to relate various macro and micro-stress indicators to plate motions, are heavily dependent on which plate vector model they are tied to (Dewey et al., 1986).

Intraplate deformation zones do not possess crustal scale shear zones displaying large displacements, and vital mineral stretching lineation data. However, this need not prevent the accurate identification of relative plate motions, although it does require a different approach. In zones of complex upper crustal deformation, such as strike-slip and transpression zones, localised strains can, and do, overprint and obscure regional strains. In the Candeeiros and Montejunto regions of the Lusitanian Basin, thrust directions are commonly determined by a complex interaction of the adjacent fault system, and the applied external stress (e.g. late NNE directed motion along the Tojeira, and Rocha Forte thrusts, in the Montejunto region, and the southerly vergent Amiais de Baixo thrust along the edge of the rotating Candeeiros block, see sections 4.5 and 3.8 respectively). Therefore, these thrust directions cannot be considered in isolation when reconstructing relative plate motions. However, where neotectonic thrust faults are found as single entities, (e.g. the Ponsul fault) the NW-SE slip direction (Dias and Cabral, 1989) equates to the relative plate motion vectors of Africa-Europe during the last 9Ma (Smith, 1971; Livermore & Smith, 1986; and Dewey et al., 1989).

As mentioned above (section 6.1), structural and kinematic analysis of the fault system as a whole, reveals two tectonically distinct regions of distributed deformation. In both cases, the structural and kinematic evolution is consistent with their development in a deformation field, within which the axis of maximum shortening rotates from a north-south, to a northwest-southeast orientation. The identification of a progressively changing axis of maximum shortening, common to two tectonically different areas, over a distance of approximately 50km, indicates that these changes in the orientation are occurring on a regional scale, and are probably due to changes in the relative plate motion vector of Africa with respect to Europe.

To test if the reconstructed regional shortening axis, and Africa-Europe plate motions coincide, an age constraint must be placed on the deformation occurring along the Serra de Montejunto-Candeeiros fault system. As mentioned in the beginning of this chapter, north-south directed thrusting initiated in the Arrábida region during the Middle Miocene, indicating that deformation related to north-south compression within the S. de Montejunto-Candeeiros fault system is likely to be coeval with this event. However, the onset of transpressive motion within the S. de Montejunto-Candeeiros fault system, cannot be relatively dated with similar confidence. Indirect evidence exists for this event in the stratigraphy of the Lower Tagus Basin Miocene sequence near Lisbon, where a depositional hiatus occurs during late Tortonian and Messinian times (Ribeiro et al., 1979). This may place an age constraint on the inversion event which occurred possibly as a direct result of the onset of transpression within the basin.

A comparison of the plate motions predicted from structural and stratigraphic data within the Lusitanian Basin with the published plate motion paths of Smith (1971), Dewey et al., (1973), and Livermore & Smith (1986), reveals a good general fit, with late northwesterly directed convergence predicted by most models. The most recent plate motion model of Dewey et al., (1989), provides a much smoother reconstruction of African plate motion, and displays a striking similarity with the plate motions predicted from the S. de Montejunto-Candeeiros fault system (figure 6.3). A slight discrepancy exists between the predicted convergence directions of Dewey et al., (1989) and those observed in the Lusitanian Basin for the Middle to Late Miocene aged motion (north-northeast, as opposed to north-south, respectively).

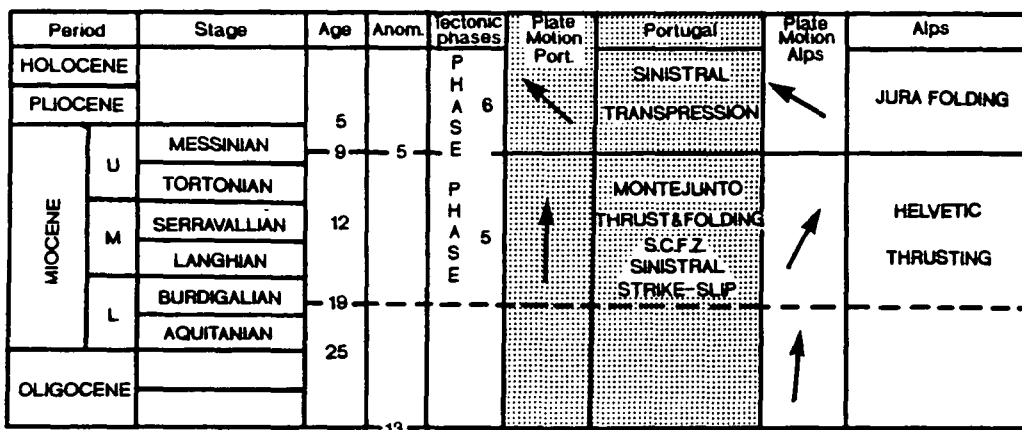


Figure 6.3 Correlation chart between the relative plate motion of Africa w.r.t. Europe, and various tectonic events in the Lusitanian Basin of Portugal (stippled), and for comparison, the European Alps. Modified from Dewey et al., (1989).

Significantly, however, the model displays a definite change from dominantly northward directed convergence, to northwestward convergence at 9Ma (middle Tortonian). This strong correlation between the change in relative convergence directions predicted from geologic observations, and the plate vector reconstruction of Dewey et al., (1989), further strengthens the indirect stratigraphic evidence, which constrains the timing of transpressive deformation along the S. de Montejunto-Candeeiros fault system.

6.3 Tectonic Style of the Lusitanian Basin

6.3.1 Previous interpretations

Interpretations of the Alpine (Miocene to Recent) tectonics of the Lusitanian Basin, vary between a thrust dominated, to a strike-slip dominated system (Ribeiro et al., 1988, 1990; and Fonseca & Long, 1989a,b, respectively). The dominant deformation style within the basin is not the only contentious point. The extent of basement involvement in Meso-Cenozoic cover deformation, raises the issue of thin-skinned versus basement driven deformation.

Ribeiro et al., (1988, 1990) present a review of the Alpine evolution of the Lusitanian Basin, in which the north-northeast trending faults "...behave as lateral ramps and transfer zones for the Alpine thrusts..." which have an approximately east-west orientation. The emphasis of this interpretation is placed on the controlling influence of the thrust faults, and the passive role of the sinistral strike-slip structures. In addition, some confusion seems to surround the role of the basement in the deformation of the cover sequence. Thin-skinned deformation has been invoked with a décollement suggested along the Hettangian evaporite horizon which separates the Hercynian basement and Meso-Cenozoic cover sequence; the Arrábida region quoted as the best example of this style. However, based on balanced cross-sections of low amplitude folds within the cover sequence of the basin, a décollement at 10 ± 2 km is proposed to separate the low-grade metamorphic Palaeozoic rocks from the underlying Precambrian basement, therefore, implying that thick-skinned tectonics were operative. Little mention is made of the detailed Quaternary tectonics within the basin, even though the change in the regional compressive stress is acknowledged. However, a change from a passive continental margin to an active margin is proposed by Ribeiro et al., (1988), due to a proposed northward propagating incipient subduction zone.

Fonseca and Long (1989a,b) proposed a neotectonic model for the Lusitanian and Lower Tagus Basins, based on seismotectonic analysis. The proposed model is dominated by strike-slip deformation along major north-northeast oriented basement faults. Deformation within the basement is suggested to decouple from the Meso-Cenozoic cover sequence along the Hettangian aged evaporites. It is suggested that

this décollement facilitates the transfer of basement fault displacements to nearby, pre-existing cover faults. Hence, the cover deformation is being driven by basement structures. Two suggestions have been offered to explain the driving mechanism of this zone of distributed strike-slip: 1) that strike-slip along NNE trending faults might occur as part of a lateral block movement to the west, accommodating crustal convergence to the south, and 2) that the strike-slip faults may be splay faults that run off-shore to the dextral, Azores-Gibraltar fracture zone. It was noted that both models may explain the distributed strike-slip seismicity observed, but if considered separately they would lead to a prediction of opposite senses of slip along the faults.

6.3.2 Revised tectonic model for the Lusitanian Basin

As described earlier in this chapter (section 6.1), the dominant deformation style within the Lusitanian Basin changed from a thrust system, to a sinistral transpressional system. The S. de Montejunto-Candeeiros fault system preserves the detail of this transformation in tectonic style, therefore, allowing the model of Ribeiro et al., (1988, 1990) to be modified.

In general, the author agrees with the kinematic interpretation of Ribeiro et al., (1990), but only for the initial period of Alpine deformation, following which the change in tectonic style, clearly documented by structural observations and the relative plate motion path of Dewey et al., (1989), must be incorporated. Thus, the post-Burdigalian thrusting event caused localised structural inversion along compressional structures, such as the Montejunto anticline, and the Arrábida region. Ribeiro et al. (1990), suggest that the basin deformed via thin-skinned thrust tectonics, although strike-slip motion along north-northeast structures appears to have played a significant role (Mauffret et al., 1989). The presence of the evaporites between the basement and cover sequence serves as an efficient décollement surface, likely to decouple the basement and cover deformation, and for this reason any attempt to relate low amplitude folds to décollement surfaces within the basement seems unrealistic. Seismic reflection profiles across the Montejunto massif indicate that basement faults have been reactivated to form continuous basement/cover structures of Miocene age. This suggests that regional thin-skinned deformation was locally influenced by basement structures.

The duration of this deformation style was short lived. In middle Tortonian times (9Ma) the relative motion of Africa-Europe changed, inducing transpressional tectonics along the S. de Montejunto-Candeeiros fault system. This oblique convergence direction persisted to the present, suggesting that, in terms of duration, transpression was the dominant deformation style within the Lusitanian Basin. However, off-shore seismic reflection profiles suggest that peak deformation occurred

during the Middle to Late Miocene, tailing off to its present level (Mauffret et al., 1989).

6.3.3 Neotectonic model for the Lusitanian Basin

Seismotectonic studies of the Lower Tagus, and Lusitanian Basins, suggest that the basement is undergoing sinistral strike-slip displacement along north-northeast trending faults. The lack of surface expression for the Lower Tagus Fault, and for a possible parallel structure, located further to the east, indicates that basement deformation is again decoupled from that of the cover. However, the main neotectonic surface structures within the Lusitanian Basin, although spatially non-coincident with the proposed basement faults, display the same sense of motion. Fonseca and Long (1989b) resolved the problem of no associated surficial deformation above the Lower Tagus Fault by suggesting that displacement associated with this fault becomes transferred along the sub-horizontal evaporite sequence to the pre-existing cover faults of the Lower Tagus Valley: the Vila Franca-Arrábida fault system. A similar scenario is proposed for the Serra dos Candeeiros fault and associated structures (Curtis, 1991). The Serra dos Candeeiros fault is considered to be neotectonic (Cabral and Ribeiro, 1988), although no seismicity has been recorded along it. However, an important linear array of earthquake epicentres lies to the immediate east of the fault trace, which have been interpreted to represent a concealed sinistral basement fault (see 5.4.3). It is suggested that displacement associated with this proposed sinistral basement fault, is prevented from propagating directly to the surface by the thick Dagorda evaporite horizon. Instead, it seems likely that the displacement associated with this basement fault explores the décollement horizon, seeking out weak, pre-existing structures. The Serra dos Candeeiros fault represents an easily exploitable structure due to the presence of a salt wall along the fault zone. Thus, due to the reduced shear stress along the Serra dos Candeeiros fault, displacement is transferred laterally by as much as 20 km. This decoupled deformation style is further suggested by the presence of the Candeeiros block, which is rotating about a vertical axis. As discussed in section 1.1.6 crustal flakes or slabs must detach along some décollement in order to facilitate the rotation, and as suggested by Brown (1928) and demonstrated by Terres and Sylvester (1981), these décollements are commonly along weak horizons or mechanical variations in the underlying lithologies. In the case of the Lusitanian Basin, it is logical to assume that the detachment surface is the Dagorda evaporites. Therefore, the evaporites appear to be providing an efficient regional detachment on a scale of at least 20x20 km, suggesting a similar décollement is likely to occur on a basin wide scale.

It appears that the Lusitanian Basin is deforming neither due to thin-skinned, nor thick-skinned tectonics. Instead, an intermediate model of decoupled cover and

basement deformation is preferred, at least for Quaternary deformation. This distinction is made because the deformation within the cover sequence is clearly related to basement deformation, although not directly by single continuous structures. Instead, the cover and basement deform in the same tectonic style, albeit detached along the evaporite horizon. Whether or not the cover and basement are deforming independently is debatable. The lack of instrumental seismicity along the Serra dos Candeeiros fault, and associated faults, possibly suggests that the Dagorda evaporite sequence may provide an all too efficient décollement, resulting in complete cover independence from the basement. However, the effects of the Candeeiros salt wall along the fault zone may facilitate aseismic creep which, coupled with the low strain rate estimates for Quaternary faults in Portugal, may have gone undetected.

As the NW-SE convergence direction between Africa-Europe has remained stable since its initiation during the late Tortonian, it seems reasonable to assume that the present tectonic style reflects the tectonic style of the basin since the late Tortonian, that is: decoupled basement and cover sinistral transpression. It is most probable that the main inversion of the Lusitanian Basin occurred during this period of sinistral transpression. Apart from the observed structural data, and seismotectonic interpretations which suggest a post-Tortonian basement driven, transpressional event, two further lines of evidence suggest that basin inversion was transpressional in nature: 1) The narrow, elongate zone of inversion, is typical of the uplift associated with transpressional fault systems (Sylvester, 1988), and 2) A positive magnetic anomaly coincides with the outcrop of inverted Mesozoic sediments, between the Montejunto Range and the Nazaré fault (Miranda et al., 1988), indicating that basement uplift may have occurred in association with the narrow zone of inversion (figure 6.4). Basement uplift related to north-south compression would be expected to be associated with localised east-west oriented structures, as structures of this orientation form a small proportion of the basin structure. The termination of the positive magnetic anomaly at the Montejunto massif, possibly suggests that inversion tectonics to the south of this structure may not include basement, and therefore, the deformation may be thin-skinned. The presence of a transpressively reactivated basement fault beneath the Montejunto massif, provides a suitable structure across which differential basement behaviour could take place.

It appears, therefore, that the inversion of the Lusitanian Basin was related to sinistral transpressive motion along two (from neotectonic evidence), and possibly more concealed basement faults. Uplift of the western side of this basement fault system, accounts for the narrow region of inversion.



Figure 6.4 Magnetic anomaly map of Portugal. Dashed line represents the eastern limit of Lusitanian Basin inversion, positive anomalies are shaded. Re-drafted from Miranda et al., (1988).

6.3.4 Summary: Alpine evolution of Lusitanian Basin Tectonics

The earlier (Langhian to late Tortonian) Alpine deformation of the Lusitanian Basin sedimentary sequence, appears to have occurred by thin-skinned thrust tectonics, in response to a dominantly north-south oriented compressive system. The regional décollement facilitating the detachment of the cover sequence was probably located within the Dagorda evaporites.

The change in relative plate motion between Africa-Europe from north-south to northwest-southeast, near the end of the Tortonian, probably induced thick-skinned transpressional deformation along NNE oriented basement faults. However, the cover deformation was most likely decoupled from the underlying basement by the thick Hettangian age Dagorda evaporites. Transpressive movement along the Lower Tagus fault, and possibly a more important parallel fault lying beneath the edge of the inversion zone, resulted in a component of upthrow to the west causing the uplift and inversion of a narrow region of the Lusitanian Basin. Wilson et al., (1990) suggest that

the Miocene inversion event is responsible for up to 1000 metres of uplift, with greater values probable, where locally intense transpression or compression has taken place (i.e. the Montejunto massif, and Serra D'Aire, respectively). Neotectonic, and seismological studies suggest that the same deformation style is continuing. The disparity in the location of basement and cover faults of the same kinematic style suggest that transpressive motion along the steep basement fault/s is transferred westward along the basement/cover evaporite decollement, to the steep S. dos Candeeiros/Cercal faults, and associated structures within the cover sequence (figure 6.5). The Lusitanian Basin is therefore displaying a tectonic style that has been increasingly recognised in southern California, with regional décollements, and lateral offsets of major strike-slip faults (Webb & Kanamori, 1985; Dewey et al., 1986; Nicholson et al., 1986; Hudnut et al., 1989; and Petersen et al., 1991).

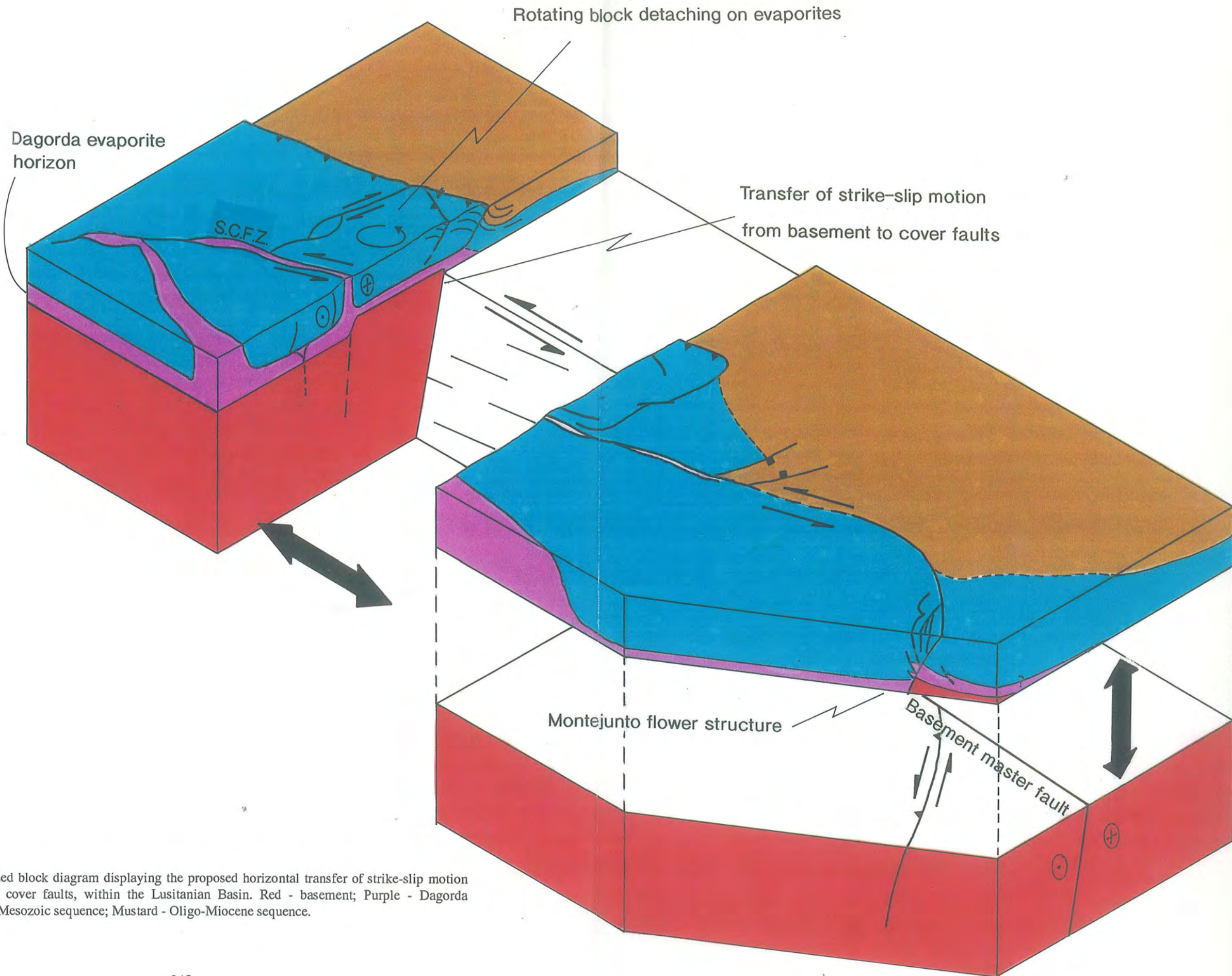


Figure 6.5 Exploded block diagram displaying the proposed horizontal transfer of strike-slip motion from basement to cover faults, within the Lusitanian Basin. Red - basement; Purple - Dagorda evaporites; Blue - Mesozoic sequence; Mustard - Oligo-Miocene sequence.

References cited in the text

- Anderson, E.M.**, 1905, The dynamics of faulting: Edinburgh Geological Society Transactions, v.8,pt.3, p.387-402.
- Anderson, E.M.**, 1942, The dynamics of faulting and dyke formation with application to Britain: Edinburgh, Scotland, Oliver and Boyd, p.206.
- Arthaud, F., and Matte, P.**, 1977, Late Palaeozoic strike-slip faulting in southern Europe and northwest Africa: result of right-lateral shear zone between the Appalachians and the Urals: Geological Society of America, Bulletin, v.88, p.1305-1320.
- Aydin, A., and Nur, A.**, 1982, Evolution of pull-apart basins and their scale independence: Tectonics, v.1, p.91-105.
- Aydin, A., and Nur, A.**, 1985, The types and role of stepovers in strike-slip tectonics, *in* Biddle, K.T., and Christie-Blick, N., eds. Strike-slip deformation, basin formation, and sedimentation: Society of Economic Paleontologists and Mineralogists Special Publication 37, p.35-43
- Aydin, A., and Page, B.M.**, 1984, Diverse Pliocene-Quaternary tectonics in a transform environment, San Francisco Bay region, California: Geological Society of America Bulletin, v.95, p.1303-1317.
- Baird, A.W., and Dewey, J.F.**, Structural evolution in thrust belts and relative plate motion: The Upper Pennine Piedmont zone of the Internal Alps, southwest Switzerland and northwest Italy: Tectonics, v.5, p.375-387.
- Bally, A.W.**, ed., 1983, Seismic expression of structural styles: American association of Petroleum geologists Studies in geology, ser. 15, 3 volumes.
- Bartlett, W.L., Friedman, M., and Logan, J.M.**, 1981, Experimental folding and faulting of rocks under confining pressure. Part IX Wrench faults in limestone layers: Tectonophysics, v.79. p.255-77.
- Bates, R.L. and Jackson, J.A.**, 1987, Glossary of geology (3rd edition): Alexandria, Virginia. American Geological Institute. p.788.
- Beach, A.**, 1975, The geometry of en echelon vein arrays: tectonophysics, v.28, p.245-263.

- Ben-Avraham, Z., and Garfunkel, Z., 1986, Character of transverse faults in the Elat pull-apart basin: Tectonics, v.5, p.1161-1169.**
- Ben-Avraham, Z., ten Brink, U., and Charrach, J., 1990, Transverse faults at the northern end of the southern basin of the Dead Sea graben: Tectonophysics, v.180, p.37-47.**
- Benson, W.N., 1952, Meeting of the geological division of the Pacific Science Congress in New Zealand, February 1949: International Proceedings: Geological Society of America Bulletin, v.63, p.11-13.**
- Bergerat, F., 1987, Stress fields in the European platform at the time of the Africa-Eurasia collision: Tectonics, v.6, p.99-132.**
- Biddle, K.T., and Christie-Blick, N., 1985, Glossary-Strike-slip deformation, basin formation, and sedimentation, *in* Biddle, K.T., and Christie-Blick, N., eds. Strike-slip deformation, basin formation, and sedimentation: Society of Economic Paleontologists and Mineralogists Special Publication 37, p.378-385.**
- Biju-Duval, B., Dercourt, J., Le Pichon, X., 1977, From the Tethys Ocean to the Mediterranean Seas: a plate tectonic model of the evolution of the western Alpine system, *in* Biju-Duval, B., & Montadert, L., eds., Structural History of the Mediterranean Basins: Proceedings of an International Symposium, Editions Technip, Paris, p.143-164.**
- Boillot, G., 1984, Some remarks on the continental margins in the Aquitaine and French Pyrenees: Geological Magazine, v.121, p.407-412.**
- Boillot, G., 1987, Proceedings of the Ocean Drilling Program, Initial Reports (Part A), v.103, p.633.**
- Borradaile, G.J., 1978, Transected folds: A study illustrated with examples from Canada and Scotland: Geological Society of America Bulletin, v.89, p.481-493.**
- Bretz, J.H., 1940, Solution cavities in the Joliet limestone of northeastern Illinois: Journal of Geology, v.50, p.675-711.**
- Brown, R.W., 1928, Experiments related to the results of horizontal shearings: American Association of Petroleum Geologists Bulletin, v.12, p.715-720.**

- Burchfiel, B.C., and Stewart, J.H., 1966, "Pull-apart" origin of the central segment of Death Valley, California: Geological Society of America Bulletin, v.77, p.439-442.**
- Bürgmann, R., 1991, Transpression along the southern San Andreas Fault, Durmid Hill, California: Tectonics, v.10, p.1152-1163.**
- Butler, R.W.H., 1982, The terminology of structures in thrust belts: Journal of Structural Geology, v.4, p.239-245.**
- Cabral, J., 1989, An example of intraplate neotectonic activity, Vilarica Basin, northeast Portugal: Tectonics, v.8, p.285-303.**
- Cabral, J., and Ribeiro, A., 1988, Carta Neotectónica de Portugal, escala 1:1,000,000, Serviços Geológicos de Portugal, Lisboa.**
- Cabral, J., Dias, R., and Brum, A., 1984, Estudo de falhas afectando formacoes Plio-Quaternarias na zona da Fonte da Telha (Peninsula de Setubal). Comun. Serv. Geol. Portugal, v.70, p.83-91.**
- Cheadle, M.J., Czuchra, B.L., Byrne, T., Ando, C.J., Oliver, J.E., Brown, L.D., Kaufman, S., Malin, P.E., and Phinney, R.A., 1986, The deep crustal structure of the Mojave desert, California, from COCORP seismic reflection data: Tectonics, v.5, p.293-320.**
- Chester, F.M., and Logan, J.M., 1987, Composite planar fabric of gouge from the Punchbowl Fault, California: Journal of Structural Geology, v.9, p.621-634.**
- Choffat, P., 1908, Éssai sur la tectonique de la chaine de L'Arrabida: Memoires e comunicação, Serviços Geológicos de Portugal, p.89.**
- Cloos, E., 1955, Experimental analysis of fracture patterns: Geological Society of America Bulletin, v.66, p.241-256.**
- Cloos, H., 1928, B, Experimente zur innern Tektonik: Zentralblatt für Mineralogie und Palaeontologie, v.1928, p.609-621.**
- Craddock, K.C., Hauser, E.C., Maher, H.D., Sun, A.Y., and Zhu, G.Q., 1985, Tectonic evolution of the West Spitsbergen fold belt: Tectonophysics, v.114, p.193-211.**

- Crowell, J.C.**, 1974a, Sedimentation along the San Andreas fault, California, *in* Dott, R.H., Jr., and Shaver, R.H., eds., Modern and ancient geosynclinal sedimentation: Society of Economic Paleontologists and Mineralogists Special Publication No.19, p.292-303
- Crowell, J.C.**, 1974b, Origin of Late Cenozoic basins in southern California, *in* Dickinson, W.R., ed., Tectonics and sedimentation: Society of Economic Paleontologists and Mineralogists Special Publication No. 22, p.190-204.
- Crowell, J.C.**, 1982a, The tectonics of Ridge basin, southern California, *in* Crowell, J.C., and Link, M.H., eds., Geological history of Ridge Basin, southern California: Society of Economic Paleontologists and Mineralogists, Pacific Section, Guidebook, p.25-41.
- Crowell, J.C.**, 1982b, The Violin breccia, Ridge Basin, southern California, *in* Crowell, J.C., and Link, M.H., eds., Geological history of Ridge Basin, southern California: Society of Economic Paleontologists and Mineralogists, Pacific Section, Guidebook, p.89-97.
- Crowell, J.C.**, Unpub. data *in* Sylvester, A.G., 1988, Strike-slip faults: Geological Society of America Bulletin, v.100, p1666-1703.
- Curtis, M.L.**, 1991, The horizontal transfer of strike-slip motion between basement and cover faults: Lusitanian Basin, Portugal: Geological Society of America, Abstracts with Programs, v.23, No.5, p.A234. Annual Meeting San Diego, October 21-24th.
- Davis, T.L., and Duebendorfer, E.M.**, 1987, Strip map of the western Big Bend segment of the San Andreas fault: Geological Society of America Map and Chart Series, Map 60, scale 1:31,682.
- Dewey, J.F., Helman, M.L., Turco, E., Hutton, D.H.W., and Knott, S.D.**, 1989, Kinematics of the Western Mediterranean, *in* Coward, M.P., Dietrich, D., and Park, R.G., eds., Alpine Tectonics, Geological Society Special Publication No. 45, p.265-283.
- Dewey, J.F., Hempton, M.R., Kidd, W.S.F., Saroglu, F., and Sengör, A.M.C.**, 1986, Shortening of continental lithosphere: the neotectonics of Eastern Anatolia - a young collision zone, *in* Coward, M.P., and Ries, A.C., eds., Collision Tectonics, Geological Society Special Publication No. 19, p.3-36.

- Dewey, J.F., Pitman, W.C.III, Ryan, W.B.F., and Bonnin, J., 1973, Plate tectonics and evolution of the Alpine systems: Geological Society of America Bulletin, v.84, p.137-180.**
- Dias, R.P., and Cabral, J., 1989, Neogene and Quaternary Reactivation of the Ponsul Fault in Portugal: Comun. Serv. Geol. Portugal, v.75, p.3-28.**
- Dickinson, W.R., 1983, Cretaceous sinistral strike-slip along Nacimiento fault in central California: American Association of Petroleum Geologists Bulletin, v.67, p.624-645.**
- Dubey, A.K., 1980, Model experiments showing simultaneous development of folds and transcurrent faults: Tectonophysics, v.65, p.69-84.**
- Dunod, 1980, 'Géologie des Pays Européens' Espagne, Grèce, Italie, Portugal, Yugoslavie, Bordas et 26^e Congrès Géologique International, p.86.**
- Durney, D.W., and Ramsay, J.G., 1973, Incremental strains measured by syntectonic crystal growths, in DeJong, K.A, and Scholten, R., eds., Gravity and Tectonics, John Wiley and Sons, New York, p.67-96.**
- Ellis, P.M., Wilson, R.C.L., and Leinfelder, R.R., 1990, Controls on Upper Jurassic carbonate build-up development in the Lusitanian Basin, Portugal: Special Publication of the International Association of Sedimentologists, v.9, p.169-202.**
- Erdlac, R.J., Jr., 1990, A Laramide-age push-up block: The structures and formation of the Terlingua-Solitario structural block, Big Bend region, Texas: Geological Society of America Bulletin, v.102, p.1065-1076.**
- Fielitz, W., 1992, Variscan transpressive inversion in the northwestern central Rhenohercynian belt of western Germany: Journal of Structural Geology, v.14, p.547-563.**
- Fischer, M.P., Woodward, N.B., and Mitchell, M.M., 1992, The kinematics of break-thrust folds: Journal of Structural Geology, v.14, p.451-460.**
- Fonseca, J.F.B.D., 1989, Seismicity and Regional Tectonics of the Estremadura, Southwestern Portugal: Unpublished Ph.D. thesis, University of Durham.**

- Fonseca, J.F.B.D., and Long, R.E., 1989a, Seismotectonics of SW Iberia: a distributed plate margin?: Symposium on the Seismicity, Seismotectonics and Seismic Risk of the Ibero-Moghrebian Region, Madrid, April 12-14th.**
- Fonseca, J.F.B.D., and Long, R.E., 1989b, Seismotectonics of western Portugal: Proceedings of the 4th International Symposium on the Analysis of Seismicity and Seismic Risk, Bechyně Castle, Czechoslovakia, September 4-9th.**
- Fonseca, J.F.B.D., Long, R.E., Costa Nunes, J., Reis, P.A.A., and Moreira, V.J.S., 1988, Seismicity and Regional Tectonics of the Portuguese Estremadura: Proceedings of the Seminar on the Prediction of Earthquakes, Lisbon, November 1988.**
- Freund, R., and Garfunkel, Z., 1976, Guidebook to the Dead Sea Rift: Jerusalem, Israel. Department of Geology, Hebrew University, 27p.**
- Fritz, H., and Neubauer, F., (in press), Displacement partitioning in a transpressional orogen: the southeastern Bohemian massif:**
- Fruend, R., 1971, The Hope fault-A strike slip fault in New Zealand: New Zealand Geological Survey Bulletin, v.86, p.1-47.**
- Fruend, R., 1974, Kinematics of transform and transcurrent faults: Tectonophysics, v.21, p.188-200.**
- Galdeano, A., Moreau, M.G., Pozzi, J.P., Berthou, P.Y., and Malod, J.A., 1989, New palaeomagnetic results from Cretaceous sediments near Lisboa (Portugal) and implications for the rotation of Iberia: Earth and Planetary Science Letters, v.92, p.95-106.**
- Gamond, J.F., 1983, Displacement features associated with fault zones: A comparison between observed examples and experimental models: Journal of Structural Geology, v.5, p.33-45.**
- Gamond, J.F., 1987, Bridge structures as sense of displacement criteria in brittle fault zones: Journal of Structural Geology, v.9, p.609-620.**
- Gamond, J.F., and Odonne, F., 1984, Critères d'identification des plis induits par un décroachment profond: Modélisation analogique et donnees de terrain: Bulletin de la Société Géologique de France, v.7, p.115-128.**

- Garfunkel, Z., and Ron, H., 1985, Block rotation and deformation by strike-slip faults 2. The properties of a type of macroscopic discontinuous deformation: Journal of Geophysical Research, v.90, p.8589-8602.**
- Geikie, J., 1905, Structural and field geology: Edinburgh, Scotland, Oliver and Boyd, p.435.**
- Group Galice, 1979, The continental margin of Galicia and Portugal: acoustical stratigraphy, dredge stratigraphy, and structural evolution, in Ryan, W.B.F., Sibuet, J.C., et Al., eds., Initial Reports of the Deep Sea Drilling Project, v.47, p.633-662.**
- Guery, F., 1984, Evolution sedimentaire et dynamique du bassin marginal ouest-Portugais Au Jurassique, Province d'Estremadura (secteur de Caldas da Rainha-Montejunto), unpublished Ph.D. Thesis, Université de Lion I.**
- Guery, F., Montenat, G., and Vanchard, D., 1986, Evolution tectono-sedimentaire de Bassin Portugais Au Mesozoique suivant la transversale de Peniche (Estremadura): Bull. Centre Rech. Explor.-Prod. Elf-Aquitaine, v.10, p.83-94.**
- Hamilton, W., and Myers, W.B., 1966, Cenozoic tectonics of the western United States: Reviews of Geophysics, v.4, p.509-549.**
- Hancock, P.L., 1985, Brittle microtectonics - Principles and practice: Journal of Structural Geology, v.7, p.437-57.**
- Harding, T.P., 1973, Newport-Inglewood Trend, California - An example of wrenching style of deformation: American Association of Petroleum Geologists Bulletin, v.57, p.97-116.**
- Harding, T.P., 1976, Tectonic significance and hydrocarbon trapping consequence of sequential folding synchronous with San Andreas faulting, San Joaquin Valley, California: American Association of Petroleum Geologists Bulletin, v.58 (7), p.356-378.**
- Harding, T.P., 1985, Seismic characteristics and identification of negative flower structures, positive flower structures, and positive structural inversion: American Association of Petroleum geologists Bulletin, v.69, p.582-600.**
- Harding, T.P., and Lowell, J.D., 1979, Structural styles, their plate-tectonic habitats, and hydrocarbon traps in petroleum provinces: American Association of Petroleum Geologists Bulletin, v.63, p.1016-1058.**

- Harding, T.P., and Tuminas, A.C., 1988, Interpretation of footwall (lowside) fault traps sealed by reverse faults and convergent wrench faults: (American Association of Petroleum Geologists Bulletin, v.72 (6), p.738-357.**
- Harland, W.B., 1971, Tectonic transpression in Caledonian Spitsbergen: Geological Magazine, v.108, p.27-42.**
- Hempton, M.R., 1983, Evolution of thought concerning sedimentation in pull-apart basins, in Boardman, S.J., ed., Revolution in earth sciences: Dubuque, Iowa, Kendal/Hunt, p.167-180.**
- Hempton, M.R., and Dunne, L.A., 1984, Sedimentation of pull-apart basins: Active examples in eastern Turkey: Journal of Geology, v.92, p.513-530.**
- Hill, M.L., and Dibblee, T.W. Jnr., 1953, San Andreas, Garlock, and Big Pine faults, California-A study of the character, history, and tectonic significance of their displacements: Geological Society of America Bulletin, v.64, p.443-458.**
- Hobbs, B.E., Means, W.D., and Williams, P.F., 1976, An Outline of Structural Geology: Wiley International Edition**
- Holdsworth, R.E., and Strachan, R., 1991, Interlinked system of ductile strike-slip and thrusting formed by Caledonian sinistral transpression in northeastern Greenland: Geology, v.19, p.510-513.**
- Horns, D.M., 1991, Block rotations within strike-slip fault zones and the presence of sub-horizontal detachments: Geological Society of America, Annual Meeting, Abstracts with Programs, (Pub. Abst.) p.A258.**
- Hudnut, K.W., Seeber, L., and Pacheco, J., 1989, Cross-fault triggering in the November 1987 Supersition Hills earthquake sequence, southern California: Geophysical Research Letters, v.16, p.199-202.**
- Hutton, D.H.W., 1988, Granite emplacement mechanisms and tectonic controls: inferences from deformation studies: Transactions of the Royal Society of Edinburgh: Earth Sciences, v.79, p.245-255.**
- Hutton, D.H.W., and Gawthorpe, R., 1988, Strike-slip inversion of the Lusitanian Basin, Portugal: Meeting of the Tectonics Studies Group of the Geological Society of London, December, (Unpub. Abst.).**

Instituto Nacional de Meteorologia e Geofisica, 1983, Portugal continental-carta sismotectónica, Lisbon.

Jones, D.L., Blake, M.C. Jr., and Rangin, C., 1976, The four Jurassic belts of northern California and their significance to the geology of the southern California borderland, *in* Howell, D.G., ed., Aspects of the geological history of the California continental borderland: American Association of Petroleum Geologists Miscellaneous Publication 24, p.343-376.

Kanaori, Y., 1990, Late Mesozoic - Cenozoic strike-slip and block rotation in the inner belt of Southwest Japan: *Tectonophysics*, v.177, p.381-399.

Keller, E.A., Bonkowski, M.S., Korsch, R.J., and Shlemon, R.J., 1982, Tectonic geomorphology of the San Andreas fault zone in the southern Indio Hills, Coachella Valley, California: *Geological Society of America Bulletin*, v.93, p.46-56.

Kennedy, W.Q., 1946, The Great Glen fault: *Geological Society of London Quarterly Journal*, v.102, p.47-76.

*

Klitgord, K.D., and Schouten, H., 1986, Kinematics of the Central Atlantic. *in* Vogt, P.R. and Tucholke, B.E., eds., *The Geology of North America, M, The western north Atlantic Region*, DNAG-GSA Series, p.351-378.

Knipe, R.J., 1986, Deformation mechanism path diagrams for sediments undergoing lithification, *in* Moore, J.C., ed., *Structural Fabrics in D.S.D.P. Cores from Forearcs*: *Memoirs of the Geological Society of America*, v.166, p.151-160.

Koral, H., 1983, Folding of strata within shear zones: Inferences from the azimuths of en echelon folds along the San Andreas fault (M.Sc. thesis): Troy, New York, Rensselaer Polytechnic Institute, 100p.

Lamb, S.H., 1987, A model for tectonic rotations about a vertical axis: *Earth and Planetary Science Letters*, v.84, p.75-86.

Leblanc, D., and Oliver, P., 1984, Role of strike-slip faults in the Betic-Rifian orogeny: *Tectonophysics*, v.101, p.345-355.

Leinfelder, R.R., and Wilson, R.C.L., 1989, Seismic and sedimentologic features of Oxfordian-Kimmeridgian syn-rift sediments on the eastern margin of the Lusitanian Basin: *Geologische Rundschau*, v.78, p.81-104.

- LePichon, X., and Sibuet, J.C., 1971, Comments on the evolution of the Northeast Atlantic: Nature, v.233, p.257-258.**
- LePichon, X., Sibuet, J.C., and Francheteau, J., 1977, The fit of the continents around the North Atlantic Ocean: Tectonophysics, v.38, p.169-209.**
- Letouzey, J., 1986, Cenozoic paleo-stress pattern in the Alpine foreland and structural interpretation in a platform basin: Tectonophysics, v.132, p.215-231.**
- Little, T.A., 1990, Kinematics of wrench and divergent wrench deformation along a central part of the Border Ranges fault system, Northern Chugach mountains, Alaska: Tectonics, v.9, p.585-611.**
- Little, T.A., 1992, Development of wrench folds along the Boarder Ranges fault system, southern Alaska, U.S.A.: Journal of Structural Geology, v.14, p.343-359.**
- Livermore, R.A., and Smith, A.G., 1985, Some boundary conditions for the evolution of the Mediterranean, in Stanley, D.G., and Wezel, F.C., eds., Geological Evolution of the Mediterranean Sea, Springer-Verlag, New York, p.89-105.**
- Logan, J.M., Friedman, M., Higgs, N., Dengo, C., and Shimamoto, T., 1979, Experimental studies of simulated gouge and their application to studies of natural fault zones: U.S. Geological Survey, Open File Report, 79-1239, p.305-343.**
- Luyendyk, B.P., 1991, A model for Neogene crustal rotations, transtension, and transpression in southern California: Geological Society of America Bulletin, v.103, p.1528-1536.**
- Luyendyk, B.P., Kamerling, M.J., and Terres, R.A., 1980, Geometric model for Neogene crustal rotations in southern California: Geological Society of America Bulletin, v.91, p.211-217.**
- Luyendyk, B.P., Kamerling, M.J., Terres, R.A., and Hornafius, J.S., 1985, Simple shear in southern California during Neogene time suggested by paleomagnetic declinations: Journal of Geophysical Research, v.90, (B14), p.12,454-12,466.**
- Maltman, A.J., 1987, Microstructures in deformed sediments, Denbigh-Moors, North Wales: Geological Journal, v.22, p.87-94.**

- Mann, P., Draper, G., and Burke, K., 1985, Neotectonics of a strike-slip restraining bend system, Jamaica, in Biddle, K.T., and Christie-Blick, N., eds. Strike-slip deformation, basin formation, and sedimentation: Society of Economic Paleontologists and Mineralogists Special Publication 37, p.211-226.**
- Mann, P., Hempton, M.R., Bradley, D.C., and Burke, K., 1983, Development of pull-apart basins: Journal of Geology, v.91, p.529-554.**
- Manspeizer, W., 1985, The Dead Sea rift: Impact of climate and tectonism on Pleistocene and Holocene sedimentation, in Biddle, K.T., and Christie-Blick, N., eds. Strike-slip deformation, basin formation, and sedimentation: Society of Economic Paleontologists and Mineralogists Special Publication 37, p.143-158.**
- Marshak, S., Geiser, P.A., Alvarez, W., and Engelder, T., 1982, Mesoscopic fault array of the northern Umbrian Apennine fold belt, Italy: geometry of conjugate shear by pressure-solution slip: Geological Society of America Bulletin, v.93, p.1013-1022.**
- Mauffret, A., Mougnot, D., Miles, P.R., and Malod, J.A., 1989, Cenozoic deformation and Mesozoic abandoned spreading centre in the Tagus Abyssal Plain (west of Portugal): results of a multichannel seismic survey: Canadian Journal of Earth Sciences, v.26, p.1101-1123.**
- McCoss, A.M., 1986, Simple construction for deformation in transpression / transtension zones: Journal of Structural Geology, v.8, p.715-718.**
- McKay, A., 1890, On the earthquakes of September 1888 in the Amuri and Marlborough Districts of the South Island: New Zealand Geological Survey Report of Geological Explorations 1888-1889, v.20, p.1-16.**
- McKay, A., 1892, On the geology of Marlborough and southeast Nelson: New Zealand Geological Survey Report of Geological Explorations 1890 1891, v. 21, p.1-28.**
- McKenzie, D., and Jackson, J., 1983, The relationship between strain rates, crustal thickening, palaeomagnetism, finite strain and fault movements within a deforming zone: Earth and Planetary Science Letters, v.65, p.183-202.**
- McKenzie, D., and Jackson, J., 1986, A block model of distributed deformation by faulting: Journal of the Geological Society, London, v.143, p.349-353.**

- Means, W.D.**, 1987, A newly recognised type of slickenside striation: *Journal of Structural Geology*, v.9, p.585-590.
- Miranda, J.M., Galdeano, A., Rossignol, J.C., and Mendes-Victor, L.A.**, 1988, The aeromagnetic survey of Portugal (1980) and some tectonic implications, *in* Banda, E., and Mendes-Victor, L.A., eds., *Proceedings of the 5th Workshop on the European Geotraverse (EGT) Project*, Lisbon, November 1988.
- Mitchell, A.H.G., and Reading, H.G.**, 1978, *Sedimentation and tectonics*: *in* Reading, H.G., ed., *Sedimentary environments and facies*: Oxford, England, Blackwell Scientific Publications, p.439-476.
- Montenat, C., Guery, F., Jamet, M., and Berthou, P.Y.**, 1988, Mesozoic evolution of the Lusitanian Basin: Comparison with the adjacent margin, *in* Boillot, G., Winterer, E.L., et Al., eds., *Proceedings of the Ocean Drilling Program, Scientific Results*, v.103, p.757-775.
- Moody, J.D., and Hill, M.J.**, 1956, Wrench-fault tectonics: *Geological Society of America Bulletin*, v.67, p.1207-1246.
- Moore, D.E. and Byerlee, J.D.**, 1991, Comparative geometry of the San Andreas fault, California, and laboratory fault zones: *Geological Society of America Bulletin*, v.103, p.762-774.
- Moore, D.E. and Byerlee, J.D.**, 1991a, Fault patterns in the San Andreas system: Possible indicators of fluid-pressure conditions?: *Geological Society of America, Abstracts with Programs*, v.23, No.5, p.A103. Annual Meeting San Diego, October 21-24th.
- Moore, J.G.**, 1963, Geology of the Mount Pinchot quadrangle, southern Sierra Nevada, California: *United States Geological Survey Bulletin* 1130, p.152
- Moreira, V.S.**, 1979, Contribuição para o conhecimento da sismicidade histórica de Portugal Continental: *Rev. Inst. Nac. Met. Geofis.*, v.2, p.121-136.
- Moreira, V.S.**, 1985, Seismotectonics of Portugal and its adjacent area in the Atlantic, *in* Eva, C., and Pavoni, N., eds., *Seismotectonics: Tectonophysics*, v.117, p.85-96.
- Morgenstern, N.R., and Tchalenko, J.S.**, 1967, Microscopic structures in kaolin subjected to direct shear: *Geotechnique*, v.17, p.309-328.

- Mount, V.S., and Suppe, J., 1987, State of stress near the San Andreas fault: Implications for wrench tectonics: *Geology*, v.15, p.1143-1146.**
- Murphy, F.C., 1985, Non-axial planar cleavage and Caledonian sinistral transpression in eastern Ireland: *Geological Journal*, v.20, p.257-279.**
- Naylor, M.A., Mandl, G., and Sijpesteijn, C.H.K., 1986, Fault geometries in basement-induced wrench faulting under different initial stress states: *Journal of Structural Geology*, v.8, p.737-752.**
- Nelson, M.R., and Jones, C.H., 1987, Paleomagnetism and crustal rotations along a shear zone, Las Vegas Range, southern Nevada: *Tectonics*, v.6, p.13-33.**
- Nicholson, C., Seeber, L., Williams, P., and Sykes, L.R., 1986, Seismic evidence for conjugate slip and block rotation within the San Andreas fault system, southern California: *Tectonics*, v.5, p.629-648.**
- Nilsen, T.H., and McLaughlin, R.J., 1985, Comparison of tectonic framework and depositional patterns of the Hornelen strike-slip basin of Norway and the Ridge and Little Sulphur Creek strike-slip basins of California: *in* Biddle, K.T., and Christie-Blick, N., eds. *Strike-slip deformation, basin formation, and sedimentation: Society of Economic Paleontologists and Mineralogists Special Publication 37*, p.79-103.**
- Nur, A., Ron, H., and Scotti, O., 1986, Fault mechanics and the kinematics of block rotations: *Geology*, v.14, p.746-749.**
- Oldow, J.S., Bally, A.W., Avé Lallemant, H.G., 1990, Transpression, orogenic float, and lithospheric balance: *Geology*, v.18, p.991-994.**
- Oxburgh, E.R., 1972, Flake tectonics and continental collision: *Nature*, v.239, p.202-204.**
- Petersen, M.D., Seeber, L., Sykes, L.R., Nàbèlek, J.L., Armbruster, J.G., Pacheco, J., and Hudnut, K.W., 1991, Seismicity and fault interaction, southern San Jacinto fault zone and adjacent faults, southern California: Implications for seismic hazard: *Tectonics*, v.10, p.1187-1203.**
- Petit, J.P., 1987, Criteria for the sense of movement on fault surfaces in brittle rocks: *Journal of Structural Geology*, v.9, p.597-608.**

- Pindell, J.L., Cande, S.C., Pitman, W.C., III, Rowley, D.B., Dewey, J.F., LaBreque, J., and Haxby, W., 1988, A plate-kinematic framework for models of Caribbean evolution: Tectonophysics, v.155, No. 1-4, p.121-138.**
- Quennell, A.M., 1958, The structure and geomorphic evolution of the Dead Sea rift: Geological Society of London Quarterly Journal, v.114, p.1-24.**
- Quennell, A.M., 1959, Tectonics of the Dead Sea rift, in International Geological Congress. 20th, Mexico City association of the Geological Service of Africa, p.385-405.**
- Ramsay, J.G., and Graham, R.M, 1970, Strain variation in shear belts: Canadian Journal of Earth Sciences, v.7, p.786-813.**
- Ramsay, J.G., and Huber, M.I., 1983, The Techniques of Modern Structural Geology, Vol. 1, Strain Analysis: Academic Press, London.**
- Ramsay, J.G., and Huber, M.I., 1987, The Techniques of Modern Structural Geology, Vol. 2: Folds and Fractures: Academic Press, London.**
- Reches, Z., 1978, Analysis of faulting in a three-dimensional strain field: Tectonophysics, v.47, p.107-129.**
- Rehault, J-P., and Mauffret, A., 1979, Relationships between tectonics and sedimentation around the northwestern Iberian margin: Initial Reports of the Deep Sea Drilling Project, v.47, p.633.**
- Ribeiro, A., Antunes, M.T., Ferreira, M.P., Rocha, R.B., Soares, A.F., Zbyszewski, G., Moitinho De Almeida, F., De Carvalho, D., and Monteiro, J.H., 1979, Introduction à la Géologie Générale du Portugal: Serviços Geológicos de Portugal.**
- Ribeiro, A., Kullberg, M.C., Cabral, J., Madeira, J., Brum, A.P., and Moniz, C., 1989, Alpine Geodynamics of the west - Iberia margin, in Banda, E., and Mendes-Victor, L.A., eds., Proceedings of the 5th Workshop on the European Geotraverse (EGT) Project, Lisbon, November 1988, p.91-98.**
- Ribeiro, A., Kullberg, M.C., Kullberg, J.C., Manupella, G., and Phipps, S., 1990, A review of Alpine tectonics in Portugal: Foreland detachment in basement and cover rocks: Tectonophysics, v.184, p.405-415.**

- Riedel, W., 1929, Zur mechanik geologischer Brucherscheinungen. Zentrablatt für Mineralogie Geologie und Palaeontologie. Abhandlung B, p.354-368.
- Rispoli, R., 1981, Stress fields about strike-slip faults inferred from stylolites and tension gashes: *Tectonophysics*, v.75, p.29-36.
- Rodgers, D.A., 1980, Analysis of pull-apart basin development produced by *en echelon* strike-slip faults, in Ballance, P.F., ed., *Sedimentation in Oblique-slip mobile zones: International Association of Sedimentology Special Publication*, v.4, p.27-41.
- Ron, H., Freund, R., Garfunkel, Z., and Nur, A., 1984, Block rotation by strike-slip faulting: Structural and paleomagnetic evidence: *Journal of Geophysical Research*, v.89, p.6256-6270.
- Rothery, E., 1988, En échelon vein array development in extension and shear: *Journal of Structural Geology*, v.10, p.63-71.
- Royden, L.H., 1985, The Vienna basin: A thin skinned pull-apart basin, in Biddle, K.T., and Christie-Blick, N., eds. *Strike-slip deformation, basin formation, and sedimentation: Society of Economic Paleontologists and Mineralogists Special Publication 37*, p.319-338.
- Rutter, E.H., and Mainprice, D.H., 1978, The effect of water on stress relaxation of faulted and unfaulted sandstones: *Pure and applied Geophysics*, v.116, p.634-654.
- Sanderson, D.J., Andrews, J.R., Phillips, W.E.A., and Hutton, D.H.W., 1980, Deformation studies in the Irish Caledonides: *Journal of the Geological Society of London*, v.137, p.289-302.
- Sanderson, D.J., and Marchini, W.R.D., 1984, Transpression: *Journal of Structural Geology*, v.6, p.449-458.
- Sanderson, D.J., Roberts, S., McGowen, J.A., and Gumiel, P., 1991, Hercynian transpressional tectonics at the southern margin of the Central Iberian Zone, west Spain: *Journal of the Geological Society of London*, v.148, p.493-498.
- Savostin, L.A., Sibuet, J.C., Zonenshain, L.P., Le Pichon, X., and Roulet, M.J., 1986, Kinematic evolution of the Tethys belt from the Atlantic Ocean to the Pamirs since the Triassic: *Tectonophysics*, v.123, p.1-35.

- Schott, J.J., and Peres, A., 1988, Palaeomagnetism of Permo-Triassic red beds in the Western Pyrenees: evidence for strong clockwise rotations of the Paleozoic units: Tectonophysics, v.156, p.75-88.**
- Segall, P., and Pollard, D.D., 1980, Mechanics of discontinuous faults: Journal of Geophysical Research, v.85, p.4337-4350.**
- Segall, P., and Pollard, D.D., 1983, Nucleation and growth of strike-slip faults in Granite: Journal of Geophysical Research, v.88, p.555-568.**
- Shackleton, R.M., and Ries, A.C., 1984, The relation between regionally consistent stretching lineations and plate motions: Journal of Structural Geology, v.6, p.111-117.**
- Sharp, R.V., 1967, San Jacinto fault zone in the Peninsular Ranges of southern California: Geological Society of America Bulletin, v.78, p.705-730.**
- Sharp, R.V., and Clark, M.M., 1972, Geological evidence for previous faulting near the 1968 rupture on the Coyote Creek fault: U.S. Geological Survey Professional Paper 787, p.131-140.**
- Sibson, R.H., 1985, Stopping earthquake ruptures at dilational fault jogs: Nature v.316, p.248-251.**
- Sibson, R.H., 1989, Earthquake faulting as a structural process: Journal of Structural Geology, v.11, p.1-14.**
- Sibuet, J-C, and Ryan, W.B.F., 1979, Initial Reports of the Deep Sea Drilling Project, v.47, Washington D.C., U.S. Government Printing Office, pt.2, p.787.**
- Skempton, A.W., 1966, Some observations on tectonic shear zones: First International Congress on Rock Mechanics, Proceedings, v.1, p.329-335.**
- Slemmons, D.B., 1982, Determination of design earthquake magnitudes for microzonation, paper presented at 3rd International Earthquake Microzonation Conference Proceedings, Univ. of Washington, Seattle, Wash., June 28-July 1.**
- Smith, A.G., 1971, Alpine deformation and the oceanic areas of the Tethys, Mediterranean, and Atlantic: Geological Society of America Bulletin, v.82, p.2039-2070.**

- Soper, N.J., 1986, Geometry of transecting, anastomosing solution cleavage in transpression zones: *Journal of Structural Geology*, v.8, p.937-940.
- Soper, N.J., and Hutton, D.H.W., 1984, Late Caledonian sinistral displacements in Britain: implications for a three-plate collision model: *Tectonics*, v.3, p.781-794.
- Soper, N.J., Webb, B.C., and Woodcock, N.H., 1987, Late Caledonian (Acadian) transpression in north-east England: timing, geometry and geotectonic significance: *Proceedings of Yorkshire Geological Society*, v.46, p.175-192.
- Srivastava, S.P., and Tapscott, C.R., 1986, Kinematics of the North Atlantic, *in* Vogt, P.R. and Tucholke, B.E., eds., *The Geology of North America, M, The western north Atlantic Region, DNAG-GSA Series*, p.379-404.
- Stam, B., 1986, Quantitative analysis of Middle and Late Jurassic foraminifera from Portugal and its implications for the Grand Banks of Newfoundland: *Utrecht Micropaleontological Bulletins*, v.34, p.168.
- Steel, R.J., and Gloppen, T.G., 1980, Late Caledonian (Devonian) basin formation, western Norway: Signs of strike-slip tectonics during infilling, *in* Ballance, P.F., and Reading, H.G., eds., *Sedimentation in oblique-slip mobile zones: International Association of Sedimentologists Special Publication 4*, p.79-103.
- Strachan, R.A., Holdsworth, R.E., Friderichsen, J.D., and Jepsen, H.F., 1992, Regional Caledonian structure within an oblique convergence zone, Dronning Louise Land, NE Greenland: *Journal of the Geological Society of London*, v.149, p.359-371.
- Suess, E., 1885, *Das Anlitz der Erde: Tempsky*, 778p.
- Swanson, M.T., 1988, Pseudotachylyte-bearing strike-slip duplex structures in the Fort Foster Brittle Zone, S. Maine: *Journal of Structural Geology*, v.10, p.813-828.
- Swanson, M.T., 1989, Sidewall ripouts in strike-slip faults: *Journal of Structural Geology*, v.11, p.933-948.
- Swanson, M.T., 1990, Extensional duplexing in the York Cliffs strike-slip fault system, southern coastal Maine: *Journal of Structural Geology*, v.12, p.499-512.

- Sylvester, A.G.**, 1988, Strike-slip faults: Geological Society of America Bulletin, v.100, p.1666-1703.
- Sylvester, A.G.**, 1991, Geological structure, transpression, and neotectonics of the San Andreas fault in the Salton Trough, California. Part 1 Palm tree structure in the central Mecca Hills, *in* Walawender, M.J., and Hanan, B.B., eds., Geological excursions in southern California and Mexico, Guidebook for the 1991 Annual Meeting Geological Society of America, San Diego, California.
- Sylvester, A.G., and Smith, R.R.**, 1976, Tectonic transpression and basement controlled deformation in the San Andreas fault zone, Salton Trough, California: American Association of Petroleum Geologists Bulletin, v.60(12), p.2081-2102.
- Tchalenko, J.S.**, 1968, The evolution of kink bands and the development of compressional textures in sheared clays: Tectonophysics, v.6, p.159-174.
- Tchalenko, J.S.**, 1970, Similarities between shear zones of different magnitudes: Geological Society of America Bulletin, v.81, p.1625-1640.
- Tchalenko, J.S., and Ambraseys, N.N.**, 1970, Structural analysis of the Dasht-e bayaz (Iran) earthquake fractures: Geological Society of America Bulletin, v.81, p.41-66.
- ten Brink, U.S., and Ben-Avraham, Z.**, 1989, The anatomy of a pull-apart basin: Seismic reflection observations of the Dead Sea basin: Tectonics, v.8, p.333-350.
- Terres, R.R., and Sylvester, A.G.**, 1981, Kinematic analysis of rotated fractures and blocks in simple shear: Seismological Society of America Bulletin, v.71, p.1593-1605.
- Treagus, S.H., and Treagus, J.E.**, 1981, Folds and the strain ellipsoid: a general model: Journal of Structural Geology, v.3, p.1-17.
- Treagus, S.H., and Treagus, J.E.**, 1992, Transected folds and transpression: how are they associated?: Journal of Structural Geology, v.14, p.361-367.
- Van der Voo, R.**, 1969, Palaeomagnetic evidence for the rotation of the Iberian Peninsula: Tectonophysics, v.7, p.5-56.

- Van der Voo, R., and Zijdeveld, J.D.A., 1971, Renewed palaeomagnetic study of the Lisbon Volcanics and implications for the rotation of the Iberian Peninsula: Journal of Geophysical Research, v.76, p.3913-3921.**
- Webb, T.H., and Kanamori, H., 1985, Earthquake focal mechanisms in the eastern Transverse Ranges and San Emigdio Mountains, southern California, evidence for a regional decollement: Seismological Society of America Bulletin, v.75, p.737-757.**
- Wellman, H.W., 1955, The geology between Bruce Bay and Haast River, South Westland: New Zealand Geological Survey Bulletin 48 (n.s.), (2nd edition), 46p.**
- Wilcox, R.E., Harding, T.P., and Seely, D.R., 1973, Basic wrench tectonics: American Association of Petroleum Geologists Bulletin, v.57, p.74-96.**
- Will, T.M., and Wilson, C.J.L., 1989, Experimentally produced slickenside lineations in pyrophyllitic clay: Journal of Structural Geology, v.11, p.657.**
- Willis, B., 1938, San Andreas rift, California: Journal of Geology, v.46, p.793-827.**
- Willis, M.G., 1988, The tectonic history of the Lusitanian basin of Portugal: Ph.D. thesis, The Open University, Milton Keynes, U.K.**
- Wilson, G., 1960, The tectonics of the 'Great Ice Chasm' Filchner Ice Shelf, Antarctica: Geologists Association Proceedings, v.71, p.130-138.**
- Wilson, R.C.L., 1975, Atlantic opening and Mesozoic continental margin basins of Iberia: Earth and Planetary Science Letters, v.25, p.33-43.**
- Wilson, R.C.L., 1979, A reconnaissance study of Upper Jurassic sediments in the Lusitanian basin: Ciências da Terra, (Univ. Nova de Lisboa), v.5, p.53-85.**
- Wilson, R.C.L., 1988, Mesozoic development of the Lusitanian Basin, Portugal: Rev. Soc. Geol. España, v.1, p.393-407.**
- Wilson, R.C.L., Hiscott, R.N., Willis, M.G., and Gradstein, F.M., 1990, The Lusitanian Basin of west-central Portugal: Mesozoic and Tertiary tectonic, stratigraphic, and subsidence history: Memoir of the American Association of Petroleum Geologists, 42, p.341-361.**

Wood, H.O., 1955, The 1857 earthquake in California: Seismological Society of America Bulletin, v.45(1), p.47-67.

Woodcock, N.H., 1986, The role of strike-slip fault systems at plate boundaries: Royal Society of London Philosophical Transactions, series A, v.317, p.13-29.

Woodcock, N.H., and Fischer, M., 1986, Strike-slip duplexes: Journal of Structural Geology, v.8, p.725-735.

Woodcock, N.H., Awan, M.A., Johnson, T.E., Mackie, A.H., and Smith, R.D.A., 1988, Acadian tectonics of Wales during Avalonia / Laurentia convergence: Tectonics, v.7, p.483-495.

Wright, V.P., and Wilson, R.C.L., 1984, A carbonate submarine fan sequence from the Jurassic of Portugal: Journal of Sedimentary Petrology, v.54, p.394-412.

Zbyszewski, G., 1959, Étude structurale de l'aire typhonique de Caldas da Rainha: Serviços Geológicos de Portugal, Memoria, v.3 (nova serie), p.184.

Ziegler, P., 1987, Geological Atlas of Western and Central Europe, Shell, The Hague.

* Kerr, D.R., and Kidwell, S.M., 1991, Late Cenozoic sedimentation and tectonics, western Salton Trough, California: Geological Excursions in Southern California and Mexico, eds., Walawender, M.J. & Hanan, B.B., Guidebook for 1991 Annual meeting of Geological Society of America, San Diego, California, October 21-24.

Appendix 1

Reconstruction of Principal strain axes from en echelon vein arrays

The determination of the orientation of principal incremental strain axes X , Y , and Z from tension gash arrays was conducted from both conjugate, and single vein arrays. The data collection procedure, and methodology of which is described below:

Data collection

Whenever possible, two sets of measurements were recorded for each vein array. 1) the orientation (strike/dip) of the vein array, denoted ϕ , and 2) the incremental orientation (strike/dip) of the individual vein.

Where vein arrays displayed sigmoidal shaped extensional veins, the orientation of the external tip of the veins was recorded as it represents the incremental orientation of the vein (figure 1a).

Construction Methodology

Conjugate arrays - Where conjugate vein arrays were encountered, the methodology of Ramsay & Huber (1987) and Hobbs et al., (1976), for determining the principal stress axes of conjugate faults, was employed. Strain axes can be substituted for stress in this method because the vein arrays record the incremental strain direction, which approximates to the principal stress axes.

The conjugate vein array orientations were plotted as cyclographic traces on an equal area stereonet, the intersection of which represents the Y axis. The Z axis lies in a plane perpendicular to the Y axis, and bisects the angle θ (figure 1b). The X axis lies mutually perpendicular to the constructed Y and Z axes, therefore, it is located at the pole to the plane containing the Y and Z .

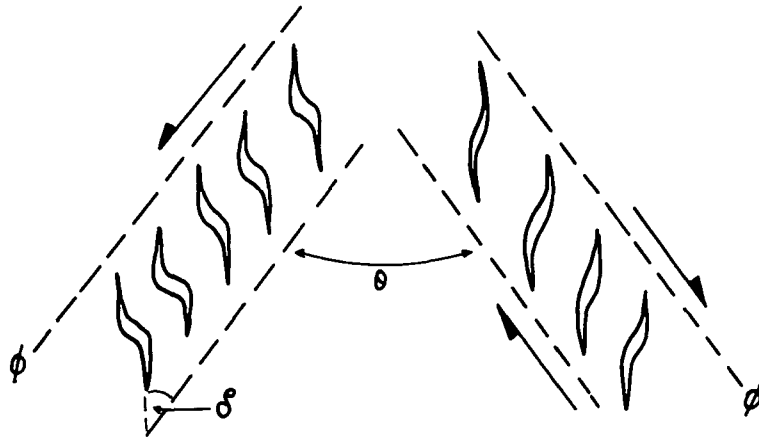
Single arrays - When only one vein array was observed, a different construction method was employed. The method is a modification of Ramsay and Huber's (1987) method for determining stress axis for a single fault plane.

- 1) The array orientation and incremental vein orientations are plotted as cyclographic traces on an equal area stereonet, the intersection of lineation (ν) of which is parallel to the intersection of the theoretical conjugate pair, and therefore, represents the Y axis (figure 1c).
- 2) A plane can be constructed perpendicular to the derived Y axis, which will contain the Z and X axes.
- 3) The Z axis will lie at an angle $\theta/2$ away from the trace of the measured vein array orientation. The angle θ can be estimated from observed conjugate vein arrays within the same lithology. However, the value of θ varies by as much as 20° depending

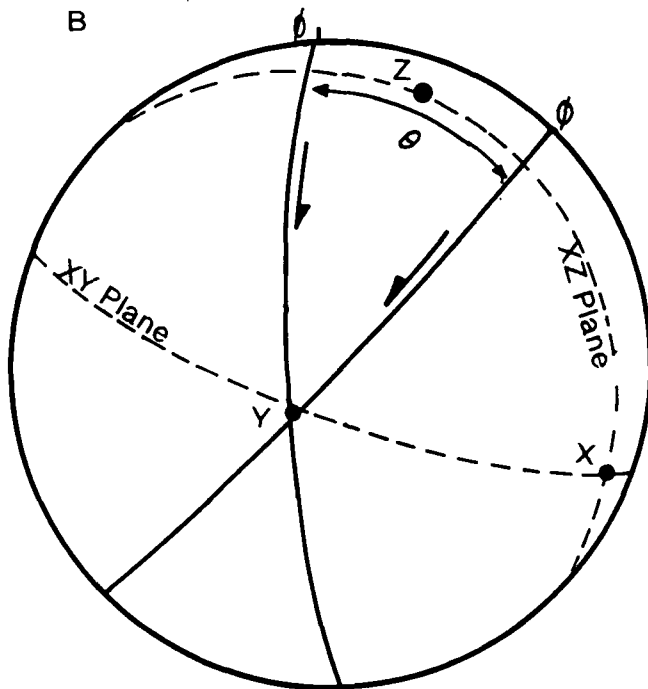
on the value of δ , the angle between the array orientation ϕ and the individual vein. However, the vein arrays display a direct relationship between the angles θ and δ . Therefore, the value of θ used in the construction depends on δ , and are based on the observed end-member variation in θ w.r.t. δ in the field. (figure 1c)

4) The X axis can be constructed in the same way as in the method for conjugate arrays.

A



B



C

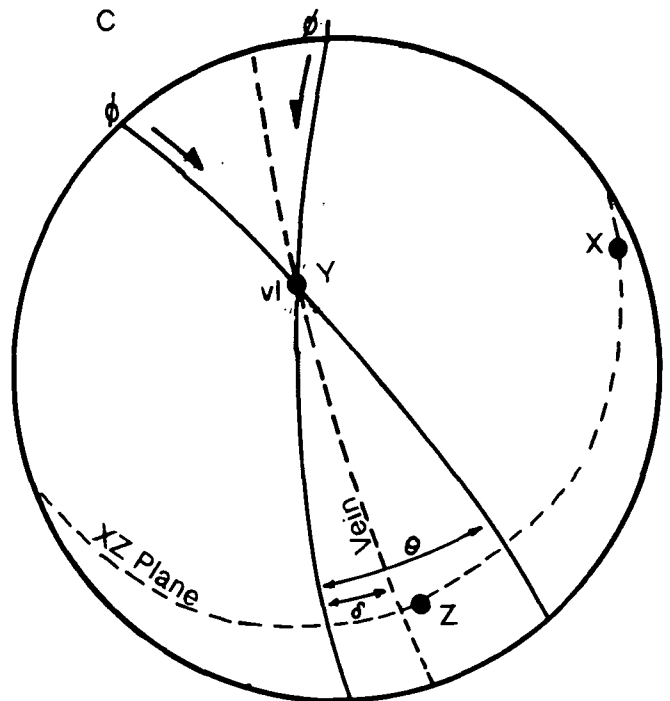
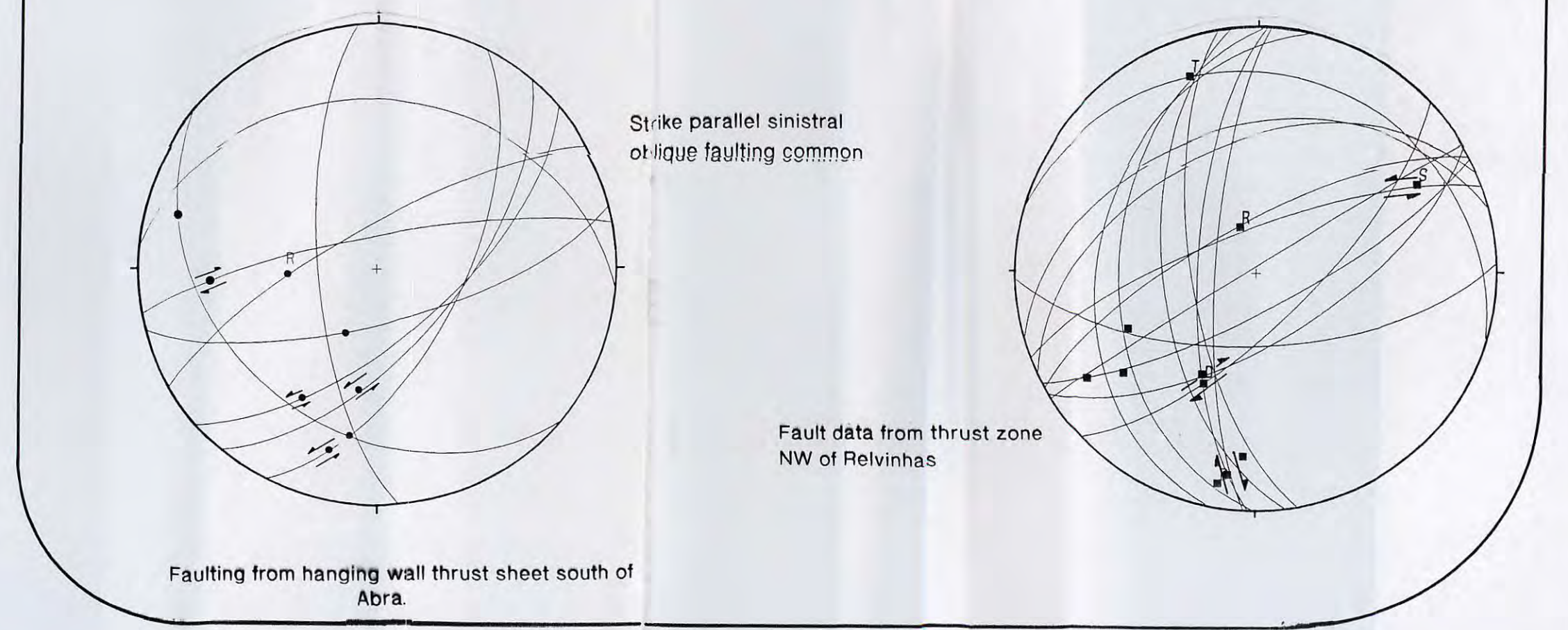
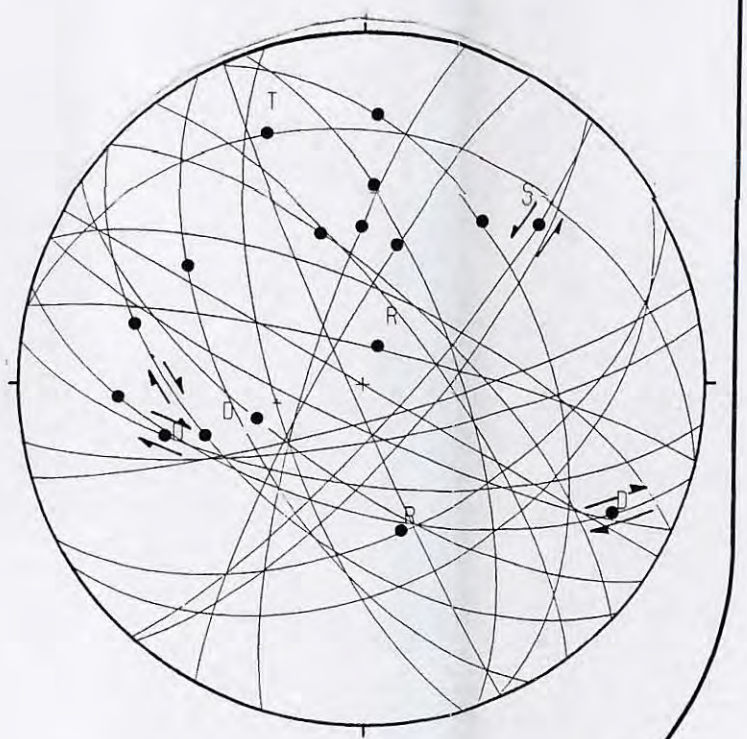
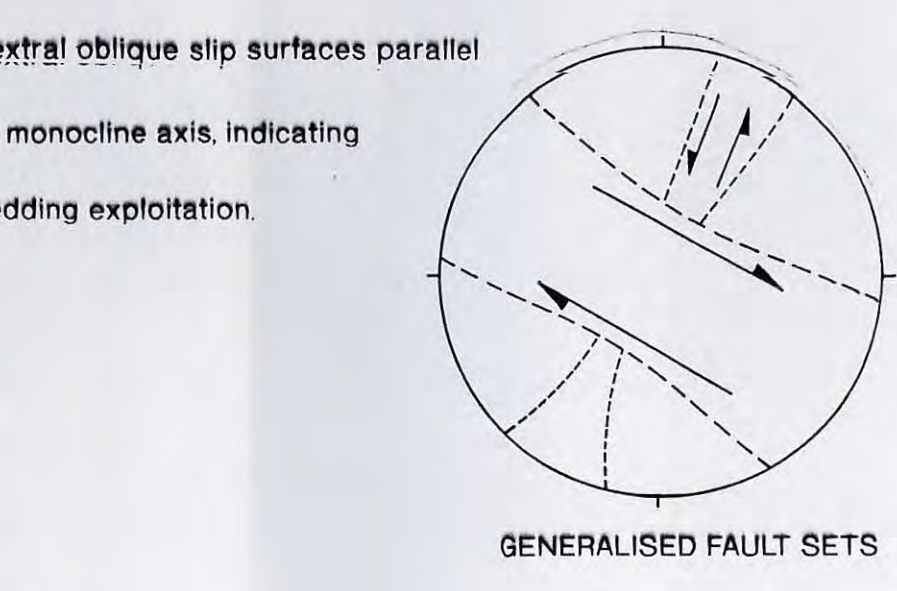
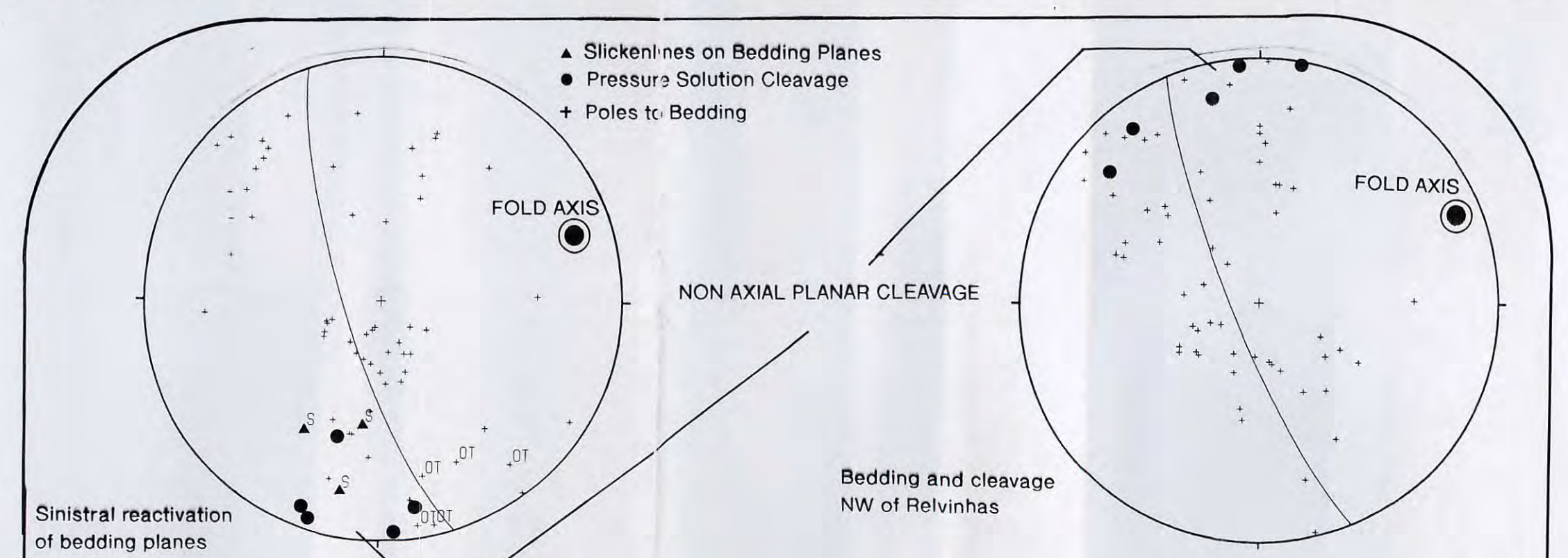
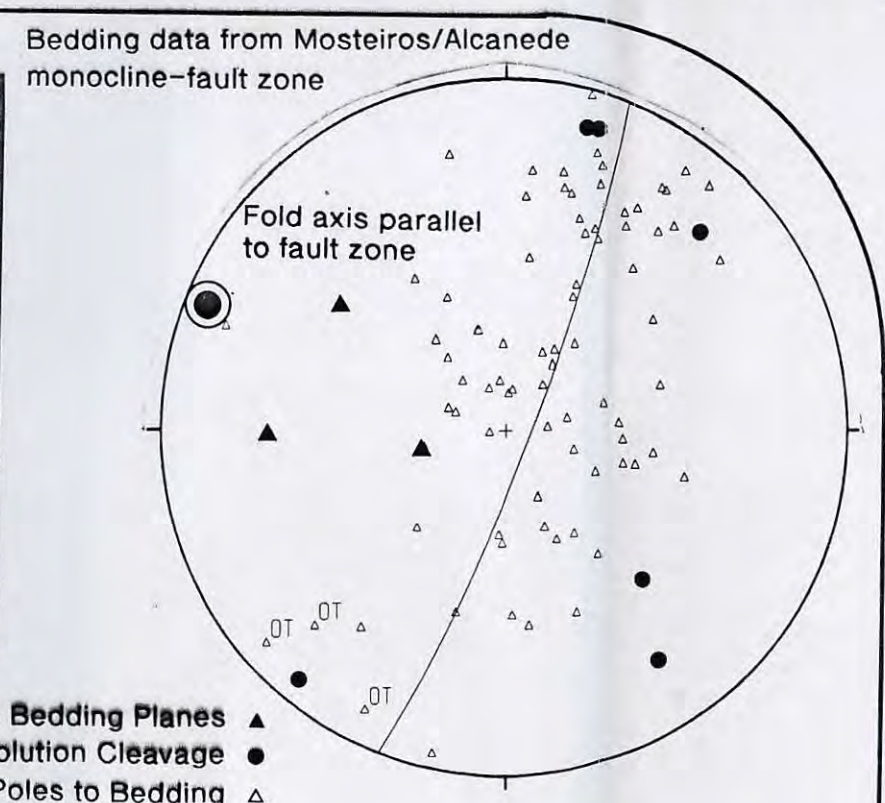
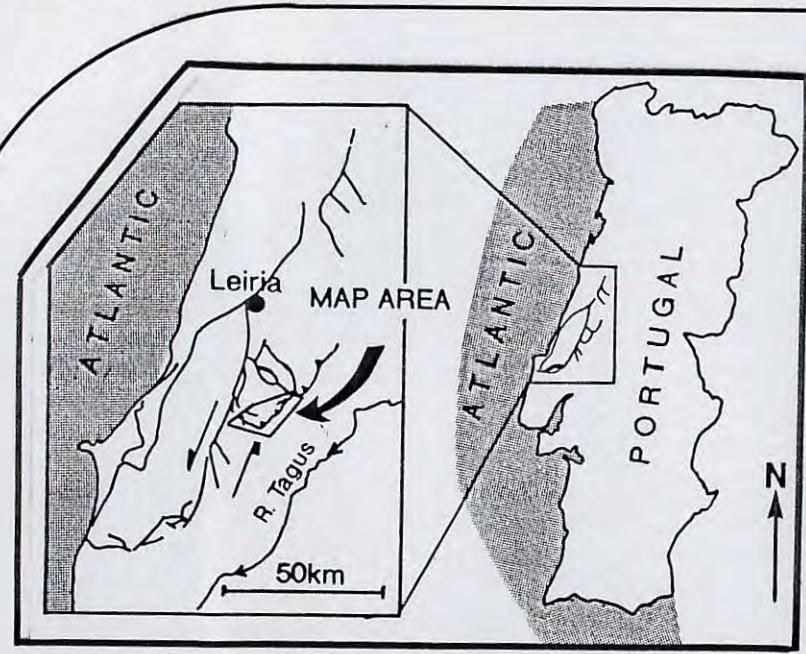
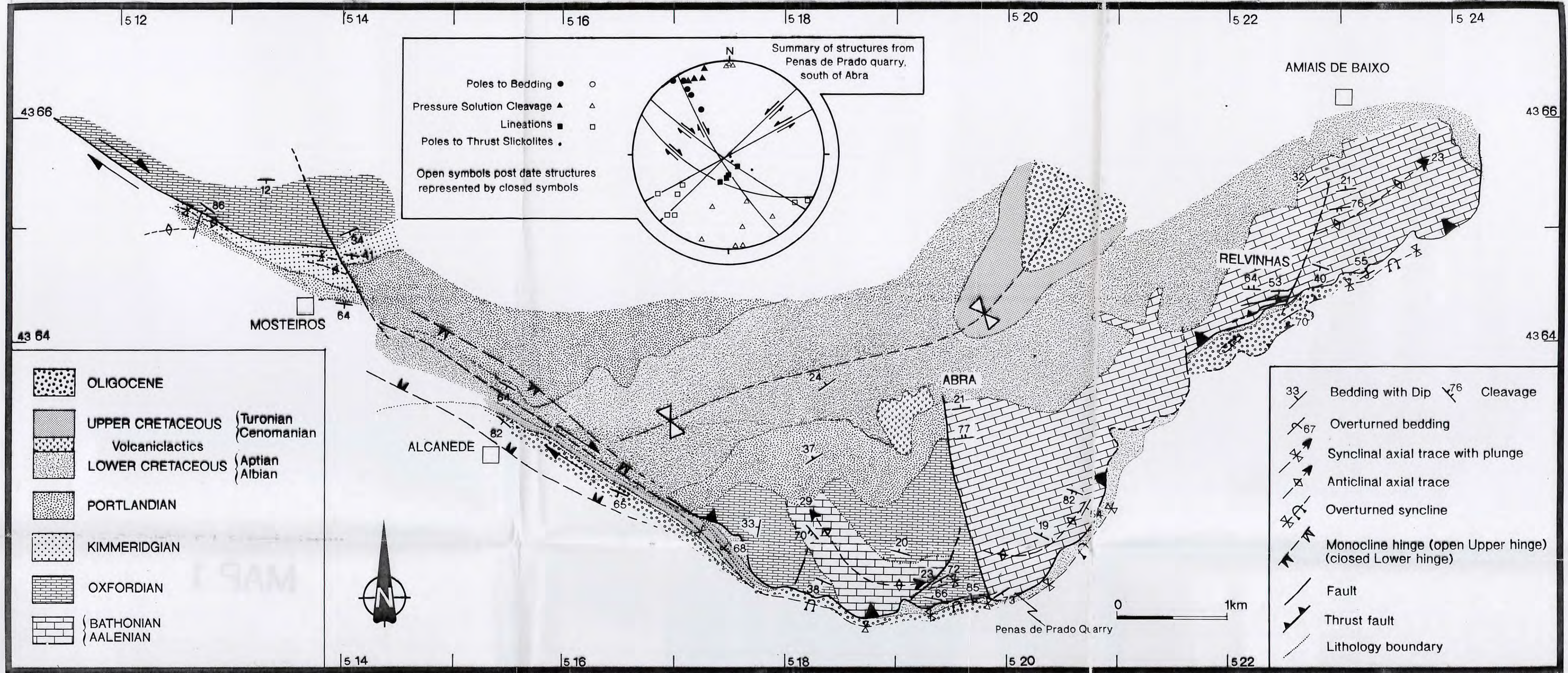


Figure 1 a) Definitions of θ , ϕ , and δ . b) Construction of strain axes from conjugate arrays. c) Construction of strain axes for single vein arrays.

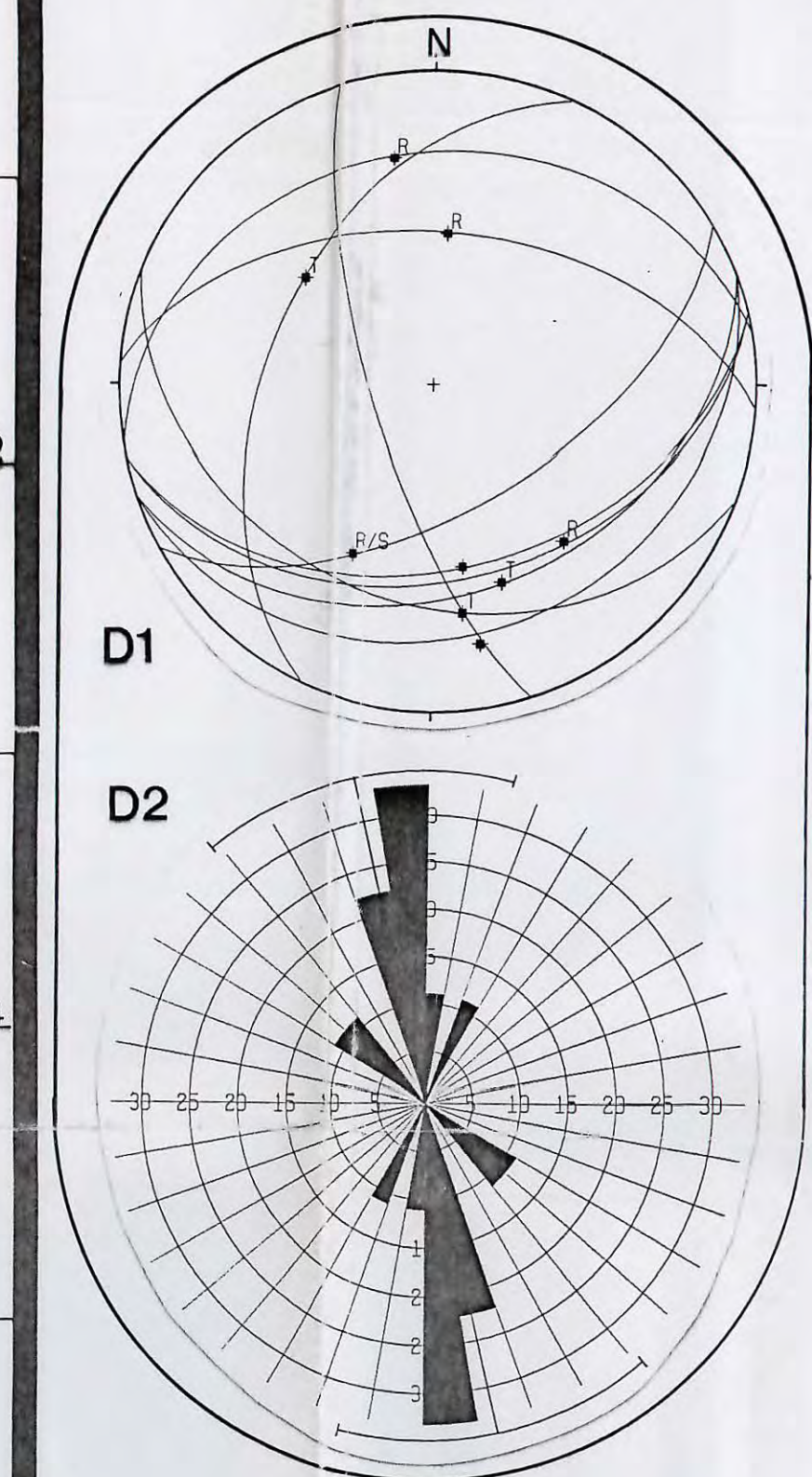
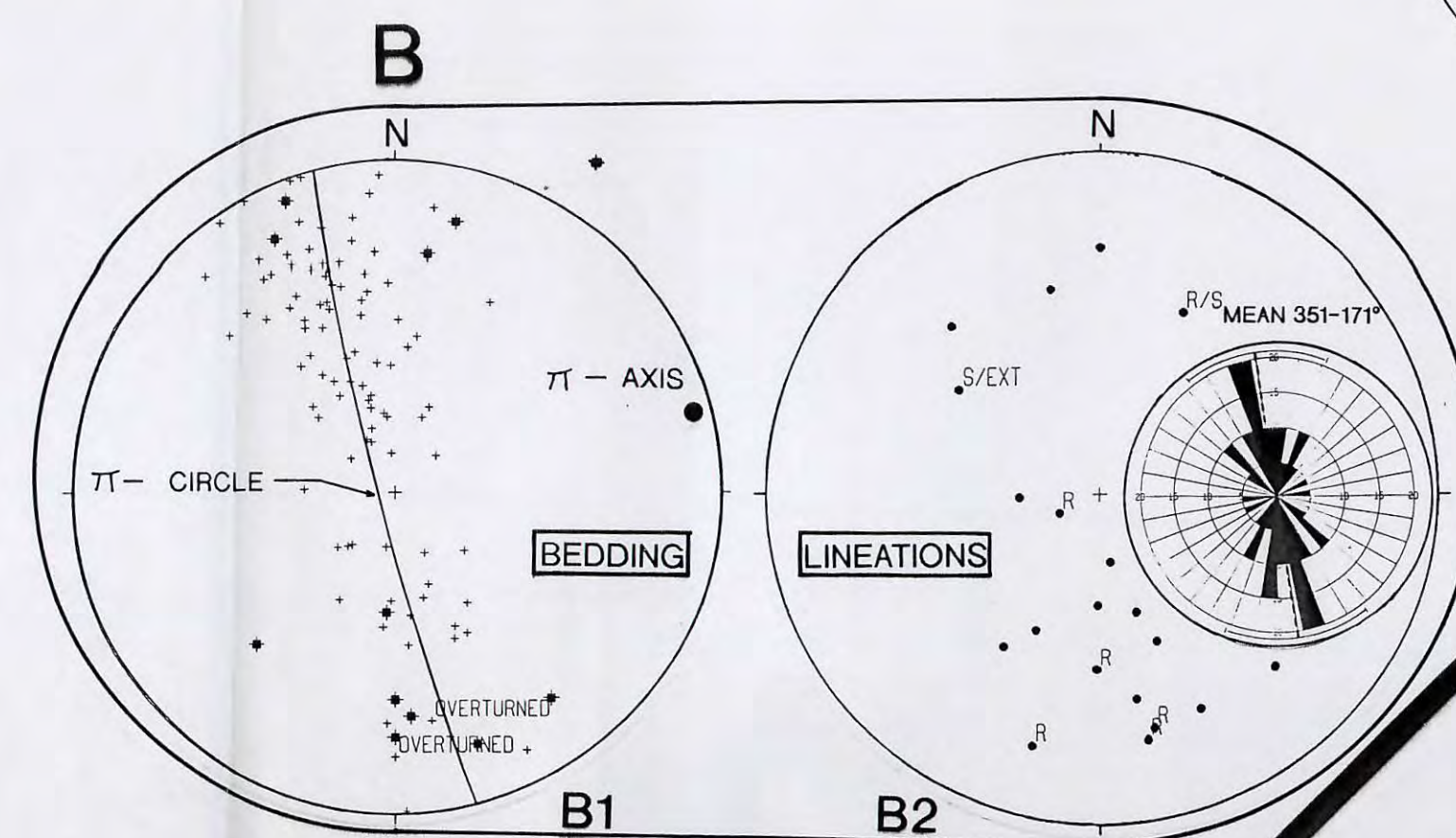
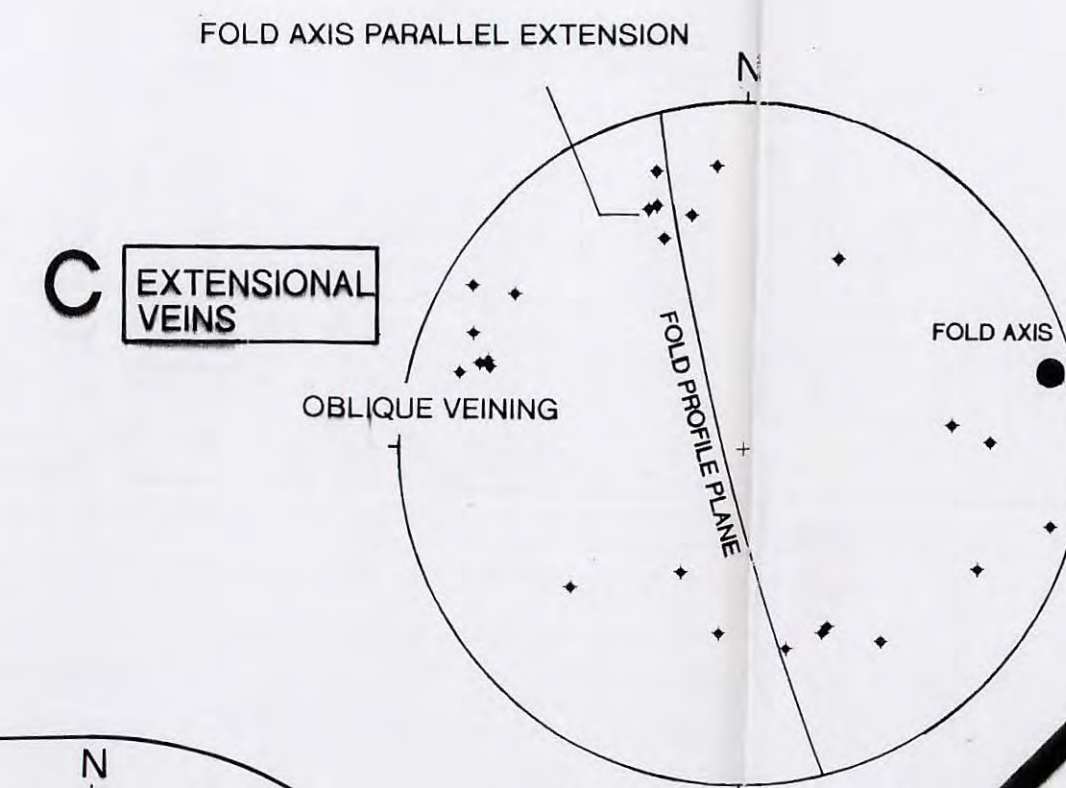
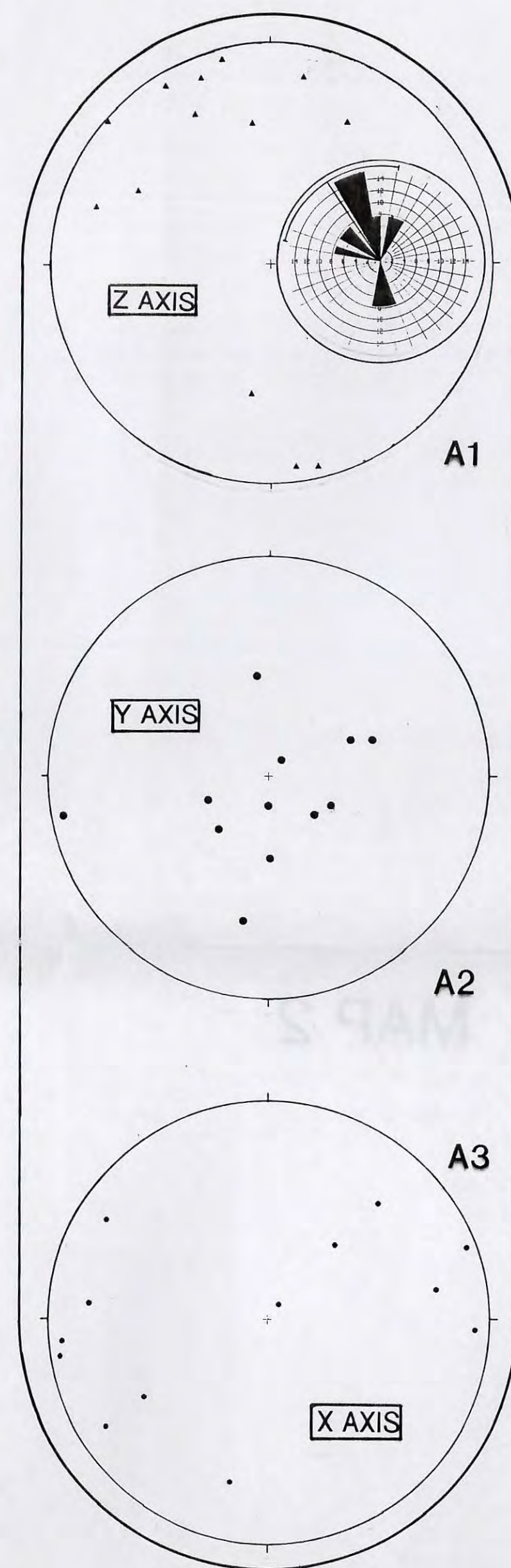
MAP 1

THE STRUCTURE AND KINEMATICS OF THE ABRA-AMIAS DE BAIXO THRUST ZONE



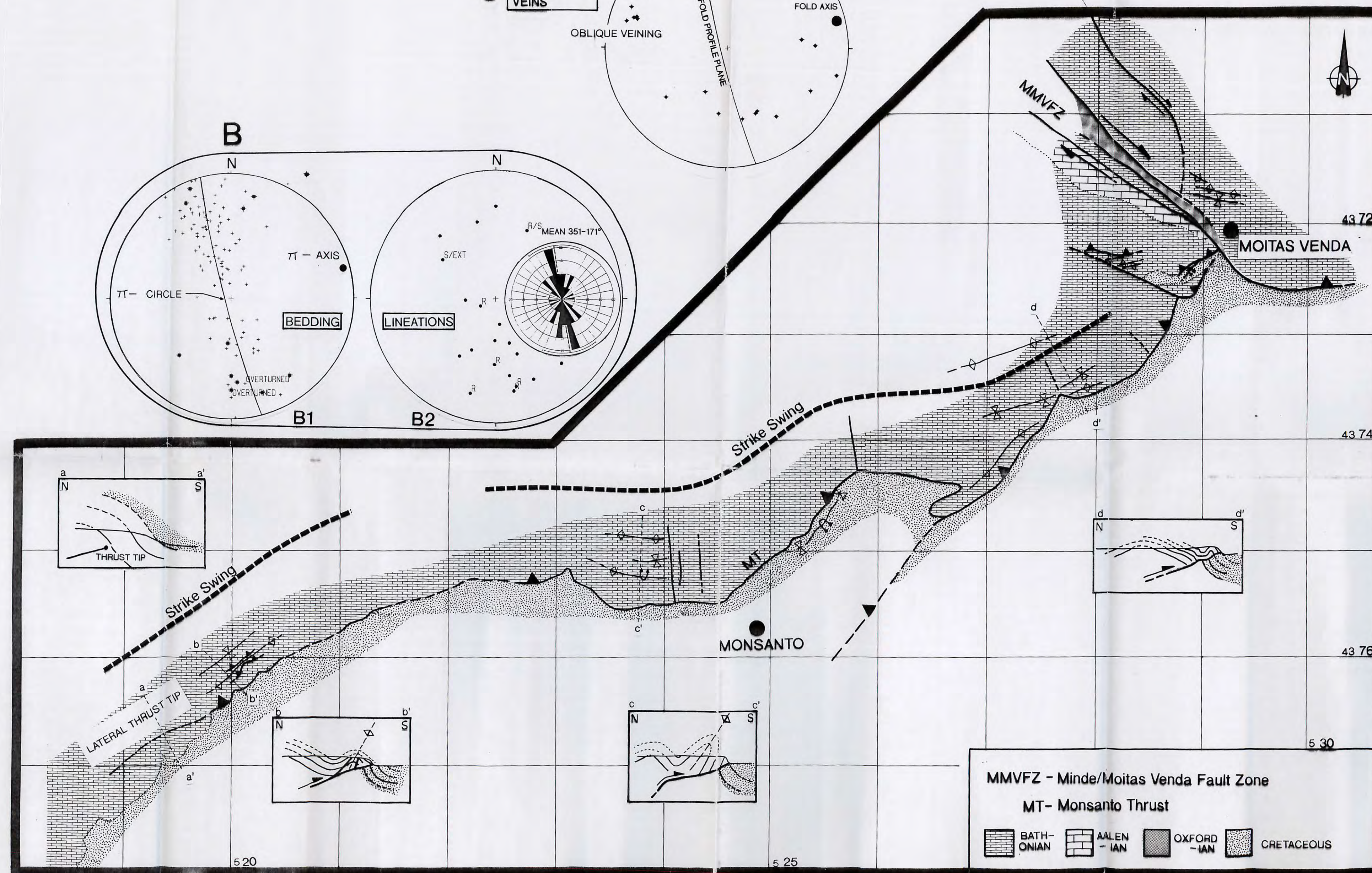
MAP 2 STRUCTURE AND KINEMATICS OF THE MONSANTO THRUST ZONE

A PRINCIPAL STRAIN AXES DERIVED FROM CONJUGATE ENNECHELON TENSION GASH ARRAYS

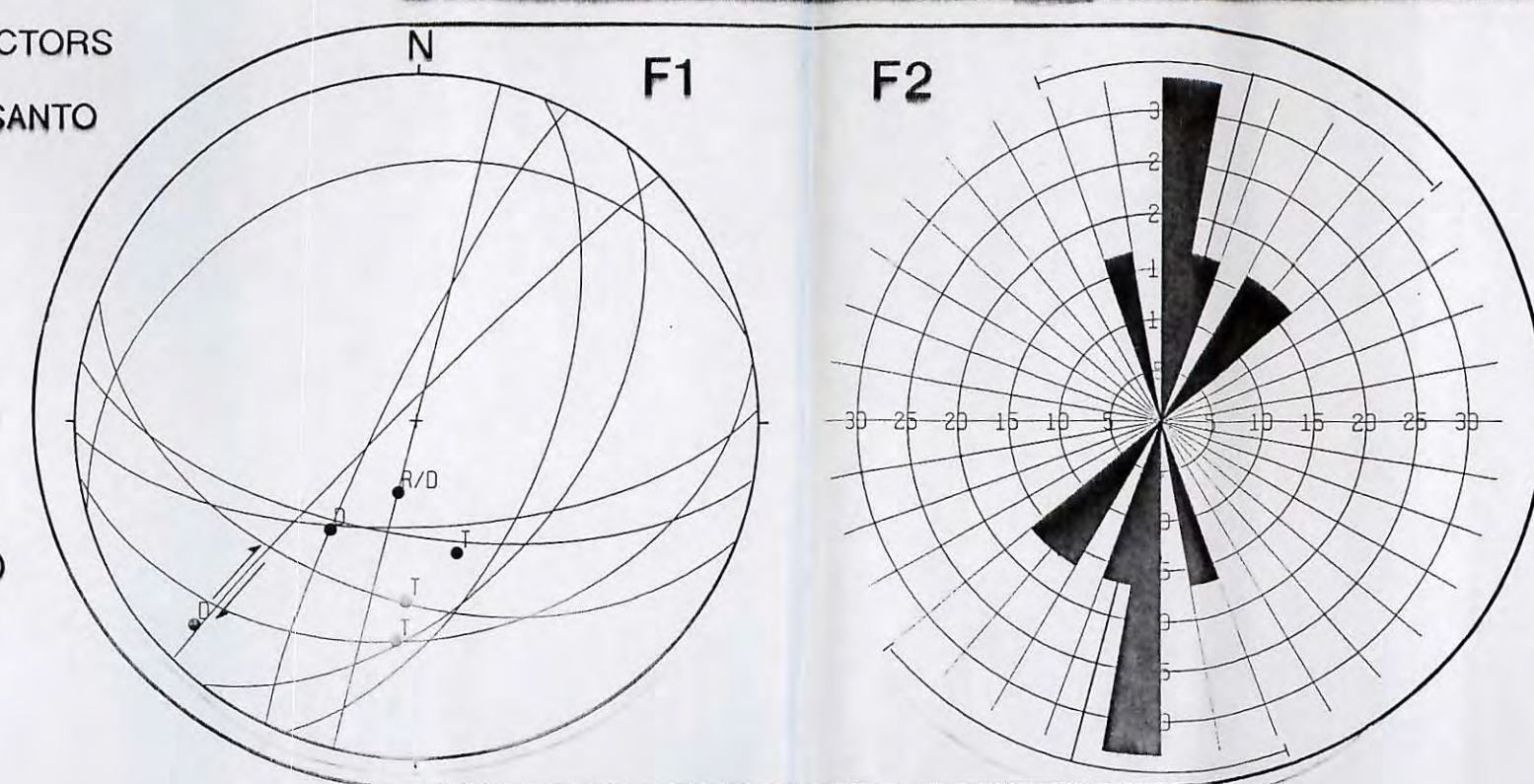


D FAULT PLANES AND MOVEMENT VECTORS FROM NE END OF THRUST SHEET

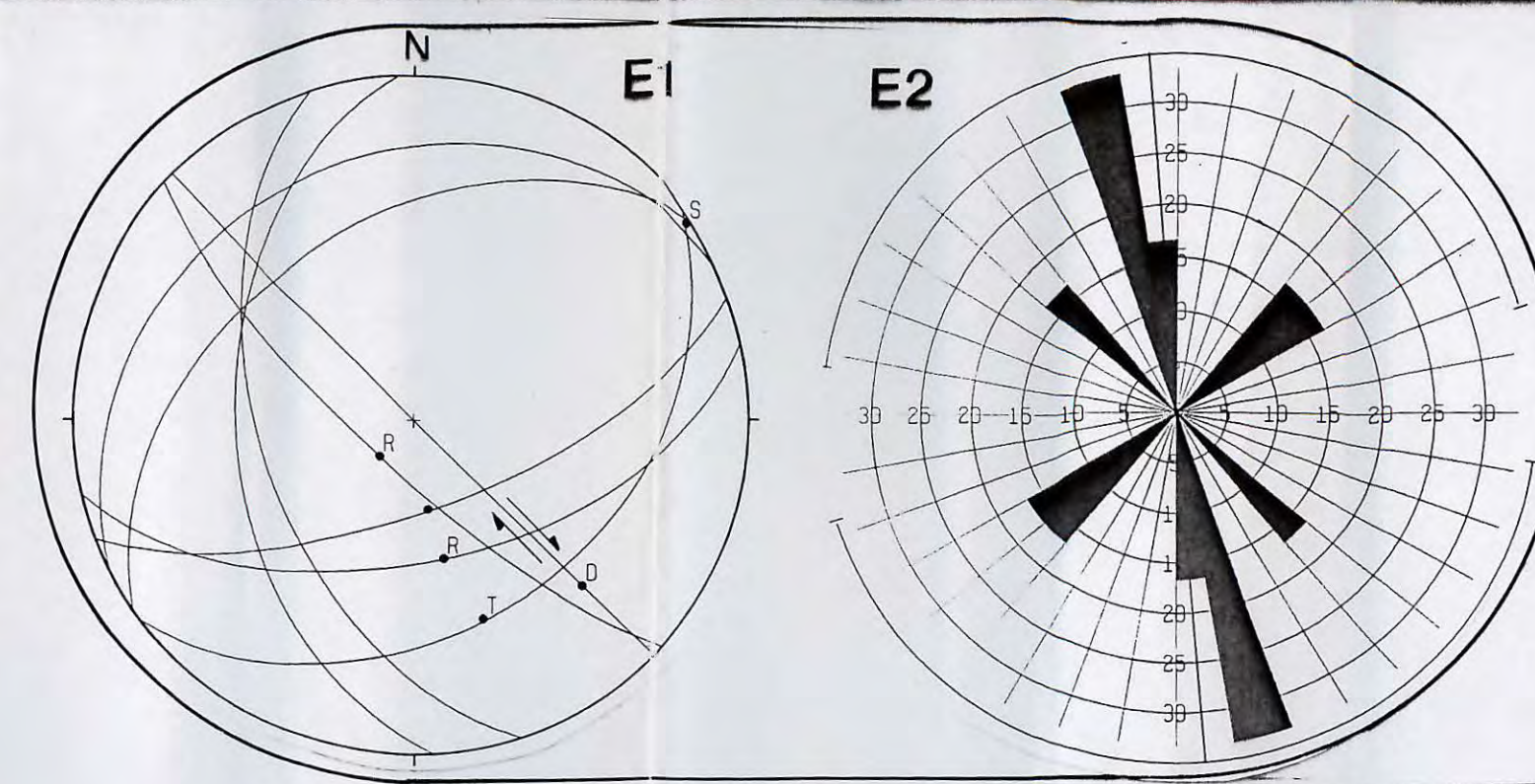
CIRCULAR HISTOGRAM OF SLICKENLINE (MOVEMENT VECTOR) AZIMUTHS
MEAN AZIMUTH 176°



FAULT PLANES AND MOVEMENT VECTORS FOR THRUST SHEET S.W. OF MONSANTO

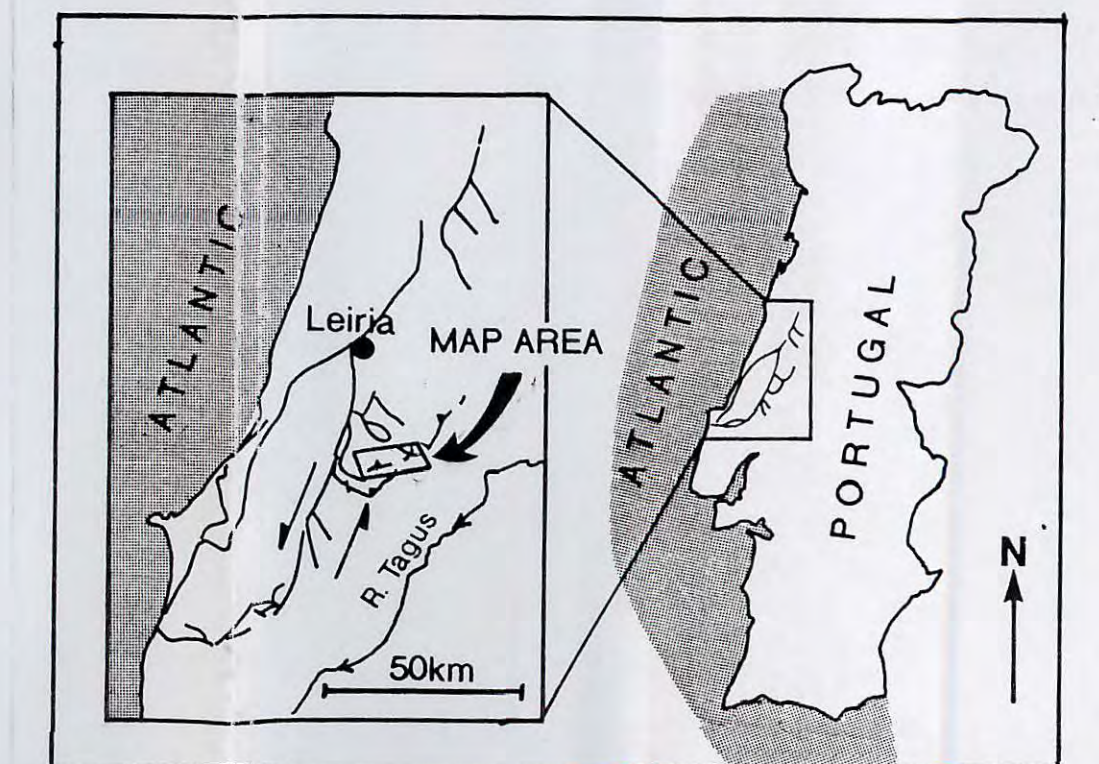


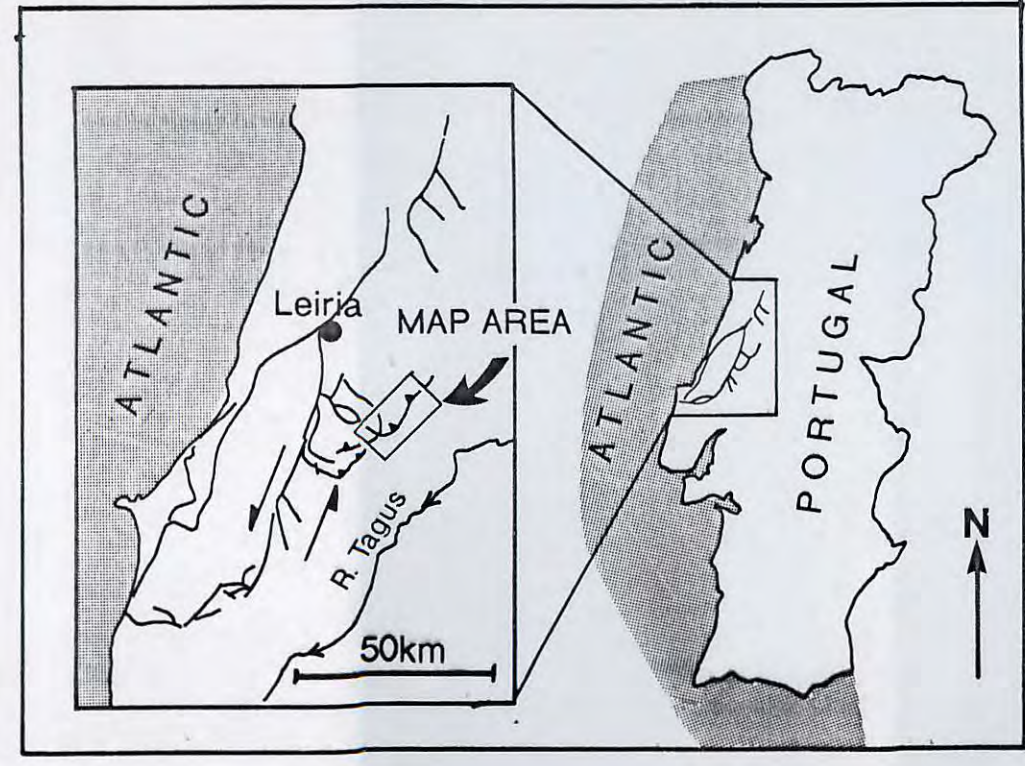
F CIRCULAR HISTOGRAM OF SLICKENLINE (MOVEMENT VECTOR) AZIMUTHS
MEAN AZIMUTH 194°



CIRCULAR HISTOGRAM OF SLICKENLINE (MOVEMENT VECTOR) AZIMUTHS
MEAN AZIMUTH 157°

E FAULT PLANES AND MOVEMENT VECTORS FROM LOCALITY 79



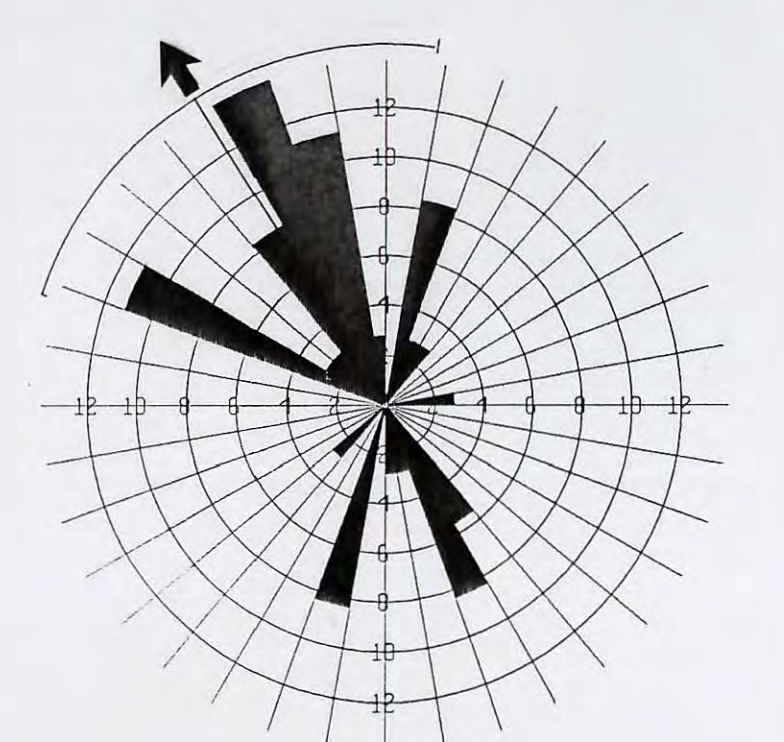
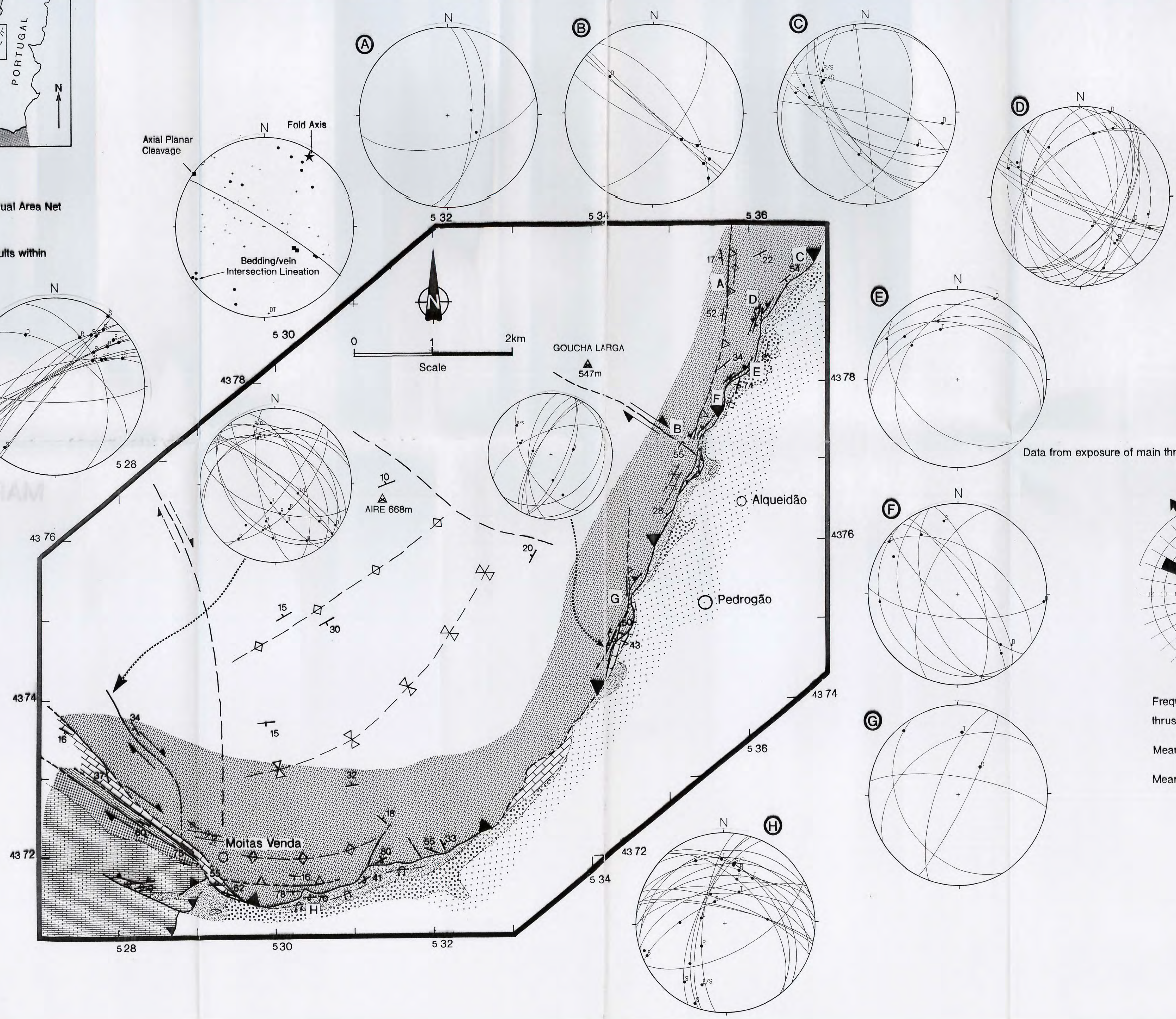


All Stereonets plotted on a Lambert Equal Area Net

Great circles represent mesoscopic faults within the hanging wall thrust sheet

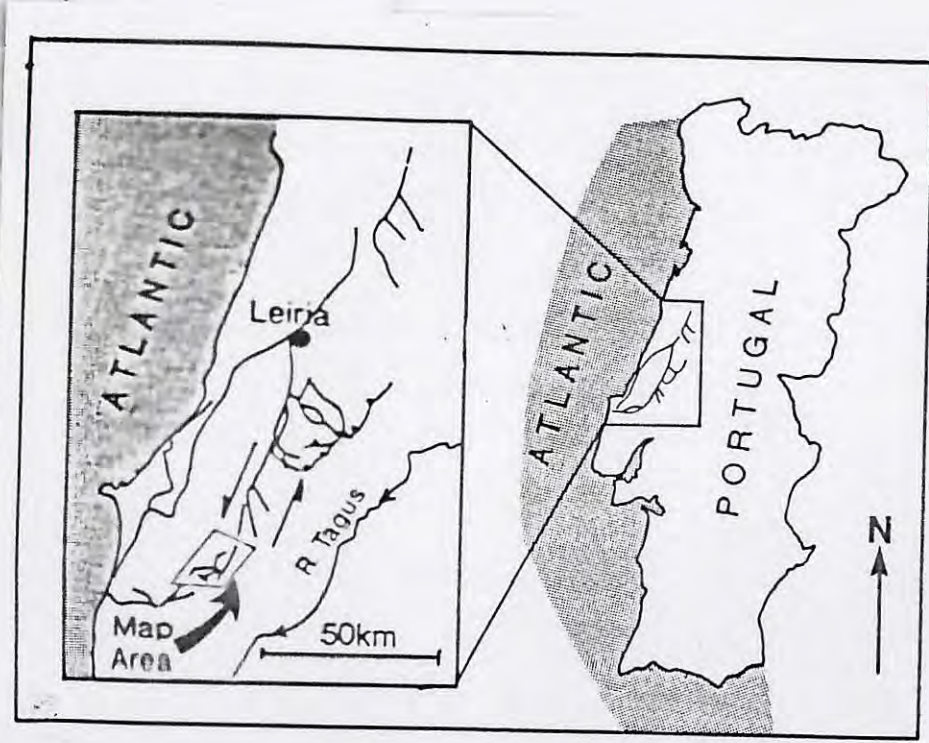
- LEGEND**
- Bedding
 - Overturned Bedding
 - Cleavage
 - Lithology boundary
 - Thrust Fault
 - Reverse Fault
 - Fault with sense of motion
 - Synclinal Trace
 - Anticlinal Trace

- KEY**
- | | |
|----------------|-----------|
| Tertiary | Miocene |
| | Oligocene |
| Cretaceous | Albian |
| | Aptian |
| Upper Jurassic | Oxfordian |
| | Bathonian |
| Mid Jurassic | Bajocian |
| | Aalenian |
| Lower Jurassic | |



Frequency = Length Rose diagram of thrust/reverse lineation azimuths.
 Mean lineation azimuth 328°
 Mean thrust transport direction 148°

MAP4 STRUCTURAL MAP OF THE MONTEJUNTO MASSIF



Stratigraphy	
	Miocene
	Kimmeridgian
	Oxfordian
	Callovian
	Bathonian
Tojeira Member } Abadia Formation } Montejunto Formation } Candeeiros Formation }	

Western & Eastern traverses through the S.M.T.

NAF - Northern Arieiro Fault
SAF - Southern Arieiro Fault

Structural symbols	
	Bedding (dip & strike)
	Overturned bedding
	Cleavage
	Thrust fault
	Strike-slip fault
	Anticline
	Syncline
with plunge } lower hinge } upper hinge } Monocline	

